Argonne NATIONAL LABORATORY

ANL/NE-07/21

Argonne Liquid-Metal Advanced Burner Reactor: Components and In-Vessel System Thermal-Hydraulic Research and Testing Experience Pathway Forward

Nuclear Engineering Division

About Argonne National Laboratory

Argonne is a U.S. Department of Energy laboratory managed by UChicago Argonne, LLC under contract DE-AC02-06CH11357. The Laboratory's main facility is outside Chicago, at 9700 South Cass Avenue, Argonne, Illinois 60439. For information about Argonne, see www.anl.gov.

Availability of This Report

This report is available, at no cost, at http://www.osti.gov/bridge. It is also available on paper to the U.S. Department of Energy and its contractors, for a processing fee, from:

U.S. Department of Energy
Office of Scientific and Technical Information
P.O. Box 62
Oak Ridge, TN 37831-0062
phone (865) 576-8401
fax (865) 576-5728
reports@adonis.osti.gov

ANL/NE-07/21

Argonne Liquid-Metal Advanced Burner Reactor: Components and In-Vessel System Thermal-Hydraulic Research and Testing Experience Pathway Forward

by
K. Kasza
with input from
C. Grandy, Y. Chang, H. Khalil, and many others
Nuclear Engineering Division, Argonne National Laboratory

May 7, 2007

Acknowledgements

The highlighted Argonne National Laboratory research represents the contributions and accomplishments of many researchers over the years and constitutes an important part of the LMR technology base that will support further reactor development under the GNEP initiative. The following list acknowledges those who have contributed to these efforts. We also gratefully acknowledge the support of the U.S. Department of Energy

R. S. Zeno
P. R. Huebotter
T. Bump
W. Simmons
A. Amorosi
J. P. Bobis
W. Brewer
A. R. Brunsvold
R. Carlson
M. M. Chen
T. Chiang
W. S. Colwell
W. Debbler
D. M. Engel
D. France
P. Fischer
P. Howard
T. M. Kuzay
W. D. Lawrence
H. C. Lin
J. J. Lorenz
A. Mele
E. W. O'hare
J. J. Oras Jr
F. J. Piotrowski
D. Pointer
R. C. Schmitt
W. T. Sha
A. Siegel
M. G. Srinivasan
C. P. Tzanos
K. L. Uherka

Contents

Executive Summary

This white paper provides an overview and status report of the thermal-hydraulic nuclear research and development, both experimental and computational, conducted predominately at Argonne National Laboratory. Argonne from the early 1970s through the early 1990s was the Department of Energy's (DOE's) lead lab for thermal-hydraulic development of Liquid Metal Reactors (LMRs). During the 1970s and into the mid-1980s, Argonne conducted thermal–hydraulic studies and experiments on individual reactor components supporting the Experimental Breeder Reactor-II (EBR-II), Fast Flux Test Facility (FFTF), and the Clinch River Breeder Reactor (CRBR). From the mid-1980s and into the early 1990s, Argonne conducted studies on phenomena related to forced- and natural-convection thermal buoyancy in complete in-vessel models of the General Electric (GE) Prototype Reactor Inherently Safe Module (PRISM) and Rockwell International (RI) Sodium Advanced Fast Reactor (SAFR). These two reactor initiatives involved Argonne working closely with U.S. industry and DOE. This paper describes the very important impact of thermal hydraulics dominated by thermal buoyancy forces on reactor global operation and on the behavior/performance of individual components during postulated off-normal accident events with low flow. Utilizing Argonne's LMR expertise and design knowledge is vital to the further development of safe, reliable, and high-performance LMRs.

Argonne believes there remains an important need for continued research and development on thermal-hydraulic design in support of DOE's and the international community's renewed thrust for developing and demonstrating the Global Nuclear Energy Partnership (GNEP) reactor(s) and the associated Argonne Liquid Metal-Advanced Burner Reactor (LM-ABR). This white paper highlights that further understanding is needed regarding reactor design under coolant low-flow events. These safety-related events are associated with the transition from normal high-flow operation to natural circulation. Low-flow coolant events are the most difficult to design for because they involve the most complex thermal-hydraulic behavior induced by the dominance of thermal-buoyancy forces acting on the coolants. Such behavior can cause multiple-component flow interaction phenomena, which are not adequately understood or appreciated by reactor designers as to their impact on reactor performance and safety.

Since the early 1990s, when DOE cancelled the U.S. Liquid Metal Fast Breeder Reactor (LMFBR) program, little has been done experimentally to further understand the importance of the complex thermal-buoyancy phenomena and their impact on reactor design or to improve the ability of three-dimensional (3-D) transient computational fluid dynamics (CFD) and structures codes to model the phenomena. An improved experimental data base and the associated improved validated codes would provide needed design tools to the reactor community. The improved codes would also facilitate scale-up from small-scale testing to prototype size and would facilitate comparing performance of one reactor/component design with another. The codes would also have relevance to the design and safety of water-cooled reactors.

To accomplish the preceding, it is proposed to establish a national GNEP-LMR research and development center at Argonne having as its foundation state-of-art science-based

infrastructure consisting of: a) thermal-hydraulic experimental capabilities for conducting both water and sodium testing of individual reactor components and complete reactor in-vessel models and b) a computational modeling development and validation capability that is strongly interfaced with the experimental facilities. The proposed center would greatly advance capabilities for reactor development by establishing the validity of high-fidelity (i.e., close to first principles) models and tools. Such tools could be used directly for reactor design or for qualifying/tuning of lower-fidelity models, which now require costly experimental qualification for each different type of design application. Capabilities required to establish and operate this center are found primarily in Argonne's Nuclear Engineering and Mathematics and Computer Science Divisions. Funding for the center would be sought from DOE-NE (GNEP/Advanced Burner Reactor and Generation IV programs), DOE-SC/ASCR, and the commercial nuclear industry.

Having the above experimental and modeling capabilities at Argonne would constitute a national/international center of excellence for conducting the research and engineering and design tool development needed to support the DOE GNEP/ LM-ABR initiative in developing safe, high-performance reactors.

1.0 Introduction

During the 1970s and 1980s, the U.S. DOE sponsored a substantial effort in the development of sodium-cooled fast nuclear reactors. Initially, these fission reactors were to be breeders with the designation Liquid Metal Fast Breeder Reactor (LMFBR). Later the breeding stipulation was dropped, and the name was changed to Liquid Metal Reactor (LMR) or Advanced Burner Reactor (ABR). The most important feature of the earlier breeder reactor was to significantly extend the useful life of the world's supply of fissionable uranium by implementing a system of breeder reactors with the goal of producing about 10% more fissionable material each year than consumed in producing electricity. At that time, LMFBRs had only been built in small size, and it was appropriate for DOE to sponsor the development of the commercial-scale technology because the project was too large for private industry and because it was of great national interest and potential benefit. To this end, DOE sponsored a variety of research and development programs to advance this technology.

In response to DOE during the 1970s, Argonne conducted thermal–hydraulic studies of individual LMR components supporting EBR-II, FFTF, and CRBR development. After cancellation of CRBR, DOE in order to begin transferring LMR technology developed under federally funded programs to the U.S. industry funded a design competition between General Electric (GE) and Rockwell International/Combustion Engineering (RI/CE) to design a commercially viable LMR for future deployment. The GE design was called PRISM (Prototype Reactor Inherently Safe Module) and the RI/CE design was called SAFR (Sodium Advanced Fast Reactor). In the mid-1980s and early 1990s, Argonne conducted forced- and natural-convection phenomena studies on complete in-vessel system experimental test models of the GE/PRISM and RI/CE/SAFR designs. These DOE-funded studies were carried out in collaboration with GE and RI/CE. Further development of LMR expertise/design knowledge is vital to the future deployment of safe, reliable, and high-performance LMR Advanced Burner Reactors (ABRs) currently being proposed by DOE under the GNEP initiative for deployment in 2025. This near-term deployment does not involve breeder reactors.

This white paper has been written to summarize the thermal-hydraulic understanding that has been developed over the last 30 plus years, highlight important phenomena that must be factored into future reactor designs, and describe additional developmental efforts still needed. In particular, it describes the need for further LM-ABR technology development support in the form of better testing infrastructure, improved engineering knowledge, and improved/validated computational modeling tools. The paper also addresses the impact of thermal hydraulics on reactor system operation and on the behavior/performance of individual components (thermal duty and structural impact) during normal operation and postulated off-normal low-flow accident events related to safety.

Argonne has been a pioneer in the study of thermal-buoyancy-force governed flows under various important reactor transient conditions, such as the transition from forced to natural convection, instabilities generated by parallel flow paths, and structural thermal stresses caused by thermal stratification and their influence on heat-sink effectiveness.

Argonne from the early 1970s through the early 1990s was DOE's lead laboratory for LMR thermal-hydraulic development. During the 1970s and into the mid-1980s, Argonne conducted thermal-hydraulic studies and experiments on individual reactor components supporting EBR-II, FFTF, and CRBR. In the 1980s and into the early 1990s, Argonne conducted studies on forced- and natural-convection (thermal-buoyancy-force) phenomena in complete in-vessel models of GE/PRISM and RI/SAFR. These two reactor initiatives involved Argonne working closely with U.S. industry and the DOE. This paper describes the very important impact of thermal hydraulics on reactor global operation and on individual component behavior/performance (thermal duty, structural impact, and safe operation) during normal operation and postulated off-normal low-flow accident events related to safety. Argonne's LMR expertise and design knowledge are vital to the further development of a safe, reliable, and high-performance LM-ABR.

In the 1980s Argonne developed/built a large water test facility called the Mixing Components Test Facility (MCTF) for performing steady and thermal-transient experimental simulations of important reactor components under a wide range of operation scenarios. (The MCTF was decommissioned in 1993.) Modeling studies were also conducted by Argonne relative to ascertaining if the thermal-buoyancy phenomena being studied could be effectively addressed through the use of water for testing of both individual LMR components and complete in-vessel system geometries. This modeling is discussed in detail in Section 4.2.1 and in Appendix 1 of this report. These modeling studies also highlighted where water testing was not adequate for addressing certain phenomena.

All of the Argonne studies involved fundamental experimental thermal-hydraulic testing and a strongly integrated component of computational fluid dynamics (CFD) code development and simulation analysis. The CFD analyses were predominately performed with the Argonne COMMIX code, which was augmented by some initial effort at utilization of commercial CFD codes like STAR-CD. One of the first uses of three-dimensional CFD analysis for addressing LMR thermal-hydraulics, which used the COMMIX code, was to address buoyancy-governed reactor flows. This computational modeling was driven and guided by Argonne's thermal-hydraulic experiments on reactor components such as piping, plenums, steam generators, and heat exchangers.

The contents of this white paper are as follows:

Section 2 briefly describes the new DOE GNEP initiative relative to the pre-conceptual design features of the Argonne proposed LM-ABR, which would be one of the GNEP building blocks. Knowing the general technical features associated with the ABR allowed us to focus on and exploit what has been learned over the last 30 plus years about LMR thermal hydraulics relative to the importance to GNEP. Finally, this section also describes, based on the 1993 GE/PRISM close-out report, what industry ideas were at that time as to what further development and testing were needed to deploy a U.S. LMR. This information helped to further focus the recommendations given in this report regarding a thermal-hydraulic pathway forward.

Section 3 describes Argonne studies and the status of our understanding of thermal buoyancy phenomena occurring in individual reactor components such as:

- Piping
- Piping/plenum interfaces and thermal plumes
- Heat exchangers
- Steam generators
- Multiple coolant stream thermal mixers

Section 4 describes Argonne's past studies on reactor in-vessel thermal hydraulics, which initially addressed generic core outlet and plenum flow interactions guided by CRBR needs. These studies in their later stages investigated forced- and natural-convection (thermal-buoyancy-force) phenomena using complete in-vessel models of the GE/PRISM and RI-CE/SAFR designs. Complete in-vessel model experiments were used because the flow and thermal behavior in a given sub-region of the reactor vessel is the result of complex interactions with the rest of the reactor in-vessel components. These interactions are especially important for pool designs under low-flow conditions and the transition to natural convection. They have the potential for strongly affecting reactor:

- Thermal-hydraulic performance
- Emergency cooling
- Structural integrity
- Heat-sink effectiveness

These complete in-vessel experimental studies provided GE and RI-CE designers with information vital to the design and assessment of the workability of the various features that were being incorporated into their innovative and inherently safe reactors.

Finally, Section 5 describes a pathway forward regarding further research and development needed to support the GNEP/LM-ABR initiative.

2.0 New DOE GNEP Initiative

The new DOE Global Nuclear Energy Partnership (GNEP) initiative [1] announced in January 2007 has as its purpose "to work with other nations to develop and deploy advanced nuclear fuel recycling and reactor technologies to make possible a dramatic expansion of safe, clean nuclear energy to help meet the growing global energy demand while decreasing the risk of nuclear weapons proliferation and effectively addressing the challenge of nuclear waste disposal." To implement the GNEP plan, three types of facilities/building blocks are required:

1. Nuclear fuel recycling centers to separate the components of spent fuel
2. Advanced recycling reactors to burn the actinide-based fuel to transform the actinides in a way that makes them easier to store as waste and produces energy
3. An advanced fuel cycle research facility to serve as an R&D center for developing improved nuclear fuels

Item 2 is believed to be satisfied by the use of a sodium-cooled fast reactor.

Section 2.1 describes within the context of the new DOE GNEP initiative, the pre-conceptual design features of a liquid-metal sodium-cooled fast reactor proposed by Argonne, called the Advanced Burner Reactor (ABR) [2], which would constitute item 2 of the GNEP building blocks. Knowing the general technical features associated with the ABR allows one to clearly focus on and exploit what has been learned over the last 30 years about LMR thermal hydraulics that is relevant to GNEP.

Section 2.2 describes, based on the 1993 GE/PRISM close-out report [3], what industry ideas were at that time as to what further development and testing were needed to deploy a U.S. LMR. The GE/PRISM LMR is similar to the proposed LM-ABR. Consideration of this past effort has helped to focus the recommendations given in Sec. 5.0 of this report regarding a thermal-hydraulic pathway forward in support of GNEP and the LM-ABR.

To establish the design/construction readiness of the LM-ABR concept proposed as part of the GNEP initiative, it is very important to assess and, if needed, further improve the understanding of and ability to model/predict the thermal hydraulics that are associated with the interplay and feedback between the various reactor in-vessel structures, such as plenums, the core, and other in-vessel components. The LM-ABR must be able to survive, with minimal operator intervention (inherently safe), such events as a loss of normal heat sink with reactor scram or a loss of coolant pumping power and normal heat sink with failure to scram by relying on passive means for heat rejection from components such as the reactor vessel walls and the other in-vessel heat sinks.

As a consequence, detailed 3-D modeling of the temperature and flow distributions occurring during various scenarios (low flow, transient and steady state, and mixed- and natural-circulation flow) is essential to the design and validation of core cooling capability as well as of the thermal-hydraulic and structural performance of other important components. A data base adequate to guide the development and the validation of computer codes for design-supporting

computational thermal-hydraulic and structural modeling must be available. The computational tools are needed to not only support assessment of general thermal-hydraulic performance and reliability of the system as a whole, but also to support design and placement of the individual components such as heat exchangers, pumps, connecting piping, plenums, and other internals within the reactor under operational scenarios causing the components to interact, because of their close coupling, in very complex ways.

2.1 LM-ABR Pre-conceptual Design Features

A pre-conceptual design of a 250 MWt LM-ABR (sodium cooled) has been developed by Argonne [2]. In addition to meeting the objectives of the GNEP initiative, the design incorporates the lessons learned from more than a dozen fast reactor programs in the U.S. and worldwide. In particular, the U.S. EBR-II operational experiences have been incorporated into the design of the ABR to the extent possible. Based on these past experiences, the pool-type reactor vessel arrangement was selected as the basis for the ABR pre-conceptual design due to its potential for design simplicity, inherent passive safety, and economics.

2.1.1 Plant Design

The plant design parameters for the proposed LM-ABR are summarized in the following table. The major primary system components and the associated thermodynamic cycle – the reactor vessel containing the reactor core and the primary heat transport system, the intermediate heat transport system with the sodium-to-CO_2 heat exchangers, and the Brayton cycle power conversion system – are shown in Figs. 2.1-1 and -2.

Table 2.1-1 Design parameters for Argonne-proposed LM-ABR plant

Reactor Power	250 MWt, 95 MWe
Coolant	Sodium
Coolant Temperature, Inlet/Outlet	355ºC/510ºC
Driver Fuel	Reference: Metal (~20% transuranics, 80% U) Backup: Oxide
Cladding and Duct Material	HT-9
Cycle Length	4 months
Plant Life	30 years with the expectation of life extension
Reactor Vessel Size	5.8-m diameter, 16-m height
Structural and Piping Material	Austenitic Stainless Steel
Primary Pump	Reference: Electromagnetic Backup: Mechanical (centrifugal)
Power Conversion Cycle	Reference: Supercritical CO_2 Brayton Backup: Steam Rankine
Thermal Efficiency	38 %

The reactor core consists of 24 assemblies in an inner enrichment zone and 30 assemblies in an outer zone. Reactivity control and neutronic shutdown are provided by 7 primary and 3 secondary control rod assemblies.

The primary system shown in Figure 2.1-1 is configured in a pool-type arrangement (similar to that used successfully in EBR-II), with the reactor core, primary pumps, intermediate heat exchangers (IHXs), and direct reactor auxiliary cooling system (DRACS) heat exchangers all immersed in a pool of sodium coolant within the reactor vessel. The pool-type arrangement was selected because of its inherent simplicity and safety. All primary coolant piping is within the sodium pool, which greatly reduces the possibility of loss of coolant, and the sodium pool provides a large thermal inertia in the system. In addition, the reactor vessel is a simple structure having no penetrations. The hot sodium at core outlet temperature is separated from the cold sodium at core inlet temperature by a structure called the "redan." The reactor vessel is exposed only to cold sodium, so it is not subjected to severe thermal transients. A guard vessel is provided as an additional passive safety feature.

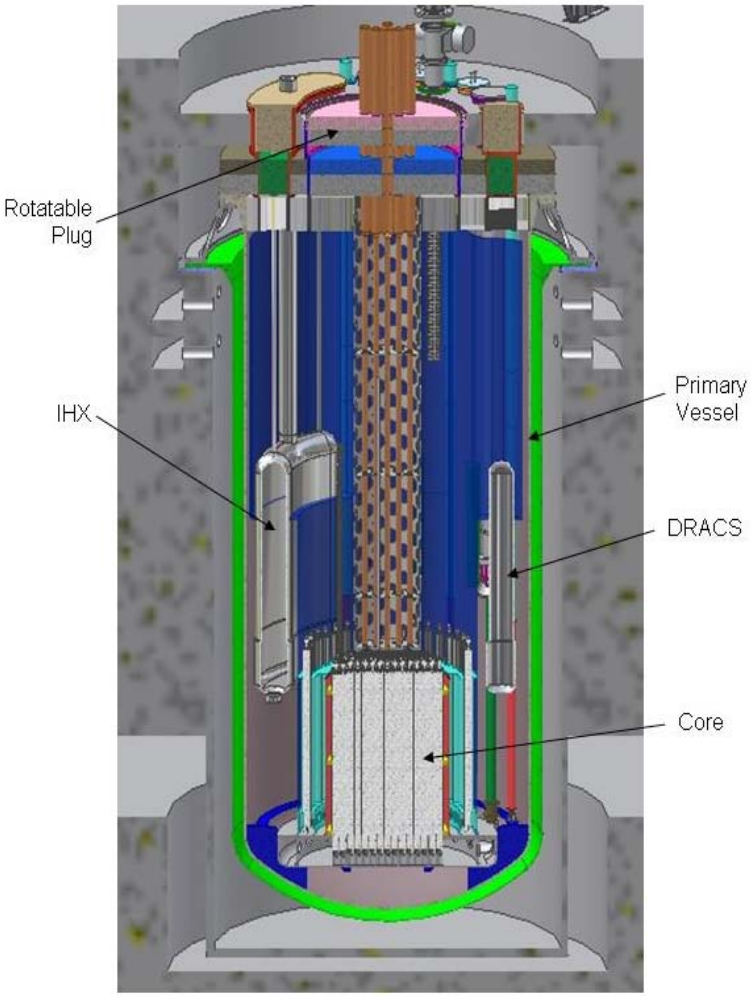

Figure 2.1-1 Schematic View of Primary System

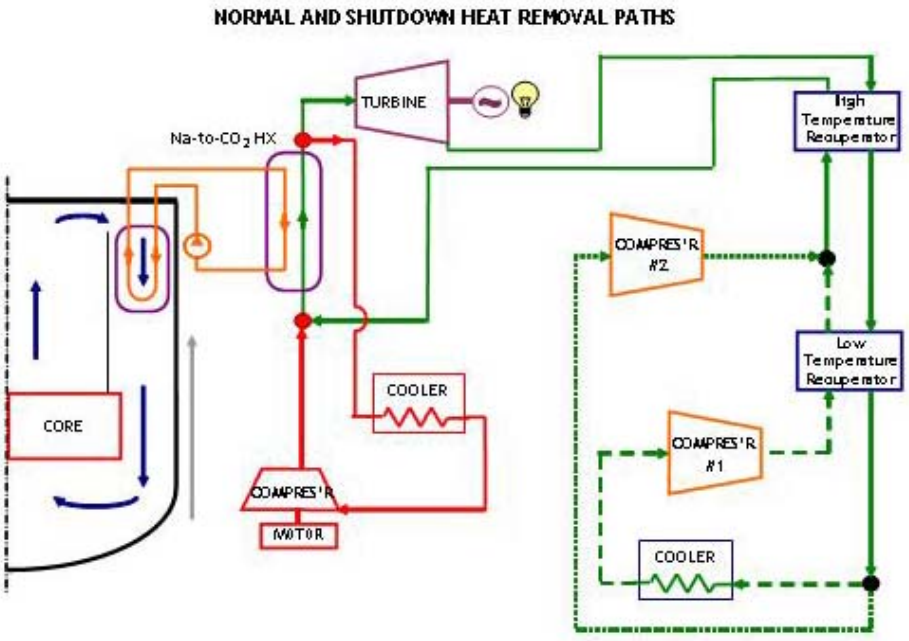

Figure 2.1-2 Overall Thermodynamic Cycle

As shown in Fig. 2.1-3, within the reactor vessel, primary electromagnetic pumps take suction from the lower regions of the cold pool and discharge the sodium into a header that distributes the sodium into three feeder pipes, which distribute sodium evenly into the inlet plenum. The inlet plenum distributes the primary sodium to the inlet of the core assemblies, which have individual orifices for proper flow distribution. The sodium is heated as it flows through the core and exits the core assemblies into the outlet plenum. The hot sodium rises into the redan and then enters the inlets of the IHXs. After the primary sodium transfers its heat to the intermediate sodium, it exits the IHXs into the lower regions of the cold pool. As shown in Fig. 2.1-4, the IHXs are contoured to the shape of the annular gap between the redan and the reactor vessel to minimize the overall diameter of the reactor vessel. The guard vessel that surrounds the reactor vessel will capture and contain any reactor vessel leakage and prevent the IHX inlet, DRACS heat exchangers, and core assemblies from being uncovered.

The basic function of the primary heat transport system (PHTS) is to transport heat from the reactor to the intermediate heat transport system (IHTS) under normal and off-normal operating conditions. The PHTS satisfies all normal and off-normal conditions specified in the duty cycle for the plant. In addition to full-power four-loop operation, the PHTS must provide heat removal for 50% power operation when only one IHTS loop is available, or 75% when one primary pump is out of service. The system, along with the core and the IHX, is arranged to remove decay heat under natural circulation conditions.

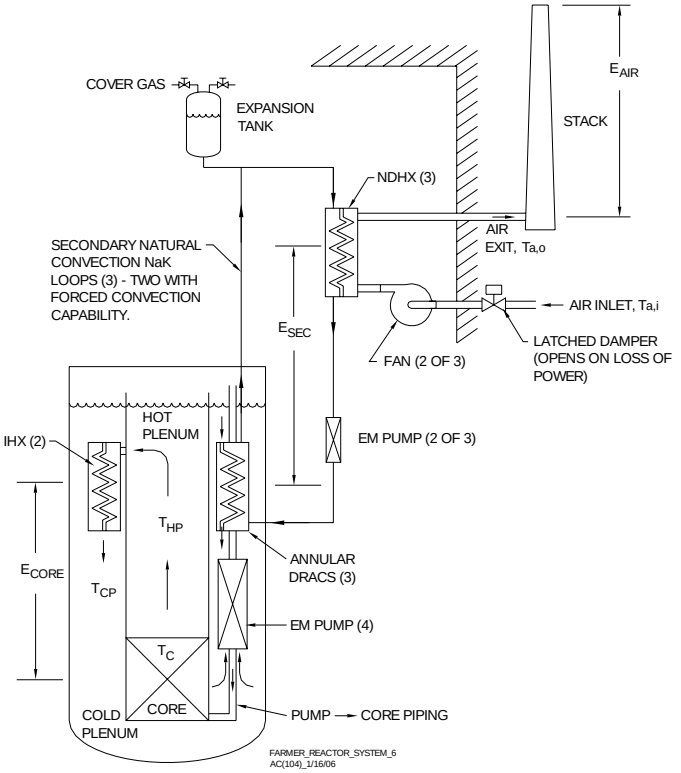

Figure 2.1-3 Schematic Diagram of Shutdown Heat Removal System

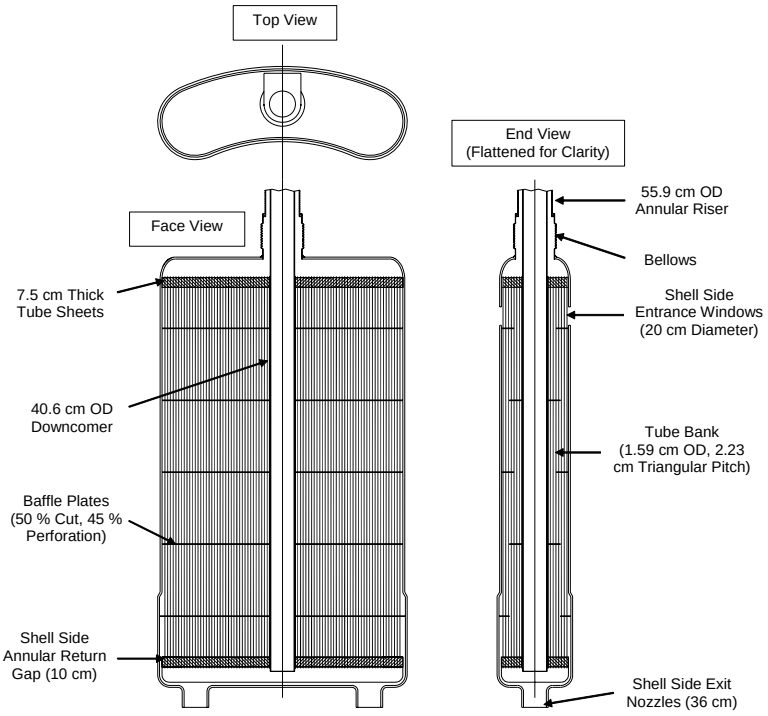

Figure 2.1-4 Intermediate Heat Exchanger Design

The PHTS consists of four primary pumps and two IHXs. The four pumps and two IHXs are located symmetrically around the reactor. The four pumps are located in the cold pool between

the redan and the reactor vessel. Each of the two IHXs is located within the redan and penetrates through the redan from the hot pool to the cold pool. Each IHX plenum is open to the reactor-vessel cover gas at the top, and each is closed at the bottom by a seal. The sodium level in the plenums around each IHX is essentially the same as in the main redan. Thus, the IHXs have no primary piping associated with them; the hot primary sodium enters the IHX inlet through openings in the IHX shell and is discharged to the cold region at the bottom of the IHX.

A total sodium flow of 10^7 lb/hr removes the heat from the core and passes it into the upper plenum at an average temperature of 510°C. The core effluent mixes with the hot sodium in the plenum and flows up into the redan to two IHXs. Approximately 125 MWt of heat is transferred from the primary to the secondary coolant in each IHX. The primary sodium leaves the IHX at 355°C and enters the cold pool region of the reactor vessel. Four pumps take the sodium from the cold pool and discharge it through inlet piping to the inlet plenum below the reactor core.

Several concepts for the LMR steam generator have been developed over the last 30 years, including the double-walled straight tube design that operated successfully for over 30 years in EBR-II. Other designs include the hockey-stick design developed by RI for the SAFR concept, and the helical coil steam generator (HCSG) developed by GE for the PRISM Mod-B concept. For the purposes of the Argonne pre-conceptual design ABR, a modified version of the GE-HCSG design was adopted. Also being considered is an innovative power conversion system using a Brayton cycle with supercritical CO_2 [2]. It is being considered because of its simple layout with relatively few components, small turbo-machinery components, and the potential for higher cycle efficiencies at higher sodium outlet temperatures. It also offers improved inherent safety because the potential for sodium-water chemical reaction is eliminated.

As noted above, a steam generator (SG) design similar to that utilized in the GE PRISM Mod-B plant concept is proposed for the LM-ABR if a steam cycle is adopted. The steam generator shown in Fig. 2.1-5 is a helical coil, vertically oriented, sodium-to-water, countercurrent flow, shell-and-tube type unit featuring once-through operation. Two 125 MWt steam generators are used; one for each IHTS loop. The steam generator design parameters are given the following table.

Table 2.1-2 Design Parameters for Steam Cycle System (PRISM Mod-B Basis)

IHTS Loop Operational Data	
Number of Intermediate Loops	2
Secondary Loop Heat Capacity	125 MWt
Loop Hot Leg Temperature	477˚C
Loop Cold Leg Temperature	326˚C
Loop Temperature Drop	151˚C
Loop Sodium Mass Flow Rate	645 kg/sec
Helical Coil Steam Generator (HCSG) Operational Data	
SG Inlet Pressure	167 bar
SG Feedwater Inlet Temperature	216˚C

SG Feedwater Mass Flow Rate	55.9 kg/sec
Steam Exit Temperature	454˚C
Steam Exit Pressure	155 bar
Saturation Temperature at Exit Pressure	345˚C
Steam Exit Superheat	109˚C

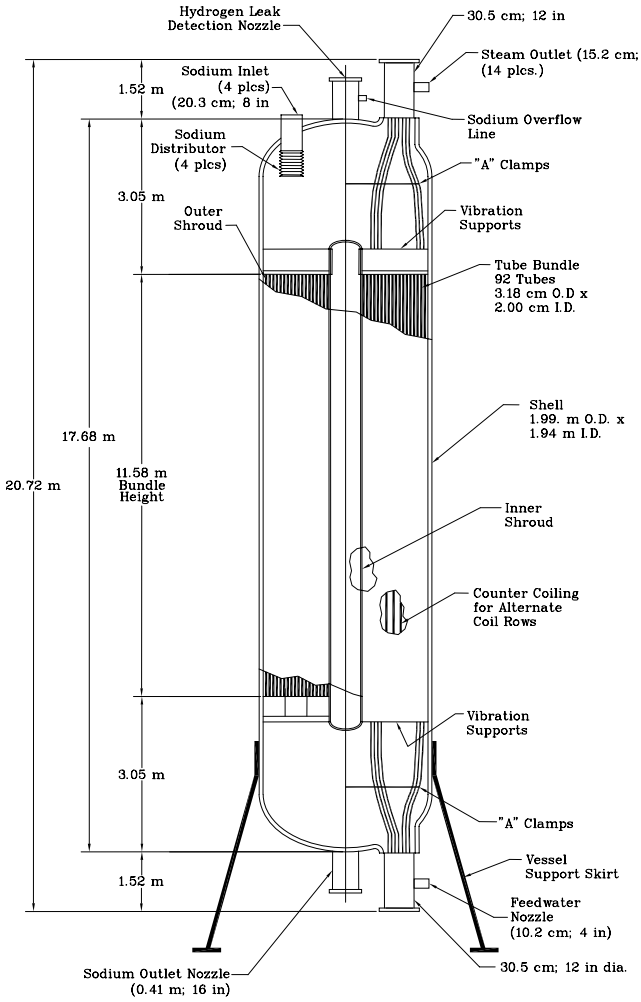

Figure 2.1-5 Helical coil steam generator for the LM-ABR (GE-PRISM Mod-B basis)

2.1.2 Shutdown Heat Removal System

The shutdown heat removal system shown in Fig. 2.1-3 is completely independent from the normal decay heat removal through the IHTS and is activated only when the normal heat removal system is disabled. The system consists of three independent, redundant, and diverse heat removal loops, with a fourth provided as a spare. Each loop consists of a small in-vessel DRACS, a secondary natural draft heat exchanger (NDHX), an expansion tank, and an exterior stack that forms the natural draft pathway for dissipating the decay heat to the atmosphere.

The DRACS heat exchangers are positioned directly in the sodium cold pool. Moreover, there are no valves or other mechanical devices that isolate the primary sodium from the DRACS. Thus, during full power operation, primary cold pool sodium circulates at a modest flow rate through the shell side of the DRACS. However, when activated, buoyancy-driven natural convection flow of the primary sodium through the DRACS is initiated.

The core decay heat is transferred by natural convection flow of primary sodium from the reactor hot pool through the IHX flow path to the cold pool. Heat from the primary sodium cold pool is then transferred through the DRACS to the secondary sodium-potassium (NaK) eutectic, passing through the heat exchanger tubes. All three loops are capable of operating in a natural convection mode, in which buoyancy-driven convection causes the secondary NaK to circulate through the NDHXs, where the air flow transfers the heat from the NaK to the atmosphere. The secondary NaK flow circuits (one for each of the three independent systems) are completely passive without any valves or constrictions to limit the flow during normal operation or shutdown conditions.

On the tertiary (air) side of the systems, the natural convection circuits are passive except for magnetically latched dampers that prevent air flow on the air inlet side of the three NDHXs. Upon loss of electrical power to the electromagnetic latch, the dampers fail by gravity in the open position. The DRACS are brought into full operation by opening of these dampers. The dampers are designed to provide an air leak rate that corresponds to nominally 1% of the full-design flow rate in the closed position, which results in a parasitic heat loss of ~18 kW during full power operation. This minor heat loss is included in the design to maintain the correct natural convection flow patterns in the primary, secondary, and tertiary sides of the system so that proper natural-convection flow patterns are established immediately upon system activation. Moreover, continuous heat addition to the system is desirable in regions where the ambient temperature can fall below the NaK freezing temperature, nominally -13˚C.

2.1.3 Computational Modeling

An initial CFD analysis was performed for the LM-ABR concept by Argonne [2] to assess at steady state the flow patterns in the primary reactor system, sodium pool temperature distributions, and temperature distributions in the reactor vessel and the reactor-vessel closure structures. For these analyses the CFD code STAR-CD was used. Ultimately this type of analysis needs to be extended to cover low-flow transient flow and thermal simulations of the entire in-vessel system and associated structure analysis of critical components to facilitate designing the reactor to operate under the cases where thermal-buoyancy forces dictate flow and thermal performance, as will be discussed in Sec. 4.0. As will also be discussed in this report, commercial CFD codes are not currently proven capable of simulating many of the important transient thermal-hydraulic phenomena of interest.

2.2 Needed Research Based on GE/PRISM

This section is based on the 1993 GE/PRISM closeout report [3] and summarizes what GE's ideas were at that time as to any further development and testing needed to deploy an LMR in the U.S. The 1993 report by GE is important because the Argonne-proposed LM-ABR associated with the current GNEP initiative described in Section 2.1 has many features similar to the GE/PRISM-LMR under development previously for the DOE. Argonne under this development program played critical roles in defining the fuel cycle and in testing a full in-vessel water model of the GE/PRISM reactor under both normal and off-normal operation conditions, as described in Section 4.2. These past studies and the resulting information have helped to focus the recommendations given in Section 5.0 regarding a thermal-hydraulic pathway forward in support of GNEP and the LM-ABR.

The GE report acknowledges the Argonne water model testing of the PRISM full-in-vessel geometry because it affected characterizing the thermal-hydraulic behavior of the design under natural circulation transient conditions and recognized the complexity of the thermal-hydraulic behavior and the value of using 3-D CFD modeling to improve the understanding of this behavior. The 1993 report also recognized the importance of thermal stripping on upper-internals structural integrity and the role that thermal stratification can play in creating large-scale temperature distributions conducive to detrimental structural stresses.

In the final part of the closeout report under the heading of "Thermal-Hydraulics" regarding the next phase of PRISM design leading to deployment, GE states under "program requirements" that the final PRISM design should be modeled and the test article be water tested at Argonne National Laboratory. GE specified: "Perform experimental evaluations of T&H characteristics for the reactor system, upper and lower plenum, and thermal barriers. Evaluate the potential for thermal stratification and stripping, and thermal shock phenomena. Apply the COMMIX (CFD) code to predict important T&H characteristics observed in the experiments." GE's reference to the COMMIX code refers to an Argonne 3-D fluids dynamics code under development in the 1970s and 1980s.

References

1. "Global Nuclear Energy Partnership Strategic Plan," GNEP-167312, Rev. 0, U.S. Department of Energy, Office of Nuclear Energy, Office of Fuel Cycle Management (January 2007).

2. Chang, Y.I., Finck, P.J., and Grandy, C., "Advanced Burner Test Reactor Pre-conceptual Design Report," ANL-ABR-1 (ANL-AFCI-173) (September 5, 2006).

3. Gluekler, E.L., "U.S. Advanced Liquid Metal Reactor Program: ALMR Technology Development Requirements Plan," GE Nuclear Energy, GEFR-00845, Rev. 4, UC-87Ta (November 1993).

3.0 Past Argonne Thermal-Hydraulic Studies on Individual Components

Beginning in the early 1970s, Argonne conducted pioneering studies on thermal-buoyancy effects in individual reactor components [1-3] and developed unique, broad understanding of how these phenomena can significantly influence component performance. In general, thermal-buoyancy-induced flow and associated thermal phenomena become important during the transition to and during natural circulation. The following is a list of individual reactor components, associated phenomena, and component issues studied by Argonne:

1) Pipe flow stratification that produces pipe stress and thermal stripping and influences energy transport between components with the potential for causing large departures from 1-D or inadequate 3-D CFD models of pipe flow

2) Stratification at pipe flow/plenum interfaces causing pipe flow recirculation zones and promoting large nozzle stresses

3) Steam-generator and heat-exchanger flow channeling and instabilities that cause tube-bundle, tube-sheet, and shell thermal stress

4) Large-scale shear flow that produces periodic eddies which strongly influence thermal-plume behavior and plenum mixing, and can cause structural fatigue (thermal stripping) induced by thermal cycling

5) Thermal-buoyancy-force-induced laminarization of stratified shear layers, a mechanism that mitigates thermal stripping and reduces plenum mixing or, if the layers are un-stable, can induce thermal stripping

6) Thermal-buoyancy-force suppression or enhancement of heat transfer under low flow, which can influence the overall heat transfer through a heat exchanger

7) Buoyancy-induced recirculation zones in baffled tube bundles and other components, which reduce heat transfer and produce radial temperature variation and "cold" spots, potentially causing large-scale detrimental structural stress.

Sections 3.1-3.5 summarize the results from Argonne studies conducted on various individual LMR components.

In proposed or built LMRs to date (sodium, lead, or others), many of the above natural convection phenomena, especially for pool-type reactors, can potentially occur within the reactor vessel (RV) and interact in a complex manner because of the close proximity of components and the multiple flow paths between the various sub-regions of the RV. This condition is especially true when operating in the low-flow thermal transient flow coast-down mode to natural circulation due to the growth of thermal-buoyancy driving forces resulting from flow-field temperature gradients. See Section 4.2.1 and Appendix 1 for discussions based on non-dimension modeling parameters that describe how thermal buoyancy can influence

individual components and the entire reactor system. Thermal buoyancy phenomena can cause significant departures from design-intended normal flow and temperature distributions. For LMR designers striving to achieve inherently safe operation, the understanding of natural-convection-dominated flows, associated thermal distributions, and their mitigation by proper design is essential. Furthermore, to accomplish this objective, they must be able to model phenomena induced by thermal-buoyancy forces with full 3-D CFD codes that incorporate the necessary physics. This requirement will be discussed further in other sections of this report.

References

1. Kasza, K.E., Kuzay, T.M., and Oras, J.J., "Overview of Thermal Buoyancy Induced Phenomena in Reactor Plant Components," 3rd International Conference on Liquid Metal Engineering and Technology in Energy Production, Oxford, England, April 9-13, 1984.

2. Kasza, K.E., Kuzay, T.M., and Oras, J.J., "Overview of Thermal-Buoyancy-Induced Phenomena in Reactor Plant Components," Symposium on Fluid Dynamics, Univ. of Ill., April 26-27, 1984.

3. Kasza, K. E., Oras, J. J., Kuzay, T. M., and Lin, H., "Thermal Buoyancy Effects in Reactor Plant Components: An Update on Recent ANL/MCTF Studies," 4th IAHR Specialists Meeting on Liquid Metals Thermal-Hydraulics, Westinghouse Hanford, Richland, Washington, July 31-Aug. 3, 1984.

3.1 Piping Thermal Stratification

During normal steady-state LMR operation, piping flow velocity in the primary and intermediate piping loops is high, and the flow is isothermal (except for small heat losses to the ambient). Under normal operation, thermal buoyancy effects produced by flow-field temperature gradients and the resulting density gradients are not important. However, for certain off-normal conditions (such as those associated with a reactor scram and pump flow coast-down), the pipe flows are low (in the range 0-7% of full flow), and large thermal transients are conveyed through the piping. The combination of low flow and thermal transients produces variations in piping fluid density conducive to flows driven by thermal-buoyancy forces.

In the late 1970s and early 1980s, Argonne conducted experimental and analytical modeling studies of thermal-buoyancy phenomena in piping for cases of steady net flow and zero net flow in pipes having differentially heated ends and for the case of buoyancy induced by thermal-hydraulic transients passing through a piping system [1-3]. Before these studies, some studies had been conducted on steady-state stratification induced by differentially heated pipe sections [4-7]. However, little information was available on thermal-buoyancy phenomena in piping when the thermal-buoyancy driving forces resulted from thermal-hydraulic transients entering the piping. Argonne's demonstration in early water experiments of the transient-induced buoyancy phenomena and the realization of its potential importance led to DOE

funding an Argonne program to assess and quantify the importance of such buoyancy effects to pipe flows and the impact on plant design and safety. Plant safety is an issue because low-flow thermal transients conducive to piping stratification occur under off-normal plant conditions, such as transition to natural circulation or under N-1 loop operation conditions. The buoyancy phenomena can induce severe pipe thermal stratification which manifests itself in horizontal piping by creating large top-to-bottom temperature differences and large structural stress. The stratification also has the potential for changing the time scale of plant global response to cool-down events.

Various thermal-hydraulic system codes exist for the analysis of LMR flow circuits (e.g., the W-ARD DEMO code [8]). One of the important reactor events analyzed is flow coast-down to natural circulation in which the flow is maintained in the reactor circuits by thermal density head variation around a pipe circuit produced by the reactor heat source, the core, and the heat sinks (see Appendix 1). The system codes have in common the fact that the flow in pipe runs connecting the various components (reactor, pumps, core, heat exchangers, evaporators, etc.) is modeled as being isothermal in planes normal to the pipe axis. Hence, thermal energy transport in the piping is assumed to be purely a 1-D transport in which possible thermal-buoyancy-induced "secondary" flows and their effects on friction factors, thermal heads, and pipe thermal stresses are neglected, and only integrated large-scale thermal density head effects are factored into the analyses in conjunction with classical pipe friction factors. The thermal-buoyancy effects, if of sufficient magnitude, will influence predictions for reactor decay heat removal and the time constants for flow coast-down. In addition, if the pipe flows are significantly altered from the classical axi-symmetrical pipe velocity profile, the distorted or thermally stratified flow entering components such as heat exchangers, pump inlets, or the pipes themselves can affect the performance of these components with regard to both actual thermal-hydraulic plant performance and inducement of structural thermal stresses.

With DOE funding, Argonne conducted the following three-phase program to evaluate the importance of thermal buoyancy in piping and generate information that could be used by the reactor designer and system analyst.

Phase I studies [1] had the objective of generating exploratory data to determine if fluid stratification could occur in the piping of the CRBR Heat Transfer System and ascertaining whether the 1-D codes were adequate to analyze the behavior of piping during a low-flow transient involving natural-circulation decay heat removal and, if not, whether 3-D CFD codes were sufficient.

Phase I studies only focused on a single event involving natural-circulation decay heat removal for CRBR. Other reactor transient events (emergency and upset events) are of interest to the general reactor community and were proven by Argonne studies to be considerably more severe from the viewpoint of pipe stratification. These events and the experimentally evidenced pipe stratification which occurs were the subject of Phases II and III of the Argonne program. Phase II studies [2] dealt with thermal buoyancy in horizontal and vertical piping segments connected with vertical elbows.

Phase III studies [3] dealt with buoyancy in a simplified pipe system consisting of two horizontal pipes connected with a horizontal elbow. The objective was to more carefully study the flow interaction between the two horizontal pipes, which allowed further generalization of a pipe stratification correlation developed initially in Phase II.

The results from all three phases of the pipe stratification program are summarized next. All testing was conducted in Argonne's Mixing Components Test Facility (MCTF), which was a water loop capable of creating transient thermal-hydraulic flows and supplying the flow to a test section under computer control. See Section 4.2.2 for a description of the facility.

3.1.1 Phase I

This phase had the objective of generating data to determine if fluid stratification could occur in the CRBR Heat Transfer System piping for a specific plant transient and ascertaining whether the 1-D codes were adequate to analyze the behavior of piping during a low-flow natural-circulation transient involving decay-heat removal and, if not, whether 3-D CFD codes were sufficient. If stratification were found to occur, it was important for designers to know whether the accompanying pipe friction pressure drops and thermal heads can be predicted correctly within typical design allowances by using reactor system pipe models that employ the assumption of a 1-D thermal-hydraulic front. This initial Phase-I exploratory study involved:

- Conducting limited water experiments in a pipe system having the important features of the CRBR cold-leg piping and simulating an envelope-case natural circulation CRBR with a decay-heat removal transient defined by the Westinghouse Advanced Reactors Division (W-ARD) and simulated by the W-ARD 1-D DEMO code [7]

- Developing a 1-D model of the Argonne test pipe system for predicting pressure differential across the piping and comparing with experimental data

- Performing a 3-D CFD simulation of pipe stratification in a CRBR pipe segment to explore use of a model based on a full Navier-Stokes equation solver

3.1.1.1 Testing of CRBR Piping Stratification

Figures 3.1-1 shows a schematic of the W-CRBR cold-leg piping used to guide the design of the Argonne pipe test section consisting of horizontal and vertical pipe runs connected by elbows. Figure 3.1-2 shows a photo of the Argonne pipe test section, which had three horizontals, two verticals, and four 90-degree elbows. This test section was a simplification of the actual CRBR piping, but it retained the essential features needed for studying thermal buoyancy (see the insert of Fig. 3.1-2 for a piping schematic).

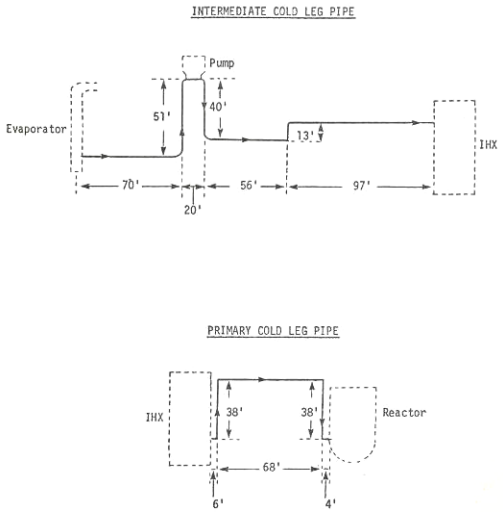

Figure 3.1-1 W-CRBR modeled cold-leg pipe configuration tested in MCTF

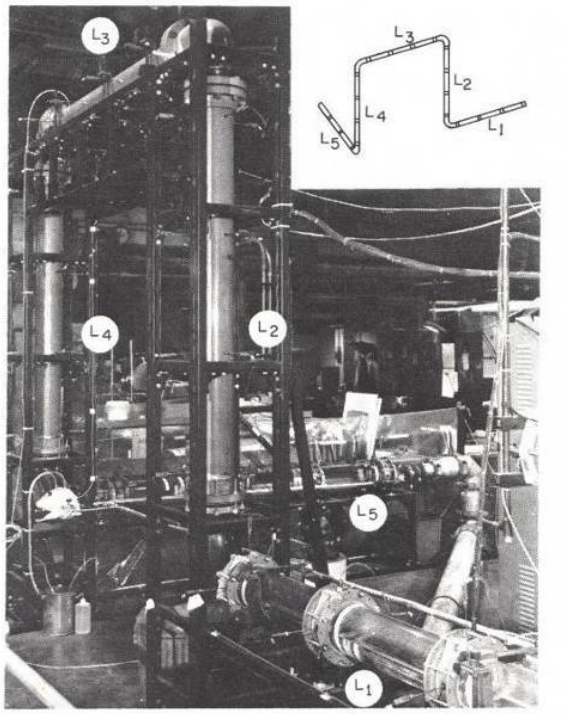

Figure 3.1-2 Pipe stratification test section

Figure 3.1-3 shows the temperatures predicted by the W-ARD 1-D DEMO code for the outlets of the IHXs. The decreasing temperature of the flow entering the piping is caused by a flow coast-down and the resulting collapse of the cold-end temperature difference.

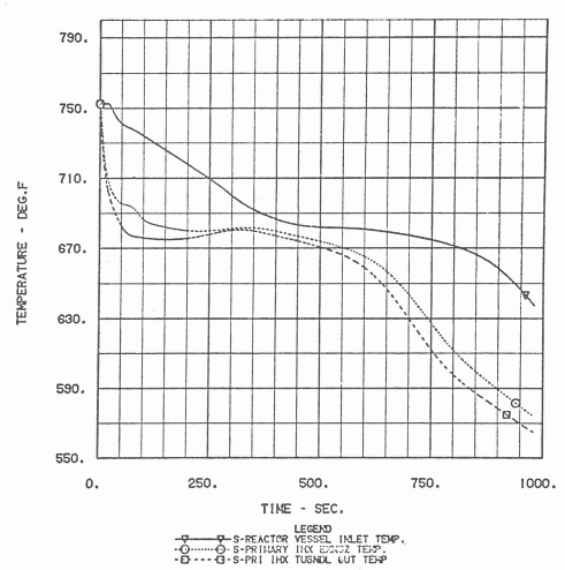

Figure 3.1-3 Natural circulation primary cold-leg temperatures

Table 3.1-1 shows the thermal-buoyancy-related test conditions for enveloping the CRBR sodium piping (based on the W-ARD specified CRBR piping and the DEMO code predictions) and the water experiment piping. As indicated, the water experiments matched the sodium prototype conditions closely or exactly in several important parameters. An exact match of the Richardson number (Ri); dimensionless thermal transient time (φ); and horizontal pipe length-to-diameter (L/D) ratio was achieved.

Table 3.1-1 Comparison of enveloping CRBR prototype sodium and water test conditions

	Envelope NA Conditions (@ 600°F)	Envelope Water Test Conditions (@ 140°F)
Velocity [m/s (ft/s)]	0.21 (0.7)	0.16 (0.53)(3)
Total Transient ΔT [°C(°F)]	56 (100)	67 (120)(2)
Temperature Gradient [°C/m(°F/ft)]	0.91 (0.5)	4.4 (2.4)(3)
Horizontal Pipe ΔT [°C(°F)]	17 (30)	20 (36)(3)
Horizontal Pipe Length [m(ft)]	18.3 (60)	4.6 (15)(1)
Pipe Diameter [m(ft)]	0.61 (2)	0.15 (0.5)(1)
Richardson Number	2.0	2.0(1)
Dimensionless Time Parameter (φ)	1.06	1.06(1)
Horizontal Pipe L/D	30	30(1)
Reynolds Number	380,000	55,600(3)
Flow Rate [m^3/hr (gpm)]	--	10.6 (46.7)(4),(3)
Input Temperature Ramp [°C/sec(°F/sec)]	--	0.71 (1.27)(4),(3)

(1) These quantities set to achieve geometric and hydraulic similarity
(2) Maximum ΔT attainable in test loop
(3) These quantities deduced from quantities in 1 and 2 above
(4) Test control quantities

For the enveloping water experiment, the flow rate entering the pipe was maintained constant at 46.7 gpm. At time zero the test section was isothermal at 200ºF. For time greater than zero and lasting for 91.4 sec, the pipe inlet temperature was decreased linearly to 80ºF. After the inlet transient time, the test was run for an additional pipe flow-through time longer to track the thermal stratification and pressure differential across the test section.

3.1.1.2 Summary of Thermal Results

Figures 3.1-4 and -5 show the temperature measured, respectively, in the first horizontal pipe L1 at the entrance of the pipe system and at a downstream location D near the exit of the horizontal pipe, just before entering the elbow into the vertical pipe. Clearly, at location D thermal stratification has developed for a period of time, with the top of the pipe becoming hotter than the bottom. Flow visualization of the cold front moving through the horizontal transparent pipe showed the flow being acted upon by thermal buoyancy causing the cold flow to sink to the bottom of the pipe and the flow in the top regions to slow down. No evidence of thermal stratification was found in the vertical pipe runs; this will be discussed more below. As will also be shown later, the flow can stagnate over a portion of the top of the pipe for cooling transients if thermal buoyancy becomes strong enough at high values of Ri. Thus, for this initial CRBR transient, pipe stratification does occur. For other types of CRBR plant transients studied in Phase I, much more severe stratification was shown to occur.

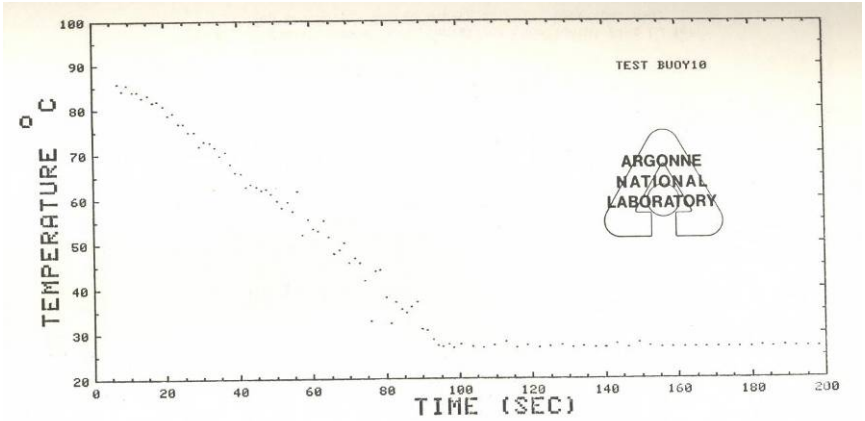

Figure 3.1-4 Inlet flow temperature transient in test section

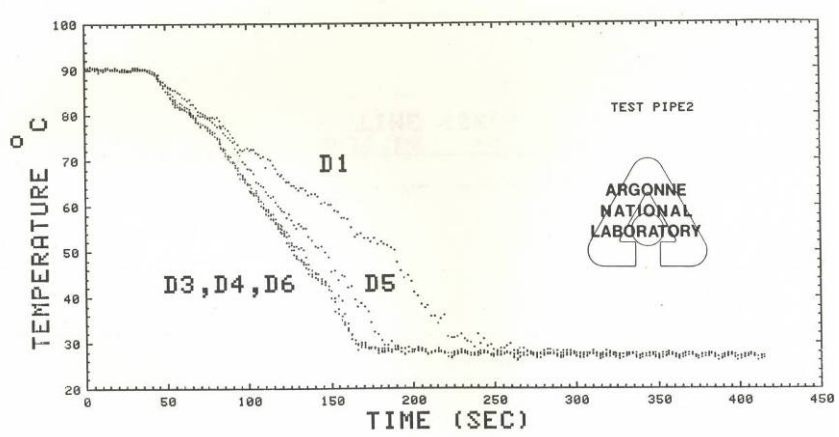

Figure 3.1-5 Circumferential transient pipe wall temperature distribution in horizontal L1 at axial location D

3.1.1.3 Influence of Stratification on 1-D Modeling of Piping

Models of 1-D pipe flow and thermal transport based on a uniform front moving perpendicular to the pipe axis were formulated [1] for predicting the pipe system inlet-to-outlet total transient pressure differential and axial temperature distribution. The predictions were compared with experimental data to evaluate the adequacy of 1-D models in the presence of thermal stratification.

The instantaneous pressure differential ΔPij between the pipe test section inlet (i; entrance to L1) and outlet (j; exit of L5) shown in Figure 3.1-2 is given by

$$\Delta P_{ij} = P_i - P_j \equiv -\int_o^h g\rho dy + \int_i^j 4f\rho \frac{U^2}{2D} dL + \sum_{n=1}^{4} C_n \frac{U^2}{2} \rho_n .$$

The first term on the right side represents the pressure change due to variations in the thermal-head fluid density in the vertical pipes. The second term accounts for the pipe wall friction losses with L as the axial distance along the piping, and the third term is the sum of the pipe elbow losses. The symbols Cn and f represent the coefficients for classical non-buoyancy-influenced friction factor loss from the elbow and pipe wall, respectively. The time-dependent nature of this equation is implicit in the temperature-dependent fluid density and viscosity properties and in the dominant thermal-head term.

In addition to the time-dependent temperature forcing function imposed upon the flow entering the pipe system, the fluid is affected by the fluid-wall heat transfer and pipe-wall heat capacitance. These effects are incorporated in the 1-D model by the two equations below:

$$\dot{m}_f C_{p,f} T_f (X) \Delta t = \dot{m}_f C_{p,f} T_f (X+\Delta X) \Delta t + \rho_w \frac{(\pi D \ell_\omega \Delta X)}{4} (2 + \ell_\omega/D) C_{p,w} \Delta T_w \quad (2)$$

$$+ \rho_f (\pi D^2/4) \Delta X C_{p,f} \Delta T_f$$

and

$$h(\pi D \Delta X) (T_f - T_w) \Delta t = \rho_w \frac{(\pi D \ell_\omega \Delta X)}{4} (2 + \ell_\omega/D) C_{p,w} \Delta T_w \quad (3)$$

where the first equation is an energy balance for an element of fluid of length Δx having velocity $\Delta x/\Delta t = U$, and the second equation represents the thermal energy transferred between the fluid and pipe wall, neglecting exchange between the pipe and the ambient. Equations 1-3 incorporate the same physics and assumptions as used in the 1-D codes such as W-DEMO. Detailed results from this 1-D model for the CRBR thermal transient are presented in Ref.1.

3.1.1.4 Summary of Pressure Results

Figure 3.1-6 shows a comparison of the predicted piping pressure differential derived from the 1-D front thermal-hydraulic pipe model and the experimental data. As shown, the 1-D model adequately predicts the transient pressure differential in the CRBR envelope test section, which includes the thermal head development in the vertical pipe runs for Ri = 2. However, for the case of Ri = 4, as shown in Figure 3.1-7, the error in the 1-D model predictions increases with the degree of stratification in the horizontal pipes, with the model overpredicting the peak values of ΔP. The major contribution to the transient pressure differential developed across the test section was found to be the integrated thermal density head. Frictional effects contributed less than a few percent due to the low-flow velocities associated with pipe stratification. Figure 3.1-8 shows a correlation developed by Argonne, included here for completeness, of the errors induced in the 1-D model of the Argonne pipe test section by stratification for additional experiments covering a wider range of Ri values. The error increases with increasing Ri. Pipe stratification behavior will be discussed more in the Phase II and III sections.

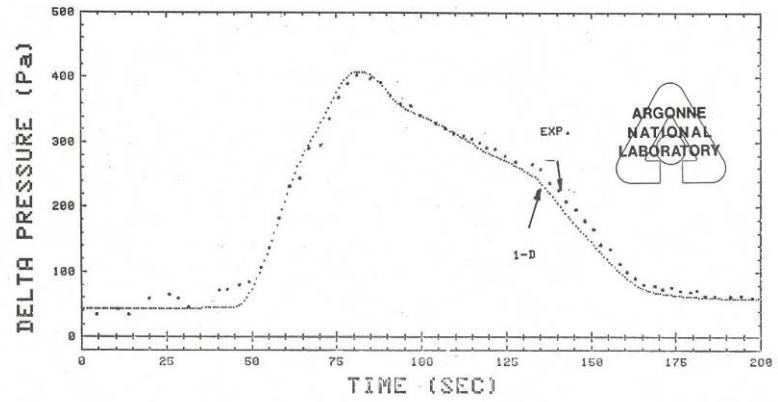

Figure 3.1-6 Comparison of pipe 1-D model predicted and experimental transient axial pressure differential for Ri = 2 (good agreement)

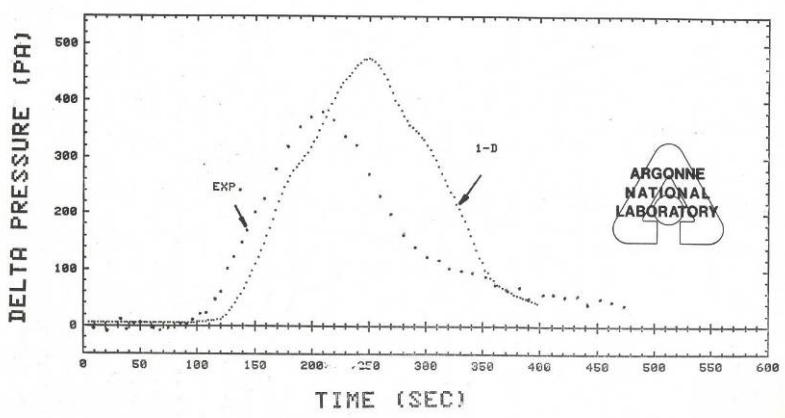

Figure 3.1-7 Comparison of pipe 1-D model predicted and experimental transient axial pressure differential for Ri = 4 (poor agreement)

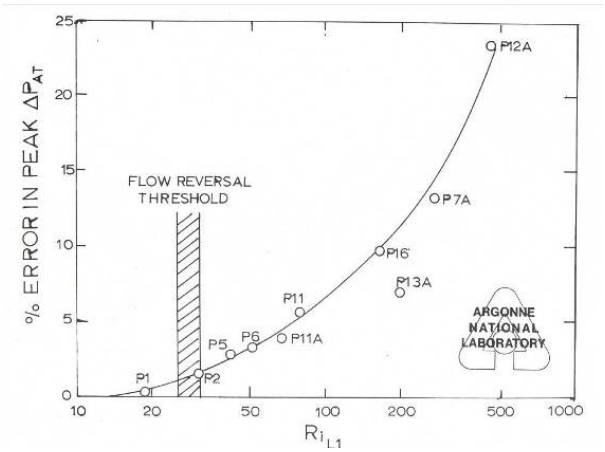

Figure 3.1-8 Correlation of the error between 1-D pipe model predicted and experimental transient axial pressure differential for a range of Ri values

3.1.1.5 Argonne CFD COMMIX Code 3-D Simulation of Pipe Stratification

Argonne, using its COMMIX code in the early stages of delineating pipe stratification under its experimental program, conducted an exploratory 3-D CFD code simulation of thermal-transient-induced stratification in a horizontal pipe [9]. Little has been done since these early simulations to further develop and validate CFD codes for simulation of the important pipe-stratification phenomena.

Thermal-buoyancy-force-created "secondary" flows in piping can be important in modeling if they are significant enough to change velocity and temperature fields in the piping and alter macroscopic integrated flow effects, such as frictional losses and thermal-density heads. Secondary flows would, in general, tend to increase piping friction over what would be gleaned

from a one-dimensional analysis and hence could have an effect on coast-down time constants for the overall reactor system and predictions of macroscopic system heat transport.

The COMMIX code was developed as an outgrowth of a code developed for the analysis of multiphase flows, which was sponsored by the Nuclear Regulatory Commission (NRC/RDD). The code can be restricted to single-phase flow calculations and hence was used as an investigative tool in analyzing the subject pipe-flow problem. The simulation of pipe flow stratification was funded by NRC.

The COMMIX code solves the complete, coupled, transient, 3-D, conservation of mass, momentum (Navier-Stokes equation), and energy equations in the primitive variables, accounting for thermal buoyancy effects and fluid property dependence on temperature. The code is based on the "time marching" scheme, which treats steady-state problems as asymptotic limit solutions in time and transient problems as the forced response to a system of forcing functions. The finite-difference equations are solved semi-implicitly, the energy equation being treated explicitly. A staggered mesh, 3-D Cartesian grid system is employed, with the velocity information being cell-surface centered and the passive scalars (temperature, density, enthalpy, etc.) cell centered.

3.1.1.6 Summary of Flow Results

Argonne simulated the influence of thermal buoyancy on flow in the CRBR IHTS piping during a pump flow-coast-down transient. A highly simplified geometry of a horizontal straight pipe located downstream of an IHTS mixing tee, which combines the flow from two evaporators, of 1.5-ft (0.46-m) diameter was analyzed. This CRBR pipe run had several elbows connecting shorter runs of straight pipe. It was assumed that this horizontal run can be straightened into a single 70-ft (21.4-m) length of pipe, even though the secondary flow generated by elbows would tend to reduce thermal buoyancy tendencies. The elbow phenomenon is discussed in the Phase III section.

In analyzing the problem, the following assumptions were employed:

1. Pipe walls were assumed to be adiabatic.
2. Pipe-wall thermal heat capacitance was neglected.
3. Turbulent eddy transport was represented by a constant eddy diffusivity parameter, which was equal for momentum and thermal transport.
4. Prior to the start of the pipe inlet transients, the pipe flow was characterized by fully developed isothermal axi-symmetrical turbulent flow.
5. The Boussinesq approximation for thermal buoyancy forces was used.
6. The turbulent velocity profiles existing at the pipe entrance at any time were assumed to be similar and axi-symmetrical over the Reynolds number range encountered during the flow transient.

7. Flow entering the pipe at any time was specified as being isothermally over the pipe circular cross section at the instantaneous DEMO code predicted temperature.
8. At the pipe exit all derivatives were assumed to be zero. This assumption is restrictive and could influence the flow somewhat upstream of the exit. However, in the absence of better information as to what conditions would be imposed at the exit by the interaction with other IHTS loop components, this approach was used.
9. The circular cross section of the pipe was approximated by a square grid array, which results in a slightly irregular approximation to a circular boundary.
10. Only the portion of the DEMO code transient from 40 to 80 sec was studied (see Figure 3.1-9). This segment of the transient represents a pipe inlet cooling transient spanning the temperature range 600°F (315.6°C) to 420°F (215.6°C) (a temperature drop of 100°C) and an inlet mean pipe flow velocity reduction of 1.9 ft/sec (0.58 m/s) to 1.1 ft/sec (0.34 m/s).
11. Initial conditions for pipe velocity were generated with the COMMIX code by solving the problem of flow development in the entrance regions of a pipe. The far-downstream velocity profile in the region of fully developed flow (pipe entrance effects no longer present) was thus used as the starting condition for fully developed flow in the subject transient calculations. A turbulent eddy viscosity of 0.07 lb/ft·sec (0.10 Pa·sec) was used in the calculations.
12. Thermal buoyancy effects on turbulent transport were ignored in the initial analysis of the problem.

The thermal-hydraulic pipe transients that might exist during a CRBR pump coast-down, as predicted by the DEMO code for the first 200 sec after a pump trip, were used for the thermal and flow-rate forcing functions at the pipe entrance, as shown in Figure 3.1-9. Only the time span from 40 to 80 sec was simulated by the COMMIX code. The flow rate was expressed as a fraction of the before-trip mass flow [i.e., 6.39×10^6 lb/hr (805 kg/s)]. Based on these transients and the 0.46-m (1.5-m)-dia pipe, the initial pipe mean velocity and Reynolds number are 18.9 ft/sec (5.77 m/s) and 8×10^6, respectively. For comparison, at approximately 100 sec into the transients, 1 ft/sec (0.305 m/s) and 4×10^5 are realized. Thus, even at the low pipe mean velocity of 0.305 m/s, the pipe flow is still turbulent.

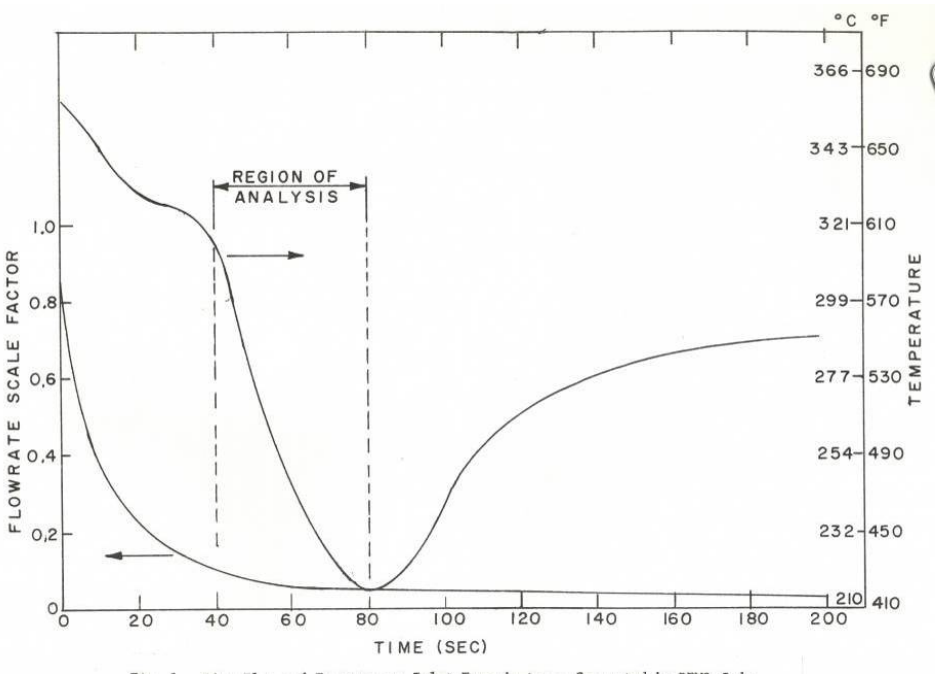

Figure 3.1-9 Pipe inlet flow and temperature transients as calculated by W-DEMO code showing the interval simulated by the Argonne COMMIX code

Figure 3.1-10 shows the simulated pipe-velocity vector profiles at various axial locations at 40 sec into the transient. At this time the velocity profiles are identical at each location and typical of fully developed turbulent flow. However, at 81 sec into the transient, as shown in Figure 3.1-11, the incoming colder flow into the pipe at reduced velocity has sunk and accelerated along the bottom of the pipe as a result of thermal buoyancy forces acting on the flow. Even more important, along the top of the pipe, flow reversal has occurred. Figure 3.1-12 shows the pipe-cross-section velocity patterns at a location of thermal stratification caused by strong buoyancy-induced flow.

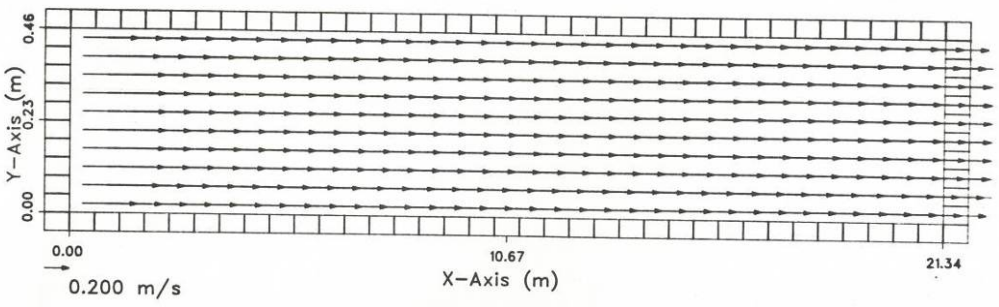

Figure 3.1-10 Velocity vector flow pattern in pipe longitudinal vertical symmetry plane at 40 sec

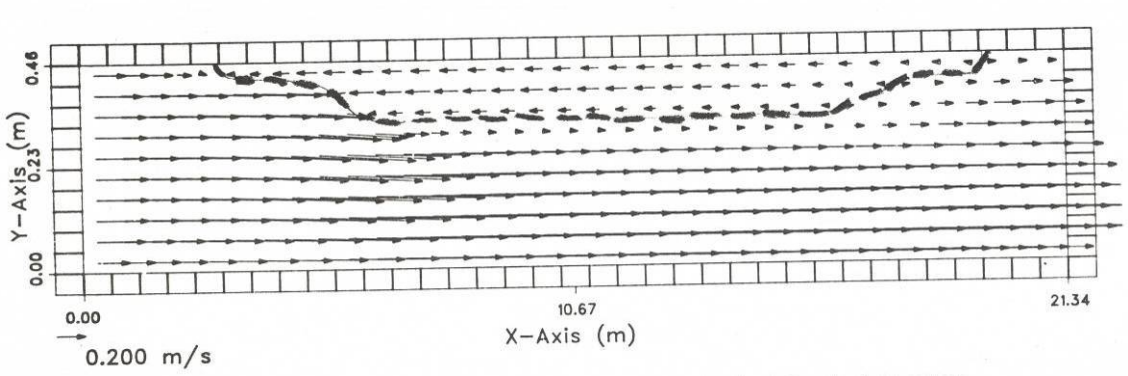

Figure 3.1-11 Velocity vector flow pattern in pipe longitudinal vertical symmetry plane at 80.8 sec

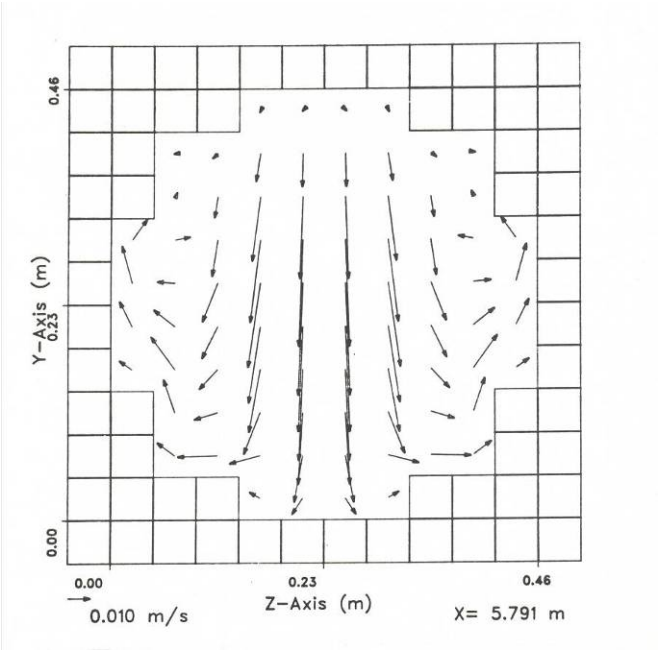

Figure 3.1-12 Velocity vector flow pattern in pipe transverse cross section at 80.8 sec and x = 5.8 m

Figure 3.1-13 shows the temperature variations along the pipe top and bottom as well as the variation in the minimum temperature from one pipe transverse cross section to the next. At the start of the pipe transient, the flow is isothermal at 600°F (315.6°C). However, at 50 sec the flow has started to stratify slightly as evidenced by a slight top-bottom temperature difference. The local minimum temperature shown plotted for this time instant physically occurred very near to the pipe centerline (i.e., the cooler core flow hasn't dropped very much in the pipe). Furthermore, the cooler inlet flow since the start of the transient (10 sec) has only advanced to about 18 diameters into the pipe. At longer times the thermal buoyancy effects become more pronounced with increasing top-bottom temperature difference. Also, as a result of the cooler core flow sinking toward the bottom of the pipe, the local minimum and pipe bottom temperatures become nearly identical (i.e., the cooler inlet flow is moving along the bottom of the pipe). Furthermore, at 80 sec, the thermal buoyancy effects have started to influence the pipe exit flow, at which point the computer simulation was stopped.

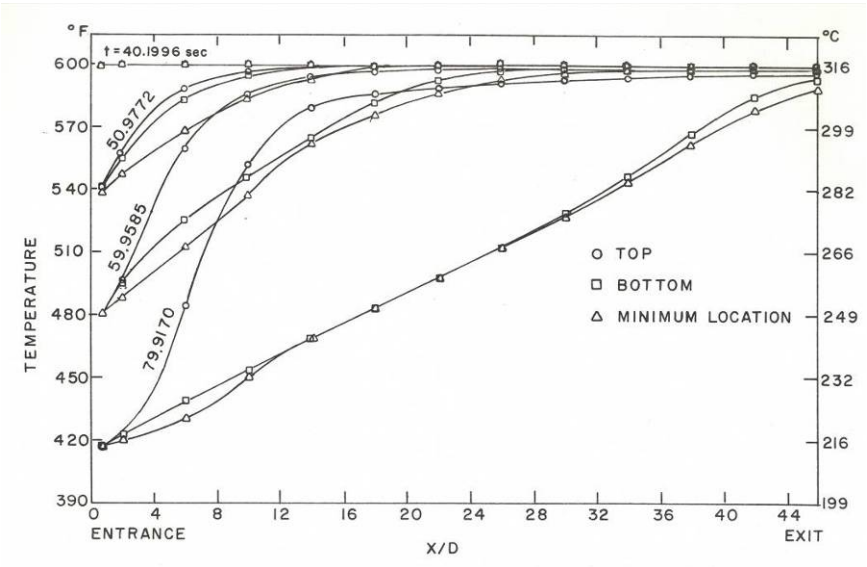

Figure 3.1-13 Axial variation of pipe fluid temperature for various times and locations within the pipe vertical symmetry plane

3.1.1.7 Future Needs

The exploratory Phase I study was based on experimental water results from a simulation of an envelope case involving a natural-circulation CRBR transient with decay heat removal, defined by W-ARD and generated by the W-ARD DEMO code. Argonne exploratory experiments showed that only moderate stratification would occur in the CRBR horizontal pipe run under the specified transient condition. However, it was also shown that only very modest variations in Ri values from the CRBR natural-circulation parametric set would lead to significant buoyancy effects, which violate the 1-D front thermal-hydraulic model used in the DEMO code. This phase also instituted the first known use of a full 3-D CFD code, the Argonne COMMIX code, to analyze pipe flows under conditions of strong thermal buoyancy force and demonstrated the need to do so when using a 1-D code is inadequate.

The preliminary results from the COMMIX simulation suggest that 3-D CFD codes are essential as tools in designing piping systems and in correctly predicting the movement of a transient front between components in an LMR. Also, the restrictiveness and correctness of several of the assumptions utilized in past studies, especially in modeling turbulence as modified by thermal buoyancy, must be investigated more thoroughly and benchmarked/validated with both water and sodium experimental data to better understand the dependence of stratification phenomena on fluid properties and to provide improved design analysis tools. This matter of turbulence modeling and the role of buoyancy on shear flows are discussed more in Section 3.2.

The COMMIX code took several hours to run the pipe simulation. Hence, future CFD simulations of this type, when addressing more complex piping systems for longer transients, must be done efficiently on powerful computers. With more experimental data to validate the codes, performing 3-D parameter studies with a validated CFD code can be used to generate a map of when thermal buoyancy is important in piping. Such information would allow first-cut estimates to be made of whether 3-D CFD analysis is needed or whether the 1-D codes like DEMO are sufficient.

3.1.2 Phase II

Phase I focused on the natural-circulation decay heat removal event postulated for CRBR. Other reactor transient events (emergency and upset events) are of interest to the general reactor community and were proven by Argonne studies to be considerably more severe from the viewpoint of pipe stratification. These events and the experimentally evidenced pipe stratification which occurs were the subject of Phases II and III of the Argonne pipe stratification program. Phase II studied thermal buoyancy in horizontal and vertical piping segments connected with vertical elbows using the same test section as in Phase I. The phenomena induced by thermal buoyancy forces (thermal stratification, flow stagnation, and flow recirculation) were delineated, and their behavior in terms of the appropriate thermal-hydraulic and geometric parameters was correlated over a wide range of conditions pertinent to LMR pipe systems. This information, subject to some restrictions, can be used to size piping to avoid or minimize thermal stratification produced by pipe-flow-convected thermal transients.

3.1.2.1 Tasks

Phase II involved the following:

1. Performing tests which enveloped thermal-hydraulic pipe transient conditions associated with LMR natural-circulation decay heat removal as well as other postulated reactor emergency and upset events deemed relevant to current and proposed reactor systems

2. Defining the threshold values of the appropriate modeling parameters for initiation of pipe thermal stratification and longitudinal flow reversal

3. Developing parametric correlations of the effect of buoyancy on pipe thermal stratification and pressure drop

3.1.2.2 Summary of Phase II Results

Phase II used the same test section as used in the Phase I pipe studies (see Fig. 3.1-2). Tests were conducted in the Argonne MCTF (see Section 4.2.2 for facility description) under the conditions of thermal transients superimposed upon constant pipe-inlet water flow. The

experiments covered a wide range of the non-dimensional modeling parameter Ri, which is the ratio of the buoyancy to inertia forces acting on the fluid. Thermal up- and down-ramp linear transients for various turbulent flow rates were studied. Data on pipe top-to-bottom temperature differences were generated for the three horizontal pipes comprising the test section: L1, L3, and L5 (see Fig. 3.1-2). The results obtained from this study were unique. The findings were as follows:

1. The individual-horizontal-pipe flow-stratified maximum top-to-bottom temperature differences developed during the passing of the thermal transient through the pipe system, as a percentage of the total transient temperature change at the pipe system entrance, as shown in Fig. 3.1-14, is correlated by the Richardson number, Ri_{Li}, which is based on individual horizontal pipe segment length (L1, L2, and L3) and the maximum axial temperature difference developed over the individual horizontal segments. This correlation allows estimating stratification in horizontal pipes in the range of 0 to 100%. The correlation was further generalized, as discussed in the Phase III studies.

2. Stratification developed in a horizontal pipe immediately upstream of a vertical pipe for thermal up- or down-ramp transients is not convected through the vertical. The flow leaving the vertical is isothermal over the pipe circular cross section. Hence, two straight horizontal pipe runs at different elevations, connected by a vertical for up- or down-flow in the vertical and subjected to either an up- or down-ramp thermal transient, behave independently for the conditions explored, as if the thermal transient was separately initiated at the entrance of each horizontal comprising the pipe system.

3. The behavior of vertical pipes in mitigating or destroying stratified flows produced in adjacent upstream horizontal pipes can be used advantageously in designing reactor piping and interfacing with various plant components in which stratified flow entering the component would be injurious to the structure or performance.

4. The threshold Ri number for the initiation of thermal-transient-induced stratification in straight horizontal pipes lies in the range $3.4 < Ri_{Li} < 4.4$ (Fig. 3.1-14).

5. Thermal-buoyancy-induced flow reversal starts to occur in a horizontal pipe for either a thermal-up or down-ramp transient when the parameter Ri_{Li} is in the range $25.5 < Ri_{Li} < 31.1$, where i = 1, 2, 3 (Fig. 3.1-14).

6. The axial location of the maximum top-bottom temperature difference occurring in a horizontal pipe during a thermal up- or down-ramp transient occurs at the downstream extremity of the horizontal pipe until the threshold value of Ri_{Li} for flow reversal is exceeded, and then it moves progressively farther upstream with increasing Ri_{Li}.

7. The information generated can be used to estimate the propensity for, and severity of, stratification in an existing pipe system. The information can also be used to

specify the transients that can be allowed in a system before exceeding an acceptable level of stratification.

8. The validity of a 1-D model of front thermal-hydraulic pipe flow in predicting the inlet-outlet transient axial pressure differential for pipe systems in which significant thermal density heads are developed in the vertical pipes deteriorates significantly when flow reversal starts to occur in the horizontal piping.

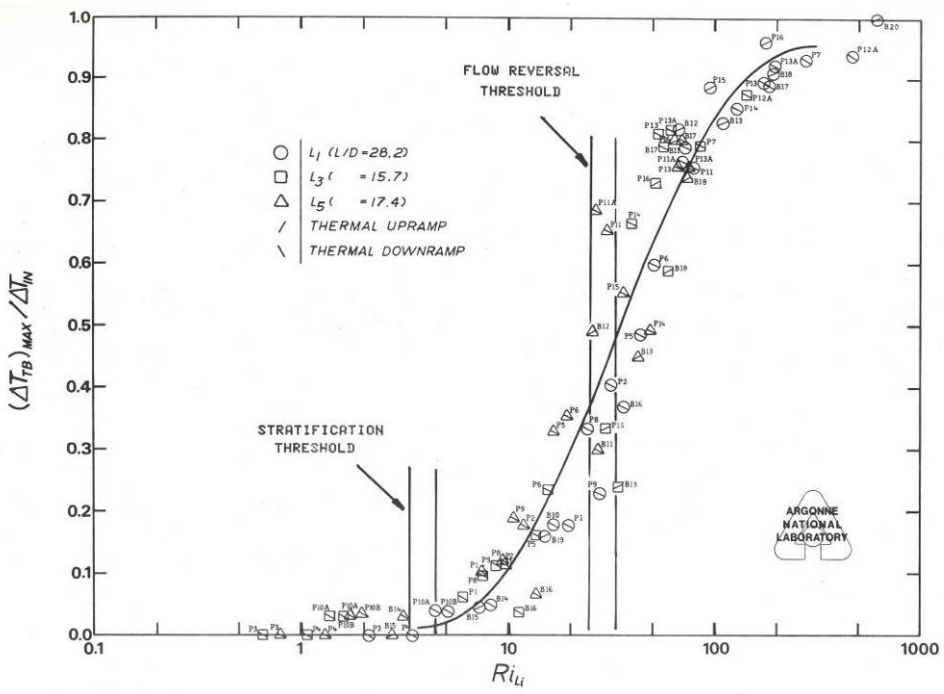

Figure 3.1-14 Correlation for horizontal-pipe flow temperature stratification resulting from thermal transients in the pipe inlet

3.1.3 Phase III

Phase II studies dealt with thermal buoyancy in pipe systems containing both horizontal and vertical piping segments connected with vertical elbows. Phase III studies dealt with buoyancy in a simplified pipe system consisting of two horizontal pipes connected with a horizontal elbow to more carefully study the flow interaction between them. This investigation allowed further generalization of the pipe stratification correlation developed in Phase II.

3.1.3.1 Tasks

Phase III involved the following:

1. Studying thermal-stratification mitigation produced by a horizontal elbow resulting from secondary corner turning vortices to determine if there is a threshold value of the governing parameters above which a horizontal non-straight pipe system behaves as a straight-run horizontal pipe of cumulative length equal to all the horizontal segments.

2. Evaluating the influence of larger values of pipe L/D on stratification. The tests performed in Phase II were for values of L/D < 28.

3. Evaluating the influence of the thermal-transient time ratio (ø). The tests performed in Phase II were on slow transients (ø > 1, which means the duration of the thermal transient was greater than the time required for flow transport through a straight pipe). Fast-transient tests were conducted in Phase III (with ø < 1.0) to establish the influence of ø on the stratification correlations developed in Phase II.

4. Determining the persistence time of stratification-induced stagnant regions and fluid "holdup" mass in piping and the resultant stratified interface thermal distribution and fluctuations relative to assessment of pipe stress levels.

5. Comparing the water-buoyancy data with the available (very limited) sodium buoyancy data to assess the applicability of the correlations to prototype sodium systems.

3.1.3.2 Summary of Phase III Results

Phase III tested a horizontal system composed of a straight pipe (L/D = 42) connected by either a 90° sweep (the elbow curvature ratio D/R = 0.5) or a mitered (D/R = infinity) to a straight downstream pipe (L/D = 15), as shown in Fig. 3.1-15. Test conditions included both fast and slow linear thermal transients superimposed upon constant turbulent pipe flow.

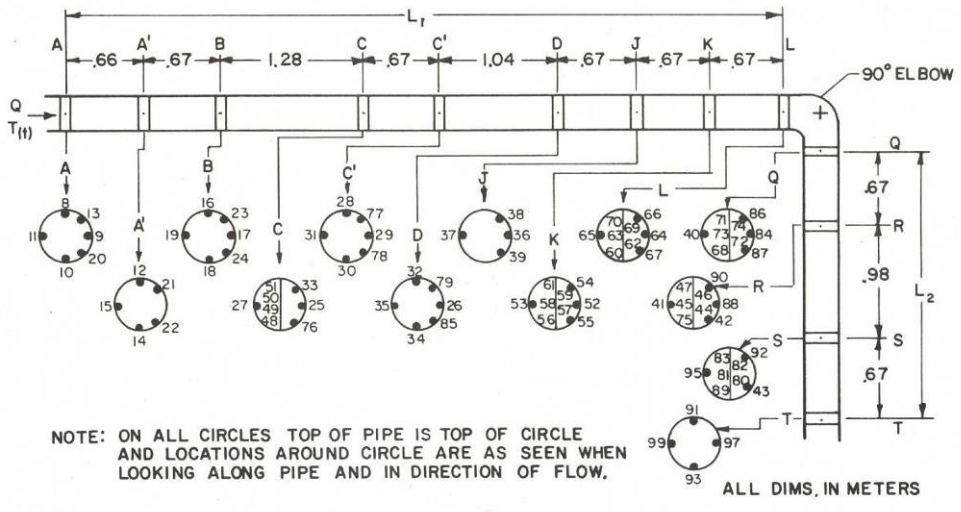

Figure 3.1-15 Argonne Phase III pipe stratification test section having only horizontal pipes

Figure 3.1-16 shows the flow temperature from a sample test for top and bottom stratification temperatures at four axial cross sections (A, B, D, and K) located in the upstream horizontal

pipe for a thermal down ramp. Figure 3.1-17 shows the top and bottom stratification temperatures for the same test at axial cross section R located in the second horizontal pipe downstream of the 90º elbow. It is clearly evident from a comparison of these two figures that the elbow-generated secondary vortex flow has reduced the temperature stratification and duration of the stratification in the downstream pipe. This behavior of the elbow is a strong function of the buoyancy forces induced by the temperature transient.

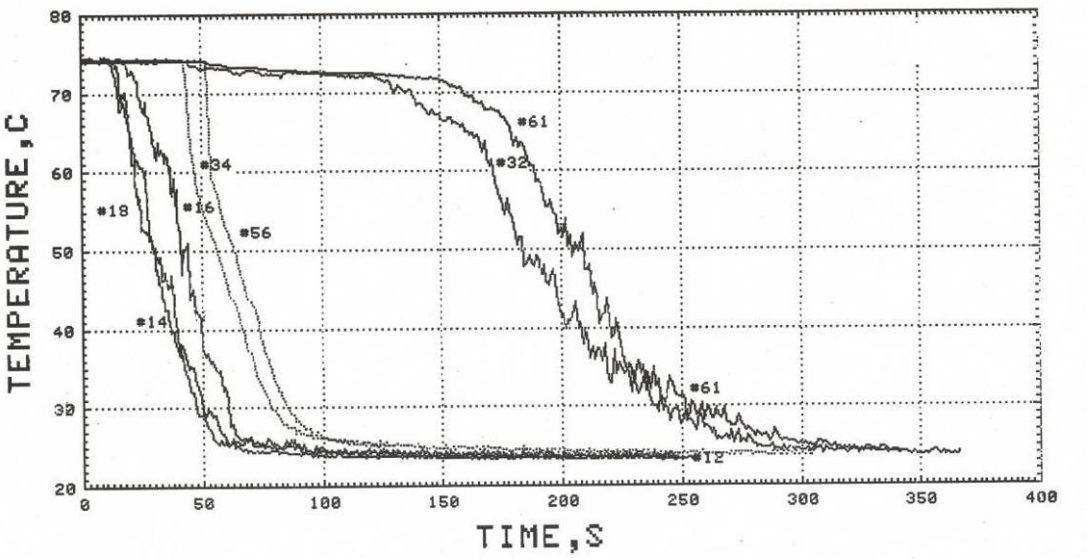

Figure 3.1-16 Top and bottom stratification temperatures at four axial cross sections (A, B, D, and K) located in upstream horizontal pipe for a thermal down ramp

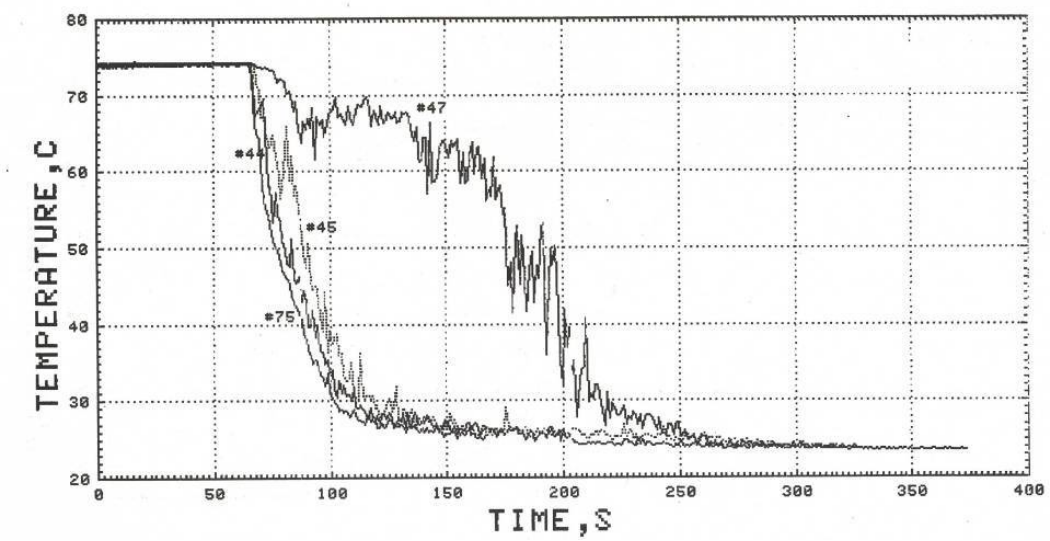

Figure 3.1-17 Top and bottom stratification temperatures for same test as shown in Fig. 3.1-16 at axial cross section R located in second horizontal downstream of a 90º elbow

The study findings were as follows:

1. The dimensionless transient time φ, which is the ratio of the linear-thermal-ramp duration to the convective transport time of flow through a given pipe, was shown to be an important parameter.

2. The correlation that was derived in Phase II for slow transients ($\varphi > 1.0$) was also able to correlate the Phase III slow-transient data, but it failed to correlate the fast-transient ($\varphi < 1.0$) Phase III flow-stratification data.

3. As shown in Fig. 3.1-18 a new generalized parameter K2 was developed. This parameter correlates the horizontal pipe stratification data from Phase II and III and accounts for thermal ramp rate for both the slow and the fast thermal-transient data. It correlates the maximum top-to-bottom stratified temperature difference, $(\Delta T_{TB})_{MAX}/\Delta T_{IN}$, developed in a given horizontal pipe during a transient with a parameter defined as $K2 = g\beta\Delta T_{IN}D/(U^2\,\varphi)$, which is a combination of Richardson number based on pipe diameter and total transient temperature change at the horizontal-pipe inlet and the dimensionless time parameter φ.

4. For the wide range of test conditions explored, the L/D ratio is found not to be an independent parameter relative to the behavior of $(\Delta T_{TB})_{MAX}/\Delta T_{IN}$.

5. Flow stratification in a horizontal straight pipe begins to develop when K2 exceeds a value of 0.05.

6. For $\varphi > 1.0$, the flow stagnation/reversal phenomenon threshold occurs when $K2 > 0.7$

7. For $\varphi < 1.0$, the flow stagnation/reversal threshold occurs when $K2\,\varphi > 0.7$

8. As shown in Fig. 3.1-19, the mitigation or mixing of stratification, developed in an adjacent upstream horizontal pipe, in its passing through a horizontal elbow of two designs (miter or sweep) can be correlated by cross-plotting the adjacent upstream (1) and downstream (2) normalized maximum top-to-bottom stratified-temperature-differences developed during the transient. The correlation is a function of the elbow curvature ratio (D/R). The larger the value of D/R, the greater is the mitigating effect of an elbow. For a given elbow, the elbow stops being effective in mitigating the stratification when a specific threshold value of K2 is exceeded in the upstream adjacent horizontal pipe. The larger the value of D/R, the larger is the threshold value of K2. When elbow secondary flow is completely suppressed, two pipes connected by the elbow become effectively one long pipe of length L1 + L2.

9. Flow visualization and thermocouple data revealed that the largest thermal fluctuations at the stratified interface occurred in the elbow exit regions on the inside radius side of the elbow. This region is thus where the greatest thermal-stripping potential exists.

10. Another parameter developed to scale the importance of thermal-buoyancy-induced stratification in horizontal pipes is γ,

$$\gamma = Ri\ Re^{-0.625}\ Pr^{-0.5}$$

where Ri, Re, and Pr are the Richardson, Reynolds, and Prandtl numbers, respectively. This parameter is preliminary and is only based on water data from which it has been established that

$\gamma \sim 0\ (10^{-4})$ threshold of buoyancy effect to correspond to item 7 above

$\gamma \sim 0\ (10^{-3})$ notable to moderate buoyancy effect

$\gamma \sim 0\ (10^{-2})$ strong buoyancy effect.

The indicated dependence of the parameter γ on Pr over a range of values from water to sodium has not been validated because of a lack of sodium data. With generation of some sodium stratification data, this expression holds some promise of furnishing a validated criterion for extrapolation of water data to sodium.

11. Figure 3.1-20 shows the K2-developed stratification correlation for both pipe test sections (vertical/horizontal and just horizontal) and the very limited sodium stratification data. The sources for the sodium data are a) a single FFTF natural-circulation test exhibiting pipe stratification in the reactor outlet plenum hot-leg horizontal pipe, b) French pipe stratification tests on a long horizontal pipe, and c) the COMMIX code computer simulation described under Phase I.

12. Valuable information has been generated to estimate the propensity for, and severity of, stratification in an existing pipe system. The information can also be used to specify the transients that can be allowed in a system before exceeding an acceptable level of stratification or as a guide in designing a new pipe system in which stratification is to be minimized.

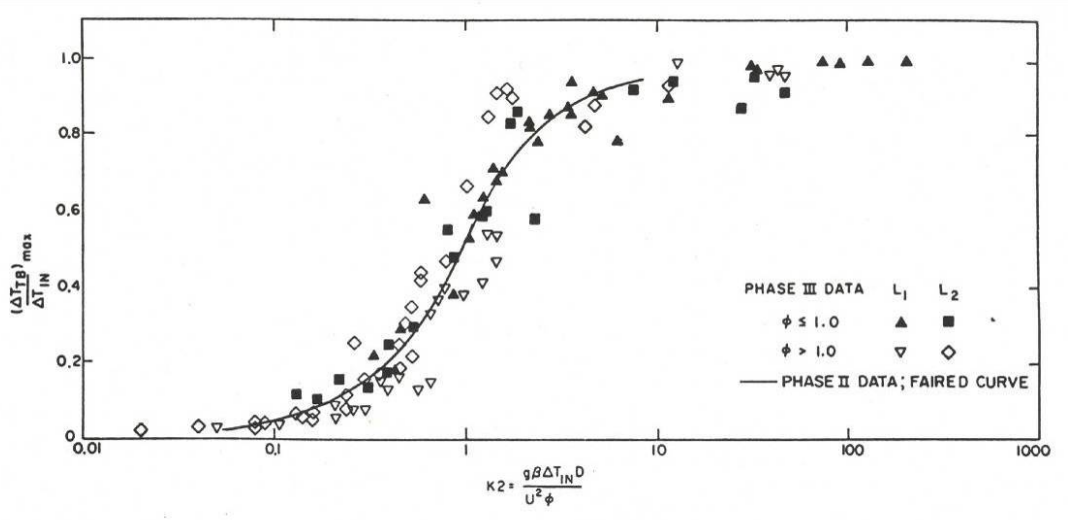

Figure 3.1-18 Correlation of Phase II and III horizontal pipe stratification data with improved parameter K2, which accounts for thermal ramp rate φ

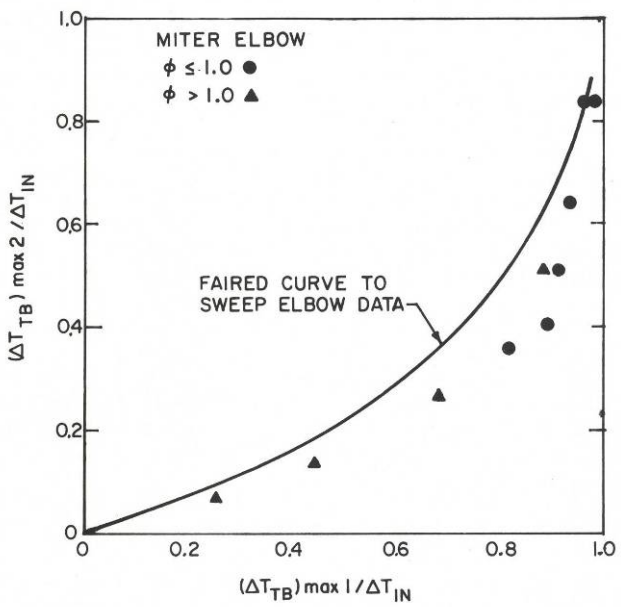

Figure 3.1-19 Correlation of horizontal pipe thermal stratification occurring upstream and downstream of a miter and a sweep elbow

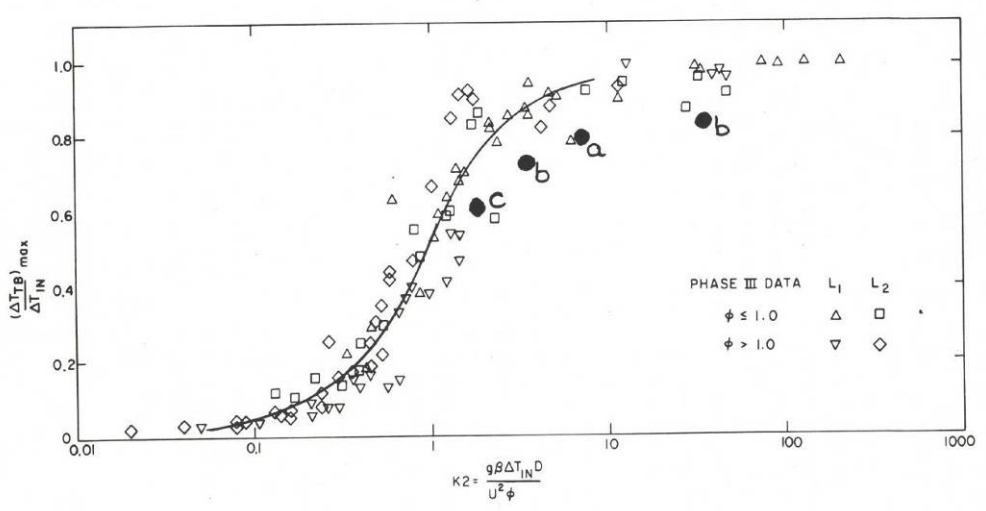

Figure 3.1-20 K2-developed stratification correlation for data from both pipe test sections (vertical/horizontal and just horizontal) and the sodium stratification data (a, b, c)

3.1.4 Future Research Needs on Pipe Stratification

Additional water testing supplemented with sodium testing is needed to broaden our understanding of pipe stratification and establish the limits of validity of current water-based correlations described in this report. The experimental activities should be conducted in parallel with an effort to establish the capability of using a 3-D commercial CFD code to simulate the complex stratification phenomena. The experimental data would be used to guide and validate development of the CFD code. The information generated, combined with the existing data

base, could be developed into a "design guide" format focused on the thermal-hydraulic aspects of the implications of stratification, including recommendations on how to size piping to avoid or minimize thermal stratification produced by pipe fluid thermal transients. The data would also be useful in telling designers when 1-D computational models are inadequate and when a 3-D CFD analysis must be used.

The experimental efforts would focus on:

1. Developing a correlation for predicting persistence time of stratification-produced stagnant zones.

2. Delineating the nature and severity of thermal oscillations occurring along a stratified interface and immediately downstream of an elbow.

3. Evaluating and quantifying the influence of the large Prandtl number difference between water and sodium on the stratification phenomena.

4. Delineating the influence of pipe drainage slope on the pipe stratification correlations.

5. Delineating the influence of turbulent to laminar transition on pipe stratification. All testing to date has been for turbulent flows. However, there are possible plant coast-down transients that may have the flow going to zero for a period of time. Testing under laminar flow would allow assessment of Reynolds number on stratification phenomena.

References

1. Kasza, K.E., Bobis, J.P., Lawrence, W.P., and Liljegren, J.C., "Thermal Transient Induced Pipe Flow Stratification: Phase I," ANL-CT-80-25 (June 1980).

2. Kasza, K.E., Bobis, J.P., Lawrence, W.P., and Liljegren, J.C., "Thermal Transient Induced Pipe Flow Stratification Phenomena and Correlations: Phase II," ANL-CT-81-19 (February 1981).

3. Kasza, K.E., and Kuzay, T.M., "Thermal Transient Induced Pipe and Elbow Flow Stratification Phenomena and Correlation (Phase-III)," ANL-82-85 (October 1982).

4. Petukhov, B. S., "Turbulent Flow and Heat Transfer in Pipes under Considerable Effect of Thermo-gravitational Forces," *Heat Transfer and Turbulent Convection*, Vol. II, Hemisphere-McGraw-Hill (1977).

5. Debler, W., "The Intrusion of Fluid Into the Inflow Branch of a 180°-Approach Mixing Tee," ANL-CT-76-47 (September 1976).

6. Fraser, J. P., and Oakley, D. J., "Turbulent Free Convection Heat Transfer Rates in a Horizontal Pipe," KAPL 1494 (1956).

7. Hong, S. W., “Natural Circulation in Horizontal Pipes,”, IJHMT Vol. 20, p. 685 (June 1977).

8. Lowrie, R. R., et al., “Preliminary Evaluation of the CRBR Natural Circulation Decay Heat Removal Capability,” Westinghouse Electric Corporation, CRBRP-ARD-0132 (November 1977).

9. Kasza, K. E., Schmitt, R. C., and Sha, W. T., “Thermal Buoyancy Phenomena in a Horizontal Pipe during a Flow Coast-down Thermal-Hydraulic Transient,” ANL-CT-77-31 (September 1977).

3.2 Thermal Stratification at Piping-Plenum Interfaces

Section 3.1 described Argonne studies of thermal stratification produced in LMR piping systems under low-flow thermal-transient conditions. These studies delineated important pipe stratification phenomena and developed correlations showing that several of the postulated transients used for reactor design will, in general, produce high levels of thermal stratification in horizontal piping. This section highlights flow thermal stratification concerns related to reactor plenums and pipe inlet/outlet nozzles [1-4].

The concerns about the LMR nozzle center on the possibility that the primary "hot-leg" piping nozzles at the reactor outlet may be subjected to stratification and backflow during some transient and steady-state conditions. The stratified flow could induce asymmetric stressing of the piping and nozzle thermal liner. Some events that could lead to these conditions are:

- Loss of one primary-pump pony motor
- Loss of one primary-pump pony motor with failure of check valve to close
- Two-loop operation (back flow in inoperative loop following plant trip)

Reactor events of the above nature can cause stratified pipe flow formed in the down loop to be convected back into the reactor-outlet nozzle region and to be back-flushed into the reactor upper plenum. This condition could produce a pipe-flow-generated thermal plume in the plenum, which would influence plenum-wall and outlet-nozzle thermal distributions. The following two phenomena were highlighted by Argonne as having a direct bearing on the problem and for which inadequate technical information existed at the time:

- The steady-state initial pipe thermal distribution induced by thermal buoyancy in the down loop is very important to the proper interpretation of the ensuing stratification after the back-flow transient begins.

- The behavior of a stratified pipe flow discharging into a large plenum has not been

studied, both from the viewpoint of how the pipe/reservoir interaction influences the pipe stratification itself (being the boundary condition on one end of the pipe) and of how the plume generated by the back-flushed pipe flow into the plenum influences the thermal distribution in the outlet-nozzle/plenum-wall region.

To address the concern and learn more about the phenomena, Argonne built the Buoyancy Effects Tank (BET) shown in Fig. 3.2-1. This tank consists of a 10.16-cm-dia straight pipe with length of 4.64 m connected to a 3.41-m^3 reservoir (either hot or cold).

3.2.1 Experimental

In testing, a temperature difference was imposed between the pipe end farthest from the reservoir and the reservoir itself. Both zero and nonzero pipe flow, as well as steady or transient water conditions, were supplied to the pipe/reservoir test section. The piping and reservoir walls were transparent to allow laser-sheet flow visualization of the pipe stratification and thermal-plume behavior in the pipe-nozzle/plenum-wall region. For this purpose, a fluorescing dye was injected into the flow entering the pipe entrance. Extensive thermocouple instrumentation was used to characterize both the pipe and plume thermal distribution, as evident in the BET schematic in Fig. 3.2-2.

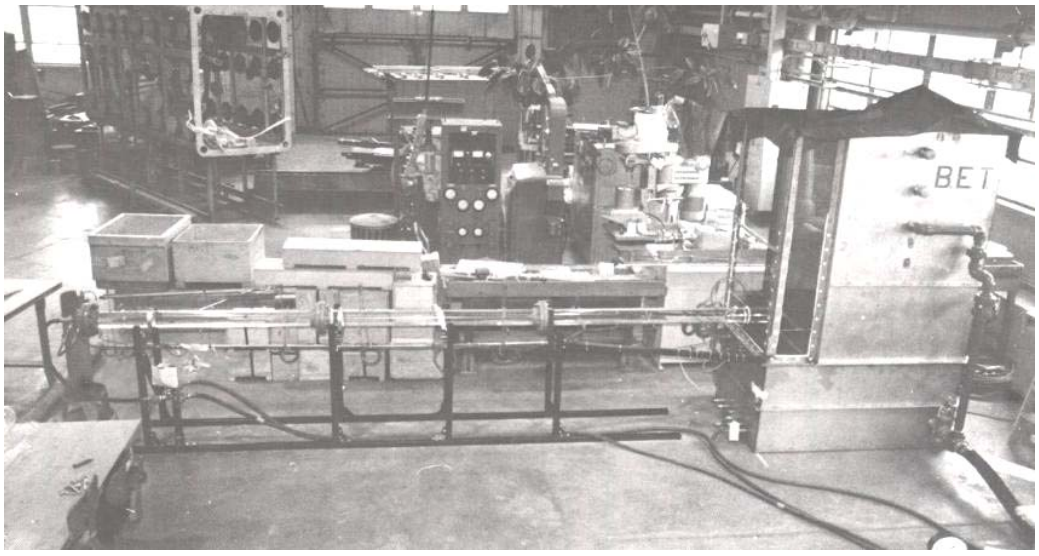

Figure 3.2-1 Argonne Buoyancy Effects Tank (BET) and piping

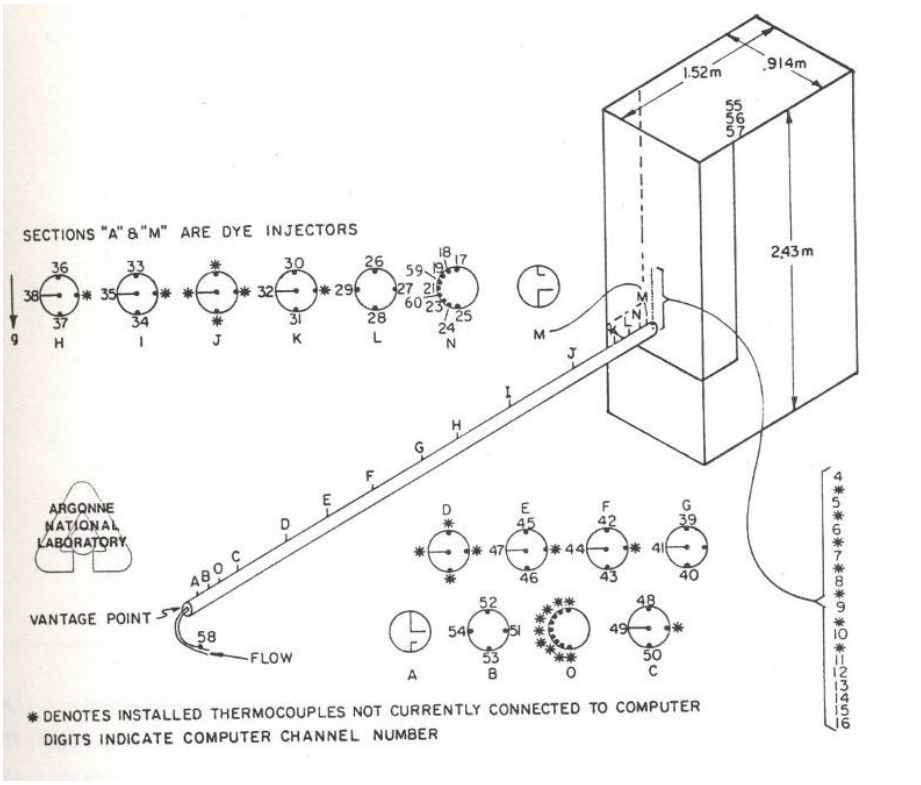

Figure 3.2-2 Temperature instrumentation for Argonne BET and piping test section

The Argonne MCTF water flow loop (see Section 4.2.2, Fig. 4.2-2) was interfaced with the BET through the 4.64-m-long horizontal pipe, which supplied water into the already filled tank at various temperatures and flow rates to create varying temperature differences for inducing thermal buoyancy forces. Initially, after turning on the pipe flow to deliver flow of a different temperature than already in the system, a temperature and flow transient occurred in the pipe and plenum and were damped out with time. Figs. 3.2-3 and -4 show the BET response to a step increase in fluid temperature entering the pipe. During this transition period, the pipe flow becomes thermally stratified, and a flow-recirculation loop forms in the pipe at the nozzle and moves upstream along the bottom of the pipe until steady state is achieved (see Fig. 3.2-4). The length of reverse flow penetration into the pipe depends on the strength of the thermal buoyancy forces, which are a function of the imposed temperature difference, pipe flow velocity, pipe size, and fluid properties. These parameters are represented by Ri, the ratio of thermal buoyancy forces to inertial forces acting on the flow (i.e., $Ri = g\beta\Delta TD /U^2$). See Section 4.2.1 and Appendix 1 for discussions of thermal-hydraulic modeling.

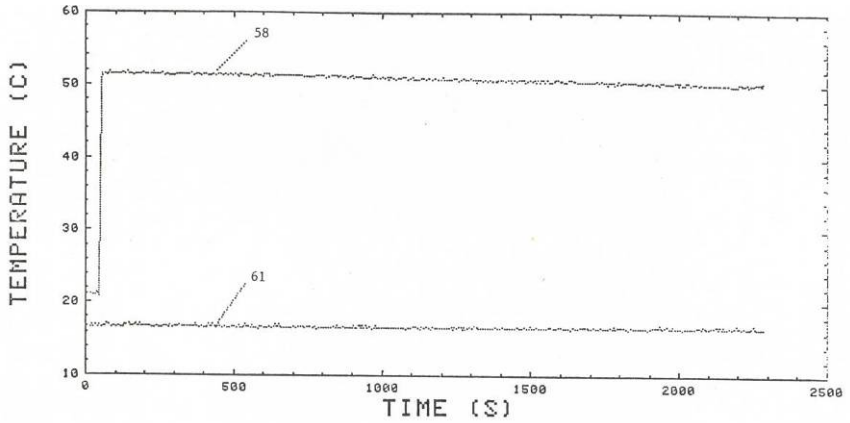

Figure 3.2-3 Inlet pipe (58) and plenum (61) temperatures for test BETC2

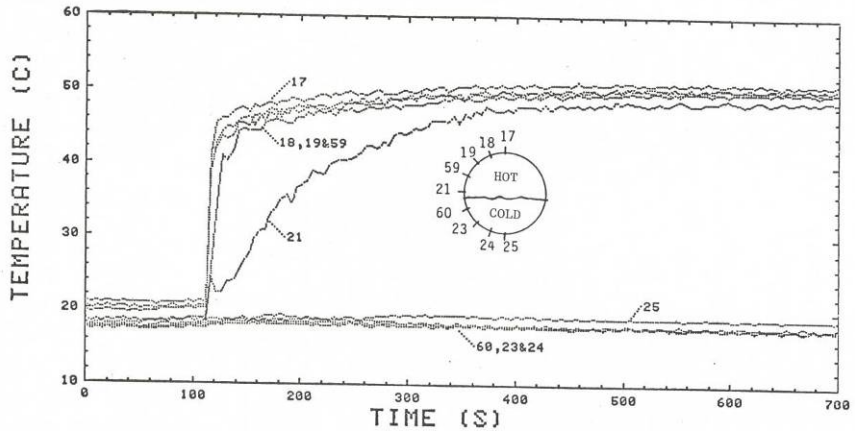

Figure 3.2-4 Pipe circumferential temperature distribution during approach to steady state at axial location N, nozzle region

3.2.2 Summary of Results

Based on flow visualization data, a thin stratified shear layer of typical thickness ~0.64-1.27 cm formed in the horizontal pipe separating the hot pipe flow at the top of the pipe from the cold recirculation zone located along the bottom of the pipe. The shear-layer velocity profile exhibits an inflection point (i.e., contains a point of zero velocity). Large temperature gradients of the order of the full ΔT/(shear layer thickness) exist in this region. Undulations of this layer produce conditions conducive to thermal stripping in piping. Furthermore, observations of the dyed shear layer indicated that, although the pipe flow (the hot region) was turbulent (as evaluated using bulk flow properties—Re >2300), the shear layer appeared laminar. That is, the thermal buoyancy forces were large enough to laminarize the shear layer and thereby suppress turbulence. An estimate of the local Ri number based on the shear layer thickness yielded 0.3, which compares favorably with the gradient Ri number of 0.45 at which turbulence has been shown to be almost completely suppressed in some shear flows [5].

In future studies, velocity and temperature gradients in this shear layer need to be measured to provide a better understanding of shear layer laminarization, a process that can occur in other flow regions within the reactor. Laminarization is important because it eliminates a source of troublesome thermal oscillations; however, the stratified shear under certain conditions, not yet understood, can undulate periodically at a much larger spatial scale. These important phenomena require further investigation, and a full 3-D CFD code must be developed and validated for modeling this important behavior.

In the plenum a thermal plume develops and large-scale periodic vortex/eddy patterns were observed (see Figs. 3.2-5 and -6). The hot flow regions, delineated by fluorescent dye injected into the bulk incoming pipe flow, appear light, while the dark areas in the pipe and plenum photos are cold regions. Clearly evident are the stratified pipe flow and plenum-thermal plume. Large eddies of low frequency formed along the bottom edge of the plume, while smaller eddies with higher frequencies occur along the top of the plume. The small eddies are flow turning vortices formed at the pipe-nozzle edge. These turning vortices penetrate through the plume farther downstream and interact with the large eddies on the lower surface of the plume, causing the entire plume to undergo large periodic displacements that greatly influence plume entrainment and its global behavior.

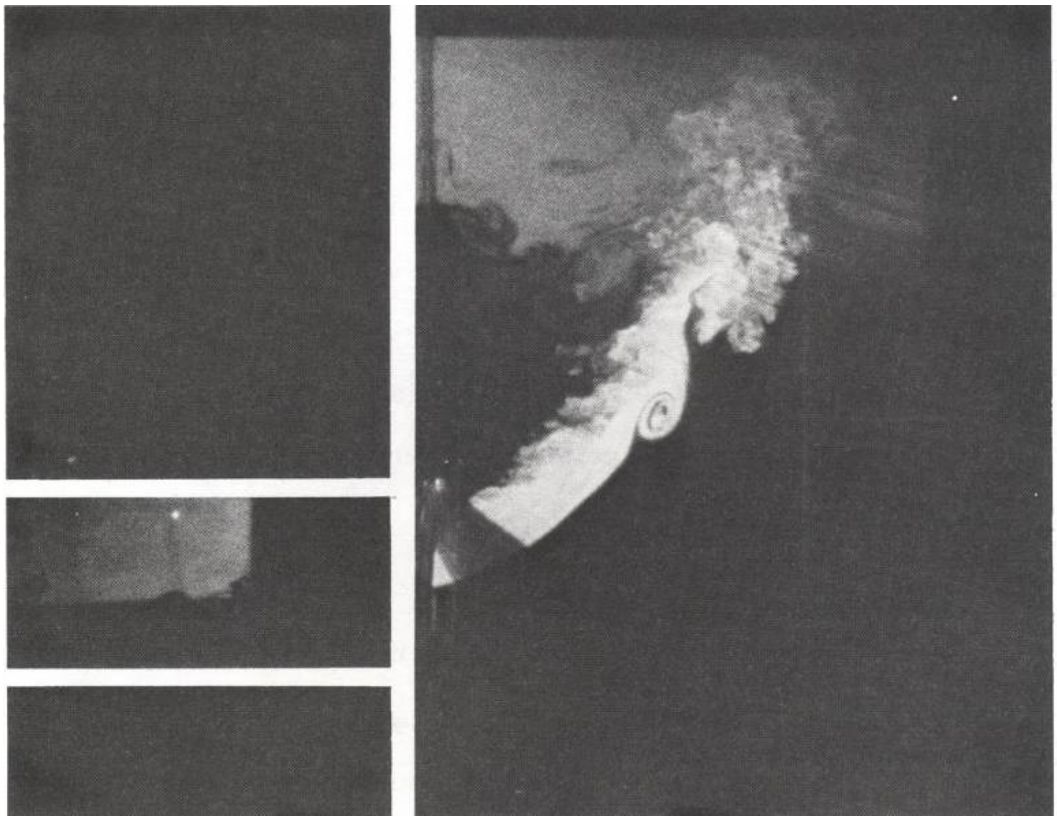

Figure 3.2-5 Pipe-nozzle stratification, BET thermal plume, and eddy pattern with thermocline

Figure 3.2-6 Large eddy pattern formed in plenum thermal plume

Figure 3.2-7 shows the temperature fluctuations measured by a thermocouple located in the plenum thermal-plume large-eddy. The fluctuation amplitude is nearly the full 30ºC temperature difference driving the buoyancy-induced flow. Figure 3.2-8 shows the power spectral frequency analysis of the eddy-produced thermal fluctuations. A dominant component occurs at 0.63 Hz. Fluctuations of this amplitude and frequency if impinging on a structure can cause thermal stripping concerns. The plume moved farther from the plenum wall as the inlet pipe flow rate was increased.

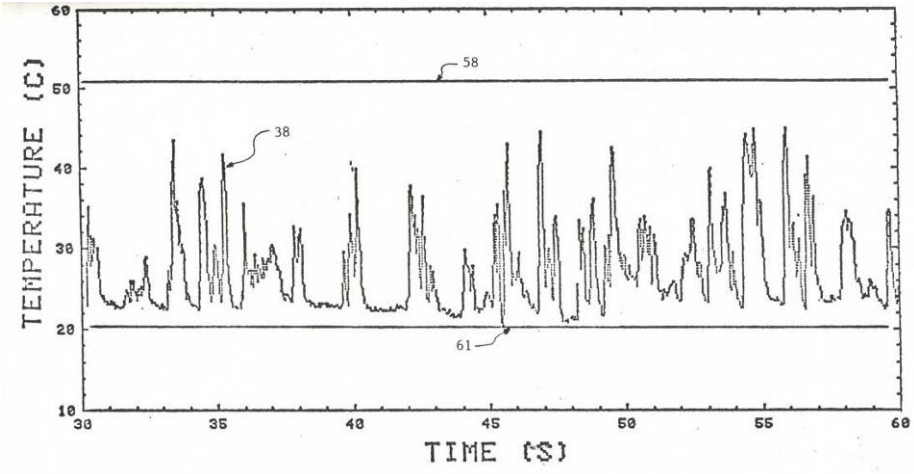

Figure 3.2-7 Response of a thermocouple positioned in the plenum thermal plume large eddy

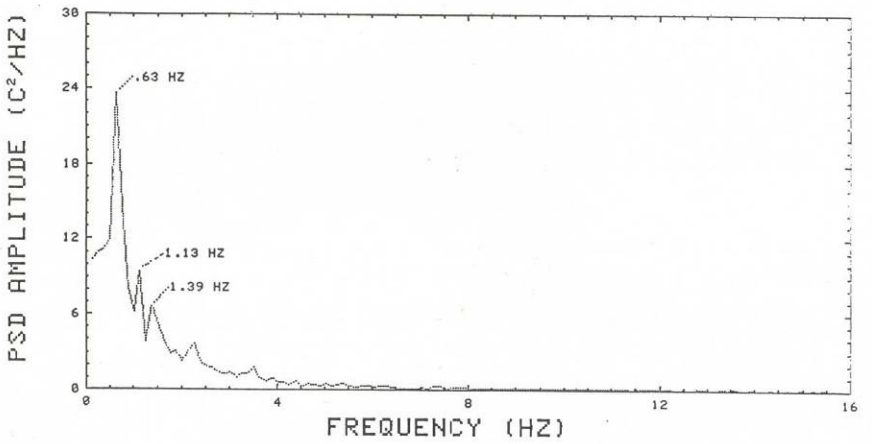

Figure 3.2-8 Power spectral density analysis of the temperature oscillations associated with the large eddies in the plenum thermal plume

The upstream axial penetration distance induced by thermal buoyancy (Zp) of the cold-back-flow recirculation zone was found to depend on both pipe flow rate and the imposed fluid temperature difference created by the pipe entrant flow. For a fixed temperature difference, as the flow rate was decreased, Zp increased until the recirculation region filled the entire pipe. This research program resulted in development of correlations for predicting the axial upstream penetration distance of the stratified pipe back-flow-recirculation region (Fig. 3.2-9) and for the height of the recirculation region in the critical nozzle region at the pipe exit (Fig. 3.2-10) in terms of Ri. In these correlations the pipe diameter D is used to normalize spatial distances.

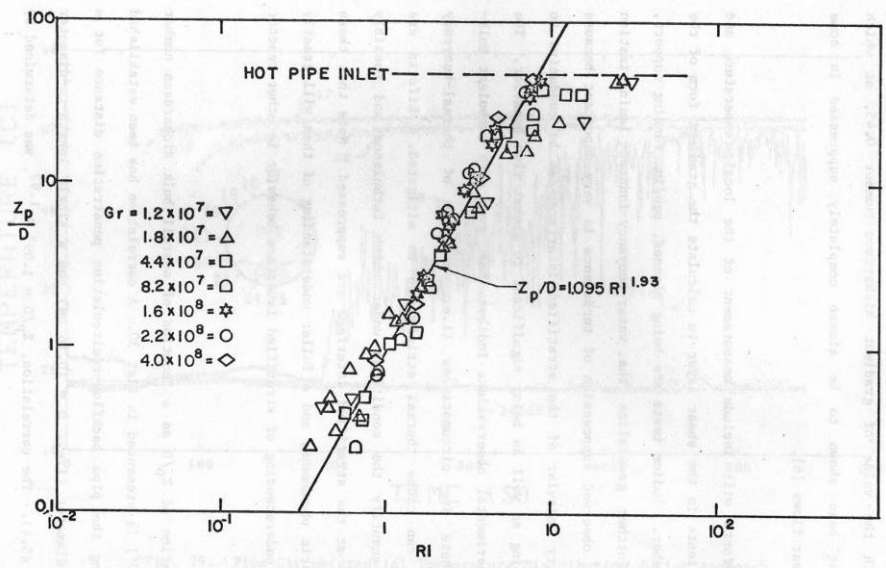

Figure 3.2-9 Variation of penetration distance in pipe-back-flow recirculation zone (Zp/D) with Ri

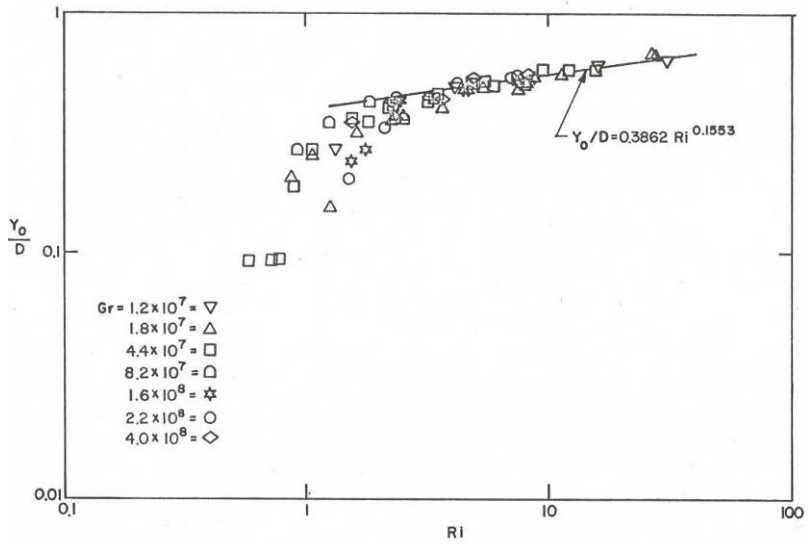

Figure 3.2-10 Variation of exit height (Y_o/D) of pipe-back-flow recirculation zone with Ri

In the BET a thermocline (i.e., hot/cold interface) developed slowly (Fig. 3.2-5) and moved downward in the plenum due to the mixing of the hot thermal plume with the cold plenum. Thus, there are three regions of different temperatures: the hot plume, the warm mixed fluid above the thermocline, and the cooler fluid below the thermocline. Figure 3.2-5 shows the thermocline high in the plenum. Under this condition, the eddy patterns are unaffected by the thermocline. When the thermocline moves lower into the region of the large eddy formation a developed eddy after hitting the thermocline breaks up due to the buoyancy forces, and dissipates. Testing showed that the plenum thermocline location does not influence the pipe stratified recirculation zone until it reaches a level of approximately the pipe centerline. This fact greatly generalizes the range of usefulness of the correlations developed. The behavior of the thermal plume and its interaction with the plenum thermocline are very complex phenomena conducive to thermal stripping, which are currently not modeled adequately by CFD codes. In conjunction with this shortcoming there is need for further investigation of these phenomena and the development/validation of a full 3-D CFD code for simulating these important phenomena.

3.2.3 Future Research Needs

The Argonne pipe-plenum stratification studies were based on water testing. Several buoyancy-induced phenomena of importance to designers were highlighted. Correlations were developed for estimating both the axial extent of the pipe back-flow-recirculation region and the height of this region at the pipe exit to the plenum. These studies suggest that stratification may occur in reactor plenum outlet nozzles under certain conditions involving N-1 loop operation. From a LMR designer's point of view, all of the above phenomena need to be evaluated carefully and their importance quantified relative to the various possible modes of plant operation.

Major findings from these studies are as follows:

- Under conditions of low flow in a horizontal pipe connected into a plenum and a temperature difference between the pipe flow and plenum, a stratified recirculation flow carries plenum fluid into the pipe, resulting in the entire pipe-to-plenum temperature difference existing between the top and bottom of the pipe.

- Thermal-buoyancy-induced laminarization of a turbulent pipe-flow stratified-shear-layer has been documented as an important mechanism of thermal oscillation (thermal stripping) suppression. Preliminary results indicate a threshold value of the local gradient Ri above which laminarization occurs. However, below this value large thermal oscillations are possible due to large scale interface oscillations.

- Large-scale periodic eddies induced by thermal buoyancy have been shown to occur in the plenum thermal plume created by the pipe discharge. These eddies interact, causing large-scale motions of the plume and greatly altering the plume/plenum mixing. The thermal plume is a source of large-amplitude thermal oscillations and thermal stripping concerns.

- The development of a plenum thermocline (i.e., plenum stratification) is shown to exert a strong influence on the behavior of a thermal plume rising upward into the thermocline. However, the developing thermocline has little effect on the pipe back-flow-recirculation correlations until it reaches the level of the pipe exit.

Important avenues for conducting further experimental research related to better understanding the phenomena and for developing the computational tools to simulate and evaluate their importance are as follows:

- An experimental program is needed to assess the influence of the pipe L/D ratio on the correlations already developed, as well as the influence of other geometrical factors such as elbows, valves, and vertical pipe runs in close proximity to the horizontal nozzle.

- Velocity and temperature gradients in the local pipe stratified-shear-zone need to be measured to gain a more thorough and generalized understanding of shear-zone laminarization caused by thermal buoyancy. Also, an improved understanding of the conditions that can produce gravity waves or undulations of the stratified interface is needed. This information is expected to have a broad range of applicability in view of the fact that stratified interfaces can occur in a variety of reactor components and are a source of potentially troublesome thermal oscillations and thermal stripping.

- Additionally, careful measurements of thermal-plume behavior and large eddies should be made to assist in modeling plume behavior. The eddy frequency and the resulting temperature fluctuation amplitude need to be characterized.

- Some of the above studies should be conducted in both water and sodium to improve understanding of the role that fluid property differences play in the behavior of these

important phenomena. There are virtually no sodium data for reactor components that can be used to validate the correlations developed for water-based buoyancy effects.

- Limited sodium experiments paralleling what has been done in the Argonne water testing should be conducted. These experiments should be sharply focused on key buoyancy phenomena. Such experiments would serve to delineate the influence of the large Prandtl number difference between water and sodium and would likely confirm the general validity of much of the water testing. The sodium information on shear zone laminarization, as well as on pipe recirculation-zone axial extent and plenum plume behavior, would furnish valuable design data for generic phenomena, which are the least well understood and provide the greatest challenge to reactor designers.

- The sodium data in conjunction with the unique Argonne reactor-component water-buoyancy effects discussed in this and other sections of this report will allow establishing a complete and in-depth body of information that can be used in the design of future LMR components.

All of the preceding experimental investigations should be done in parallel with the development and validation of sub-models for thermal-buoyancy-influenced turbulence and the incorporation of them into a robust full 3-D CFD. This work should also involve coupling a CFD code with a structural code to correctly impose the thermal stripping boundary condition on a structural member and evaluate the potential for fatigue cracking.

References

1. Oras, J.J., and Kasza, K.E., "Periodic Large-Amplitude Thermal Oscillations Occurring in a Buoyant Plume," Trans. Am. Nucl. Soc., Vol. 45 (1983).

2. Oras, J.J., and Kasza, K.E., Argonne National Laboratory, unpublished information, October 1983.

3. Oras, J.J., and Kasza, K.E., "Thermal Laminarization of a Stratified Pipe Flow," Trans. Am. Nucl. Soc., Vol. 46 (1984).

4. Kasza, K.E., Oras, J.J., and Kolman, R., "Measurement of Velocity Profiles in a Stratified Pipe Flow Recirculatory Shear Zone Using Laser Flow Visualization," Trans. Am. Nucl. Soc., Vol. 48 (1985).

5. Tritton, D.J., *Physical Fluid Dynamics*, Van Nostrand Reinhold Co., New York, p. 287 (1977).

3.3 Thermal-Buoyancy Modified Behavior in Heat Exchangers

Sodium-to-sodium IHXs in LMRs under full-flow, steady-state normal operating conditions are not to any measurable degree influenced by thermal buoyancy. However, as discovered in past Argonne studies [1-3], heat-exchanger/system interactions can occur during various reactor operation modes for which buoyancy has the potential for adversely influencing the thermal-hydraulic and structural performance of IHXs and, as will be discussed in Section 3.4, the performance of steam generators.

There are several areas in which questions have been raised relative to the importance of thermal buoyancy to IHX performance. First, with regard to normal operation high-flow steady-state design conditions, one of the reasons for the use of flow control orifices in the shell-side inlet plenum and tube-bundle/baffle design is to minimize radial tube-bundle temperature variation in order to minimize differential tube expansion and possible buckling problems. However, under low-flow conditions, the shell-inlet plenum and tube-bundle flow paths may be altered by thermal-buoyancy forces. Hence, the tube-bundle thermal field can be changed from the "as designed" thermal distribution. The propensity for the preceding to occur in the IHX, as well as in steam generators, under various operating conditions has not been adequately studied and evaluated.

Second, the thermal-hydraulic behavior of the LMFBR system under various types of plant transients (reactor scrams, flow coast-down to natural circulation, evaporator dumps, N-1 loop operation, etc.) has been studied using 1-D flow and energy transport models of the system components. Many of the transient events studied involve the passing from a "high" to a "low" flow with an accompanying rise and/or fall in temperature of the fluid passing through the components. The thermal transients in conjunction with the "low" flow create conditions conducive to thermal-buoyancy effects. The system codes, in addition to using the 1-D assumption, also assume that the classical (neglecting buoyancy) friction and heat-transfer coefficients can be used. Thermal buoyancy can exert its influence on system dynamic-energy transport predictions through alteration of flow and thermal distributions in the reactor components, which in turn can influence decay heat removal, system-response time constants, heat transport between primary and secondary loops (via the IHX), and thermal-energy rejection at the reactor heat sink (the steam generators). The influence of thermal buoyancy on the above system and component considerations has not been investigated in great detail.

In addition to the 1-D system-analysis codes, 3-D computer codes called COMMIX-IHX and COMMIX-SG were partially developed at Argonne for the analysis of heat exchangers and steam generators. However, currently, there are no validated 3-D codes available to analyze these LMR components under the conditions discussed in this section. The codes to be developed will require benchmark data for guidance in modeling and validation, especially in the transient low-flow thermal-buoyancy regime, where heat transfer and turbulence modeling are not well understood.

The overall objectives of the past Argonne studies on heat-exchanger buoyancy effects were to:

- Delineate the nature of thermal-buoyancy phenomena that can occur in IHXs and SGs under off-normal conditions.
- Determine parameters for buoyancy-phenomena models and develop thermal-hydraulic correlations.
- Develop thermal-hydraulic guidelines that can be used by component designers and system analysts for evaluating the importance of buoyancy to prototype reactor components.
- Generate benchmark data that can be used for 3-D code development and validation.

For these studies transient and steady-state experiments under low-flow, non-isothermal water conditions were performed with two test articles:

- A 360°, 1/5-scale, complete geometric model of a generic IHX.
- A 60° pie sector, 0.46-scale, reduced-length hydraulic model of the shell side in the Westinghouse-Tampa Intermediate "A" steam generator, under development earlier for the DOE initiative on Rfuture advanced reactor components.

These experiments were conducted in Argonne's MCTF water facility described in Section 4.2.2. Similar tests were performed on the shell sides of both test articles. The testing of the Westinghouse SG model is described in Section 3.4.

3.3.1 Preliminary Work

3.3.1.1 Paper Studies

As groundwork for conducting the heat-exchanger water tests, Argonne conducted initial paper studies of the propensity for thermal buoyancy to alter the performance of LMR IHXs under low-flow thermal-transient operation [1,2]. Part of the paper study involved surveying the various IHX designs in existence or being proposed at that time. This survey allowed characterization of the geometric and thermal-hydraulic modeling parameters, which were then used to describe a generic IHX and evaluate the potential for thermal-buoyancy phenomena to occur. This survey is summarized next.

The following seven LMR IHX designs proposed for the Fast Flux Test Facility (FFTF), Clinch River Breeder Reactor Plant (CRBRP), and the Prototype Large Breeder Reactor (PLBR) were characterized:

- Foster Wheeler FFTF [4, 5]

- Foster Wheeler CRBRP [6]
- Foster Wheeler Commercial Design [7, 8]
- Foster Wheeler for GE PLBR [9]
- Combustion Engineering "Optimum Design" [10]
- Westinghouse PLBR Concept [11]
- Atomics International PLBR Concept [12]

All of the IHX concepts were vertical, counter-flow, shell-and-tube type with primary sodium flowing downward on the shell side and intermediate sodium flowing upward on the tube side. Three of the seven designs featured a central down-comer. All of the designs, with the exception of FFTF, had a straight tube design. Each tube in the FFTF design had an expansion bend in the region above the lower tube sheet to absorb differences in thermal expansion between the tubes and the down-comer and between active and plugged tubes. Tube outside diameters for the various units ranged from 7/8 in. (2.22 cm) to 1-1/4 in. (3.18 cm) with a representative tube wall thickness of 0.047 in. (0.119 cm). With the exception of FFTF, all had triangular pitch with a representative P/D of 1.5. The ratio of tube length to outer tube bundle diameter ranged from 3.8 to 5.0.

All designs except FFTF had nominally 13 flow-control baffle plates. Baffle plate span ranged from 15 to 40 in. (0.4 to 1.0 m), with three of the designs ranging from 38 to 40 in. (0.97 to 1.0 m). Baffle plate designs were of two basic types. For designs featuring a central down-comer, the plates were of disc and donut type. For IHXs without a central down-comer for flow control, baffles were typified by Foster Wheeler's design for the GE-PLBR, which consisted of alternating type A and type B plates. The A-type orificed plates had a 24% perforated region around the periphery with a 60% perforated central region. The highly perforated central region was off-centered in successive baffles to promote swirling downward flow through the tube bundle in order to prevent streaming down the center of the tube bundle. Type B plates had 24% perforation.

The following conclusions were reached from the Argonne scoping paper studies:

- The open literature was nearly devoid of quantitative information that could be used to assess the importance of buoyancy to LMR-IHX performance. Thermal-hydraulic knowledge relative to buoyancy effects was found to be weakest for the shell side in the areas of tube-bundle flow and heat transfer,, recirculation flows, turbulent structure, and shear flows.
- For flow levels that are a few percent of prototype full flow, both transient and steady-state conditions can possibly cause buoyancy forces of a magnitude having a potential impact on the IHX.
- From the viewpoint of ascertaining the influence of thermal buoyancy on sodium IHX performance, water testing can be used to obtain information on flow-field/thermal-

buoyancy force interaction which is conservative, but not unrealistically conservative. However, in regard to solid-surface heat transfer and boundary-layer behavior, extrapolation to sodium would not be of quantitative utility due to the large differences in Peclet number (Pe = Re Pr) between water and sodium.

- The water data would serve as a valuable first step toward validating and guiding development of computer codes aimed at calculation of IHX thermal-hydraulic thermal-buoyancy conditions. However, "fine tuning" of a code for predicting heat transfer, under strong buoyancy forces, would have to be done against sodium data.

- Of all the phenomena considered in assessing possible IHX thermal-buoyancy effects, two were found to have the greatest potential for producing global effects on IHX performance: the influence of buoyancy on flow recirculation zones and buoyancy-induced flow channeling on the shell side of the tube bundle, which could be adequately studied by water testing.

3.3.1.2 Modeling

The preceding survey of the various IHX designs allowed characterizations of the geometric and thermal-hydraulic parameters that can be used to describe a generic IHX and evaluate its potential for thermal buoyancy effects. As a result of various plant-system operational events, the inlet flows to the primary and secondary loops of the IHX undergo flow coast-down and large thermal transients. A reactor scram in conjunction with loss of power to primary and secondary pumps is typical of these events. For this event, in about 30 to 40 sec after the pump trip, the primary and secondary flows have fallen to about 5% of full flow, and large temperature transients of ~ ±5°F/sec with falling and rising ramps enter the IHX. At this point, depending on plant design, the flow is maintained by either pony motors or driven entirely by thermal density heads existing in the loop. The question then arises as to whether the low flow and the temperature transient produce thermal buoyancy forces within the IHXs are significant enough to alter unit performance (and ultimately overall plant transient behavior) from that which would be predicted from using classical flow and heat-transfer 1-D models. To answer this question, the IHX geometry was divided into the following geometric sub-regions:

Primary Side	Secondary Side
▪ Inlet nozzle	▪ Inlet nozzle
▪ Inlet plenum	▪ Down-comer
▪ Tube bundle	▪ Tube bundle
▪ Outlet plenum	▪ Exit nozzle

The thermal-hydraulic non-dimensional parameters defining these various regions and associated buoyancy phenomena were evaluated, and the various thermal buoyancy-related phenomena were investigated for their propensity to occur. The influence of thermal buoyancy on the following flow phenomena was considered [1]:

- Boundary layer flows
- Pipe flows
- Tube bundles
- Recirculation flows
- Thermal instabilities
- Shear flow instabilities
- Turbulent structure/thermal buoyancy interaction

This evaluation showed that the following three thermal-hydraulic independent non-dimensional parameters (Re, Pr, and Ri numbers), in addition to the appropriate thermal-hydraulic transient time constants, are important for the general case of IHX behavior. The available literature also showed that the buoyancy effects can be modeled by just two parameters and even just one Ri under some conditions. These parameters were evaluated for the various IHX sub-regions at 5% of full flow. These results were used to estimate the importance of the various phenomena and guide specification of the test articles.

Relative to the transient time constants, for the reactor system operational transients considered, the flow reaches within a few percent of its steady low-flow value of nominally 5% before the thermal transients begin to enter the IHX (due to system transport times). Thus, considerable information on IHX thermal buoyancy effects was obtained with experiments using steady low flow at the IHX inlet with the proper thermal transients superimposed. The preceding simplified experimental techniques.

The above initial modeling studies showed that Ri (the ratio of buoyant to inertia forces) can be used as a measure of the importance of buoyancy. The Ri for 5% prototype flow was found to vary from ~0.3-25.0 in the various regions of the IHX. Under these conditions, the buoyant forces were evaluated to be as important as the inertia forces, and thermal buoyancy was estimated to have a significant effect upon flow and heat transfer in all regions of the IHX. Special attention was given to assessing buoyancy effects in the tube bundle region on both the shell and tube sides. This region is important because heat transfer between shell- and tube-side flows is the sole mode of communication between the primary and secondary loops. Considerable literature was found to be available for evaluating when buoyancy becomes important to heat transfer for flow over and within a single tube under steady-state conditions. However, this information was judged to be of little value in estimating buoyancy effects for flows over tube bundles due to strong tube-to-tube interactions. Within the tubes, nevertheless, the single-tube information is more useful. Based on the appropriate criteria, the internal tube flows at 5% prototype flow were estimated to experience significant buoyancy effects, which would be reflected in an alteration of the tube-side pressure drop and heat transfer from their

classical values (i.e. neglecting buoyancy). It would appear that the literature today for the above considerations has not greatly expanded beyond what was generated at Argonne.

Of all the phenomena considered in assessing IHX thermal-buoyancy effects, the recirculation flow regions were estimated as having the greatest possibility of producing global effects on IHX performance. Recirculation flow regions may be present before the initiation of a flow coast-down transient resulting from geometrical design, or they may be produced by buoyancy forces during coast-down. Recirculation zones can occur in IHX plenums and under or above flow-control baffle plates, as will be shown when experimental data are presented. The formation and behavior of recirculation zones, as will be shown, are strongly governed by the parameter Ri. This finding was supported by earlier Argonne buoyancy studies [13] conducted with both water and sodium on reactor upper-plenum flow exiting the core. Since Ri is of order of 1 in all regions where recirculation can occur, thermal buoyancy can exert a strong influence on IHX behavior, causing flow path alteration from that intended, channeling of flow down through the tube bundle and subsequent alterations of pressure drop, and heat transfer leading potentially to large temperature gradients across the diameter of the tube bundle.

In summary, from the viewpoint of ascertaining the effect of thermal buoyancy on sodium IHX performance, it was concluded that conservative information can be obtained on IHX flow field/thermal buoyancy interactions through use of water testing. The water testing is capable of generating all the thermal-buoyancy-related phenomena, even though in some areas such as heat transfer and boundary layer effects, extrapolation to sodium would not be of quantitative utility due to the difficulty of simulating with water the low value of the Peclet number (Pe = Re Pr) associated with sodium flows; however, regarding the most important case of flow recirculation/thermal buoyancy interaction, the Pe identity need not be maintained between sodium and water. In the areas where the Pe difference between water and sodium is important, the determination of when buoyancy starts to exert its influence using water will establish criteria for which one can be sure no buoyancy is present in the sodium prototype. Furthermore, in a code validation effort directed at verifying whether a code predicts the various thermal-buoyancy-related phenomena that can possibly occur in a sodium IHX, a comparison with more readily obtainable water data, in which buoyancy effects (if they exist) would be equal to or greater than the effects in sodium, would constitute a strong test of code capability. In this regard, however, the final "fine tuning" of the code for sodium IHX calculations for predicting heat transfer would have to be done against sodium data in order to assure that the code properly accounts for Pe (or Pr) effects on heat transfer.

The IHX test article used in the Argonne water experiments is described next.

3.3.1.3 IHX Testing

The Ri value for the prototype IHX at 5% shell-side tube-bundle-flow is of order one. When this value of Ri is imposed on the Argonne water test article (assuming test article primary and secondary inlet water temperatures of 200 and 70°F, respectively), the test article used yielded a tube bundle Re = 5000, which is close to the prototype value at 5%-flow and supports the

claim that a water IHX test model can be used to study important thermal buoyancy phenomena that may occur in a sodium IHX.

The test article used [3] was an approximately 1/5-scale model of a vertically oriented, single-pass, counter-flow LMR IHX of the shell-and-tube type. The test article was a modified Corning all-glass (Pyrex) heat exchanger, which allowed flow visualization. The test article as shown in Fig. 3.3-1 contains most of the geometric generic features of an LMR-IHX, including (1) shell-inlet plenum with 360° annular-flow distribution, (2) straight tube bundle, (3) flow-control orificed baffle plates for the tube bundle, and (4) tube-side inlet/outlet plenum chambers.

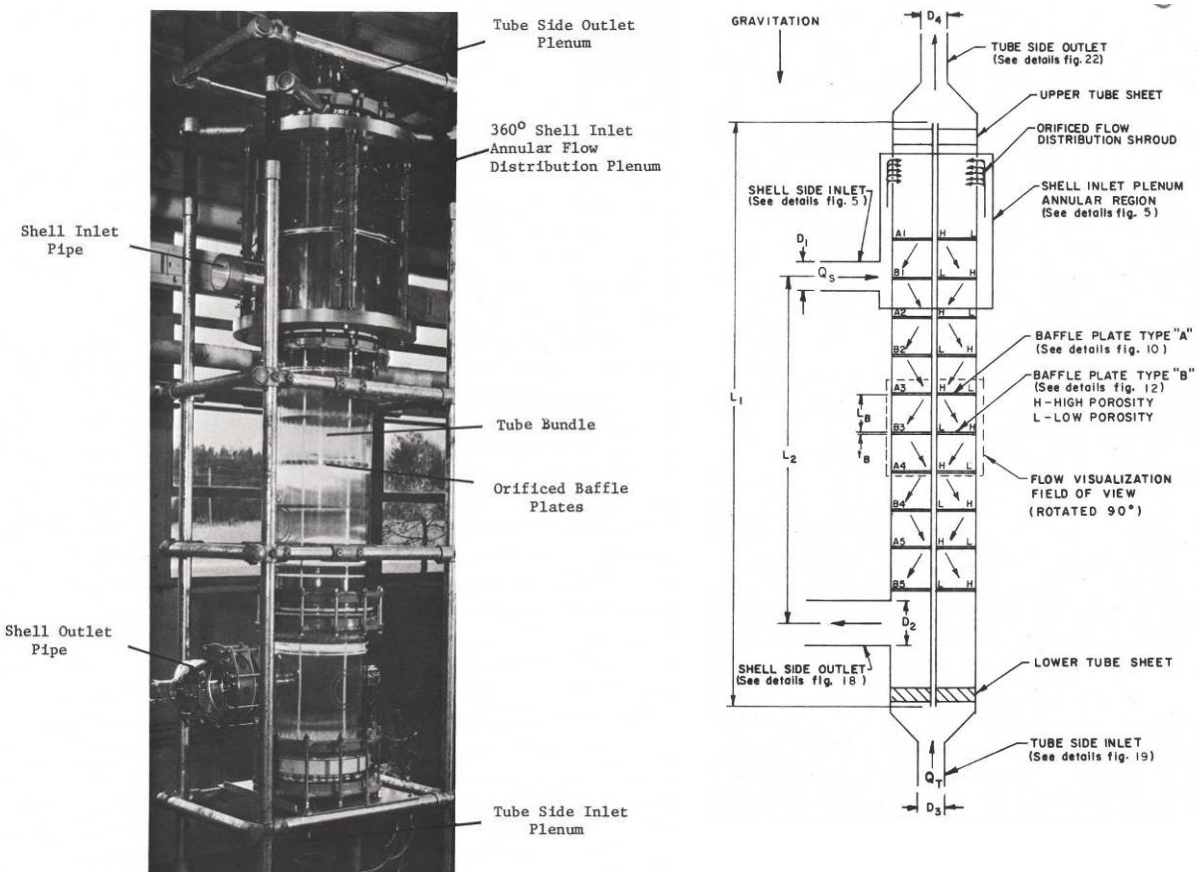

Figure 3.3-1 Photo and schematic of Argonne 360^0 glass IHX test article

The shell inlet plenum and tube bundle orificed baffles of the purchased Corning unit were reconstructed out of Lexan in order to achieve prototype LMR-IHX features. As shown in the IHX schematics of Figs. 3.3-1 and -2, the primary hot-side flow on the shell side enters the inlet pipe, flows into the annular flow-redistribution plenum, and then enters the tube-bundle shell side through an orificed flow-distribution shroud. The fluid then flows downward over the 145-tube bundle, where mixed axial/cross-flow is created by ten full-disk orificed baffle plates, as shown in Fig. 3.3-3 and then exits the tube bundle at the bottom through an outlet pipe.. The secondary flow, as shown in Fig. 3.3-4, enters the tube-side inlet pipe at the bottom of the IHX and then flows upward through a plenum region and into the tubes. The tube flow exits the tube

bundle into a plenum and leaves the plenum through a vertical outlet pipe. Figure 3.3-5 shows the extensive thermocouple instrumentation used to monitor thermal distributions during the low-flow thermal transient testing.

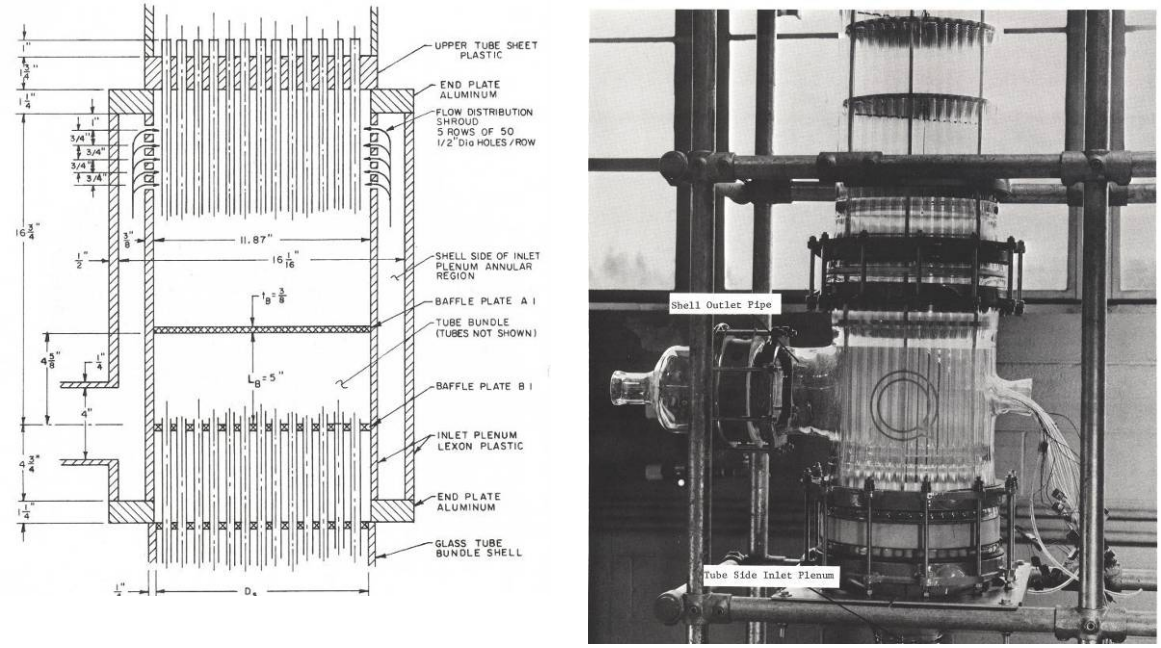

Figure 3.3-2 Primary-side flow inlet plenum (left) and outlet pipe (right) for IHX shell

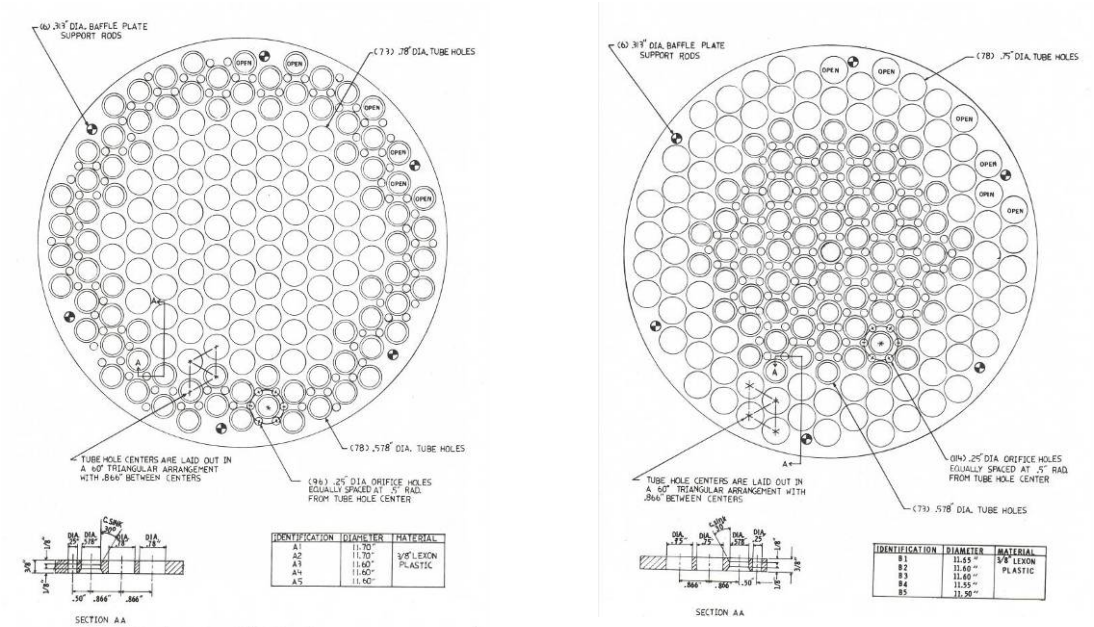

Figure 3.3-3 Flow-distribution orificed baffle plates for IHX: type A and B

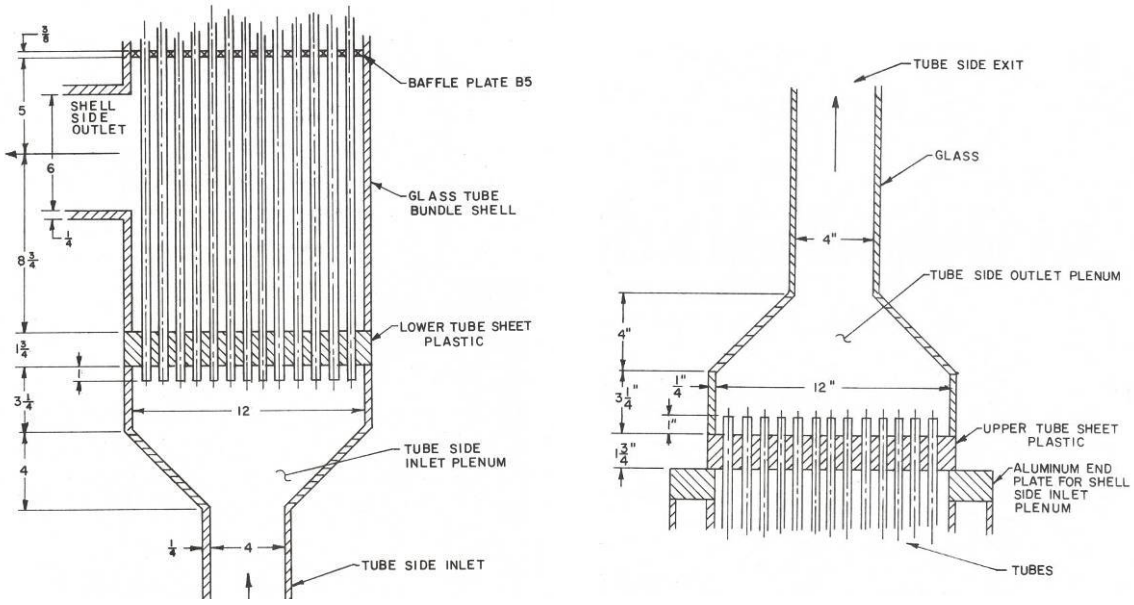

Figure 3.3-4 Secondary tube-side flow inlet region (left) and outlet region (right) for IHX

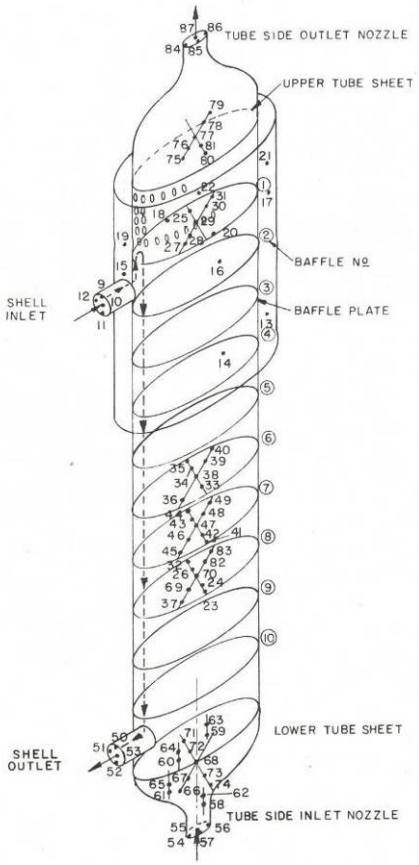

Figure 3.3-5 Thermocouple instrumentation used to monitor IHX thermal distributions during low-flow thermal transient testing

The inside diameter of the IHX shell was 11.8 in. (30 cm). The 145 glass tubes of the IHX had 0.55-in. (1.4-cm) outside diameter and a wall thickness of 0.039 in. (0.099 cm). They were laid out on a 60^0 triangular pitch with 0.87 in. (2.2 cm) between centers, yielding a pitch-to-diameter ratio of 1.58. As shown in Fig. 3.3-3, the tube bundle contained ten solid-disk orificed flow-control baffle plates of alternating type A and B spaced 5-in. (13-cm) apart and having a difference in porosity between an inner circular region of radius 3.87 in. (10 cm) and an outer annular region. This type of design induces bundle cross-flow and minimizes radial temperature variation in the tube bundle, reducing chances for differential tube elongations that stress the tube sheets. Type A baffles had an inner-region porosity of 37.2% and an outer porosity ~ 20%. Type B baffles had an inner-region porosity of 15.7% and an outer porosity of 33.5%.

3.3.2 Shell-Side Behavior in Heat Exchanger

The Argonne water experiments were conducted under low-flow scenarios for both steady-state and transient thermal operation to ascertain how thermal buoyancy can influence IHX thermal-hydraulic and structural performance.

3.3.2.1 Steady-State Thermal Buoyancy

An initial series of tests was conducted to determine the possible influence of buoyancy on the overall heat-transfer coefficient, U, of the IHX tube bundle under steady-state operation. Thermal buoyancy can influence U under low flow by altering the boundary layers on the heat transfer surfaces which then alters tube heat transfer coefficients as well as friction coefficients. This information is of interest to both LMR system analysts and IHX designers. One of the reactor transients given considerable attention is a natural-circulation event. The system behavior has been studied using 1-D thermal-hydraulic models for all the reactor-plant components in conjunction with heat-transfer coefficients, which do not account for buoyancy. Hence, errors in U associated with IHXs as well as other heat transfer devices can lead to errors in system-code prediction for the rate of decay-heat removal. The preceding is a result of the feedback effect that errors in IHX heat transfer have on predicted thermal head development and, hence, on the flow rates for heat-transport systems.

Additionally, 2-D and 3-D thermal-hydraulic codes in current use to aid design of IHXs also use empirical tube heat-transfer correlations, which neglect buoyancy. Thus, under low-flow conditions, even though these codes properly solve the conservation equations for the shell- and tube-side flows, errors can be introduced through the use of fluid/tube-wall heat-transfer coefficients that do not account for buoyancy.

Argonne IHX testing under the subject conditions was for the steady-state conditions of nominally balanced shell- and tube-side flows, $Q_s = Q_{T,}$ in the range of 14.8 m^3/h (65 gpm) to 0.91 m^3/h (4 gpm) and for nominal shell- and tube-inlet temperatures of 79°C (174°F) and 26°C (78°F), respectively. The shell- and tube-side bundle Re numbers varied from Re_S = 339

to 5815 and Re_T = 325 to 3790, respectively. For these test conditions, the bundle overall U was determined from experimental data, and its behavior with flow and varying strength of thermal buoyancy force was studied.

The tube-bundle coefficient, U, is defined by $Q = UA\Delta T_m$, where Q is the heat transferred between the shell- and tube-side fluids, A is the total effective heat-transfer area of the tube bundle, and ΔT_m is a representative temperature difference between the shell and tube fluids in the tube bundle. To calculate U from experimental data, Argonne used the standard textbook equation for a counter-flow IHX based on the assumptions of constant fluid thermal properties and U over the axial length of the tube bundle, velocity, and temperature as a function of axial location only. Negligible heat loss through the shell to the ambient was assumed. The equation used for calculating U from experimental data was

$$U = \frac{\dot{m}_T C_{PT}}{A(1-\phi)} \ln\left[1 + (1-\phi)\frac{T_{TO} - T_{TI}}{T_{SI} - T_{TO}}\right]$$

where m_T is the mass flow rate on the tube side, C_{PT} is the fluid-specific heat on the tube side, and $\varphi = (m_T C_{PT})/(m_S C_{PS})$. All fluid properties on a given side of the IHX were based on the average of the inlet and outlet temperatures for that side.

In a classical analysis (i.e. neglecting buoyancy) of IHX tube-bundle heat transfer, U is evaluated through the use of empirical correlations for the heat transfer coefficients of the inner and outer tube wall (h_T and h_S, respectively), which were used in the following equation for U:

$$U = 1/\left[\frac{A_S}{A_T}\frac{1}{h_T} + A_s \ln(r_s/r_t)/2\pi k_T L + \frac{1}{h_S}\right]$$

In the denominator, the first and last terms represent, respectively, the heat-transfer resistances of the fluid/wall interface on the tube and shell sides and the middle term the tube-wall resistance. The terms h_T and h_s are based on experimental correlations which do not account for thermal-buoyancy influences. The situation is further complicated by the fact that at the time of the Argonne studies no generally accepted criterion existed for determining when thermal buoyancy in a tube bundle becomes important to heat-transfer considerations.

Table 3.3-1 summarizes the calculated experimentally derived U values and the shell- and tube-side Richardson numbers, $Ri_S = (g\beta_S \Delta T_M D_S)/uS$ and $Ri_T = (g\beta_T \Delta T_M D_T)/(u_T)$, respectively, for each test (β is the coefficient of volumetric thermal expansion). The fluid properties in Re and Ri for a given side of the IHX were based on the average of the inlet and outlet temperatures. The characteristic lengths in Re and Ri are the tube-bundle shell and tube-side hydraulic diameters (D_s and D_T). The reference temperatures used in both Ri_s and Ri_T are the same and taken as the log mean-temperature difference, ΔT_M. The actual reference-temperature differences in Ri_s and Ri_T are most likely different and equal to their respective bulk-fluid to wall-temperature difference. However, because of buoyancy, the wall-surface temperatures on the inner- and outer-tube walls are not known and cannot be calculated by existing correlations. Thus, ΔT_M was used as the thermal-buoyancy-driving temperature difference. ΔT_M represents an upper bound on the actual shell- and tube-side thermal-buoyancy-driving temperature

differences, which individually are some fraction of ΔT_M that depends on h_s, h_T, and the tube-wall resistance.

Table 3.3-1 Summary of results from steady-state heat transfer test of IHX

Test Identifier	Re_S	Re_T	$U\left[W/(m^2{}^0C)\right]$	Ri_S	Ri_T
SHX657	5815	3790	465	0.93	.027
SHX564	4993	3319	366	1.29	.038
SHX421	3745	2503	294	2.12	.061
SHX281	2470	1738	264	4.41	.128
SHX143	1151	943	268	13.80	.432
SHX075	537	502	268	34.50	1.32
SHX046	339	325	304	58.50	2.99

Figure 3.3-6 shows a plot of U versus both Re_S and Re_T. With decreasing Re, U reaches a minimum value and then increases with further reduction in Re. In the absence of buoyancy, existing heat-transfer correlations would yield a U that does not exhibit a minimum plateau value and then increase with further reductions in Re at small Re. This behavior of U is a result of the buoyancy forces as measured by Ri becoming more and more dominant with decreasing Re, relative to the viscous and inertial forces in the shell- and tube-side flows, as the flow is reduced.

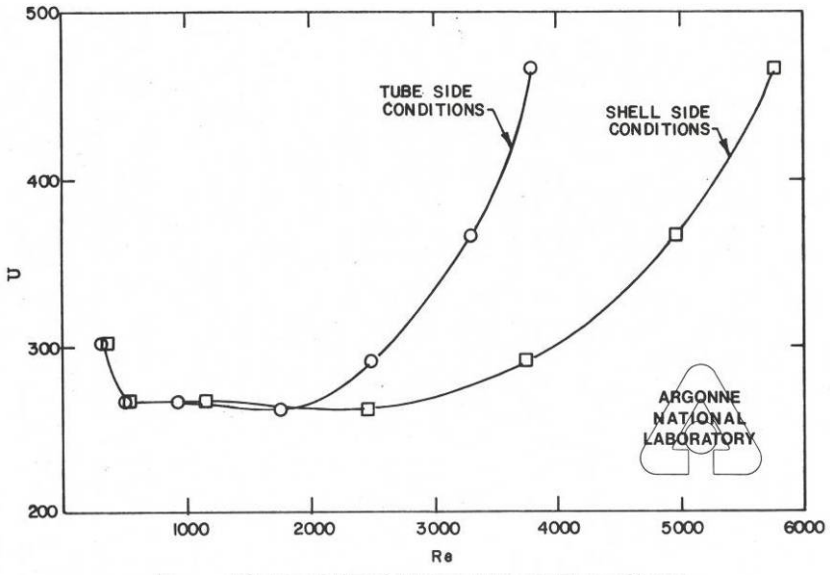

Figure 3.3-6 Influence of thermal buoyancy forces on overall heat transfer coefficient U of IHX

The influence of thermal buoyancy on tube heat transfer as discussed next is even more complex because multiple tube interactions are possible, as is the case for IHXs. As a result of the vertical orientation of the IHX, and the fact that the cooling primary shell-side flow is downward and the heated tube-side flow is upward, the buoyancy forces acting on the fluid-boundary layers on both the tube outer and inner surfaces, when large enough, can enhance the overall heat transfer by individually increasing the shell- and tube-side heat-transfer coefficients. For example, at the tube inner surfaces, the fluid near the wall is warmer than that at the center. Hence, if the buoyancy forces are of sufficient magnitude, the fluid will be buoyed upward near the tube wall, altering the near-wall velocity. Because the buoyancy forces act in the same direction as the tube-side mean flow, the wall heat-transfer coefficient is increased as a result of an increase in the near-wall fluid velocity. Note that the IHX heat-transfer data, when compared with available empirical correlations on non-buoyancy heat transfer, show less heat transfer than indicated by the correlations for conditions of negligible-to-moderate buoyancy forces. However, under conditions of large buoyancy forces, the IHX heat transfer is larger than that predicted by heat-transfer correlations neglecting buoyancy. This behavior is similar to that uncovered by Petukhov [1] in his studies of heat transfer for a single vertical tube.

For a complex piece of equipment like a heat exchanger, it is not readily apparent that Ri must necessarily increase with reducing shell- and tube-side flows. For example, under the conditions of $Q_S = Q_T$, ΔT_M decreases as the flow rate through the IHX is reduced. Hence, for Ri, which is proportional to $\Delta T_M/Q^2$, to increase with decreasing IHX flow, ΔT_M must decrease at a lower rate than $1/Q^2$ increases. Indeed, Table 3.3-1 shows that the data do exhibit increasing Ri as the flow is reduced, and Ri_S and Ri_T do attain values greater than 1. The behavior of Ri with decreasing flow will depend on IHX geometry and fluid type, as well as on Re. This type of behavior needs to be studied in more detail along with sodium testing to assess the influence of the Peclet number on the heat transfer behavior on the tube surfaces.

Thus, under low-flow levels, even under conditions of steady-state flow and coolant temperature, thermal buoyancy can alter the convection-flow heat transfer film coefficients on the tube surfaces, causing a departure in overall heat transfer predicted across the heat exchanger tube bundle. This departure has the potential for causing significant errors in 1-D models of IHXs and the resulting predicted system behavior.

Under steady-state IHX operation, Argonne also showed that the outlet-pipe plenums can exhibit thermal stratification. As shown in Fig. 3.3-7, the thermal distributions in the shell-outlet pipe for the steady-state testing used to explore U behavior exhibited a large top-to-bottom temperature difference, T_{SOT} - T_{SOB}. This asymmetry in the outlet-pipe thermal distribution has the potential for producing significant pipe-nozzle structural stresses.

The exit-pipe stratification was correlated in terms of the Richardson number $Ri_{DSO} = [g\beta D_{SO} (T_{SO} - T_{TI})/u_{SO}^2]$, where β is the coefficient of volumetric thermal expansion, D_{SO} is the exit-pipe diameter, and U_{SO} is the mean velocity in the exit pipe. Clearly, the stratification correlates with Ri_{DSO} and reaches 99% of the maximum temperature difference possible at $Ri_{DSO} = 39$. Although the data have been correlated for the present geometry, the subject phenomenon is so complex that additional study will be required to establish whether the reference length (D_{so})

and velocity (U_{so}) chosen for Ri are the best choices. Additionally, there are most likely other parameters, representing at a minimum the characterization of the geometry in the lower tube bundle, which exert an influence over this phenomenon and which must be studied.

The preceding phenomenon is the result of the formation of a geometry-induced, large, nearly stagnant flow-recirculation zone in the tube-bundle region on the lower shell side adjacent to the shell outlet pipe (see inset in Fig. 3.3-7). This recirculation zone is a result of the shell flow turning 90° to leave the IHX through the side of the shell. Note that even for an IHX design with a central down-comer pipe and multiple ports for circumferential shell exit flow, a recirculation zone in the shape of a toroid centered about the down-comer would exist. These recirculation zones are present even under isothermal conditions.

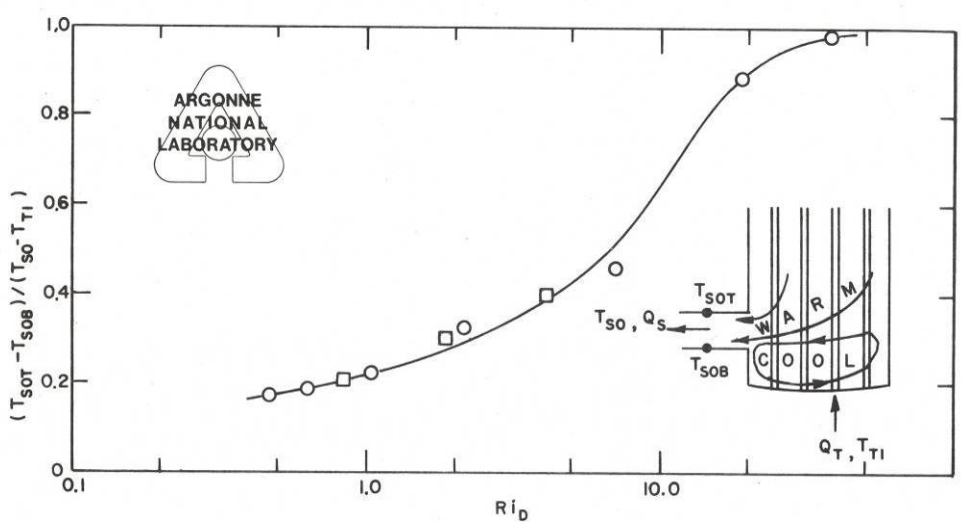

Figure 3.3-7 Steady-state IHX shell outlet pipe normalized stratification top-to-bottom temperature difference versus Richardson number Ri_D

Under steady-state non-isothermal conditions, a large temperature difference can exist between the cooler fluid within the recirculation zone and the hotter main flow, even under high-flow conditions. However, under low-flow conditions, as a result of the large temperature differences, buoyancy forces cause alteration of the shape of the recirculation zone, and stratified flow can spill out into the outlet piping, producing possible thermal-stress problems in the outlet as well as in the tube bundle. In conclusion,, even under steady-state IHX operation, thermal-buoyancy conditions may cause problems under low-flow operation. This situation would be further aggravated when a plant-produced thermal transient flow passes through the IHX shell [14].

Note that the preceding phenomenon constitutes a situation of significant complexity for the new generation of 3-D thermal-hydraulic computer codes. The phenomenon encompasses nearly all the major modeling uncertainties that still exist. Specifically, modeling the transport of momentum and heat across the shear zone separating the recirculation zone and the main shell bypass stream involves many of the uncertainties present in turbulent modeling. The problem is further complicated by the presence of the tube-bundle structure and the uncertainties related to the lack of knowledge concerning the heat transfer between the tubes

and the shell fluid. The entire problem is additionally complicated by the presence of significant buoyancy forces, the influence of which has not been adequately factored into turbulent transport models. The preceding problem area is a recommended topic for additional fundamental study and for the development of a validated 3-D computational CFD code.

3.3.2.2 Thermal-Transient Induced Buoyancy

In this section, thermal-transient-induced buoyancy phenomena are discussed as presented in Ref. [3]. A fairly extensive series of transient tests was performed on the IHX. These tests involved equal and constant shell- and tube-side inlet flows ($Q_S = Q_T$) with a linear-down-ramp thermal transient superimposed on the shell-side inlet flow of duration t_t, with constant temperature flow into the tube-side inlet flow. The thermal-down-ramp transient on the shell side of an IHX is of considerable interest because this transient puts cooler flow on top of warm flow for a period of time. Because of buoyancy forces, this is potentially an unstable configuration. Prior to initiation of the thermal transient, the IHX was in thermal-hydraulic equilibrium. Data were recorded long enough after the passage of thermal transient to allow the IHX to reach final equilibrium state.

To illustrate the various buoyancy-induced phenomena that can occur in the tube bundle, data for test TX1410 are presented. Figures 3.3-8 and -9 show the behavior of the shell-side and tube-side inlet temperatures and radial temperature variation within the shell-side of the tube bundle, respectively, during the transient as a function of time. Q_S and Q_T are approximately equal and constant for the duration of the test (= 14.75 gpm). $T_{TI} = 25^oC$ for the test duration, and T_{SI} undergoes an approximately linear decrease from 80°C to 40°C in a time of 29.1 sec. Hence, the thermal down-ramp rate was K = -1.33°C/s.

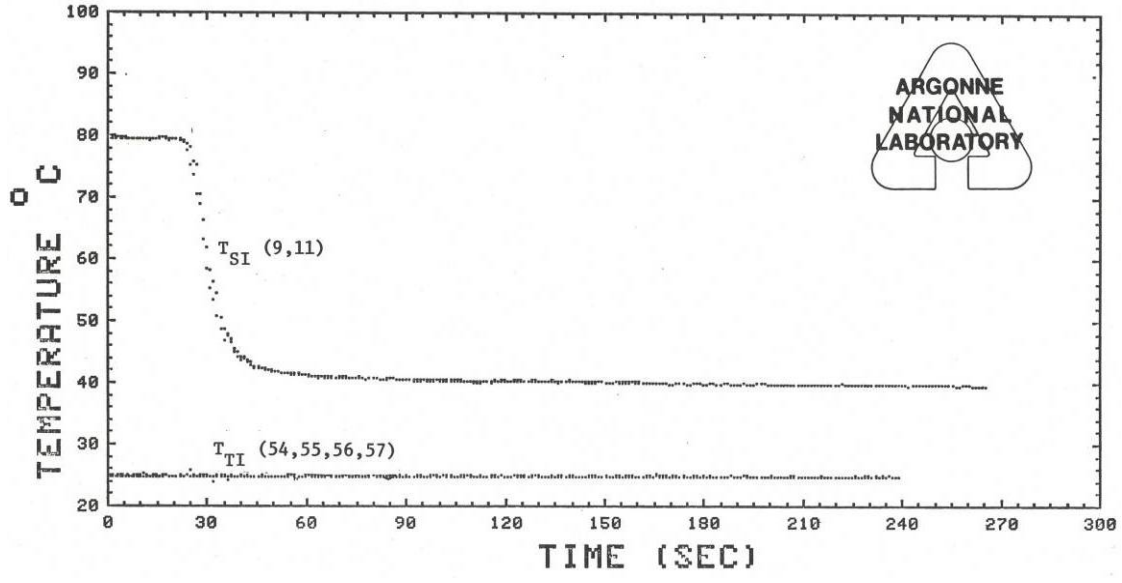

Figure 3.3-8 Shell- (T_{SI}) and tube-side (T_{TI}) inlet temperatures of IHX during transient test TX1410

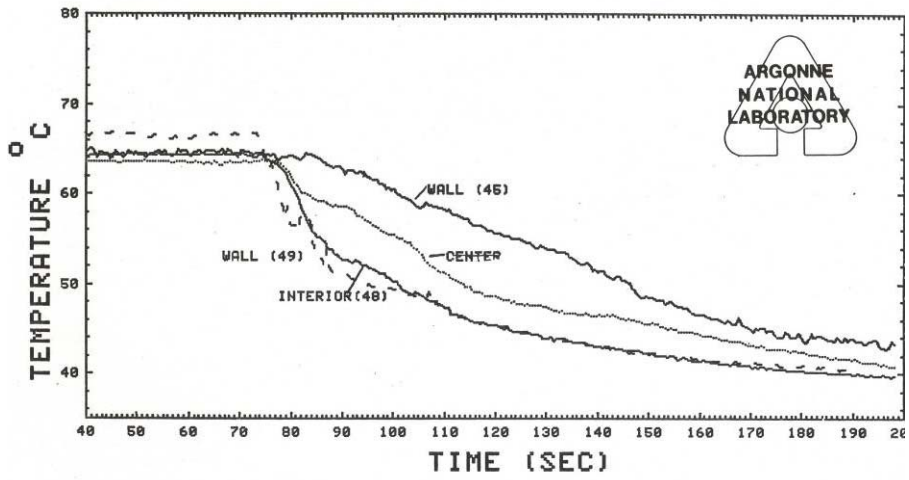

Figure 3.3-9 Radial temperature variation in IHX shell-side tube bundle at baffle location A4, Test TX1410

As shown in Fig. 3.3-9, after the thermal front reached baffle axial location A4 (see Fig. 3.3-1) and during the approach to final steady state, large radial-temperature variations develop across the bundle. At this baffle axial location, the radial variation in temperature across the tube bundle reached 12°C, which is nearly 50% of the temporal change in mean temperature that occurred at this location as a result of the thermal transient passing through the heat-exchanger shell. This radial temperature variation existed over a significant portion of the total bundle tube length. Before the transient, the steady-state radial variation in temperature at location A4 was only a couple of degrees. Furthermore, the tube-bundle thermal distribution does not remain axi-symmetrical during the transient. The preceding growth of radial-temperature variation in the tube bundle during the transient, if large enough and lasting for sufficient time, can promote tube-stress problems.

Flow visualization using a plane of laser light that passed through the glass IHX test article in conjunction with seeding of the flow with neutrally buoyant fluorescent beads (tuned to the laser illumination) was used to delineate shell-side flow patterns between baffle plates during the testing. Figures 3.3-10 and -11 for test TX1410 show, respectively, the flow patterns for the shell-side tube bundle in a vertical laser plane slice before initiation of the shell thermal transient and during the transient when large thermal buoyancy forces were created.

The photograph in Fig. 3.3-10 was taken with a 3-sec exposure, causing the tracer particles to show up as streak lines. A high level of flow detail is depicted. The mixed axial/cross-flow created by the alternating A- and B-type orificed baffles is shown. After the flow passes through baffle A3 (high porosity in the center and low in the peripheral region), the flow expands radially outward in the tube bundle as it approaches baffle B3 (low porosity in the center and high in the peripheral region). After the flow leaves baffle B3, it moves radially inward as it approaches baffle A4, which completes the repetitive characteristic flow pattern created by the A- and B-type baffles. Small flow-recirculation zones are also shown immediately downstream of each A- and B-type baffle in the peripheral region of the tube bundle. In three dimensions, the recirculation zones are toroidal. The direction of recirculation is different for the A- and B-type baffles. Under the A-type baffles the flow at the inner surface of the toroid (i.e., nearest the center of the tube bundle) is in the bundle mean-flow direction

and upward at the shell side of the toroid, whereas for the B-type baffles the recirculation flow opposes the mean flow at the inner toroid surface and is downward at the shell side of the toroid. The preceding behavior is explainable in terms of the flow mechanism producing the recirculation zones. The recirculation zones are produced by the shear layer, which exists at the "high"- and "low"-velocity interface downstream of the baffle plates. Thus, when thermal buoyancy is not present before the start of the thermal transient, good cross flow is created by the perforated baffle plates, with only a very small recirculation zone under each baffle. Also important, a radial component of flow is induced by the baffles across the tubes, which minimizes cross-bundle radial temperature gradients.

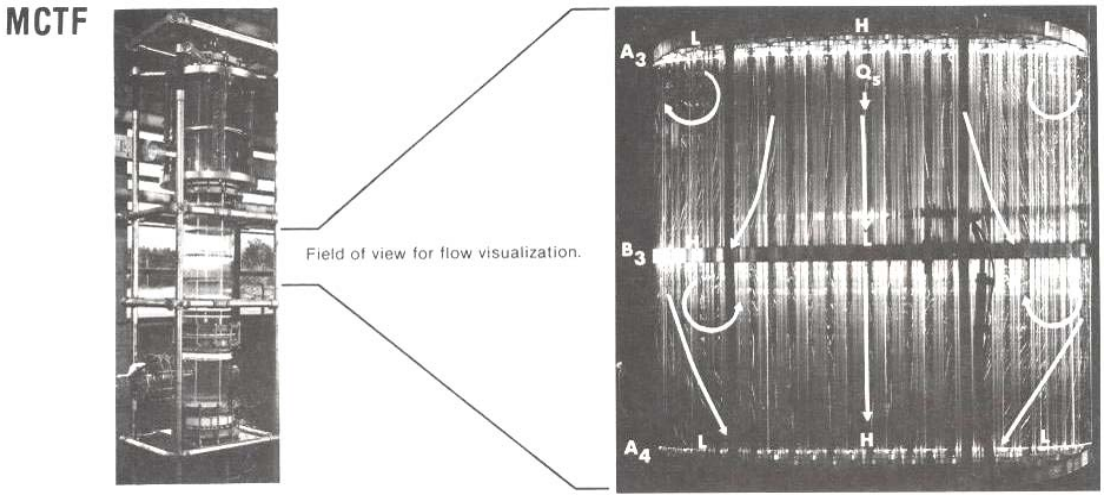

Figure 3.3-10 IHX tube bundle shell-side pre-transient flow pattern in the absence of thermal buoyancy for test TX1410

Figure 3.3-11 shows the IHX inlet thermal down-ramp transient induced flow channeling down the center of the shell-side of the tube bundle. This behavior is produced by strong thermal buoyancy forces and causes dramatic breakdown of the effectiveness of the orificed flow-distribution baffle plates. It also creates large radial temperature gradients in the tube bundle (Fig. 3.3-9) and stresses in the IHX structure.

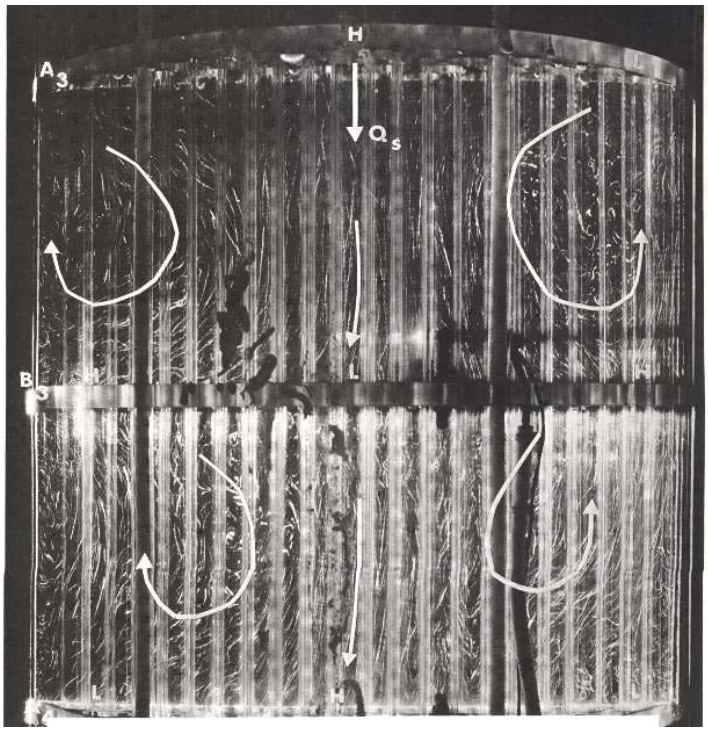

Figure 3.3-11 IHX tube bundle shell-side flow pattern during a thermal transient producing strong thermal buoyancy forces for test TX1410.and extensive flow channeling and eddies

Thermal buoyancy was also shown to influence the flow behavior in the shell-inlet plenums of IHXs. For test TX1410 the thermal distribution in the shell-inlet annular flow-redistribution plenum at the bottom, middle, and top exhibited considerable circumferential variation in temperature at the three elevations during the transient. For this transient, the buoyancy forces were strong enough to cause the incoming cooler fluid to stratify and fill the annular plenum from the bottom upward with a fairly distinct stratified interface moving upward. This buoyancy-induced behavior causes the flow and thermal distribution of the flow entering the tube bundle to undergo changes for a period of time during the transient. Because the thermal-hydraulic conditions at the tube-bundle inlet are no longer circumferentially uniform during the transient, due to the buoyancy, the inlet-plenum and tube-bundle regions can no longer be treated as separate regions when being analyzed. The extent of the interaction will depend on the strength of the buoyancy forces developed in the shell-inlet plenum and in the bundle itself if feedback occurs between the two regions. Note that currently most thermal-hydraulic 2-D and 3-D codes treat the analysis of the annular plenum and tube bundle as two separate problems and assume circumferential symmetry of flow and temperature as the boundary condition connecting the two regions.

Argonne also found that flow channeling through an IHX tube bundle can be aggravated by buoyancy-induced failure of the shell annular-inlet plenum to continue to circumferentially supply a flow of uniform temperature to the entrance of the tube bundle. Figures 3.3-10 and -11 show very vividly for this thermal-transient test with constant mean flow (TX1410) the manner in which thermal-buoyancy forces induced in a flow field by a thermal-down-ramp transient can influence the flow and thermal distribution on the shell side of the tube bundle. The

thermal-down-ramp transient, when severe enough, by producing cool fluid on top of warm fluid, induces density gradients in the flow field. When of sufficient magnitude, these density gradients create gravitational buoyancy forces that strongly couple the governing fluid momentum and energy equations. As a result, variations occur in the flow patterns and, in turn, the temperature field during the transient. When the buoyancy forces are not of sufficient strength, the momentum and energy equations are essentially uncoupled, and the thermal transient passes through the IHX without producing any change in flow pattern or adverse radial-temperature variation under constant mean-flow conditions.

The thermal head developed in a vertical-orientated IHX and its temporal behavior are important to the dynamic system analysis of the LMR. Under various plant transients, such as the natural-circulation event, the thermal head drives the flow in the reactor circuits. If the thermal head in an IHX is inadequately predicted by the currently used 1-D thermal-hydraulic system models, then errors will result in predicted flow rates and possibly in decay heat removal. The acceleration of the flow through the tube bundle causes the thermal disturbance initiated at the shell inlet to travel faster through the tube bundle than would be indicated by a 1-D thermal-hydraulic model. A 1-D model would overestimate the thermal-disturbance transit time through the heat exchanger and, as a consequence, wrongly predict the axial temperature distribution through the IHX. The preceding would further manifest itself by causing uncertainties in the shell-to-tube-side heat transfer predicted by the 1-D model and in the thermal-density head developed in the vertical IHX, which, in turn, can influence the flow rate established in the reactor circuits under natural circulation. Note that because flow channeling reduces the area in the tube bundle available for transferring heat, the effect is to also reduce the net heat transfer during a thermal-down-ramp transient on the shell side of the IHX.

Because of the importance of being able to correctly use 1-D models of the IHX, Argonne compared predictions of a 1-D front or slug-based IHX model for transit time of a thermal front moving through the IHX tube bundle with the test results for transport time. These comparisons furnished preliminary guidelines as to the importance of thermal buoyancy phenomena in making 1-D thermal-hydraulic predictions. A similar procedure was used in the Argonne pipe-stratification studies discussed in Section 3.1, which yielded criteria for assessing when 1-D pipe models start to break down due to thermal buoyancy.

The 1-D slug model of the shell flow was based on the following assumptions. On the shell side of the tube bundle, the fluid velocity was assumed to be constant and equal to the flow rate Q_S divided by the cross-sectional flow area. Based on a 1-D slug flow, the shell-flow transit time is given by

$$t_{F(1-D)}\ [s] = 1470.7/Q_S\ [gpm].$$

Test TX1410 had constant flow during the thermal transient, Q_S = 14.75 gpm. Hence, $t_{F(1-D)}$ = 99.7 sec. The flow transit time of the thermal transient from the inlet to the outlet of the IHX for test TX1410 was $t_{F(EXP)}$ = 71.4 sec. Thus, the thermal transient travels faster through the IHX shell than is predicted by the 1-D model. The preceding is a result of the buoyancy-force-induced flow channeling discussed earlier. As a measure of the degree of channeling, the transit time error parameter, $[t_{F(1-D)} - t_{F(EXP)}] / t_{F(EXP)}$, was computed for each test. For test TX1410, $[t_{F(1-D)} - t_{F(EXP)}] / t_{F(EXP)} = 0.396$.

Argonne established that $[t_{F(1\text{-}D)} - t_{F(EXP)}]/t_{F(EXP)}$ could be correlated in terms of the flow rate, thermal-transient characteristics, and tube-bundle geometry over the range of conditions explored in terms of a buoyant-to-viscous force ratio. The correlation parameter is given by $Ri_{LB}\ Re_{DH}$, the product of the Richardson and Reynolds numbers, where $Ri_{LB} = (g\beta L_B \Delta T_B)/u^2$ and $Re_{DH} = u\ D_H/\upsilon$. Hence, $Ri_{LB}\ Re_{DH} = (g\beta L_B D_H \Delta T_B)/\upsilon u$, where β and υ are, respectively, the coefficient of volumetric thermal expansion and the kinematic viscosity of the fluid, L_B is the axial distance between adjacent baffle plates, D_H is the hydraulic diameter of the shell-side tube bundle, ΔT_B is the maximum-occurring temperature difference between two adjacent baffle plates based on the thermal-transient characteristics at the shell inlet and 1-D slug flow in the tube bundle, and u is the mean axial velocity of the shell-side tube bundle. The fluid properties are evaluated at the average of the shell inlet and outlet temperatures before the start of the transient. For test TX1410, $Ri_{LB} = 40.5$ and $Re_{DH} = 1191$. Hence, $Ri_{LB}\ Re_{DH} = 48{,}213$. Figure 3.3-12 shows a plot of IHX transit time error for the 1-D model using this correlation parameter.

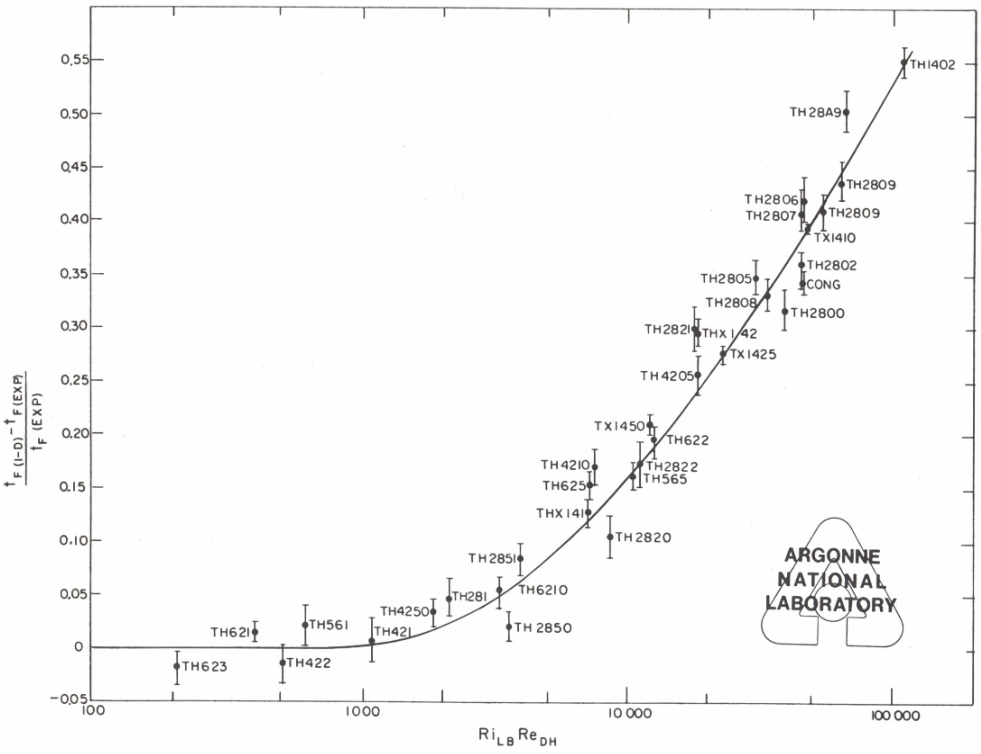

Figure 3.3-12 Plot of transit-time error with 1-D model caused by flow channeling induced by thermal buoyancy in the IHX shell-side during thermal down-ramps correlated with the Argonne thermal buoyancy parameter

As shown in Fig. 3.3-12, below $Ri_{LB}\ Re_{DH} = 800$, $[t_{F(1\text{-}D)} - t_{F(EXP)}]/t_{EXP} = 0$, and the flow channeling is insignificant, with the flow moving through the shell effectively as a slug. Under these conditions, the 1-D slug model of the thermal-hydraulic behavior yields a good prediction

of the transit time, $T_{f(EXP)}$. The preceding assumes that the shell-side design is adequate relative to effectively achieving 1-D flow under insignificant buoyancy forces. Furthermore, when Ri_{LB} Re_{DH} <800, the radial temperature variation across the tube bundle is minimal, and 1-D model predictions of the thermal-density head developed in the vertical IHX should be valid.

Above Ri_{LB} Re_{DH} = 800, $[t_{F(1\text{-}D)} - t_{F(EXP)}]/t_{EXP}$ increases continuously with increasing Ri_{LB} Re_{DH}. At the upper limit of investigation, Ri_{LB} Re_{DH} = 110,000, $[t_{F(1\text{-}D)} - t_{F(EXP)}]/t_{EXP}$ = 0.6. Under this condition, strong thermal-buoyancy forces relative to the viscous forces are induced into the flow field by the thermal-down-ramp transient, and significant flow channeling occurs. The thermal-transient disturbance convected into the shell of the IHX travels much faster through the shell than is predicted by a 1-D model, and the radial temperature variation across the tube bundle increases considerably during the flow-channeling period, and thus 1-D models of thermal-density head and heat transfer would be in significant error.

3.3.2.3 Summary

The correlation just presented for thermal-buoyancy-induced flow channeling is unique. Before Argonne studies there was, for the most part, not even qualitative appreciation of this phenomenon. This correlation, however, still has important uncertainties associated with it. For example, the characteristic length used in Ri_{LB} is the distance between adjacent baffle plates, L_B. In the subject tests, tube-bundle geometry such as baffle plate design and tube spacing were not varied as a check on the appropriateness of L_B. Additionally, the influence of the large difference between water and sodium thermal conductivity on the developed correlation must be assessed in order to establish how conservative the correlation is when used to extrapolate to sodium. Nevertheless, it is felt that the correlation can be helpful in making a scoping estimate of the tendency for flow channeling to occur in vertical-oriented LMR heat exchangers and steam generators. In Section 3.4, additional data are provided from Argonne steam generator testing.

The Argonne studies under low flow also raise additional questions about the design process used to achieve a “good” tube-bundle design. In the design of IHXs and also steam generators, one of the design objectives is to minimize the radial temperature variation in the tube bundle, which, in turn, minimizes tube/structural stress concerns. The geometry used to achieve this objective frequently involves (i) a shell-inlet annular plenum having an orificed shroud to promote circumferential uniformity of the flow entering the tube bundle and (ii) tube-bundle baffles for promoting mixed axial/cross-flow over the tubes.

Currently, the design process of optimizing the two preceding IHX geometric features is based mainly on testing in conjunction with trial-and-error manipulation of test-article geometry. The testing is usually performed under isothermal steady-flow conditions, and the inlet plenum and tube bundle are frequently tested as separate articles. The logic employed when using separate inlet-plenum and tube-bundle test articles is that, if uniform flow exiting from the inlet plenum can be achieved through plenum-shroud porosity distribution design in the absence of a simulation of downstream tube-bundle resistance, then the tendency for flow uniformity will be enhanced in the final component due to the downstream flow resistance of the tube bundle. The

previous assumption is correct under steady-state operation of the IHX; however, there are two shortcomings of this approach. First, this procedure does not account for thermal-hydraulic behavior under low-flow thermal-transient conditions, as presented in this section. This condition is conducive to thermal-buoyant-force alteration of the "as designed" flow and thermal distributions. Second, using the porosity-induced flow resistance in the shell-inlet plenum orifice as a sole means of achieving uniformity of flow to the tube-bundle entrance promotes a high-pressure-drop IHX design and possible tube-vibration concerns resulting from the high-velocity orifice jets impacting the tubes.

The data just presented, under steady state conditions prior to initiation of the thermal transient, exhibited a fairly uniform radial temperature distribution in the tube bundle, in spite of the fact that the flow distribution shroud to the shell inlet plenum employed uniform porosity, rather than a circumferential variation. The shroud porosity was 35%. Hence, it appears that the downstream flow resistance in the tube bundle plays a strong role in smoothing out flow asymmetries which may be present in the tube-bundle entrant flow. The role of downstream flow resistance in reducing entrant flow asymmetries is not well understood and constitutes an area of further needed investigation. The benefit from this type of study would be a IHX design with lower pressure drop and a design that maintains good flow distribution even when strong thermal buoyancy forces are present during plant transients.

3.3.3 Tube-Side Buoyancy-Induced Instabilities in Heat Exchanger

Section 3.3.2 discussed the importance of thermal buoyancy to the shell-side flow and thermal behavior of an IHX. This section discusses how thermal transients under low-flow conditions entering the tube side of an IHX can cause parallel channel flow instabilities.

In Ref. [2] analytical modeling and sample calculations were presented by Argonne to show that during low-flow episodes accompanied by inlet thermal transients, LMR heat exchanger tube bundles may experience a form of parallel channel instability induced by thermal buoyancy in the tube-side flow, which could lead to significant flow “mal-distribution” among the tubes. One facet of this study addressed tube-bundle flow instability with respect to a continuous perturbation associated with the relative advance/delay of fluid entry into various sub-geometric regions of the tube-bundle inlet. This advance/delay phenomenon was found to possess the potential for producing extensive flow mal-distribution during complicated inlet thermal transients. On the basis of typical thermal transients at the IHX inlet predicted by 1-D system dynamic energy transport codes for LMRs, Argonne showed that the flow mal-distribution as represented by variations in tube flow velocity over the tube-bundle cross section may reach the same order of magnitude as the mean flow velocity. Although the study was based on a linearized analysis, not valid for large relative velocities, the results should be a conservative indicator for estimating the tendency of IHXs to develop tube-side flow mal-distributions and/or instabilities.

When a bank of parallel, vertical heat-exchanger tubes, as shown in Fig. 3.3-13, is subjected to an inlet thermal transient during some period of time, lighter warm fluid may lie under denser cold fluid. Such a condition leads to a form of buoyancy-induced flow instability that can result

in flow mal-distribution among tubes. Under certain circumstances, flow oscillations or even reversals may also occur. It should be noted that a somewhat analogous, but more complicated phenomena can occur in fuel rod bundles. The possibility that this thermal-hydraulic behavior may lead to unacceptable thermal stressing of the heat exchangers used in LMRs or departures from anticipated performance was the motivation for the study.

The possible existence of such phenomenon can be illustrated by the following two simple examples. Consider a bank of tubes as shown in Fig. 3.3-13, with a common inlet manifold at the bottom and a common exit manifold at the top. It is assumed that the total flow Q is constant for all time, and that the inlet temperature $T_i(t)$ has been constant for $t < 0$ and increases monotonically for $t > 0$. Two possible origins for flow "perturbation," which refers to departures from the steady, uniform average flow velocity, were considered in Ref. [2]. One of these perturbations, which is associated with a continuously disturbed tube-bundle entrance, is described next.

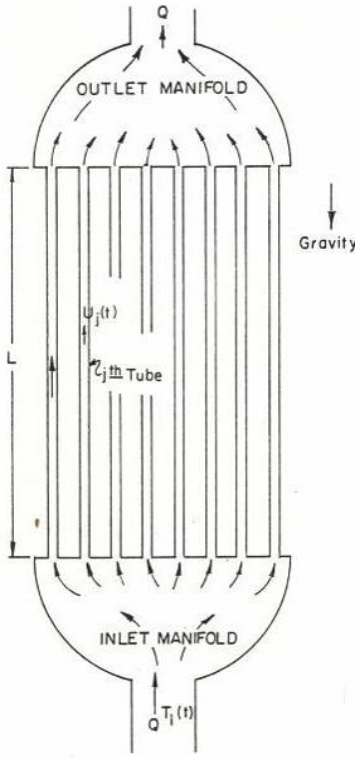

Figure 3.3-13 Schematic of parallel-channel flow system forming the tube side of vertical IHX

3.3.3.1 Continuously Disturbed System

In a typical heat exchanger, there is likely to be some delay between the time the fluid enters the tube-side inlet manifold and the time it enters a tube, as shown in Fig. 3.3-14 for two inlet manifold designs. Furthermore, the delay is expected to vary from tube to tube. During a temperature-rise episode, tubes with a shorter-than-average entrance delay will continuously

get warmer fluid than their neighbors and, consequently, will develop a higher velocity because of the upward higher buoyancy force. The increased velocity, of course, will further aggravate the situation by drawing additional warmer fluid into the tube.

The study of tube-side flow instability in two-phase (boiling) flows has been extensive [15-18]. However, few investigators have studied the case of a single-phase fluid with a continuously variable temperature dependent on density. This case was addressed by Argonne [2]. The origin of the instability is the positive feedback between increased tube flow velocity and increased buoyancy force from the entering warmer fluid. A measure of the severity of this feedback process is the Richardson number R, defined as:

$$R = \frac{g\beta\Delta T\, L}{u_o^2}$$

where L is the tube length, ΔT is the imposed temperature difference, β is the volumetric thermal expansion coefficient of the fluid, and U_o is the fluid velocity. The Richardson number represents the ratio of thermal buoyancy to inertia forces acting on the flow and was estimated to be of the order of $10^2 - 10^3$ for IHXs under typical reduced flow conditions associated with pump coast-down.

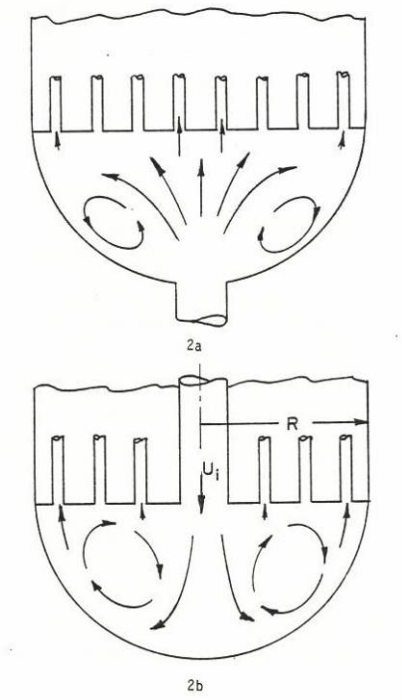

Figure 3.3-14 Relationship between the tube-bundle entrance delay/advance and the flow pattern in the IHX inlet manifold: (2a) without down-comer and (2b) with down-comer

An important delineated mechanism which triggers this type of instability is the variations of the time delay δ between coolant entry into the inlet plenum and coolant entry into various tube-inlet sub-regions, as shown in Fig. 3.3-14, for two inlet manifold designs. A dimensionless measure of the variation is α, the entry-time advance/delay parameter given by

$$\alpha \equiv (\bar{\delta} - \delta_i) u_o / L$$

The order of magnitude of α for typical heat exchangers has been estimated to be 10^{-1}–10^{-2}.

For typical thermal-hydraulic conditions and prevailing IHX designs, the pressure drop through individual tubes under low flow conditions was shown to have very little influence on the instability. The pressure drop effects were expressed through a damping parameter γ defined by

$$\gamma = K \left[2 C_f \frac{L}{D} + \frac{1}{2} C_L \right]$$

where K is a constant lying between 1 and 1.8 and C_f and C_L are the tube frictional and entrance loss coefficients respectively. For typical IHXs, $10 < \gamma < 20$.

The severity of the flow mal-distribution/instability oscillations generated in the tube bundle was expressed through the dimensionless perturbation velocity parameter defined by

$$\frac{\hat{u}(\tau)}{u_o} \sim \alpha\, G(\tau)$$

where G(τ) was evaluated for a number of design-basis IHX transients. Values of G(τ) as high as 104 were obtained, indicating that the velocity perturbation on the basis of linear theory and neglecting tube-to-primary side heat transfer could be many times higher than the mean tube flow velocity u_o.

Based on the above analysis, the following expression was found to provide an easy-to-use semi-quantitative estimate of the tendency for tube-bundle flow instability:

$$\ln (G_{max}) \sim R^{1/2}\, \Delta\tau_u \quad \text{if } \gamma^2/4R << 1$$

where $\Delta\tau_u$ is the duration of the unstable episode in dimensionless time units ($\Delta\tau_u = \Delta t_u\, u_o/L$). This approximate result also indicates that for systems with large R, increasing the pressure drop through the tube bundle would have little effect on mitigating the instability unless γ is increased to an order of $(4R)^{1/2}$.

3.3.3.2 Summary

While nonlinear effects were neglected in the analysis and will certainly alter these results, the possibility of instabilities being generated in the tube-side of vertical IHX tube bundles under low flow during thermal-ramp-up transients should be considered in more detail.

Furthermore, the above results were obtained under the assumption of negligible tube heat transfer. Using physical arguments, Argonne estimated that the effect of heat transfer would be to moderate the instability. However, whether the instability can be moderated sufficiently to prevent large flow mal-distributions and oscillations cannot be answered without a more refined analysis.

The above results clearly point out the potential importance of the instability phenomenon and the need for better understanding of the problem. In this connection, the consideration of heat transfer effects is particularly important. Finally, experiments on vertical tube bundles in water and with sodium to study the role of heat transfer in mitigating instabilities during low-flow thermal transients should be conducted to verify the theoretical conclusions.

References

1. Kasza, K.E., Chen, M.M., and Binder, M.J., "Initial Considerations on the Influence of Thermal Buoyancy on Heat Exchanger Performance," ANL-CT-78-47 (August 1978).

2. Kasza, K.E., and Chen, M.M., "Tube Bundle/Tube Side (Parallel Channel) Thermal Buoyancy Induced Flow Mal-distribution and Instability during Thermal Transients," ANL-CT-80-9 (December 1979).

3. Kasza, K.E., Bobis, J.P., Lawrence, W.P., and Kuzay, T.M., "Heat-Exchanger Thermal - Buoyancy Effects: Design and Performance Comments (Phase I)," ANL-CT-81-31 (Apri1 1982).

4. Foster Wheeler Corporation, ND/74/59, Issue 2 (November 12, 1974).

5. Wolowodiuk, W., "Development of Intermediate Heat Exchanger for Liquid Metal Fast Breeder Reactor Plants," Foster Wheeler Energy Corporation (May 11, 1976).

6. Foster Wheeler Corporation, ND/74/32 (July 15, 1974).

7. Foster Wheeler Energy Corporation, ND/76/14 (May 7, 1976).

8. Foster Wheeler Energy Corporation, ND/76/40 (July 30, 1976).

9. General Electric Company, GEFR-00099 (June 1977).

10. Combustion Engineering, CENC 1304 (September 30, 1977).

11. Westinghouse Electric Corporation, "ERDA-EPRI LMFBR Design Projects, Phase II, Final Report," Vol. B1, PLBR Design Characteristics (June 1977).

12. Rockwell International, Burns and Roe, Inc., FBR-77-3, Vol. II (May 1977).

13. Lorenz, J. J., et al., "Influence of Size Scale and Fluid Thermal Properties in Simulating LMFBR Outlet Plenum Behavior," AIChE Symp., *73*, 120 (1977).

14. Oras, J.J., and Kasza, K.E., "Mitigation of Thermal Transients by Tube Bundle Inlet Plenum Design," Trans. Am. Nucl. Soc., Vol. 46 (1984).

15. Ledinegg, M., "Instability of Flow during Natural and Forced Circulation," Die Warme, *61*, 891-898 (1938): Translation: AEC-TR-1861.

16. Boure, J.A., Bergles, A.E., and Tong, L.S., "Review of Two-Phase Flow Instability," Paper presented at ASME-AICHE National Heat Transfer Conference, Tulsa, Okla. (August 1971).

17. *Proceedings Symposium on Two-Phase Flow Dynamics*, Eindhoven (1967).

18. *Proceedings, Second Two-Phase Flow and Heat Transfer Symposium/Workshop*, Miami, Hemisphere Publishers (April 1979).

3.4 Steam Generator Behavior

During the 1970s and 1980s, DOE sponsored a substantial effort in the development of sodium-cooled LMRs. A significant part of this effort was devoted to development of a sodium-heated steam generator.

Argonne in the 1980s conducted two experimental studies focused on the thermal-hydraulic behavior of the LMR steam generator. The first study involved water testing in the MCTF of a 60^{o}-sector shell-side model of the Westinghouse-Tampa steam generator to explore the potential for buoyancy-influenced behavior on the shell of the unit. The experimental protocols were similar to those used on a 360^{o} model of an IHX presented in Section 3.3.1.3. The second study was conducted in Argonne's Steam Generator Test Facility to study sodium-to-water heat transfer associated with a single tube of prototypic length and to study phenomena like boiling induced dry-out and two-phase flow instabilities that can occur during LMR steam-generator operation.

3.4.1 Argonne Shell-Flow Studies of Westinghouse CRBR Steam Generator

In 1983-84 tests were conducted in the Argonne MCTF on a 60°-sector shell-side flow model of the straight-tube steam generator of Westinghouse-Tampa (Fig. 3.4-1) being developed under the DOE Large Component Development Program. The model was built by Westinghouse Tampa Division (WTD) and first tested at Westinghouse Advanced Reactors Division (WARD) [1] under isothermal conditions to generate design input on flow-control orificing of the inlet plenum and baffle plate to achieve uniform flow through the tube bundle. After this testing, the model was shipped to Argonne for water testing under low-flow thermal transient conditions to explore the potential for buoyancy-influenced behavior on the shell of the unit. The testing protocols were similar to those conducted on the 360^{o} Argonne model of an IHX presented in Sec. 3.3.1.3. In a similar fashion to the IHX studies, Argonne also assessed the validity of 1-D flow models of this tube bundle in predicting, under varying degrees of thermal-buoyancy-induced flow, channeling transit time through the tube bundle and the thermal density head developed in the tube bundle. One-dimensional modeling is used

extensively by industry to study the dynamics of LMRs under a wide variety of thermal-hydraulic transients.

The shell-side flow model shown in Fig. 3.4-1 represents a 60° wedge of the straight-tube steam generator in the WTD Intermediate A plant. The tube bundle was 0.462 scale. One flat side was made of clear plastic so that the flow patterns in the bundle could be viewed. Water enters the shell through a 20.32-cm nozzle and vertical elbow; upstream of this are 15.24-, 10.16-, and 5.08-cm-diameter transition pipes. Flow-distribution perforated flat plates A and B for the inlet plenum were used to straighten the flow prior to entering the bundle region through perforated distribution shroud C. The flow control baffles were designed by WTD to uncouple nonprototypic inlet conditions from the tube bundle of the flow model. The baffles provided increased mixing, relative to the prototype inlet plenum design, due to orificed jets. Although the 60°-sector SG flow model did not have a prototypic inlet plenum, it did allow Argonne to study the role of plenum mixing on flow channeling by porosity variation of the perforated flow-control baffle in the model.

The 561 tubes of the tube bundle each had 0.95-cm outside diameter and were laid out in a 60° triangular array with a tube pitch to diameter ratio P/D = 1.77. The bundle radius was 52.1 cm. The tube bundle baffles were located 22.50 cm between adjacent surfaces, except the uppermost span, which was 27.7 cm. Plate T simulated the sodium tube sheet. Plate D was a distributor plate that helped even out the axial flow by counteracting the cross-flow bundle losses between C and D. All E-type plates were uniform-porosity tube-support plates containing large flow holes between the tubes spaced on a triangular pitch. All plates of a given letter designation were identical. Plate F was similar to E. Plates X and Y were full plates with radially varying porosity to create shell-side cross-flow. The region of the tube bundle with X and Y baffle plates was prototypic. Plate G was similar to E but of lower porosity to decouple the exit region effects from the bundle region.

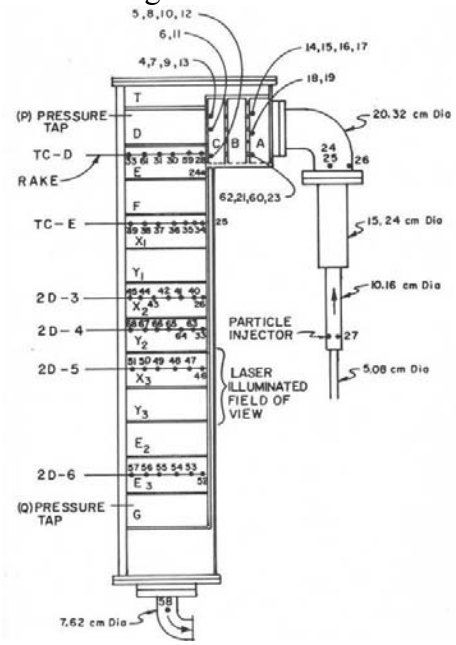

Figure 3.4-1 Westinghouse-Tampa 60°-sector steam generator shell-side flow model tested at Argonne

3.4.1.1 Flow Channeling Correlation

Based on the Argonne 360° IHX water experiments, a flow-channeling correlation for a tube bundle was presented in Sec 3.3.2.2 in terms of the parameter Ri_{DS} Re_{DH}, a ratio of buoyant to viscous forces in the tube bundle. This parameter correlated the error between 1-D predicted transit time through the tube bundle and the experimental value for various degrees of buoyancy-induced flow channeling. Similar testing was conducted on the Westinghouse steam generator test article, which was subjected to various constant inlet flows upon which were superimposed linear thermal down ramp transients for different flow rates and magnitudes of temperature change. Figures 3.4-2 and -3 show steam generator inlet/exit temperatures and flows (top) and pressure differentials across the unit (bottom) for a typical test with no buoyancy-induced channeling and with significant channeling respectively.

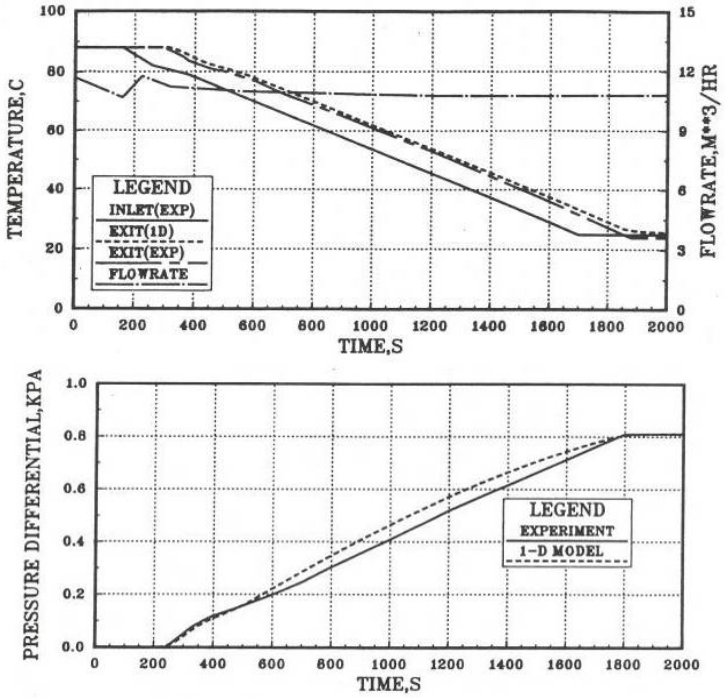

Figure 3.4-2 Steam generator inlet/exit temperature and flow (top) and pressure differential across the unit (bottom) for a test with <u>no buoyancy-induced channeling</u>. Also shows 1-D model predictions.

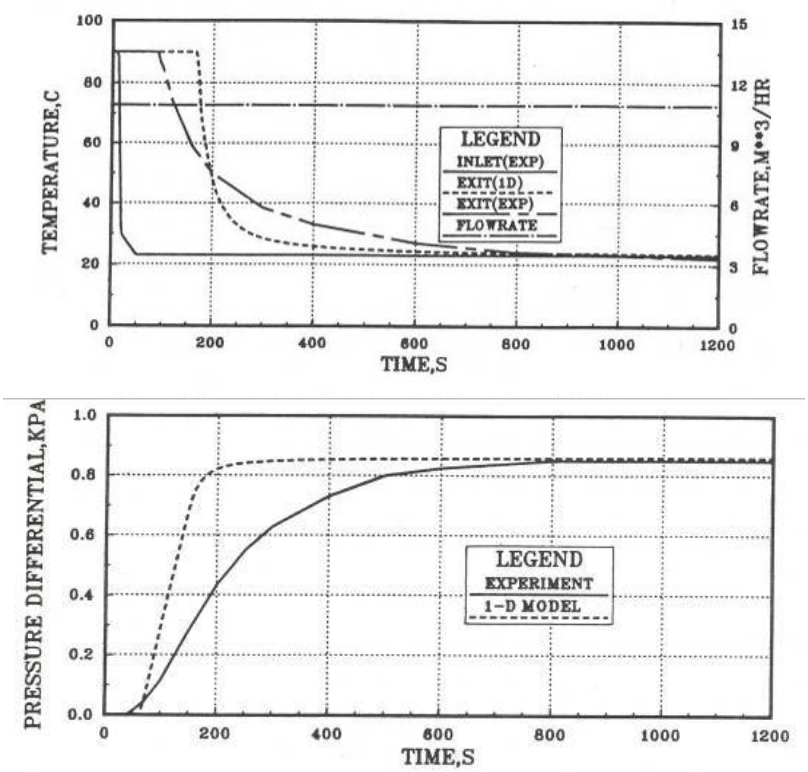

Figure 3.4-3 Steam generator inlet/exit temperature and flow (top) and pressure differential across the unit (bottom) for another test with significant buoyancy-induced channeling. Also shows 1-D model predictions.

Figures 3.4-2 and -3 also show 1-D model predictions for these tests based on Argonne modeling [2,3] of transit time through the tube bundle and pressure differential across the unit. Under low-flow conditions, note that the thermal density head in the vertical unit is the main contributor; frictional losses are small. For the test case shown in Fig. 3.4-2 with negligible thermal buoyancy, the agreement between the 1-D model and experiment is good for both thermal disturbance transit time and pressure differential across the bundle. Just the opposite is true for Fig. 3.4-3. Due to flow channeling induced by strong thermal buoyancy, the 1-D model predictions are not in agreement with experiments for a significant period of time. As discussed in previous sections, the correct prediction of thermal density head in the various vertical components composing the reactor plant is very important under certain conditions relative to obtaining valid predictions of plant flow. For example, during natural circulation it is the net thermal density head that drives the flow and dictates the capability for decay heat removal.

Figure 3.4-4 shows a typical data set for temperature variation radially across the tube-bundle shell-side, midway down the tube bundle, for the test shown in Fig. 3.4-3. As seen, the flow channeling produced a large radial-temperature variation across the tube bundle as the thermal transient passed through the tube bundle. This condition raises possible tube-bundle differential stress concerns similar to what happened in the 360^{o} IHX model tests described in Section 3.3.2.2.

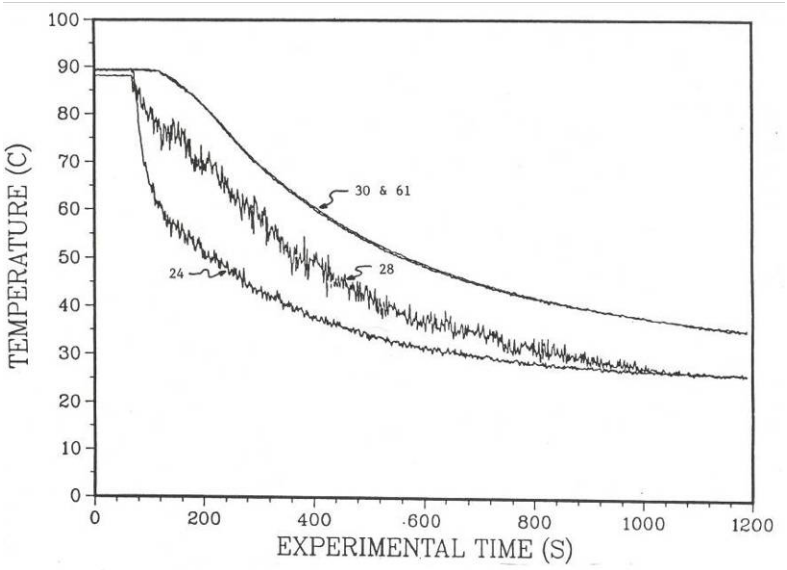

Figure 3.4-4 Radial temperature variation across the tube bundle shell-side at mid-elevation caused by flow channeling versus time

The testing under thermal transients as shown in the Figs. 3.4-2, -3, and -4 in terms of the Argonne modeling parameter Ri_{DS} Re_{DH} covered the range of values associated with testing of the IHX but also extended the range from 4.0×10^5 out to 1.3×10^6. As shown in Fig. 3.4-5 the same modeling parameter correlated the error between the 1-D model predicted value for the thermal front transit time through the steam generator tube bundle and the experimentally determined value. The range extension resulted from testing with faster thermal transients and the fact that the steam generator model was larger, with the size reflected in the modeling parameter. The curves for the IHX and SG data sets show some difference because of differences in baffle designs and the thermal masses of the two test articles. Also shown in Fig. 3.4-5 are two points entered by computing values of the modeling parameter for the prototype Westinghouse steam generator and anticipated thermal-hydraulic transients under low flow. It appears that flow channeling will probably occur in the prototype.

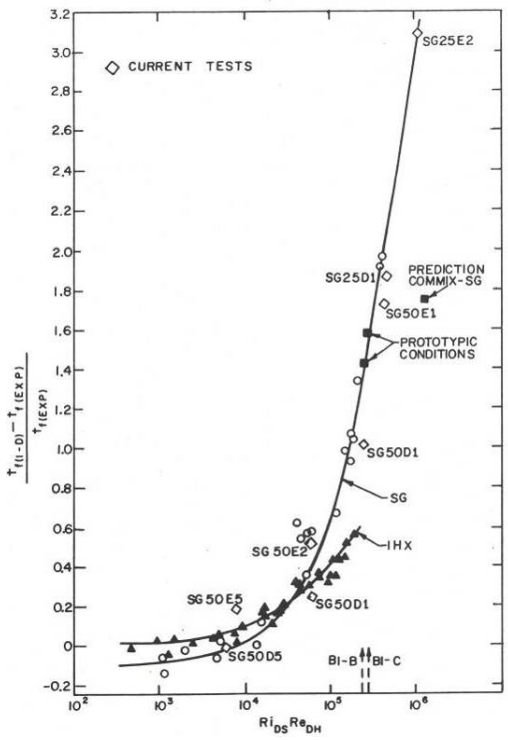

Figure 3.4-5 Argonne developed correlation for shell-side thermal-buoyancy-induced flow channeling transit time for the Westinghouse SG and the Argonne IHX tube bundles

As mentioned earlier, Argonne modeled under 1-D assumptions the advancement of thermal front transit times through the Westinghouse steam-generation test article and the pressure differential across the unit. Figure 3.4-6 shows the errors in temperature and pressure prediction in comparison with the experimental data. The error growth in each prediction as a result of thermal-buoyancy-induced flow channeling starts at zero at about $Ri_{DS}\ Re_{DH} = 1000$ and grows quickly with increasing buoyancy parameter.

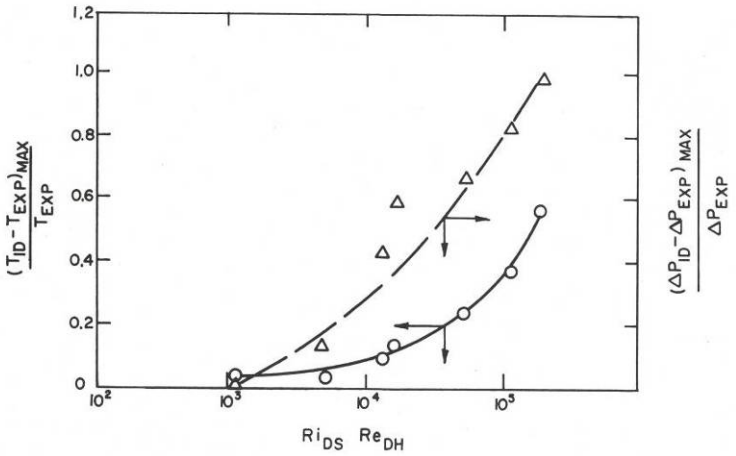

Figure 3.4-6 Errors in 1-D model predictions for Westinghouse SG tube-bundle temperature and pressure differential versus buoyancy parameter $Ri_{DS}\ Re_{DH}$

3.4.1.2 Summary and Research Needs

A multiphase DOE-funded program was conducted to investigate the importance of thermal buoyancy to LMR steam generators and heat exchangers under low-flow thermal transient conditions. A 60°-sector shell-side flow model of the Westinghouse straight-tube steam generator and a generic 360° IHX were water tested at Argonne. These tests focused on the potential for buoyancy in the plenums and on the phenomenon of thermal-buoyancy-induced flow channeling in the vertical tube bundles. In addition, Argonne studied the potential that flow channeling and thermal stratification could invalidate the use of 1-D thermal-hydraulic models to predict the temperature distributions in the tube bundles and the thermal density heads in these vertical units as a function of time.

The major findings were:

- Both LMR IHXs and steam generators will experience performance-degrading thermal buoyancy phenomena under low-flow thermal transient operation.

- Performance-degrading flow channeling was found to be correlated by the non-dimensional parameter $Ri_{DS}\ Re_{DH}$, which is the ratio of thermal buoyancy to viscous forces acting on the flows fields during low-flow thermal transient conditions. The testing with both test articles covered a $Ri_{DS}\ Re_{DH}$ range from 3.0×10^2 to 1.3×10^6. It was found that when $Ri_{DS}\ Re_{DH} < 800$ no flow channeling induced by thermal buoyancy is present, and 1-D modeling is good provided the units are correctly designed with baffles and orificing to achieve uniform flow. However, Argonne also showed that, even with good flow uniformity under high-flow conditions achieved using conventional design practices, the thermal buoyancy forces under low-flow conditions can still cause large departures from the uniform flow that was intended.

- Increasing the porosity of the perforated flow-control baffle (i.e., reducing mixing) in the shell inlet plenum of a tube bundle decreases the transient mitigation capability of the inlet plenum and increases the flow channeling. Designers would do well to design inlet plenums not only with the viewpoint of providing uniform flow distribution to the tube bundle, but also mitigating thermal down-ramp transients (i.e., promoting plenum mixing) and thus flow channeling.

- Under the flow-channeling conditions explored, tube-bundle baffle plates with both uniform and non-uniform porosity were equally ineffective in eliminating flow channeling and radial temperature variation. Hence, it is believed that the design philosophy behind the tube bundle should be re-evaluated.

- Flow channeling induced by thermal buoyancy has been shown to cause significant departures from 1-D thermal-hydraulic model predictions of thermal distributions and thermal density heads developed in vertical tube bundles. When the channeling modeling parameter $Ri_{DS}\ Re_{DH}$ exceeded 1000, appreciable departure from 1-D predictions occurred and grew significantly with further increases in $Ri_{DS}\ Re_{DH}$.

Research needs in this subject area relate to assessing the influence of shell-to-tube-side heat transfer and structural heat capacitance on the flow-channeling correlation and exploring the influence of the large Prandtl number difference between water and sodium on the water-based correlation. Sodium transient tests with small-scale tube bundles would serve very well; there is no need to use prototypic or near-prototypic tube bundle lengths. The resulting sodium data will yield a validated flow-channeling correlation that can be used to extrapolate to prototype performance and thus will allow designers to predict whether a potentially important phenomenon will occur in SGs or IHXs. If designers find it difficult to avoid thermal buoyancy in the tube bundles, then 3-D CFD codes should be developed and benchmarked with experimental data and used by designers to quantify the performance of their design and the severity of the thermal-buoyancy-induced phenomena both in the IHX or steam generator and to the rest of the plant related to correctly predicting flow coast-downs and decay heat removal. As highlighted in earlier sections, this design work will also require use of 3-D CFD codes for modeling piping flows in the presence of pipe thermal stratification.

3.4.2 Single-Tube Studies at Argonne

The sodium-heated steam generators of LMRs have many favorable features, including the low pressure of the sodium coolant. However, the steam generator is the only LMR plant component in which sodium and water are present in close proximity; separated by only the heat transfer tube of the steam generator. Because of a possible reaction between the two, this proximity is one reason that this component received so much attention in the 1970s and 1980s. However, there was much more involved than safety considerations alone. A sodium-heated steam generator was one of the least developed components for commercial scale-up. Interestingly, for a component with no moving parts, it has required considerable research and development with regard to heat transfer, flow distribution, plant upset conditions, and more. Argonne played a key role in the heat transfer development area in the mid-1970s through the mid-1980s. The following is a summary of Argonne studies covering heat transfer and flow stability aspects of the design of LMR steam generators.

In the past, the worldwide LMR development effort for commercialization took the position that a prototype reactor should be built to gain experience before a full-scale commercial reactor was attempted. The prototype size was to be between the very small LMFBR reactors of the time, including Argonne's Experimental Breeder Reactor II (EBR-II), and the commercial size of approximately 1000 MW electric. The prototype size was set at about 1/3 of this commercial size, and the first U.S. version was called the Clinch River Breeder Reactor (CRBR), which was then followed by the GE PRISM development initiative. The CRBR steam generator was designed by Atomics International (AI), and it was a recirculation type with an evaporator and superheater separated by a steam drum. The steam-water mixture exited the evaporator in the mid-quality range, and this feature resulted in critical heat flux (CHF) behavior being present in this unit over a range of normal operating conditions [4,5]. [CHF is also referred to as departure from nucleate boiling (DNB.)] This feature also required investigations concerning steam generator tube corrosion and spalling of the corrosion layer and prediction of the occurrence of CHF itself. One of the first areas investigated by Argonne was the spalling of the oxide scale on the water tube walls due to thermal fluctuations induced

by CHF [6]. The Argonne study showed the potential for shortened tube life due to this phenomenon and led to a series of experiments to quantify the effect more accurately [7]. These experiments were then followed by more studies directed at generating additional thermal-hydraulic performance data for steam generators. All these experiments were performed in Argonne's Steam Generator Single Tube Test Facility, which was built for DOE [8].

3.4.2.1 Argonne Steam Generator Test Facility

Figures 3.4-7 and -8 show schematics of the Argonne Steam Generator Test Facility (SGTF). The SGTF was a sodium/water system designed to accommodate testing of full-scale LMR steam-generator tube designs (straight or bayonet type) or other vertically oriented components as tall as 80 ft (24 m). The SGTF could be operated in the recirculation mode for testing steam generator evaporators or in the once-through mode for integrated units. Figure 3.4-9 shows photos of the SGTF tower and control room. The SGTF was used for studying:

- Overall thermal performance of full-scale tubes
- Heat transfer from a liquid-metal across a tube wall to boiling water and CHF/DNB
- Oscillatory boiling regime generated tube thermal fluctuations and stresses and the influence on tube-scale build up.
- Steam generator response to system upsets

The following table gives the maximum operating parameters for the SGTF.

Table 3.4-1 Maximum SGTF operating parameters

Sodium System	
Heat input	550 kW
Operating temperature	1000^{o}F
Flow rate	56 gpm
Operating pressure	70 psig
Water System	
Operating temperature	900^{o}F
Flow rate	165 gpm
Operating pressure	500-2300 psig
Pressure drop	130 psi

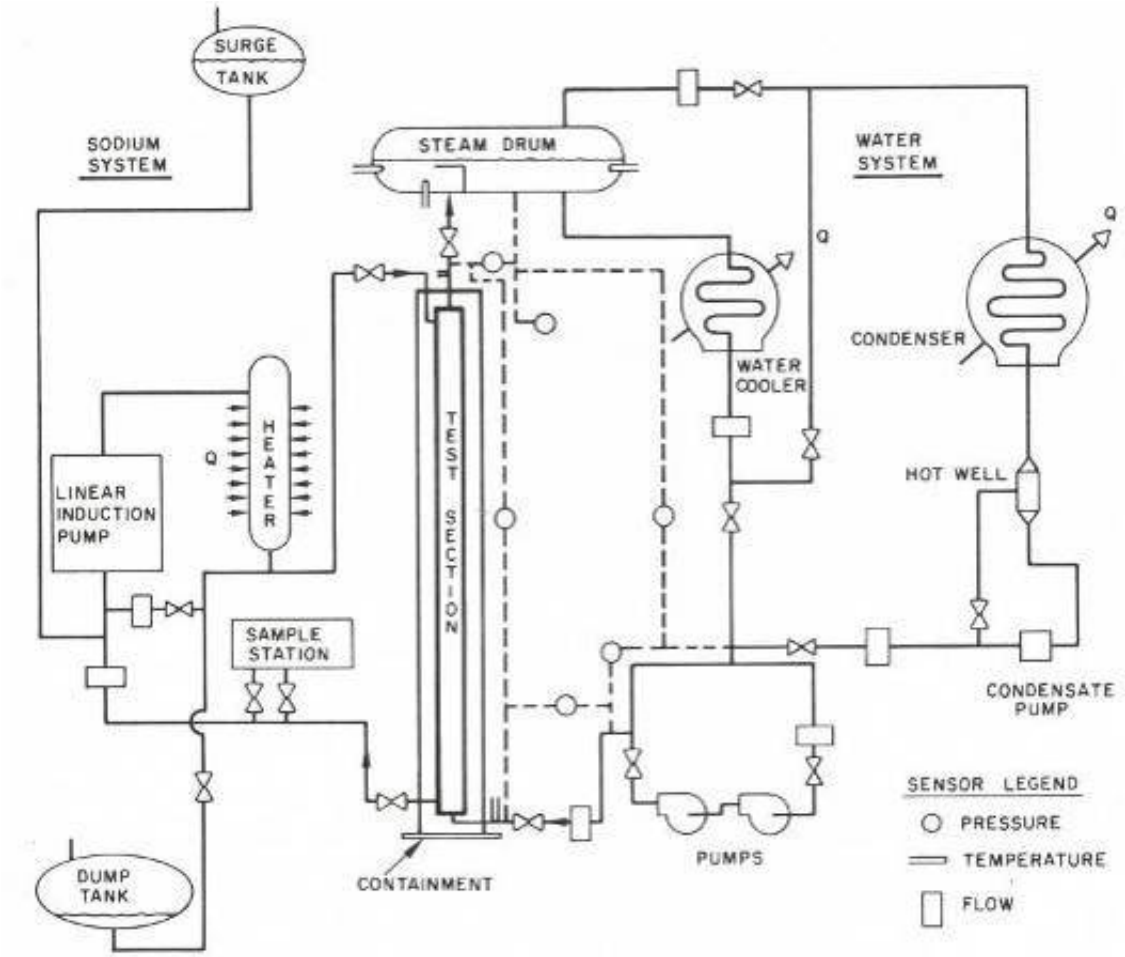

Figure 3.4-7 Schematic of Argonne's Steam Generator Test Facility

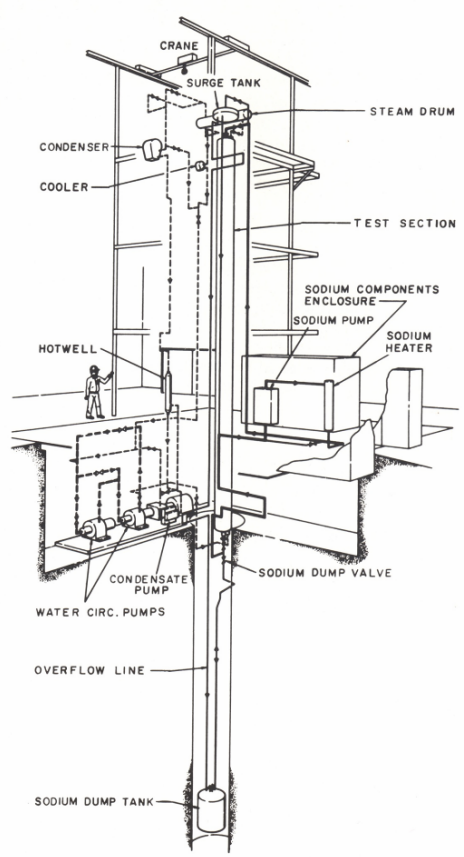

Figure 3.4-8 Scaled pictorial of Argonne's Steam Generator Test Facility

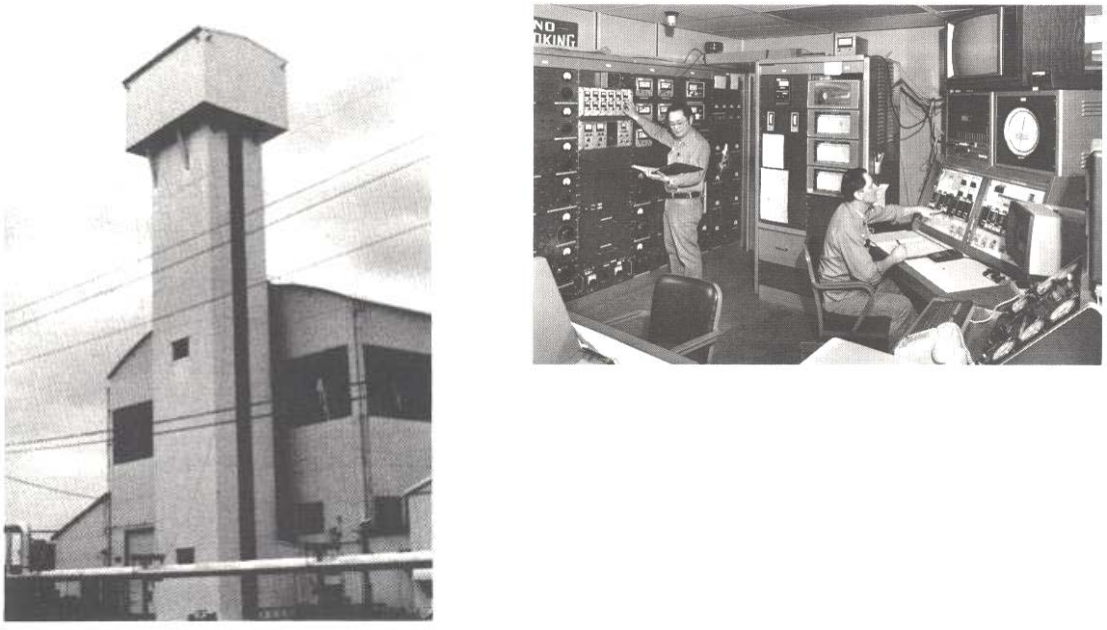

Figure 3.4-9 Photos of Argonne's SGTF tower (left) and control room (right)

The following provides highlights of the studies conducted by Argonne in the SGTF:

3.4.2.2 CHF and Sub-Cooled Heat Transfer in Steam Generator Tubes

Extensive tests were performed in the SGTF for the purpose of defining the conditions when CHF occurred. These results were necessary for thermal sizing of LMFBR steam generators. They were pertinent to CRBR directly and to future sodium-heated steam generator designs. The term CHF (critical heat flux) is used to refer to the point along a tube on the water side at which the wall surface temperature increases rapidly in response to a temperature-controlled or heat-flux controlled boundary condition on the sodium side. CHF serves as a generic term covering the two separate and distinct processes of 'departure from nucleate boiling' (DNB) and 'dryout'. Upstream of the CHF zone, heat transfer is very effective and is characterized by a high heat transfer coefficient, h, as for nucleate-type boiling by analogy to pool boiling even though nucleation may be suppressed as for when dryout occurs. Downstream of the CHF, the wall is covered by bulk vapor with entrained droplets, and the heat transfer is by a film-type of boiling, with an h-value considerably lower than for nucleate boiling.

The following highlights Argonne's CHF studies covering normal- and low-flow steam generator operation, behavior upstream and downstream of the CHF zone, and exploratory use of computer simulation to model tube boiling.

Normal-Flow

Critical heat flux (CHF) experiments [9] were performed in the SGTF for general application to Liquid Metal Fast Breeder Reactor (LMFBR) steam generators. A single, straight, vertical, full scale LMFBR steam generator tube was tested with water flow boiling upwards inside the tube heated by sodium flowing countercurrent in a surrounding annulus. The test section tube parameters were: inside diameter = 10 mm, outside diameter = 15.8 mm, material = 2 1/4 Cr - 1 Mosteel, and heated length = 13.1 m. Experiments were performed in the normal water pressure range of 7.0 to 15.3 MPa and the water mass flux range of 720 to 3200 $kg/m^2.s$. The data exhibited two trends: heat flux independent and heat flux dependent. The CHF data from the 398 tests in the SGTF were presented along with an empirical correlation having a root mean square deviation of 14.7 percent from the data. The correlation was compared to other CHF data in the same parameter range.

Low-Flow

The data from the preceding SGTF experiments pointed to low-flow operating conditions in the steam generators as the most severe condition for CHF induced thermal stresses in the units. CHF and the associated thermal fluctuations were then studied under low-flow conditions.. Initially nine experiments were conducted on the same tube as above [10] with 7.3 MPa water pressure and mass fluxes of 550, 270 and 140 $kg/m^2.s$ covering a broad range of critical heat flux. Measured and analyzed tube wall, thermal fluctuation data and thermal stresses were presented for each test. Only one test at the highest heat flux of 0.76 MW/m^2 and 270 $kg/m^2.s$

mass flux exhibited cyclic thermal stresses in the marginal range for meeting ASME requirements for 30 years lifetime. All other tests showed considerably lower stresses.

To supplement the previous nine tests, seventy CHF experiments were performed [11] on the same tube. The water mass flux was relatively low ranging from 100 to 600 $kg/m^2.s$, and the majority of the data were obtained at a water pressure of 7.3 MPa. The critical quality and thermal stress in the tube wall at the CHF zone were evaluated and compared to extrapolations of previously derived empirical correlation equations.

Upstream CHF

Sodium LMR steam generators for electric power plants have been designed with a variety of configurations. Once-through, recirculation, and saturated heating modes have been used. However, most of these units have the common features of shell and tube type designs, with high-pressure water boiling inside the tubes heated by liquid sodium on the shell side. LMR steam generators have been developed for use in electric power plants operating on Rankine thermodynamic cycles. Consequently, subcooled liquid water enters the steam generators to begin the heating process. Water may exit the steam generators as superheated or saturated vapor, and critical heat flux may or may not be present, depending on the design. As a minimum, the water in the steam generators experiences heat transfer in the single-phase liquid, subcooled boiling, and bulk boiling modes. Heat transfer from sodium to single-phase, subcooled, liquid water over the steam generator length from the water inlet to the initiation of subcooled boiling is termed the preheat region and was studied by ANL. Heat transfer to the water in the preheat region of LMR steam generators is an application of convection heat transfer to a liquid flowing.

There was concern that the subcooled liquid heat transfer in LMFBR steam generators might not be well enough predicted by standard correlations. Tests in the SGTF [12] and by Westinghouse Electric Corp.(W) were conducted to address this concern.

Both experimental investigations were performed in full-scale LMFBR model steam generator test sections in which water flowed inside tubes heated by flowing liquid sodium on the outside. Forty tests performed by ANL and five tests performed by W were analyzed. The water parameter ranges were 7 to 16 MPa pressure and 180 to 800 $kg/m^2 \bullet s$ mass flux. The data were compared with estimates from standard heat transfer correlation equations. Differences between results were examined and deviations from the standard correlation equation predictions were assessed.

Downstream CHF

In the heat transfer region downstream of CHF, the heat transfer rates are relatively low. Accurate knowledge of these rates is necessary for the accurate sizing of steam generators. As input to the sizing process, CHF test data from one hundred thirty-five post-critical heat flux (post-CHF) experiments performed in the SGTF were analyzed [13]. The tests employed the same straight, vertical steam generator tube of 13.1 m length and 10 mm inside diameter. The water pressure ranged from 7.0 to 15.3 MPa, and the water mass flux ranged from 0.72 to 3.2

Mg/m^2•s. The data and a developed post-CHF heat transfer correlation equation were presented. Also presented were the results of analyses of transition boiling region characterization which showed that the previously observed heat flux dependent and heat flux independent trends of critical heat flux data are a consequence of a change of the hydrodynamic structure of the two-phase flow.

Boiling CFD Simulation

ANL was a leader in the early development of 3-D CFD codes for nuclear reactor component thermal and fluid analyses including steam generators. In Ref. [14], SGTF experimental information was used to guide modeling with the ANL 3-D COMMIX CFD code. Promising improvements in steam generator tube heat transfer predictions resulted from a change in the critical heat flux correlation employed in the code and the long CPU times were shortened somewhat. Results were compared to experimental data obtained under steady state conditions in a single-tube sodium-heated steam generator experimental facility. Sample predictions for a full size liquid metal fast breeder reactor steam generator were also presented.

3.4.2.3 Steam Generator Tube Fatigue, Corrosion, and Corrosion Layer Spauling

For a large number of SGTF tests, covering a wide range of parameters, the measured CHF zone thermal fluctuations were used to make steam generator tube thermal stress and fatigue calculations. Some of the results are highlighted next.

The thermal induced alternating strains occurring in the tubes of steam generator evaporators result from departure from nucleate boiling (DNB) which occurs between the nucleate boiling regime and the film boiling regime. In the nucleate boiling regime the inner surface of the tube is coated with water, which has a relatively high heat transfer coefficient. In the film boiling regime, there exists a layer of vapor between the tube and the water. The heat transfer coefficients of the film of vapor are low compared to those in the nucleate boiling regime. The temperature of the outer surface of the tube is approximately the temperature of the sodium which remains almost constant along the tube in the DNB region. Since the temperature of the outside surface remains relatively constant, the temperature gradient through the wall will be larger in the nucleate boiling regime than in the film boiling regime. The exact location of DNB fluctuates with time, and it is this fluctuation that causes an oscillating temperature gradient. If the amplitudes of the alternating strains and mean stress induced by the tube wall temperature cycling are sufficiently large, they can cause fatigue damage to the tubes.

The CRBR steam generator was designed by Atomics International (AI), and it was a recirculation type with an evaporator and superheater separated by a steam drum. The steam-water mixture exited the evaporator in the mid-quality range, and this feature resulted in CHF and DNB being present in this unit over a range of normal operating conditions. This phenomenon was studied and evaluated by Argonne concerning the potential for tube fatigue damage and the influence on corrosion and corrosion layer spauling.

The study in Ref. [15] showed the potential for shortened tube life due to this phenomenon and lead to a series of experiments to quantify the effect more accurately. Transient temperature distributions and thermal stresses were calculated for a sodium heated steam generator evaporator tube and water side oxide layer in the DNB region. The pertinent thermal hydraulic parameter ranges and geometry were adopted from the Atomics International reference design for the steam generators of the CRBRP. The tube wall and the oxide scale layer on the water side of the tube (treated as either a powdery substance or a dense protective film) were subjected to periodic water heat transfer coefficient fluctuations simulating the effect of DNB in that area of the tube. The stresses obtained were employed in estimating the life expectancy of the steam generator tube based on fatigue of the tube wall and repeated exfoliation of the oxide layers.

Additional Argonne studies of tube fatigue [16] were conducted over a broader range of CRBRP parameters on a sodium-heated vertical full-length tube of length = 13.1 m, I.D. = 10.1 mm, O.D. = 15.9 mm and was made of 2-1/4 Cr - 1 Mo steel. Water was circulated vertically upwards through the tube and was heated by sodium flowing counter-current in a surrounding annulus. The nominal thermal-hydraulic parameters for these tests were: water mass flux = 2480 kg/m^2.s, water pressure = 12.8 MPa, CHF quality = 0.2, and sodium temperature = 420°C. The measured thermal fluctuation amplitude and calculated results for tube thermal stresses were presented showing the influence of sodium temperature and water pressure separately on the severity of the fluctuations and stresses. Results were also presented for a series of tests simulating various operational conditions of the CRBR steam generator evaporators including full and 64 % load. The latter case was shown to be the most severe load for this unit from the standpoint of the potential for fatigue damage to the tubes due to thermal fluctuations in the tube wall CHF/DNB region.

In Ref. [17], CHF data was presented for 406 experiments conducted in the Argonne SGTF. The same tube was used as in the previous study. The parametric range of the data was pressure = 7.0 - 15.3 MPa, water mass flux = 0.72 - 3.2 Mg/m^2.s, critical heat flux = 0.3 - 1.8 MW/m^2, and critical quality = 0.1 - 0.8. Complete parametric results were presented for all tests as well as calculated results for thermal fluctuations and thermal stresses in the tube wall. The thermal fluctuation results are discussed and parametric trends identified. An empirical equation was developed that correlated all of the thermal fluctuation data.

3.4.2.4 Dynamic Instabilities Associated With Boiling Parallel Channels

Parallel channel dynamic flow instability is a condition to be avoided in LMR steam generators. In support, of LMFBR development effort of the CRBR steam generators, tests were performed in the Argonne SGTF to ascertain the potential for such instabilities. The results from an initial study were presented in Ref. [18]. Eighteen dynamic stability tests employing a full scale LMFBR steam generator tube were conducted. Parallel channel flow of boiling water in full length steam generator tubes was simulated with flowing sodium used as the heating fluid. The tests corresponded to normal and abnormal operation of the CRBRP steam generators. All tests were pushed toward instability using test section throttling with all other parameters maintained constant. Dynamic instability, characterized by large amplitude fluctuations in the water flowrate, was reached in sixteen of the tests. Steady and dynamic results were presented for each test.

Following the preceding study, additional tests were performed in the SGTF simulating specific full and part load operating conditions in the CRBR. The results were presented in Ref. [19]. The testing involved the same test configuration as used in the preceding study. Sixteen hydrodynamic stability tests were performed. Results were presented for four tests simulating the CRBR normal load levels of 120, 100, 80 and 40 percent power, and for five tests representing post-transient steam generator operation. In addition, the results of seven parametric sensitivity tests were presented. Hydrodynamic instability was encountered in almost every test with some of the thresholds of instability occurring within the range of CRBR operating conditions.

3.4.2.5 Improving Heat Transfer in Duplex Steam Generator Tubes

For over two decades, Argonne had operated the EBR-II fast breeder reactor including its steam generators without a sodium/water interaction. The following highlights some of the insight gained from this experience regarding the steam generators which used duplex (double-wall) tubes.

EBR-II was located at the former Argonne-West site on the Idaho National Engineering Laboratory. It consisted of an unmoderated sodium-cooled reactor with a thermal power output of 62.5 MW, an intermediate closed loop of secondary sodium coolant, and a steam plant that produced 19.5 MW of electrical power through a conventional turbine-generator. The steam-generator system consisted of a conventional steam drum, eight shell-and tube, natural-circulation evaporators, and two shell-and-tube superheaters. After 17 years of operation, one of the superheater evaporators was removed from the system in 1981 due to performance degradation and evaluated by Argonne [20, 21]. It had delivered steam at increasingly and erratically reduced temperatures beginning in 1974 until its removal. It was disassembled and subjected to materials examinations and physical tests; and operating-data, structural, and heat-transfer analyses were performed.

The heat-transfer across prestressed duplex tubes in the steam generating system of the Experimental Breeder Reactor II progressively deteriorated with time and certain anomalies in steady-state heat-transfer were noted. Analytical modeling of the steady-state counterflow heat-transfer in the duplex tubes showed that more than one steady-state solution for heat-transfer may exist when the room-temperature prestress had relaxed sufficiently. The room temperature prestress determined for two individual tubes were used to determine steady-state solutions at different plant operating conditions and compared with measured values. These results were used to explain the apparently anomalous behavior. A sensitivity study also indicated that small perturbations in the steam flow rate might be sufficient to cause disproportionate loss in heat transfer when the prestress has relaxed sufficiently.

It was established that the tube heat transfer degradation was caused by separation of the duplex-tubing interface resulting from material creep and deterioration of the interface environment. The implication of these findings were that these effects should in future designs of duplex-tube steam generators be accounted for. For example, high-strength, high-temperature, low-creep materials should be used or the thermal conductivity at the interface should be enhanced by metallurgical bonding or a "filler" gas.

When the CRBR project was cancelled, DOE changed its fast reactor development efforts to modular plants that would be easier to deploy, more economical, and reliable. Two new steam generators were designed for these plants, and ANL had programs associated with both. SGTF testing was in support of the Westinghouse steam generator design based on the EBR-II double-walled concept with the addition of a sodium/water safety detection system. Because of the double-walled tube design, the use of heat transfer enhancement devices was attractive for reducing the heat transfer penalty of the thick tube walls. Experiments were performed in the SGTF to quantify the benefits of two such devices and the results were presented [22].

To reduce the size and cost of steam generators in LMRs, some U.S. designers considered using heat transfer augmentation devices in the tubes to improve thermal efficiency and reduce steam generator size. Argonne investigated tube heat transfer, pressure drop, and dynamic stability with two types of inserts: twisted tapes and core tubes forming flow annuli. Water was boiled at full pressure, heated by liquid sodium at full temperature. The water tube diameter was prototypic and the test section was half length. A search of the engineering literature existing at the time of the study revealed that there are thousands of references to augmented heat transfer schemes, but there is very little information that can be applied directly to LMR steam generator designs where water is boiled at pressures between 7 and 16 MPa.

Experimental results were presented for both types of enhancers -- twisted tapes and core tubes inserted into the steam generator tube. Test parameters were prototypical of LMR steam generator design. The best insert based on heat transfer enhancement was found to be a full-length twisted tape with a twist ratio of 15. Although both enhancer types increased overall performance, the enhancement mechanisms were different.

3.4.2.6 Plant Upsets Causing Fast Transients in the Steam System

LMR plant upset conditions such as a water or steam line rupture can cause fast transients in the steam system including the steam generators. Most of the experimental work done in the past has addressed steady-state or oscillatory CHF type phenomena in steam generators. More global hydrodynamic stability of steam generators for LMR electric power plants is an important consideration in the design and operation of these components. Dynamic instabilities have occurred in steam generators. An important design consideration is the avoidance of hydrodynamic instabilities, and the design input is the conditions under which instabilities will initiate--the threshold of the instabilities. Experiments were performed in Argonne's SGTF to provide dynamic-stability design information for steam generators [23, 24].

The test section used was typical of full-scale tubes used in LMR steam generators. Liquid sodium at temperatures up to 500°C provided heat to boil water at pressures of 3-16 MPa and mass fluxes of 170-800 kg/m's. Special attention was given to developing the test protocols relative to the method of triggering the instabilities, and to the determination of the instability thresholds from the measurement of water mass flux. The test section was operated in the once-through mode with superheated steam exiting in all tests.

To initially address the influence of plant upset transients, a series of nine fast depressurization and dump (blow-down) transient tests were performed in the SGTF [23]. The tests were

initiated from steady-state conditions indicative of LMR steam generators operating in the once-through mode. In all tests, water entered the test section subcooled and exited superheated. Three parameters were varied among the nine tests performed: the initial water pressure, the use of top and bottom or bottom-only blowdown valves, and the rate of blowdown. Initial water pressures of 16, 8.5, and 3.6 MPa were used, and water exited the test section to the atmosphere in times ranging from 14 to 35 s. Under these test protocols, large gradients in water mass flux were observed in all tests, and similar pressure gradients occurred in most tests. The movement of the blowdown activating water valves that initiated the transients were closely monitored, and it was found that the steepest gradients occurred during this movement period.

A second series of 80 dynamic instability experiments were performed in the SGTF [24]. The experimental results were found to correlate well with a modified stability equation developed by Argonne.

3.4.2.7 Summary

By the early-1990's politics were negative towards nuclear energy. A long time had passed since the mid-east oil embargo of 1973, and the world's energy supply was stable on the short term. As a result, nuclear energy research and development efforts were significantly reduced. Today's sobering realizations concerning worldwide energy supply have turned the political climate to some degree, and the need for nuclear electric power plants for the future is again being proposed. However, most of the research facilities used to support previous LMR development have been decommissioned and/or dismantled. Such is the case of the SGTF. Design and construction of replacement facilities of this type are not small undertakings and will likely be needed to support new LMFBR designs. Although considerable LMR steam generator development work was performed previously, some of which is described above, future support work will depend on how closely new steam generator designs resemble previous designs. ANL was a key contributor to experimental support for LMFBR steam generators in the 1970's and 1980's. There were other experimental investigations mainly at General Electric (GE) and Energy Technology Engineering Center (ETEC). These facilities have also been decommissioned. A very good summary of the technical status of LMR steam generator technology was published in 1993 [25].

References

1. Harris, W.G., et al., "Westinghouse Benson Cycle Steam Generator Flow Models Mechanical Design and Fabrication Report," WNCD-BRCP-80-005 (February 1980).

2. Oras, J.J., and Kasza, K.E., "Thermal Transient Induced Buoyant Flow Channeling in a Vertical Steam Generator Tube Bundle," ANL-83-109 (October 1983).

3. Oras, J.J., Kasza, K.E., and Lin, H.C., "Thermal Transient-Induced Buoyant Flow Channeling in a Vertical Steam Generator Tube Bundle: Effect of Inlet Plenum Design and Validity of 1-D Modeling," ANL-84-97 (October 1984).

4. France, D.M., "DNB in Liquid Metal-Heated Forced-Convection Boiling," J. Heat Mass Transfer, *16*, 2343-2354 (1973).

5. France, D.M., et al., "Incipient Boiling Superheat Measurements at LMFBR Conditions," Trans. Am. Nucl. Soc., *18*, 202 (1974).

6. France, D.M., et al., "Experimental Observations of Thermal Oscillations in LMFBR Steam Generator Tubes," Trans. Am. Nucl. Soc., *23*, 386 (1976).

7. Chiang, T. et al., "Calculation of Tube Degradation Induced by Dryout Instability in Sodium Heated Steam Generators," Nucl. Eng. Des., *41*(2), 181-191 (1977).

8. Stevens, H.C., and France, D.M., "Development of a Thermal-hydraulic Test Facility for Full-Scale LMFBR Steam Generator Tubes," Trans. Am. Nucl. Soc., *22*, 538-540 (1975).

9. D. M. France, T. Chiang, R. D. Carlson, and W. J. Minkowycz, "Measurement and Correlation of Critical Heat Flux in a Sodium Heated Steam Generator Tube," ANL-CT-78-15 (January 1978).

10. D. M. France, T. Chiang, and R. D. Carlson, "Critical Heat Flux Tests at Low Water Flow and 7.3 MPa-Interim Report," ANL-CT-78-10 (October 1977).

11. D. M. France, T. Chiang, R. D. Carlson, et al., "Critical Heat Flux Measurements with Sodium Heating and Low Water Flowrate," ANL-CT-78-39 (July 1978).

12. D. M. France, R. D. Carlson, W. J. Minkowycz, Argonne National Laboratory, unpublished information, 1985.

13. T. Chiang, D. M. France, and R. D. Carlson, "Post-CHF Heat Transfer and Transition Boiling Characteristics in an LMFBR Steam Generator Tube," ANL-CT-79-14 (December 1978).

14. K. C. Chan, T.T. Kao, J.G. Bartzis, D. M. France, and W. T. Sha, "Modifications To and Results From COMMIX-SG: A 3-D Thermal-Hydraulic Code For Steam Generators," ANL-CT-80-20 (March 1980).

15. T. Chiang, D. M. France, and T. R. Bump, "DNB Induced Thermal Stress and Fatigue in LMFBR Evaporator Tubes with Oxide Scale," ANL-CT-75-24 (December 1974).

16. D. M. France, R. D. Carlson, T. Chiang, et al., "CHF-Induced Thermal Oscillations Measured in an LMFBR Steam Generator Tube wall," ANL-CT-78-1 (October 1977).

17. D. M. France, T. Chiang, R. D. Carlson, et al., "Critical Heat Flux Data with Stress Calculations in an LMFBR Steam Generator Tube," ANL-CT-78-27 (April 1978).

18. D. M. France, T. Chiang, R. D. Carlson, et al., "Dynamic Stability Simulation Tests of an LMFBR Steam Generator," ANL-CT-81-20 (1981).

19. D. M. France, T. Chiang, and R. D. Carlson, "Dynamic Stability Simulation Tests For The CRBR Steam Generators," ANL-CT-82-18 (1982).

20. M. G. Srinivasan, D. M. France, H. J. Haupt, A. R. Brunsvold, Argonne National Laboratory, unpublished information, 1983.

21. Wm. H. Penney, A. R. Brunsvold, et al., Argonne National Laboratory, unpublished information, 1984.

22. R. D. Carlson, D. M. France, W. P. Lawrence, W. E. Brewer, E. R. Koehl, E. W. O'hare, J. V. Killelea, Argonne National Laboratory, unpublished information, 1986.

23. D. M. France, R. D. Carlson, T. Chiang, et al., Argonne National Laboratory, unpublished information, 1984.

24. D. M. France, R. D. Carlson, R. P. Roy, et al., Argonne National Laboratory, unpublished information, 1984.

25. A. T. Onesto, H. R. Zweig, D. C. Gibbs, R. D. Carlson, et al., "The Case For Endurance Testing of Sodium-Heated Steam Generators," Nuclear Technology Vol. 103, 168-186 (August 1993).

3.5 Thermal Mixing of Multiple Coolant Streams

Thermal-fatigue failures have been reported in liquid metal and water thermal mixers [1-6, 22]. They were caused by thermal stripping produced by mixing of two streams of coolant at different temperatures. In view of this, Argonne investigated the thermal-hydraulic performance of various types of thermal mixers. The objective was to generate information that could be used to design thermal-fatigue-free mixing components for LMR service. Both pipe tee and advanced design thermal mixers were studied [7-11, 17-19].

.

The thermal mixing studied occurs when two fluid streams having constant flow rate and constant but different temperatures are mixed. Using flow visualization studies performed on a Plexiglas model of a pipe tee [12,13,21], Argonne showed that combining two fluid streams within a confined space can produce flow instabilities, which generate large-scale, often periodic, transient fluid motions (Fig. 3.5-1) in addition to random smaller turbulent fluctuations. These transient fluid motions generate temperature fluctuations at the mixer wall-fluid interface (thermal stripping), which produce fluctuating thermal wall stresses. The thermal stresses, if severe enough and of significant duration, can lead to thermal-fatigue cracking.

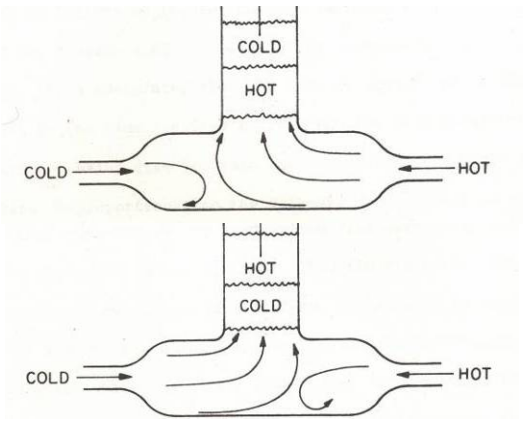

Figure 3.5-1 Large-scale transient fluidic motions generated in a 180^{o} inlet tee mixer

Thermal stress analysis of a mixer, or any structure subjected to thermal stripping, requires knowledge of the fluid temperature fluctuations at the mixer walls. Prototype sodium mixer testing is usually not possible due to test facility thermal-hydraulic limitations and is more readily accomplished in water. Thus, knowledge of size scaling, thermal-hydraulics, and fluid medium dependence is required for modeling the temperature fluctuations and extrapolation to prototype performance. Prior to the Argonne studies, the design of thermal mixers was hindered by the lack of thermal mixing data. The information generated was used to (a) evaluate the FFTF secondary-loop mixer design; (b) extrapolate the water data to the thermal mixer sodium performance of the CRBR Intermediate Heat Transfer System (IHTS); (c) develop improved mixers; and finally, (d) furnish data that can be used to evaluate the effectiveness of pipe tee mixer designs for future LMR plants.

To ascertain the thermal mixing characteristics of pipe tee mixers, Argonne performed a series of tests on various mixers utilizing both water and sodium fluid mediums. These tests consisted of the following:

i) Flow-visualization water studies on a Plexiglas model of a 4-in. (10-cm) pipe tee

ii) Pipe-tee water mixing studies of low-flow inlet-leg stratification and flow intrusion

iii) Temperature fluctuation measurements on a 4-in. (10-cm) water tee mixer

iv) Temperature fluctuation measurements on a 8-in.(20-cm) water tee mixer

v) Temperature fluctuation measurements on two 4-in. (10-cm) sodium tees (ANL/FFM Tees No. 2a, b)

vi) Development and testing of two improved mixers

The studies of thermal mixing in 4-in. (10-cm) water pipe tees [6-15] were conducted first with a transparent tee (Fig. 3.5-2) and then with a standard pipe tee (Fig. 3.5-3) with various inlet leg reducer inserts (Fig. 3.5-4). These experiments documented the thermal-fatigue propensity of pipe tees. Subsequent studies on the 8-in. (20-cm) water tee focused on the size scaling laws for temperature fluctuations [20]. Then, experimental data from a 4-in. (10-cm) sodium pipe tee mixer [9,11,14] were generated and compared with the 4-in. (10-cm) and 8-in. (20-cm) water mixing data from the earlier tests [20]. This comparison yielded correlations for sodium/water temperature fluctuation, which in conjunction with the water data greatly enhanced the general knowledge concerning thermal mixing in the complex confined flows and contributed to the development of thermal-fatigue-free mixers.

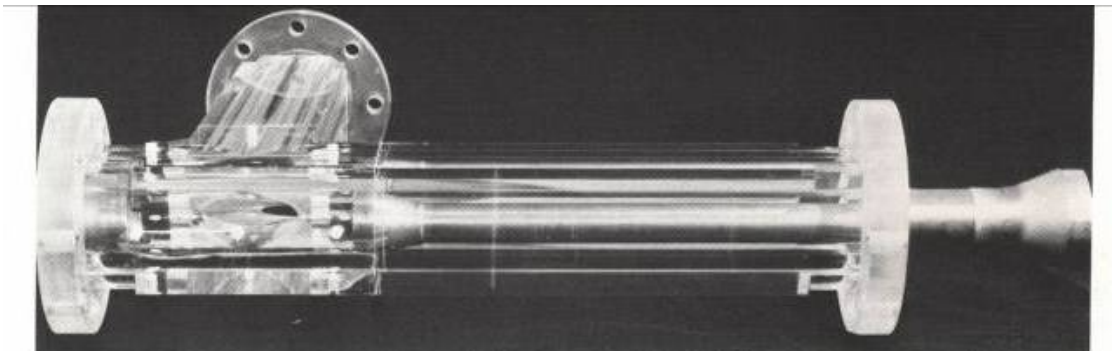

Figure 3.5-2 Plastic pipe-tee test article which facilitated understanding large-scale transient flow patterns

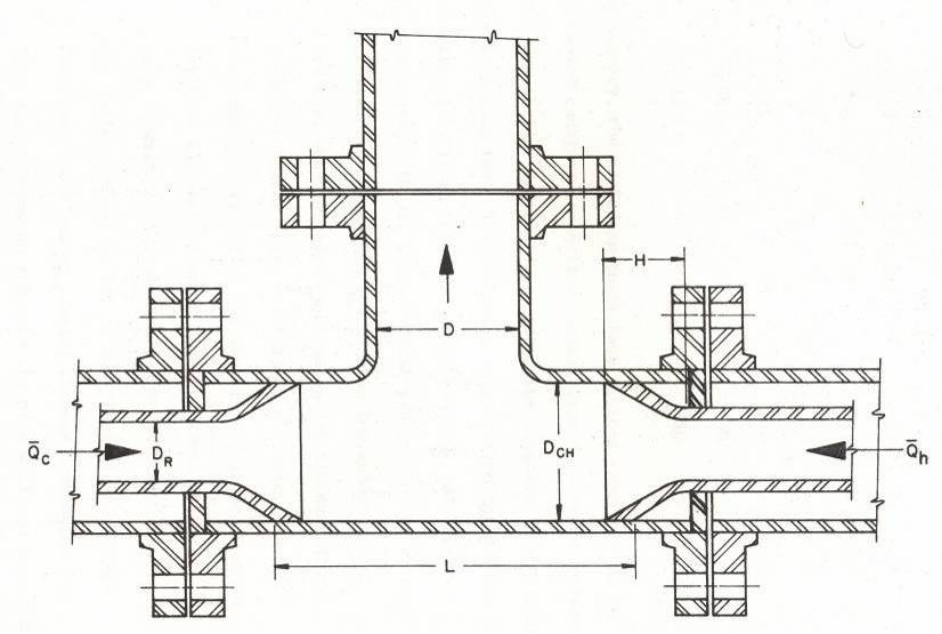

Figure 3.5-3 Pipe mixing tee geometry with 180^o inlet legs containing reducers

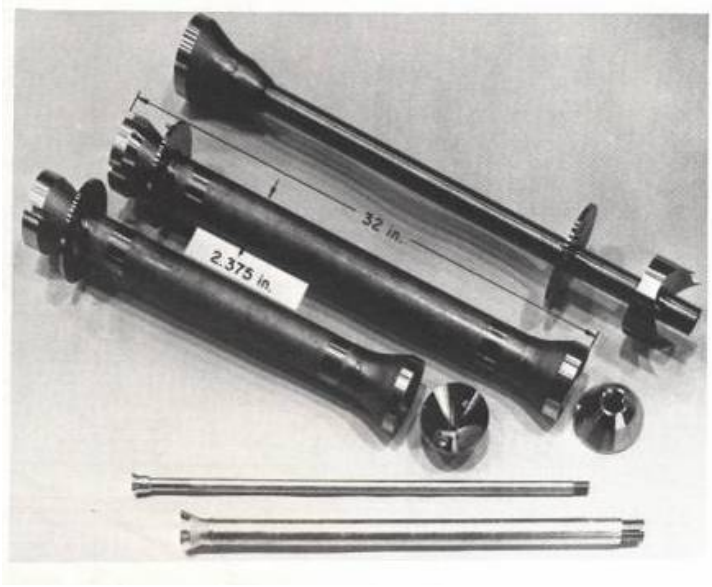

Figure 3.5-4 Pipe tee reducer inserts used to vary diameter of test section (Fig. 3.5-3) inlet legs

The water testing was performed in Argonne's MCTF (see Sec. 4.2.2). The sodium testing program was planned and developed by Argonne and conducted by Oak Ridge National Laboratory (ORNL) and Argonne in the ORNL Fuel Failure Mockup (FFM) sodium loop (also called the Thermal-Hydraulic Out-of-Reactor Safety facility, THORS). All test sections except the flow visualization model were instrumented with approximately 40 fast-response thermocouples (time constants < 30 msec). In light of the fact that the temperature fluctuation

at the tee inner wall is the prime input to a thermal-stress analysis, the majority of the thermocouples were located at the fluid-mixer wall interface.

Figure 3.5-5 shows typical thermocouple placements in a test article. The pipe tee chamber size, D_{ch}, was used as the geometric scale factor for locating thermocouples at similar locations in the several mixer test articles tested. Thermocouples were located in the tee chamber as well as in the exit leg out to a distance of approximately seven pipe diameters (i.e., $L/D_{ch} = 7$, where L is the axial distance into the mixer exit leg as referenced to the juncture between the centerlines for the inlet- and outlet-leg pipes).

For all cases the tees had equal exit leg (D) and D_{ch},sizes with inlet-leg pipes of sizes either equal to D or D/2. All tests were performed with the plane of the tee legs horizontal and with the "hot" and "cold" temperatures and flow rates of the inlet-legs constant over time.

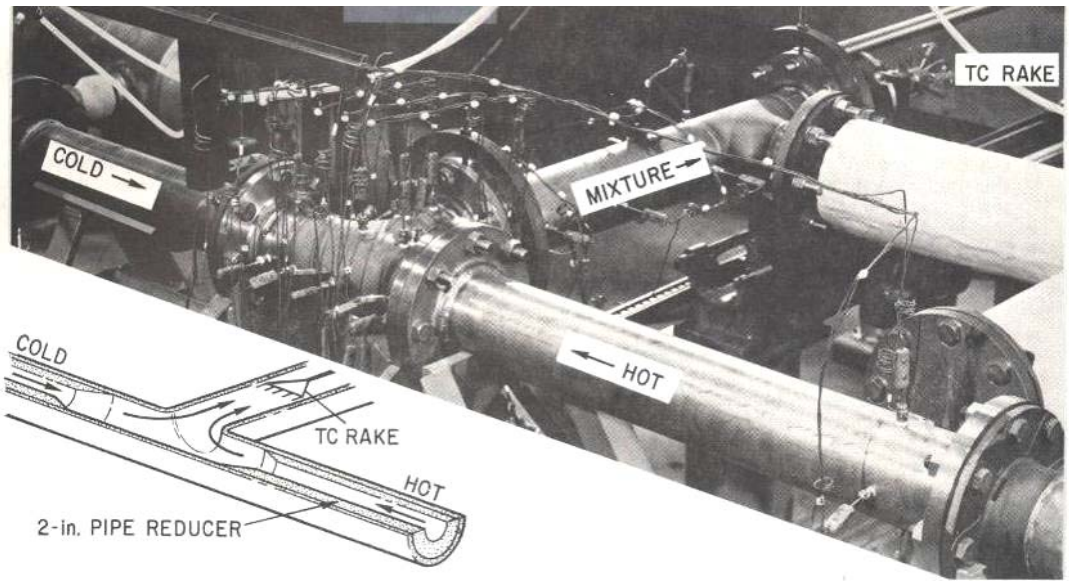

Figure 3.5-5 Argonne pipe tee mixer with thermocouples mounted in tee chamber and outlet leg

3.5.1 Flow Visualization

Flow visualization experiments were first conducted with the 4-in. (10-cm) transparent tee test article (Fig. 3.5-2) to allow study of the large-scale fluid motions. The fluid motions were delineated and photographed using small hydrogen-bubble flow tracers generated by electrolysis from fine wires stretched across the pipe flow regions. The following describes the various fluid motions occurring in mixing tees.

3.5.1.1 Inlet-Leg Flow Intrusion

The flow rates in the two inlet legs of a 180°-approach mixing tee can be greatly different and of the same temperature. In this case, as shown in Fig. 3.5-6, where the high-flow inlet leg is on the left, the fluid with a high velocity (entering from the left) may intrude into the opposite leg if the flow in that leg is entering with much lower velocity. Such an intrusion, which is a region of intense mixing, would not extend more than one or two pipe diameters into the low-flow inlet leg. However, if the streams were at different temperatures, large temperature fluctuations were generated in this intrusion zone. Additionally, depending on the temperature difference between the two streams and how low the velocity is in the low-flow inlet leg, significant thermal stratification can occur in the low-flow leg.

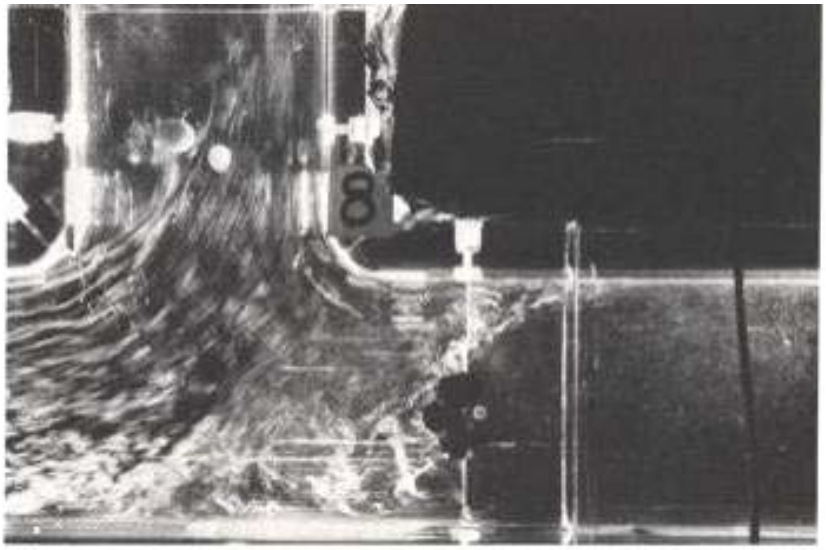

Figure 3.5-6 Visualization of flow patterns in 180^{o} inlet-leg tee chamber showing intrusion of high flow from left into low-flow on right

The 180°-approach mixing tee is used in power-generation plants to mix hot and cold liquid streams and thereby achieve the desired fluid temperature for subsequent stages of the thermodynamic cycle. Under some conditions of operation, the flow of one fluid may be reduced when a large flow rate of the other fluid is wanted from the tee, or when one leg in a standby condition has little or no flow. Under these conditions, Argonne testing showed that the high-flow-rate fluid intruded into the low-flow-rate inlet branch much more than a couple of pipe diameters when the two streams were of different temperature. This situation evidenced itself when the lower surface of the low-flow-rate (hot water) inlet leg was found to be cool (consistent with the temperature of the high-flow-rate cold leg) at distances of 75 diameters (D = 10 cm) upstream in the hot-water inlet leg extending upstream beyond several 90^{o} pipe elbows in the horizontal pipe system. This intrusion of warm fluid in the cool fluid branch produced large temperature differences between the top and bottom of the pipe. Such behavior in LMR pipe systems can produce deleterious pipe thermal stresses and complicate the mounting/hanging of the pipes. Argonne developed a preliminary mathematical model based on a perturbation solution for a low Reynolds number flow that illustrated some of the factors controlling this phenomenon [15].

3.5.1.2 Large-Scale Mixer Fluctuating Fluid Motions

If the two streams of different temperature entering a mixer undergo large-scale fluctuating motions, they produce large-amplitude thermal oscillations in the tee chamber and, for some distance, into the exit leg of the mixer. Flow visualization tests were performed in the transparent mixer test article shown in Fig. 3.5-2 to study the mixer-generated fluid fluctuations. Figures 3.5-7 and -8 show the large ordered fluid motions occurring in a 180^o inlet-leg mixer with no inlet reducers for equal inlet-leg flows. Figure 3.5-7 shows the flow behavior in the tee chamber at two instants of time. This behavior is highlighted by nitrogen bubbles generated from a wire stretched horizontally across each inlet leg. The view is looking into the tee chamber and along the centerline of the exit leg. As shown at instant a), the left stream is deflected downward and the right stream is deflected upward; at instant b), both streams are colliding head on. Not shown is that at another instant the two streams are deflected just the opposite as at instant a). Clearly, the two inlet streams undergo large-scale coherent period motions.

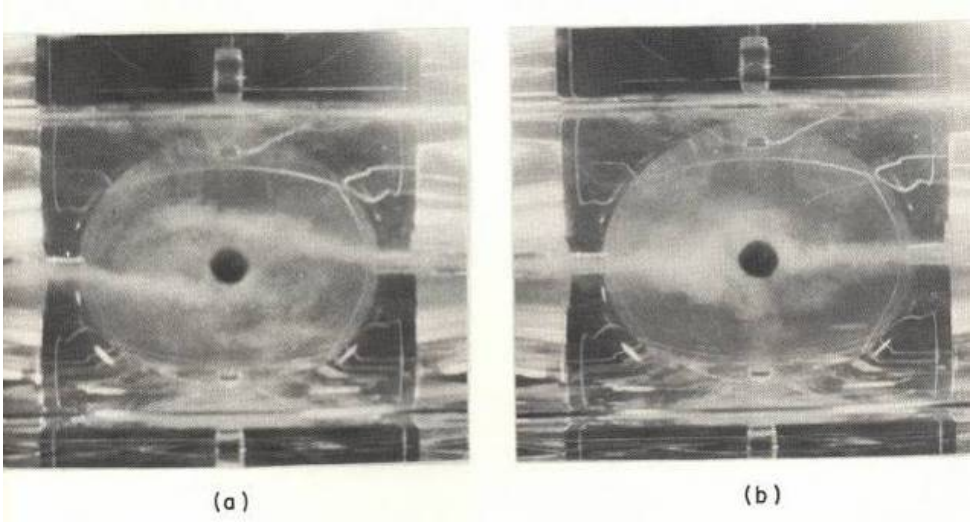

Figure 3.5-7 Front view flow patterns in 180^o inlet-leg tee-chamber showing up and down motion of the inlet-leg flows

Figure 3.5-8 shows, for the same tee and conditions as in Fig. 3.5-7, at four instants of time what happens to the inlet-leg streams tagged by the bubbles as the two streams interact in the tee exit leg. In the exit leg the streams intermittently change position in the top and bottom of the pipe. Large vortices were formed by the inlet streams turning the 90^o corner to enter the exit leg. Clearly, thermocouples mounted at the fluid pipe-wall interface would sense large temperature fluctuations associated with the large-scale fluid motions. Because the large-scale fluid motions persist far into the exit leg of conventional tee mixers, they are poor performers and subject the pipe walls to thermal stripping.

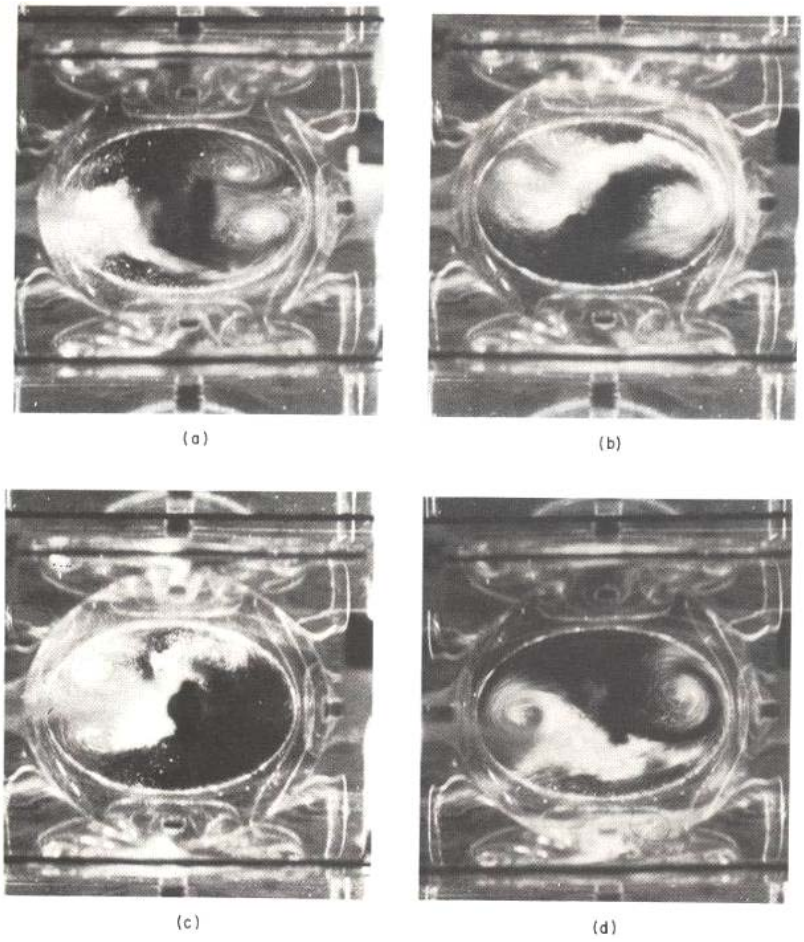

Figure 3.5-8 Visualization of flow patterns in 180^o inlet-leg tee showing periodic large-scale interaction of the inlet-leg flows in the exit leg

Figure 3.5-9 shows the flow patterns in the tee chamber as viewed looking down on the plane of the mixer for the same 180^o inlet-leg tee but now fitted with inlet-leg pipe diameter reducers similar to that shown in Fig. 3.5-3. The electrolysis wires are now stretched vertically across the two inlet legs just downstream of each reducer. As shown for this instant of time, the inlet flow from the right leg is predominately channeling into the exit leg, and the inlet flow from the left leg is accumulating in the chamber. A photo an instant later would show the two streams having switched locations. This fluidic flip-flop of alternating hot and cold flow into the exit leg is shown schematically in Fig. 3.5-1 and, as will be discussed later, results in large temperature fluctuations and mixer shaking forces.

In the next section the temperature fluctuations associated with these large-scale fluctuating fluid motions are presented.

Figure 3.5-9 Plan view of flow patterns in 180° inlet-leg tee chamber fitted with inlet-leg-pipe diameter reducers

3.5.2 Tee Temperature Fluctuations

The large-scale fluid motions produced in mixing tees, as described above, can generate large temperature oscillations when the inlet streams are at different temperatures. Figure 3.5-10 shows the typical thermal oscillations generated in a 180° inlet-leg 4-in. (10-cm) pipe tee mixer with a 40°F temperature difference between the two inlet streams at the entrance of the exit leg. The fluctuation amplitude reaches 75% of the entering difference in inlet-leg fluid temperature and subjects the walls of the mixer to thermal stripping [1,2,6,21,22].

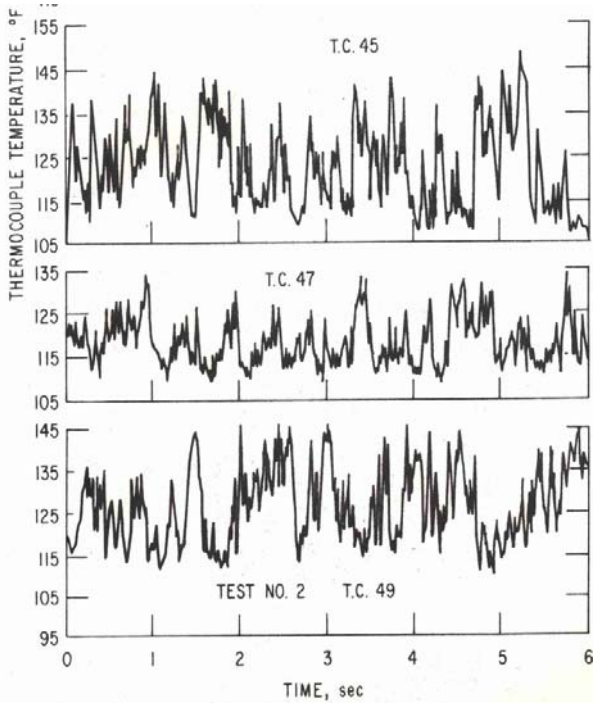

Figure 3.5-10 Temperature fluctuation traces from the exit leg of a 180° inlet-leg tee without inlet-leg reducers

Figure 3.5-11 shows, for the preceding 180° inlet-leg mixer test, the variation of the maximum temperature fluctuation amplitude $(\Delta T_{Fluct})_{max}$ occurring at a given wall axial location L along the centerline of the exit pipe. The axial distance is normalized by the pipe diameter D and the maximum temperature-fluctuation amplitude by the inlet-leg temperature difference ΔT_{inlet} . As shown, the maximum temperature fluctuations reach 90% of the inlet-leg temperature difference at about 2 pipe diameters into the exit leg. This location coincides with the location of the large-scale flow patterns shown in Fig. 3.5-8.

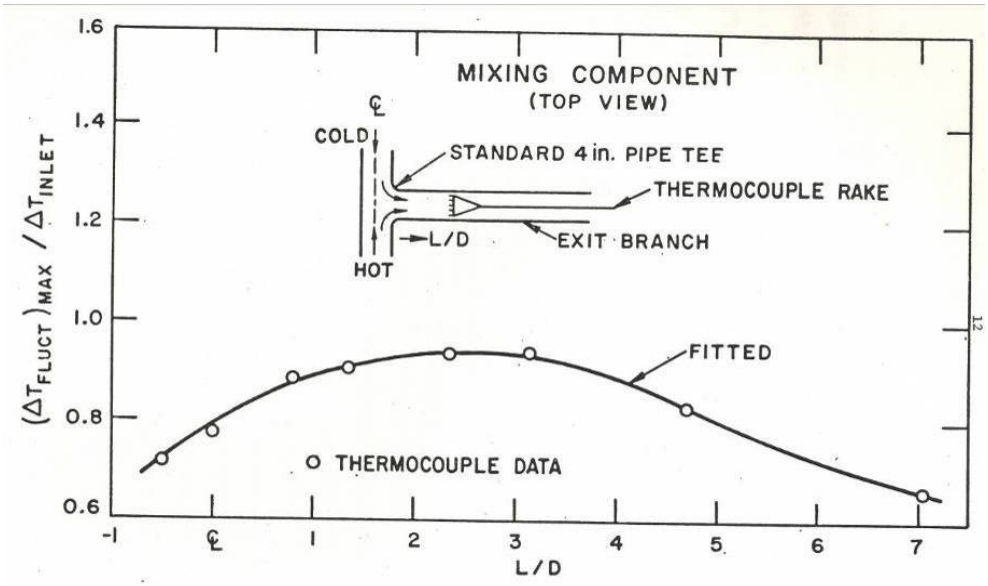

Figure 3.5-11 Variation of maximum temperature fluctuation in a tee without inlet reducers versus cross-section location

Figure 3.5-12 shows, for the same test, the power spectral density (PSD) plot of the temperature fluctuations occurring in the tee chamber. Clearly, a large fluctuation component occurs at a dominant frequency of 0.4 Hz (cps). This fluctuation is a result of the large-scale fluctuating flow patterns evident in the flow visualization photo of Fig. 3.5-7. Thus, even without inlet-leg reducers, large-scale transient fluid stream interactions still occur with a characteristic low frequency conducive to thermal stripping of the exit leg and chamber pipe walls.

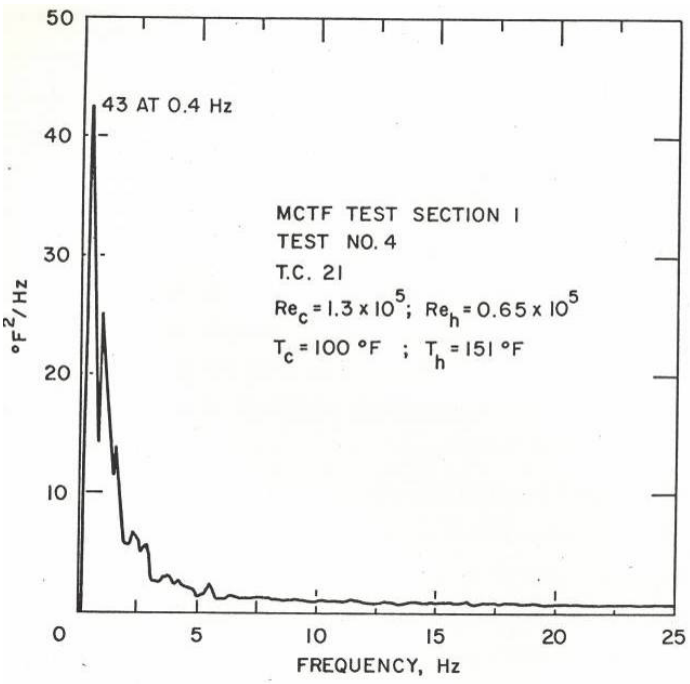

Figure 3.5-12 PSD plot of temperature fluctuations occurring in the chamber of a 180° inlet-leg tee without inlet-leg reducers

The next two figures present data for a 180° inlet-leg tee with inlet-leg pipe reducers similar to the tee without reducers. Figure 3.5-13 shows the normalized temperature-fluctuation amplitudes versus location in the tee for three test conditions. All three cases had equal inlet-leg flows but differed in that they were at different flow levels, as reflected by the range of Reynolds numbers. All tests had high Reynolds numbers and were turbulent flows but with large-scale ordered fluid motions. As shown, the maximum fluctuations, reaching almost 100% of the inlet-leg temperature difference, occur in the tee chamber, in contrast to the tee without reducers where the maximum occurred in the exit leg. Similar to the tee tests without inlet-leg reducers, the temperature-fluctuation amplitude remains 40 to 70% of the inlet-leg temperature difference at seven diameters into the exit-leg. Again, these large fluctuations result from the large-scale fluctuating fluid motions produced by the interacting inlet flows shown in Fig. 3.5-9. However, in contrast to the tee without reducers, the tee with reducers exhibits temperature fluctuations at a given exit-leg location at a given instant of time that are of similar amplitude, periodic, and in-phase. This behavior is associated with the inlet-leg reducers of this tee geometry producing the alternate fluidic flip-flop of the hot and cold streams into the exit leg. Figure 3.5-14 shows the PSD plot for the temperature fluctuations occurring in the exit leg of a 180° inlet-leg tee with reducers. There is a very dominant frequency component at 1.2 Hz.

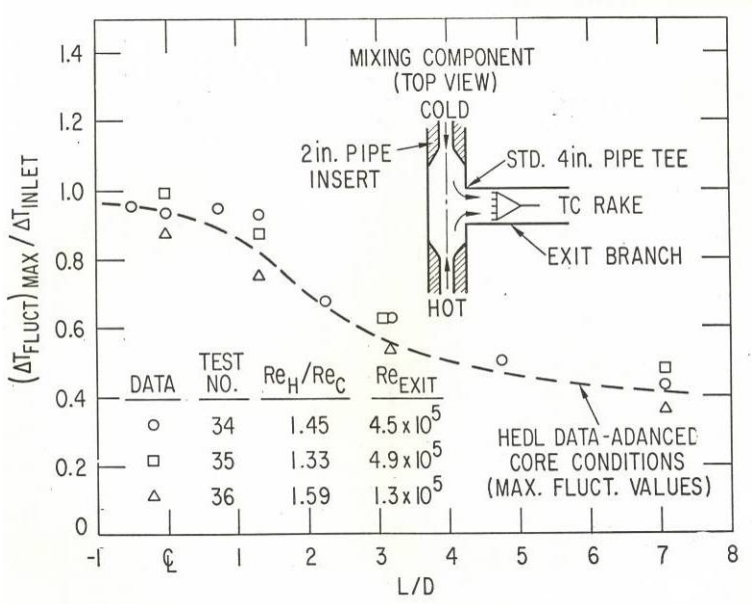

Figure 3.5-13 Variation of maximum temperature fluctuation in a tee with inlet reducers versus exit-leg cross section location

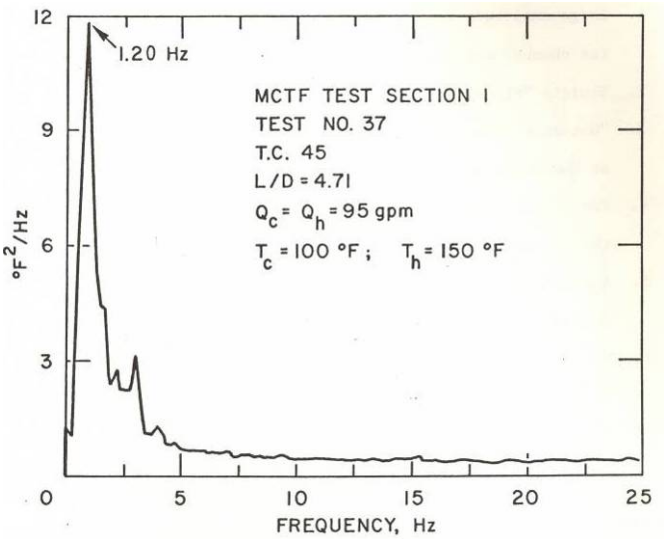

Figure 3.5-14 PSD plot of temperature fluctuations occurring in the exit leg of a 180° inlet-leg tee with inlet-leg reducers

Argonne also explored the thermal mixing associated with 90° inlet-leg mixers, as shown in the insets of Figs. 3.5-15 and -16. Figure 3.5-15 shows the variation in maximum temperature fluctuation with L/D, the distance into the exit leg, for various ratios of hot-to-cold inlet-leg pipe diameters (D_H/D_C) for $D_C/D_E = 1$ and $Re_H/Re_C = 1$ for 90° inlet-leg tees. As depicted, as the sidearm pipe diameter is reduced relative to the other inlet leg for the same flow rates, the mixing becomes more intense due to the side jet being of higher relative velocity and thus more disruptive, thereby causing attenuation of the fluctuations at larger L/D. Note that the largest temperature fluctuations extending over the greatest spatial extent are for the case where both inlet legs are of the same diameter, $D_H/D_C = 1$. Even though increasing the side-arm relative velocity promotes more rapid mixing, it also produces larger fluctuations in the tee chamber

region because the sidearm jet penetrates towards the opposite wall of the tee, as shown in Fig. 3.5-16. This figure shows the behavior of the normalized location L*/D, where the sidearm jet impacts the opposite wall of the tee in terms of an Argonne-developed correlation parameter ξ, which represents the influence of jet velocity ratio between the two inlet streams and tee geometry. In general, the 90° inlet-leg mixing tee, like the 180° inlet-leg mixing tee, is a poor geometry for mixing two streams of large temperature difference because of the potential for structural thermal-fatigue induced by thermal stripping.

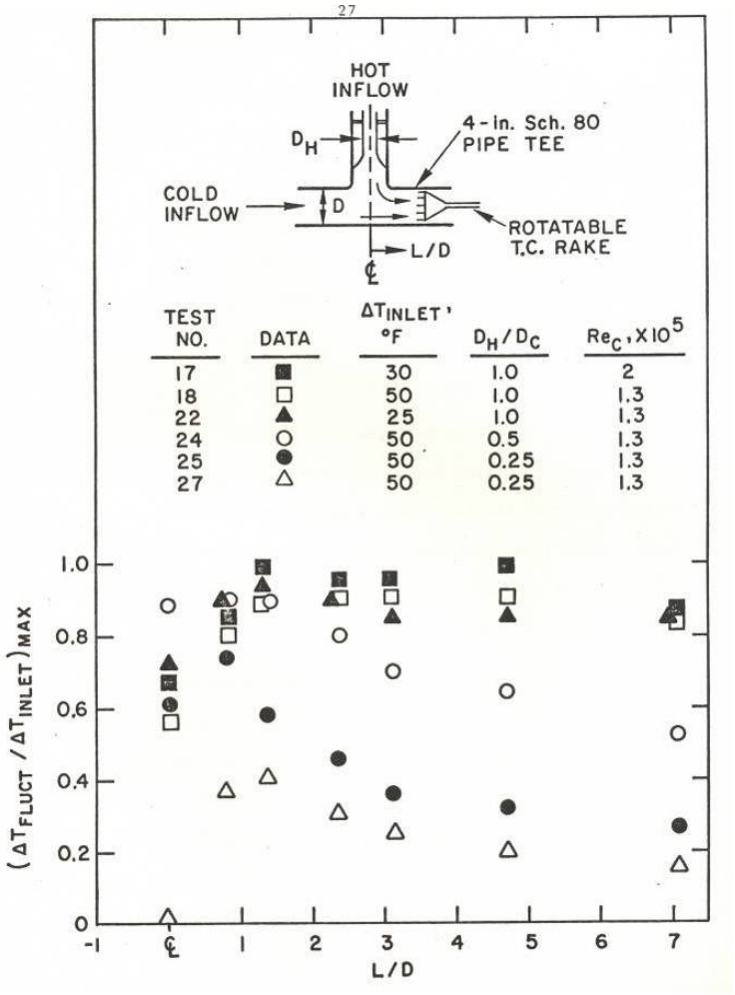

Figure 3.5-15 Variation in maximum temperature fluctuation with L/D for various sidearm pipe sizes ($D_C/D_E = 1$ and $Re_H/Re_C = 1$ for 90° inlet-leg tees)

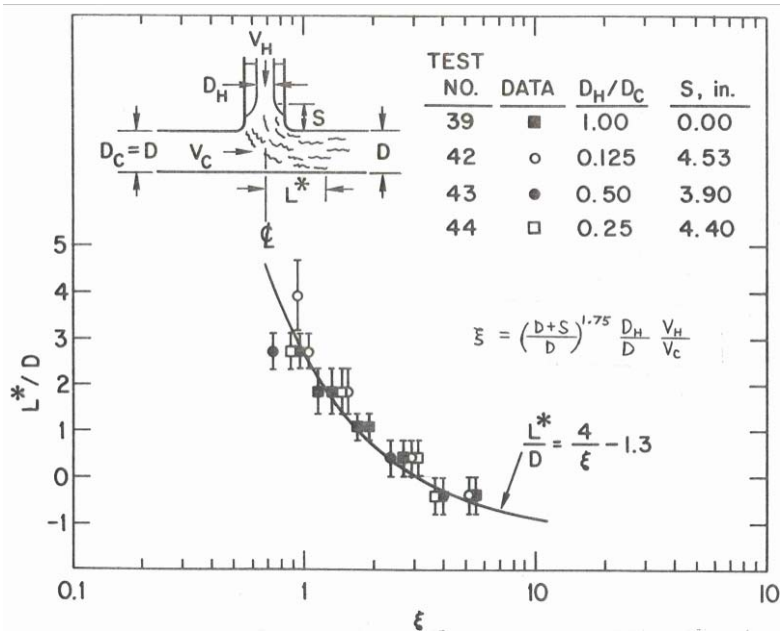

Figure 3.5-16 Correlation of side-stream impingement position (L*/D) with Argonne modeling parameter ξ

3.5.3 Tee Shaking Forces

The Argonne study of pipe tee mixers showed that tees with inlet-leg pipe reducers and a 180° angle between the two inlet legs exhibited thermal-hydraulic behavior different from that in tees not having inlet-leg reducers. It was found that:

1. The temperature fluctuations in the tee are periodic and occur at a single predominant well-defined frequency, f_p.
2. The flow in the exit-leg of the tee consists of "hot" and "cold" slugs; consequently, the predominant frequency of the temperature fluctuation is the same over the entire length of the exit leg.
3. Accompanying the slug flow are pressure and flow fluctuations in the tee, which occur at the same frequency as the temperature fluctuations.
4. The flow and pressure fluctuations of item 3 subject the tee to cyclic shaking forces, which occur at the frequency f_p.
5. Depending on the frequency and magnitude of the tee shaking force, a given piping system may be subjected to mechanical vibration fatigue as well as thermal fatigue.

Argonne developed a model to explain the flip-flop fluidic action occurring in 180^o inlet-leg mixing tees with reducer pipes [6,7,18]. It was discovered from flow visualization studies, as shown in Fig. 3.5-17, that the slug flow and the pressure and flow fluctuations are produced by an alternating fluidic "flip-flop" of the hot and cold inlet streams into the exit leg of the tee.

Based on this flow model, analytical expressions which predict the fluctuation frequency f_p and the magnitude of the tee shaking force were developed, as described next.

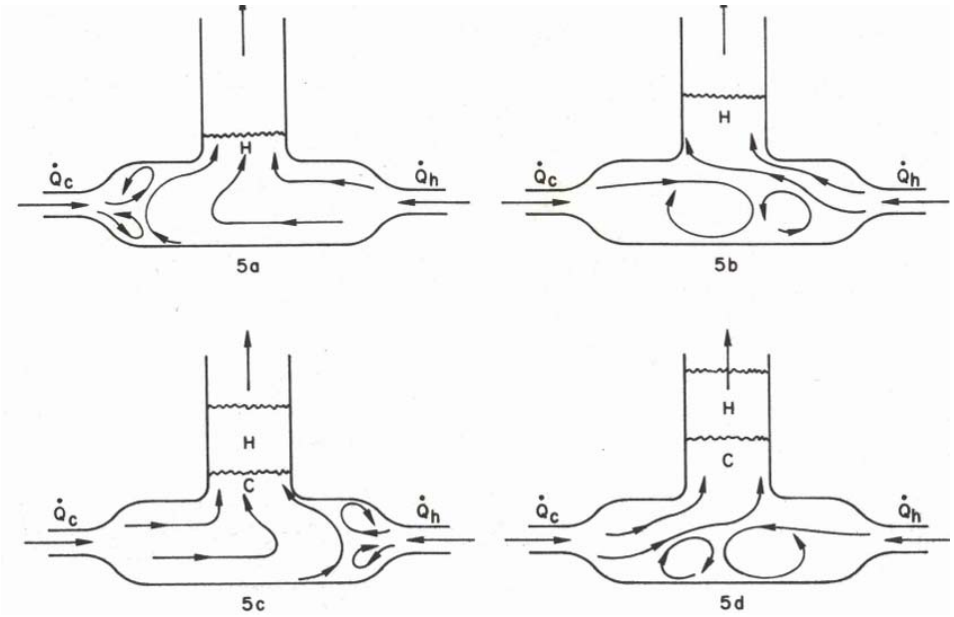

Figure 3.5-17 Schematic of the slug flow and fluidic flow fluctuations produced in a 180° inlet-leg pipe tee with inlet reducers

3.5.3.1 Fluidic Frequency Model

Equation 1 below was derived for predicting the fluidic flip-flop frequency f_P using conservation of mass applied to a control volume comprising the mixing tee chamber shown in Figs. 3.5-17 and -18.

$$f_p = \left[\frac{4}{\pi D_{CH}^2 L}\right] \frac{\bar{Q}_c \bar{Q}_h}{(k_c \bar{Q}_h + k_h \bar{Q}_c)} \qquad (1)$$

where D_{CH} and L are the tee-chamber pipe diameter and length, respectively; Q_C and Q_H are the volumetric flow rates of the two inlet-legs; and k_C and k_H are inlet-flow interaction parameters dependent weakly on the tee design and Reynolds numbers of the streams. Some features of the model are now discussed.

It has already been mentioned that the temperature fluctuations are most periodic in tees having inlet-leg reducers. This fact is also predicted by Eq. (1), which shows that the frequency of periodic fluctuations is inversely proportional to the tee chamber volume. If one thus visualizes a tee without reducers as one in which the chamber length L has become very large, Eq. (1) predicts, in agreement with experiment, that the frequency f_p of the periodic fluctuations becomes zero in the limit of very large L. The preceding does not imply that the temperature ceases to fluctuate as L goes to infinity, but only that the fluctuations are no longer predominantly “flip-flop” in nature.

From Eq. (1) the effect of an inlet flow unbalance on temperature fluctuation frequency can also be deduced. The expression in brackets is a constant for a given tee size and design. Furthermore, if the parameters k_c and k_h are weak functions of the inlet-stream Reynolds numbers and of order unity ($k_c \simeq k_h \simeq 1$), which was substantiated by experimental data, the above equation can be written as

$$f_p = \left[\frac{4}{\pi D_{CH}^2 L}\right] \frac{\bar{Q}_c \bar{Q}_h}{\bar{Q}_h + \bar{Q}_c}$$

Thus, if the total volumetric flow rate in the outlet leg, $Q_h + Q_c$, is held constant but the inlet-leg flow rates are allowed to become unbalanced, the effect is to reduce the frequency of fluctuation. Furthermore, the greater the unbalance, the lower will be the frequency of fluctuation.

Equation (1) can also be reduced to a form applicable to tees with equal inlet volumetric flow rates. In particular, it is assumed that $Q_h = Q_c = Q$ and that $k_c = k_h = k$. The last assumption is approximately true because of the near symmetry of the hot- and cold-stream chamber filling processes and the parameters k_c and k_h are weak functions of the inlet-stream Reynolds numbers. Equation (1) thus can be written as

$$f_p = \frac{2\bar{Q}}{\pi k D_{CH}^2 L} \tag{2}$$

Equation (2) can then be rewritten in terms of the non-dimensional frequency Strouhal number, S_L. If the density of the fluid is a weak function of temperature, the total flow in the exit leg of the tee is given by

$$\bar{Q}_T = 2\bar{Q} = V_T \frac{\pi D^2}{4}$$

where V_T is the average velocity in the exit leg. Thus

$$f_p = \frac{V_T}{4kL} \frac{D^2}{D_{CH}^2}$$

and

$$S_L = \frac{f_p L}{V_T} = \frac{1}{4k} \frac{D^2}{D_{CH}^2} \tag{3}$$

The Strouhal number defined in Eq. (3) is not the same as that used in the Handford Engineering Development Laboratory (HEDL) report [3]. The present definition, however, follows very readily and conveniently from this analytical study. Note that for standard commercial tees the exit-leg diameter, D, is usually equal to the chamber diameter, D_{CH}, and thus

$$S_L = \frac{1}{4k} \tag{4}$$

Equation (4) thus states that insofar as k is at most a weak function of the inlet-stream Reynolds number, the Strouhal number can be assumed to be a constant. For some other types of periodic flow phenomena (for example, vortex shedding behind a cylinder in cross flow [5]), the Strouhal number indeed is a constant for moderate- and high-flow Reynolds number but depends on the Reynolds number when the flow is laminar. More extensive experimental work over a wider range of inlet flow conditions may show this to also be true for the fluidic "flip-flop" in mixing tees. Comparisons with Argonne experimental data support that $k \sim 1$. Thus, under the present assumptions

$$S_L = 0.25$$

for a large class of commercial mixing tees with inlet-leg reducers and balanced inflow, and $D = D_{CH}$.

3.5.3.2 Model for Mixing Tee Shaking Force

This section describes the model developed for predicting the magnitude of the shaking forces acting on the mixing tee as a result of the fluidic "flip-flop" of the fluid within the tee [6,7,18]. In the analysis, it is assumed that the gravitational force acts normal to the plane of the tee. To analyze the problem, the momentum and continuity equations in their control volume forms were applied to the inertial control volume shown in Fig. 3.5-18 as a dashed line. The flow in the tee is most likely three-dimensional. However, insofar as force predictions are desired, the assumption of two-dimensionality is adequate to describe the problem. This assumption is based on the fact that the time rate of change of the fluid momentum normal to the plane of the tee is negligible, and thus the tee shaking force lies in the plane of the tee.

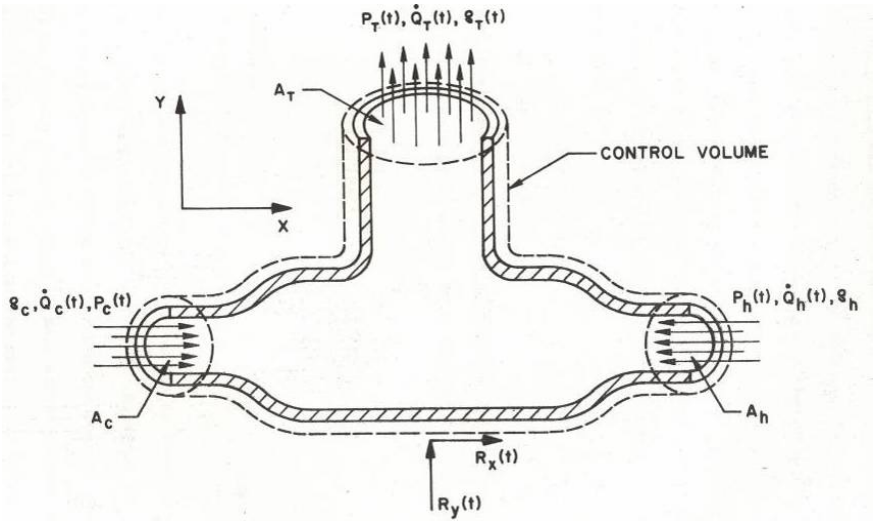

Figure 3.5-18 Control volume and variables used in modeling fluidic action and shaking forces generated by a 180° inlet-leg mixing tee

All the flow properties shown in Fig. 3.5-18 are periodic functions of time and fluctuate at frequency f_p. These quantities are, however, in general not fluctuating in phase. The quantities $[P_c(t), Q_c(t)]$ and $[P_h(t), Q_h(t)]$ represent the instantaneous gauge pressure and volumetric flow rate for the cold- and hot-inlet streams, respectively. The quantities $P_T(t)$, $Q_T(t)$, and $\rho_T(t)$ represent the instantaneous gauge pressure, volumetric flow rate, and fluid density at the exit leg. The circular cross-sectional areas of the cold and hot inlet legs are represented by A_c and A_h and the outlet-leg cross section by A_T. The quantities $R_x(t)$ and $R_y(t)$ represent the instantaneous components of the total force R(t) that would be required to hold the mixing tee in equilibrium. These desired shaking forces (SFs) are denoted by

$$SF_x(t) = -R_x(t)$$

$$SF_y(t) = -R_y(t)$$

By applying the control volume form of the conservation of mass- and momentum-governing equations to the control volume of Fig. 3.5-18, Argonne found that the amplitude of the cyclic shaking force in the x-direction is given by:

$$|SF_x|_{max} = \frac{2\rho\bar{Q}^2}{A_R}\left\{\left(1 - \frac{\mu A_R}{A_{CH}}\right) C_1 \sin(\beta) + \frac{\mu A_R}{A_{CH}}\left[1 + \frac{\pi C_1}{2}\cos(\beta)\right]\right\}$$

where

$$\beta = \tan^{-1}\left[\frac{2}{\pi}\left(\frac{A_{CH}}{\mu A_R} - 1\right)\right]$$

It was shown that the cyclic shaking force acts in line with the two inlet-legs of the tee, and that the force "flip-flops" back and forth between the hot and cold inlet sides of the tee at a frequency f_p under the condition of balanced inlet volumetric flow rates Q.

It was also shown that the force SF_y acting in line with the exit leg is only weakly time dependent, always acts in the negative y-direction, changes little from its dominant mean value with time, and is given by

$$SF_{y\ ave} = -A_T\left[P_T + \frac{4\rho\bar{Q}^2}{A_T^2}\right]$$

The preceding equations for tee shacking forces include a number of calibration factors to permit their use over a wide range of conditions. Based on Argonne data, a value of unity was shown to be adequate for the conditions explored. The predictions for temperature fluctuation frequency were in agreement with data. In applying these equations for predicting mixing tee shaking forces and frequency of fluctuation and assessing the impact on a piping system, it must be remembered that system vibration susceptibility depends strongly on the characteristics of the adjacent piping stiffness and mounting.

To illustrate the importance of the tee shaking force SF_x, which acts in-line with the inlet-legs of the 180° inlet-leg mixers with inlet reducers, the predictions of shaking force and fluctuation frequency were made for two prototype thermal LMR mixers designed for combining flows from the FFTF dump heat exchangers [16-in.(04.-m) tee with 8-in. (0.2-m) inlet pipes] and the CRBR intermediate heat exchangers [24-in. (0.6-m) tee with 18-in. (0.5-m) inlet pipes]. These predictions are shown in the following table.

Mixing Component	Inlet flows equal (gpm)	Shaking frequency (cps)	Peak shaking force (lb)
FFTF/DHX tee	2,428	0.67	51.3
CRBR/IHX tee	14,700	1.3	583

The predicted forces would be present at all times the tees are at nominal operating conditions, even in the absence of an inlet temperature difference. The shaking force predicted for the CRBR tee is in contrast to a probable tee structural weight of about 1000 lb and is large because the flow rates projected for this tee were high and the shaking force varies as the square of the inlet flow rate. In determining whether this shaking force is an important design consideration, the entire piping system associated with the tee would need to be studied.

3.5.4 Thermal Mixing: Sodium Compared to Water

This section presents a comparison of the mixing tee data generated by Argonne for both sodium and water [9,10,13,14]. All the sodium tests were conducted on a 4-in. (10-cm) 180° inlet-leg pipe tee. The water data were obtained from tests on both a 4-in. (10- cm) and an 8-in. (20-cm) 180° inlet-leg pipe tees to explore size scale influence. The 4-in. (10-cm) water and sodium test articles are shown in Figs. 3.5-19 and -20 and were heavily instrumented with thermocouples.

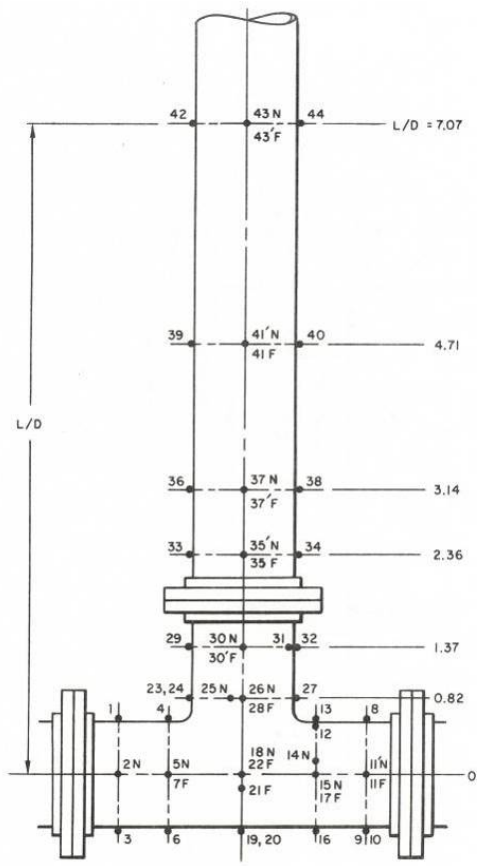

Figure 3.5-19 Argonne 4-in. (10-cm) water tested 180° inlet-leg pipe tee mixer showing thermocouple locations matching those of the sodium test article tested by Argonne at ORNL

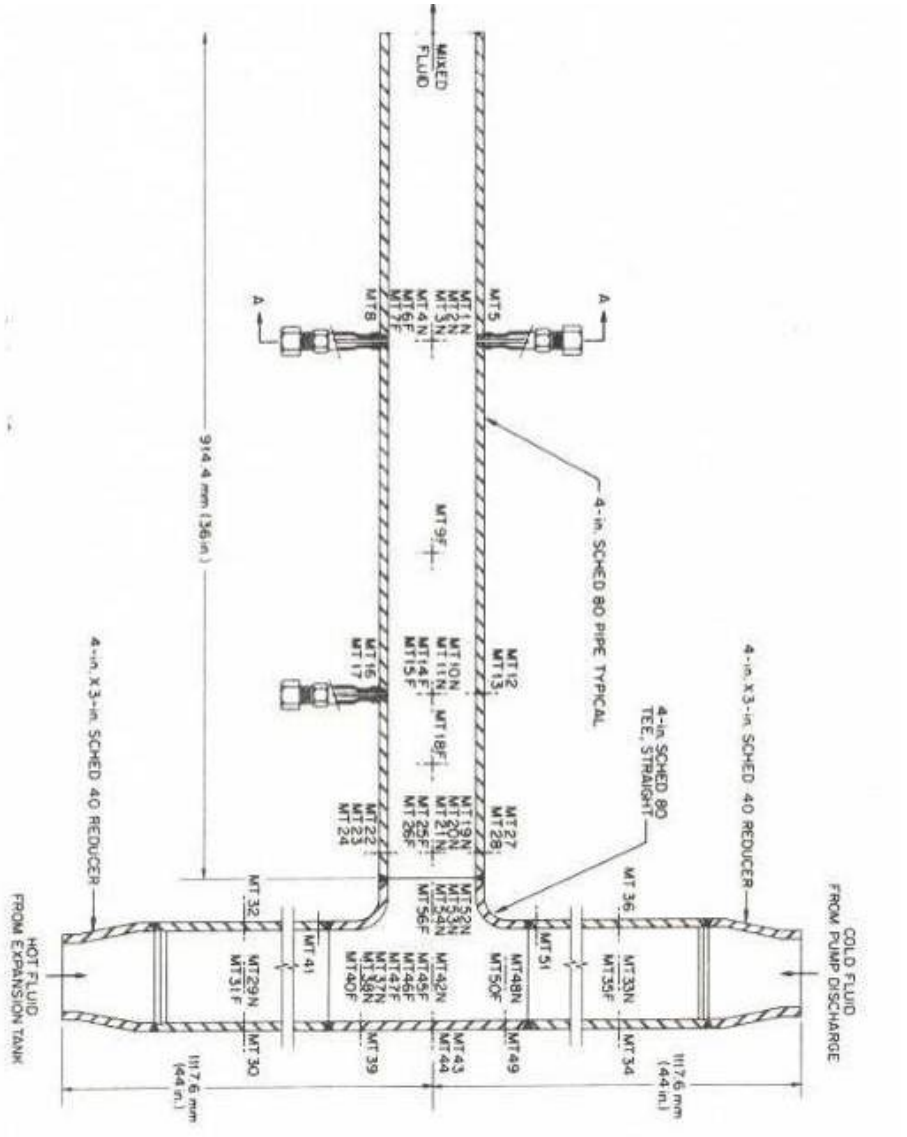

Figure 3.5-20 Argonne 4-in. (10-cm) sodium tested 180° inlet-leg pipe tee mixer showing thermocouple locations; tested at ORNL

From sodium testing of the 180° inlet-leg pipe tee without inlet reducers, as shown in Fig. 3.5-21, inlet flow-level differences for the four tests depicted having a four different inlet flow levels but the same level of inlet flow unbalance of $Q_C/Q_H = 1.56$ had no effect on temperature fluctuation amplitude. The flows were all fully turbulent, and varying the Reynolds number had no influence on the amplitude of the maximum temperature fluctuation at each location in the mixer.

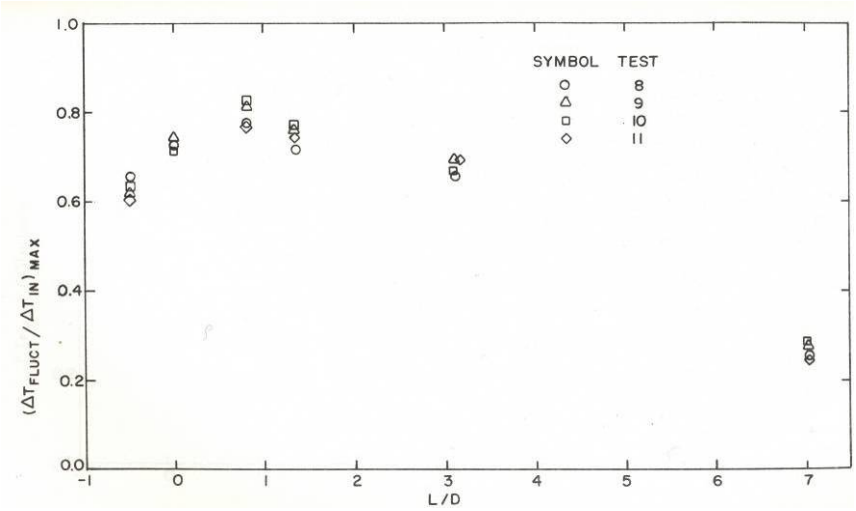

Figure 3.5-21 Temperature fluctuation amplitude as function of exit-leg location in sodium 180° inlet-leg tee with no inlet reducers (inlet flows unbalanced $Q_C/Q_H = 1.56$; four different inlet flow levels)

Figure 3.5-22 shows more sodium data from the preceding pipe tee and that for inlet-leg flow unbalances of up to Q_C/Q_H = 1.8 the flow unbalance has no influence on $\Delta T_{FLUCT}/\Delta T_{IN}$ variation throughout the tee. However, for greater unbalances the fluctuation amplitude falls off because the flow from the high-flow inlet leg overwhelms the flow from the low-flow inlet leg, and mixing takes place primarily in the tee chamber.

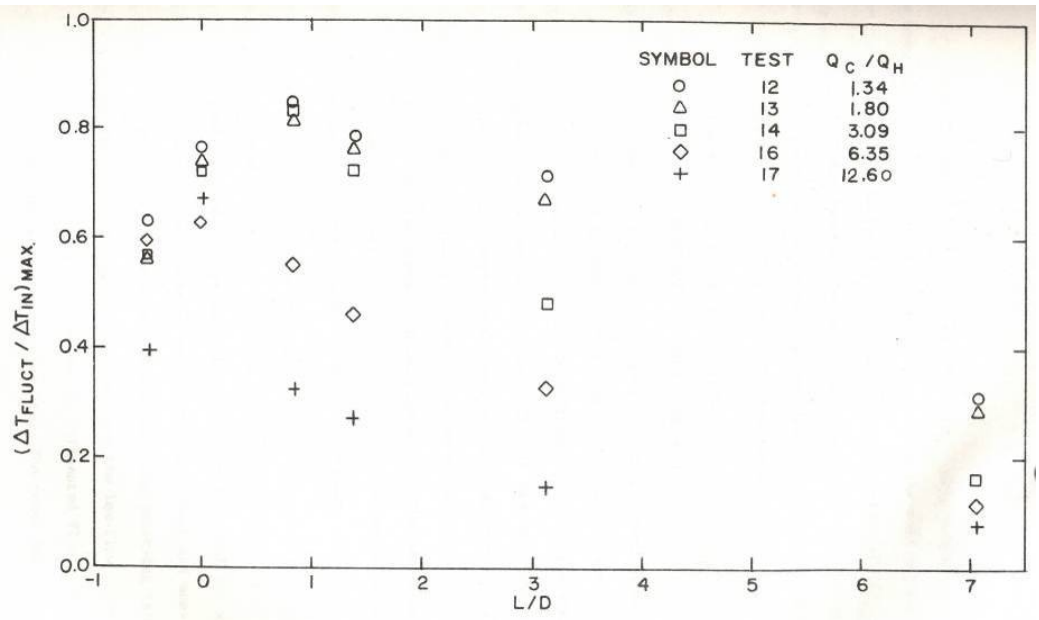

Figure 3.5-22 Temperature fluctuation amplitude as function of exit-leg location for sodium 180° inlet-leg tee with <u>no inlet reducers</u> (various degrees of flow unbalance Q_C/Q_H ; various inlet flow levels)

From sodium testing of a 180° inlet-leg pipe tee <u>with inlet reducers</u>, as shown in Fig. 3.5-23, more effective mixing takes place in the tee chamber with reducers, but the temperature fluctuations are still potentially large enough to subject the tee structure to detrimental thermal stripping. The same was true for the water testing of the geometrically similar tee. Also note

that moderate levels of inflow unbalance have no effect on the temperature fluctuation amplitude, just as was the case for the tee without inlet reducers (see Fig. 3.5-21).

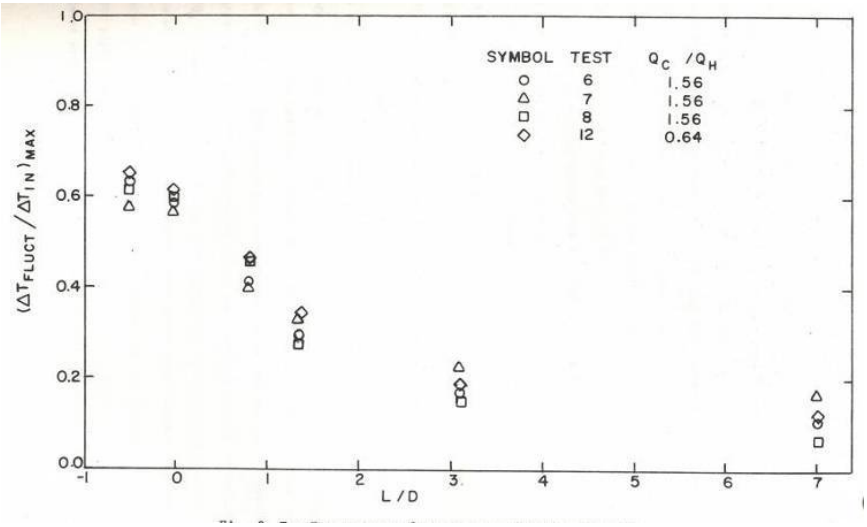

Figure 3.5-23 Temperature fluctuation amplitude as function of exit-leg location for sodium 180° inlet-leg tee <u>with inlet reducers</u> (various degrees of flow unbalance Q_C/Q_H and various inlet flow levels)

Figure 3.5-24 shows plots of sodium and water temperature fluctuation from the Argonne tests in geometrically identical pipe tee mixers <u>with no inlet reducers</u>, as well as the ratio of sodium-to-water temperature fluctuation amplitude. The curves are each an average of several tests. As shown, for both the water and sodium tees the maximum fluctuations occur just downstream of the tee chamber in the exit leg pipe, and the ratio between sodium and water data is ~ 0.8 in the tee chamber and in the entry region of the exit pipe. The lower fluctuation amplitude in sodium is the result of the higher thermal conductivity of sodium than water, which causes more rapid attenuation of the mixing-generated thermal oscillations caused by the temperature difference of the inlet streams. Also note that tee size has no effect on the behavior of the temperature fluctuations, as was evident from the data for the 4-in. (10-cm) and 8-in. (20-cm) water mixer tests.

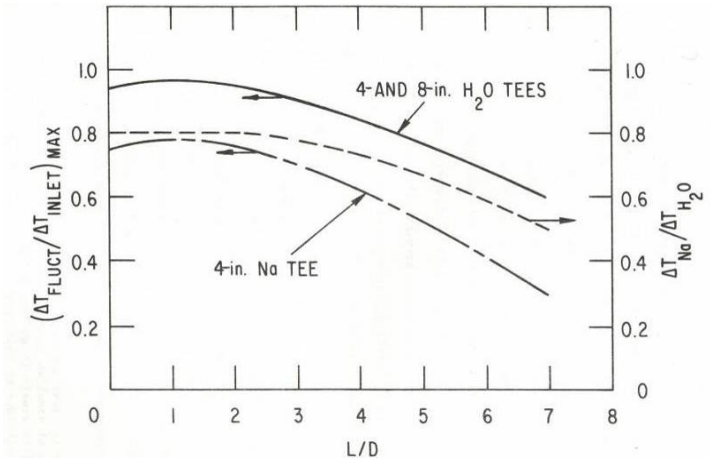

Figure 3.5-24 Comparison of H_2O and Na temperature fluctuation amplitude in a 180° inlet tee <u>with no inlet reducers</u>; ($Q_{LOW}/Q_{HIGH} > 0.32$)

Figure 3.5-25 shows data similar to that in Fig. 3.5-24, but for tees with inlet reducers and balanced inlet flow rates $Q_C/Q_H = 1$. The curves for the sodium and water data as well as the ratio between sodium and water temperature are very similar to those from tees without reducers. However, with reducers the maximum temperature fluctuations occur in the tee chamber proper, in contrast to the previous case without reducers, where the maximum fluctuations occurred in the exit leg just downstream of the tee chamber.

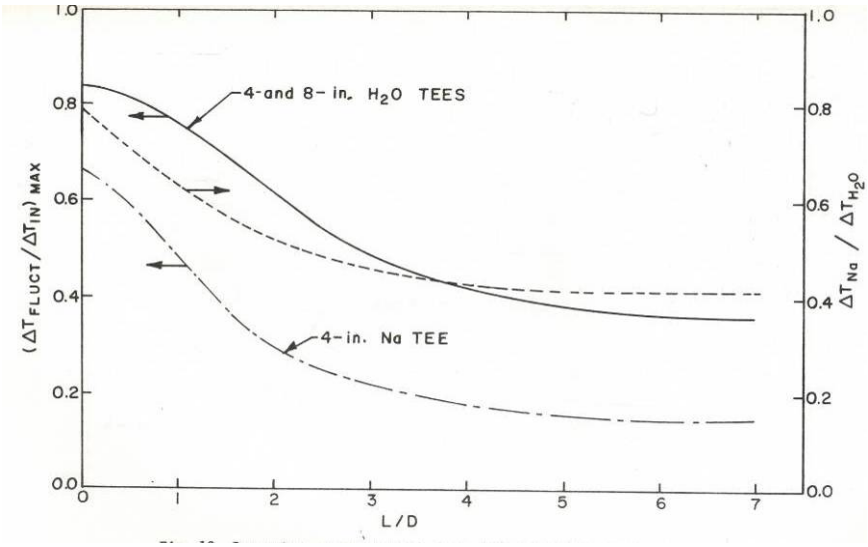

Figure 3.5-25 Comparison of H_2O and Na temperature fluctuation amplitude in a 180° inlet tee with inlet reducers; ($Q_C/Q_H = 1$)

Figure 3.5-26 shows data similar to those in Fig. 3.5-25 for tees with inlet reducers but with significantly unbalanced inlet flows of $Q_C/Q_H = 2.44$. Compared to Fig. 3.5-25 for tests of the same geometry but with balanced inlet flows, the fluctuation amplitude is reduced, but the ratio of sodium-to-water temperature fluctuation amplitude is very similar. In all these comparisons of temperature fluctuation amplitude for sodium and water, the data are for cases in which there is no thermal-buoyancy-induced flow stratification into the lowest flow inlet leg as described in Section 3.1.

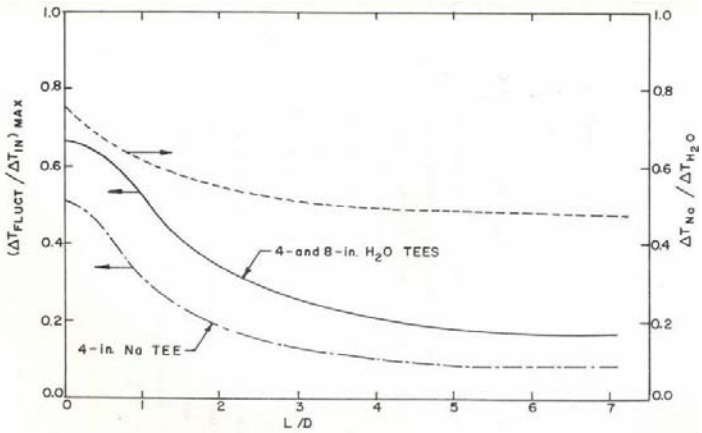

Figure 3.5-26 Comparison of H_2O and Na temperature fluctuation amplitude in 180° inlet tees with inlet reducers; (unbalanced inlet flows, $Q_C/Q_H = 2.44$)

Figure 3.5-27 shows a typical PSD plot for temperature fluctuation data from a sodium mixing tee test for a mixer having 180^o inlet legs and inlet reducers. Clearly, just as was the case for the water testing, the sodium mixer shows a dominant frequency created by the fluid flip-flop action associated with this mixer geometry. The modeling of the characteristic frequency was discussed in Section 3.5.3. For this case the dominant frequency is 0.79 Hz.

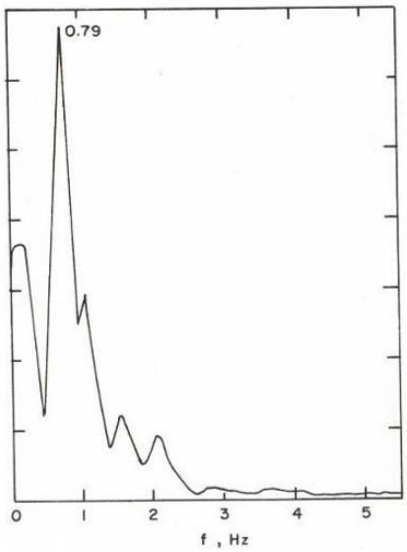

Figure 3.5-27 PSD plot for Na temperature fluctuation data from a mixing tee having 180^o inlet legs and inlet reducers

Figure 3.5-28 shows a graph of both sodium and water pipe tee large-scale fluid motion generated dominant component temperature fluctuation frequency data plotted as a function of the exit-leg Reynolds number Re_E in terms of the nondimensional frequency Strouhal number, S_t. These data were obtained from tees having 180^o inlets and no reducers for balanced and moderate unbalance inlet flows. The frequency data were determined by PSD analysis of the temperature data. As discussed in Sections 3.5.2 and 3.5.3, tees with and without inlet reducers generate large-scale but different fluid motions having characteristic frequencies. Clearly, for tees without reducers having either balanced or an unbalanced inlet-flow ratio of $Q_C/Q_H = 1.5$, the frequency of dominant temperature fluctuation is represented by a constant value of S_t, which varies with the degree of inlet-flow unbalance and is insensitive to Re_E.

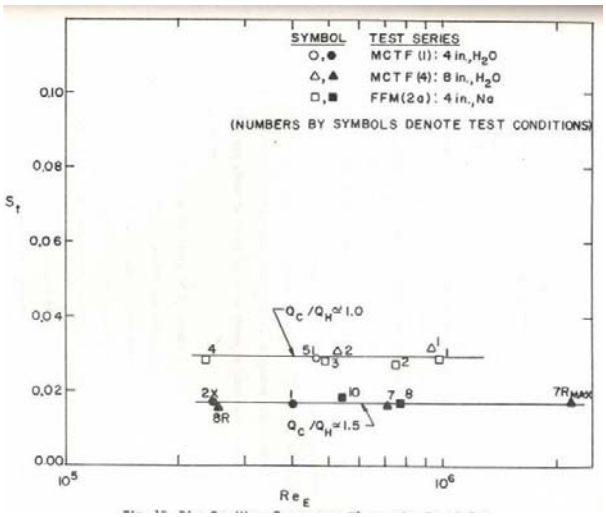

Figure 3.5-28 Sodium and water pipe tee temperature fluctuation Strouhal number (S_t) versus tee exit-leg Reynolds number (Re_E); for tees with 180° inlets and <u>no reducers</u>

Figure 3.5-29 shows sodium and water temperature fluctuation frequency data for 180° tees with inlet reducers in terms of S_t versus the exit-leg Reynolds number Re_E. Data for balanced and unbalanced inlet-flow cases are presented. Clearly, the inlet-leg reducer generated fluidic flip-flop action creates a dominant temperature fluctuation frequency and associated constant Strouhal number, which as shown is not a function of the exit-leg Reynolds number for both water and sodium data. Also plotted in Fig. 3.5-29 are the predictions from the Argonne flip-flop model (see Section 3.5.3) for the Strouhal for two cases of inlet-flow ratio. Very good agreement between data and model is evident, and the behavior of St is the same in water and sodium.

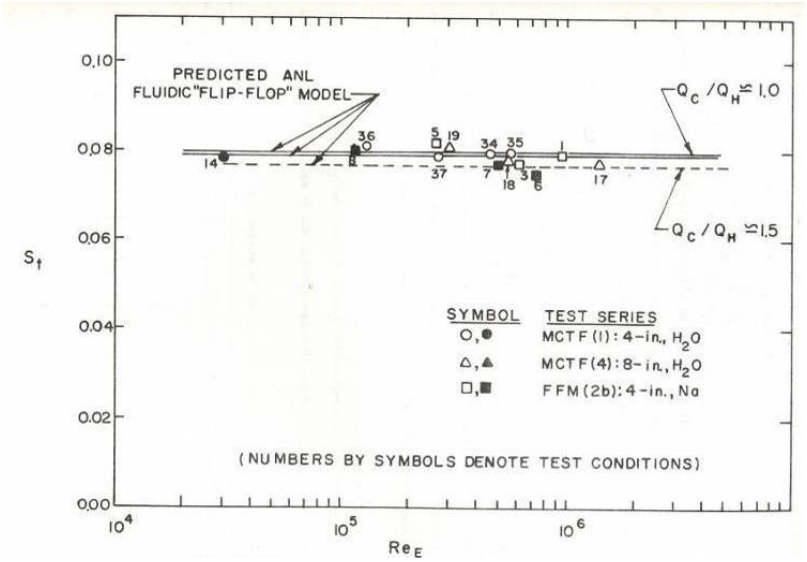

Figure 3.5-29 Sodium and water pipe tee temperature fluctuation Strouhal number (S_t) versus tee exit-leg Reynolds number (Re_E); for tees with 180° inlets and <u>inlet reducers</u>; Also plotted are Argonne flip-flop model predictions.

3.5.5 Conclusions

From the preceding it can be concluded that the behavior of $(\Delta T_{FLUCT}/\Delta T_{in})_{MAX}$ versus L/D for a standard 180° inlet tee mixer without inlet reducers can be represented by a single curve that is valid for a given fluid (this has been done for both sodium and water) over a wide range of thermal-hydraulic tee inlet conditions. Guidelines have been established for determining when the universal curve is valid. It has been found that two phenomena can cause deviations from the universal behavior: (i) thermal-buoyancy-induced intrusion of either the "hot" or "cold" inlet fluids into the opposite inlet pipe and ii) the occurrence of "corner cut-off" in the inlet flow tee chamber when a certain degree of inlet flow unbalance is exceeded. These phenomena occur for tees with significantly unbalanced inlet flows and operating with large inlet temperature differences. Comparing sodium and water data for $(\Delta T_{FLUCT}/\Delta T_{in})_{MAX}$ shows that the temperature fluctuations in a sodium tee operating under the same conditions are 20% lower than in water in the locations of maximum fluctuation amplitude. The ratio of sodium-to-water temperature fluctuation amplitude for tees with reducers is found to be at most a weak function of inlet flow rate ratio. As for the tee without reducers, the upper bound on this ratio is 0.8. Hence, water testing of a tee as a simulation of prototype sodium tee performance yields inherently a built-in factor of safety with respect to temperature fluctuation amplitude.

A comparison of the temperature fluctuation data for tees with and without inlet-pipe reducers in the absence of thermal buoyancy and "corner cut-off" effects shows that $(\Delta T_{FLUCT}/\Delta T_{IN})_{MAX}$ is a little lower with pipe reducers. Hence, the addition of inlet pipe reducers improves thermal mixing a little, but they also can produce large structural tee shaking forces resulting from the fluidic flip-flop motion of the two inlet streams. The Argonne flow visualization studies showed that inlet pipe reducers increase the degree of "hot-cold" stream interaction within the tee chamber. Without reducer pipes and in the absence of "corner cut-off" effects, the two inlet streams were found to interact very little in the tee chamber and channel separate paths into the exit leg. In the absence of "corner cut-off" and inlet-leg thermal stratification effects, mixer size effects are properly accounted for by the non-dimensional length parameter L/D. The influence of tee size is identical for sodium and water. The temperature-fluctuation-frequency Strouhal number for balanced and 50% unbalanced inlet flows for tees with inlet reducers was found to be well predicted by the Argonne fluidic flip-flop model. The temperature fluctuation Strouhal number for geometrically similar tees with reducers was also found to be a function of inlet flow-rate ratio, but not a function of exit-leg Reynolds number, tee size, or fluid medium.

Earlier efforts by Argonne at developing an analytical predictive model for the ratio of the temperature fluctuation amplitude between sodium and water for a coaxial two-stream mixer [5,17] yielded a large-eddy thermal conduction model that was in qualitative agreement with experimental trends. With additional research and the possible use of direct eddy simulation CFD approaches, the temperature fluctuation model could be improved to allow quantitative assessment of temperature fluctuation attenuation with location in a mixer.

In conclusion, Argonne has characterized the temperature fluctuations occurring in thermal mixers having 180° inlet-leg angle pipes, with and without inlet reducer pipes. Sodium and water data from different sized tees have allowed delineation of the size and fluid medium modeling laws required for the extrapolation of reduced-scale water model temperature

fluctuation to prototype sodium mixers. The information presented is vital to the design of thermal-fatigue-free mixers.

3.5.6 Advanced Design Thermal Mixers

Standard mixing tees using either 180° or 90° inlet-leg flow geometries with equal inlet leg and tee-chamber pipe sizes are plagued by similar thermal-hydraulic conditions conducive to thermal fatigue. The thermal-hydraulic conditions of concern are those which occur when the inlet flows are steady and the mixing tee is operated with a constant inlet-leg temperature difference. The mixing action produces large amplitude temperature fluctuations, and when inlet-leg reducers are present on 180^o inlet-leg mixers, large shaking forces can occur.

In summary, 180° inlet-leg angle mixing tees fitted with inlet pipe reducers exhibit the following traits:

- Large amplitude temperature fluctuations occur in the tee chamber and exit leg.
- Fluidic "flip-flop" occurs in the tee chamber.
- "Hot-cold" slug flow occurs in the exit leg at the frequency f_p.
- Tee pressure and flow fluctuations occur at the frequency f_p.
- A cyclic tee shaking force is produced at the frequency f_p.
- Thermal fatigue and mechanical vibration fatigue of the tee are possible.
- Both f_p and the shaking force can be predicted by models developed at Argonne

The conventional 90° inlet-leg angle mixing tee, like the 180° inlet angle tee, was also shown to produce thermal-hydraulic conditions conducive to thermal-fatigue problems. The performance characteristics of this tee geometry are as follows:

- Performance is generally poor.
- "Hot-cold" inlet streams tend to channel separate paths through the exit leg.
- Mixing occurs along a plane separating "hot-cold" regions.
- In general 90° inlet-leg angle tees are poorer mixers than 180° tees with large temperature fluctuations occurring at L/D > 7.
- If sidearm in-flow is much larger than through-flow, severe thermal-fatigue conditions can be present directly opposite the sidearm pipe.

Argonne has developed two improved mixer designs, which are described in this section: the CRBR 180^o inlet-leg mixer [17,18] shown in Fig. 3.5-30 and a 90^o inlet-leg mixer [19] shown in Fig. 3.5-31. These improved designs were developed to eliminate tee-generated shaking forces and to reduce thermal oscillations produced by two-stream mixing, which have the potential to cause structural thermal stripping in the piping.

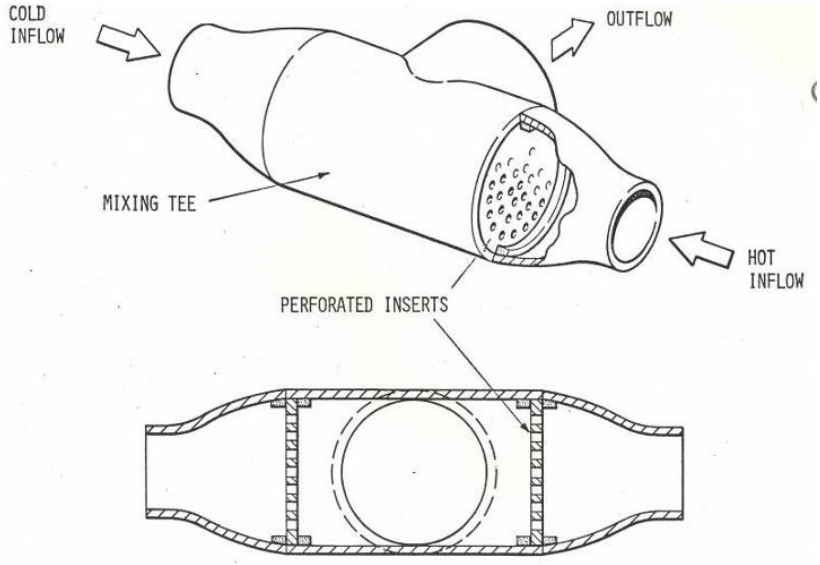

Figure 3.5-30 Argonne developed improved 180^{o} inlet-leg thermal mixer for CRBR

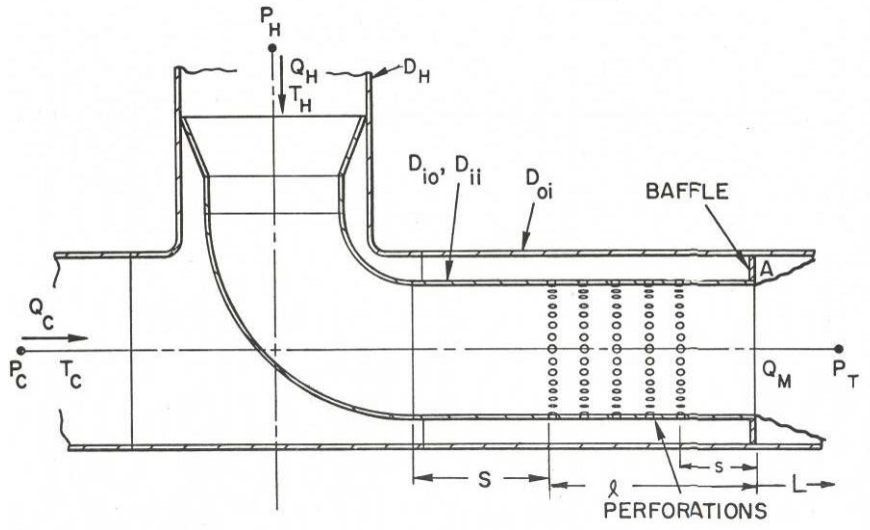

Figure 3.5-31 Argonne developed improved 90^{o} inlet-leg thermal mixer

3.5.6.1 Improved 180^{o} Inlet -Leg Mixer for CRBR

The improved thermal mixer developed for CRBR (Fig. 3.5-30) consists of mounting perforated plate inserts in the "hot-cold" inlet legs of a 180° angle mixing tee. Although the concept was only tested for the 180° inlet-leg angle tee, it can also be used for the 90° inlet angle tee advantageously. The improved tee design outperforms the conventional mixing tee design (tee without perforated plates). Multiple jet interactions formed by the plate holes within

the tee chamber increase thermal mixing and eliminate large-scale transient flow behavior within the tee, which can produce tee shaking forces.

The opposing circular plate inserts in each inlet leg contain discrete circular flow holes. A pressure differential across these plates produces "hot and cold" fluid jets issuing into the tee chamber proper, the region between the two perforated inserts. The degree of increased thermal mixing performance over the conventional tee design is thus directly related to the amount of "hot-cold" stream interaction that occurs in the tee chamber. The greater the interaction of the "hot and cold" jets, the greater will be the thermal mixing of the two temperature inlet streams before they enter the exit pipe. Increasing jet interaction, while improving thermal mixing performance, involves a design trade-off as a result of the increase in tee pressure losses. In general, this design trade-off is always present when seeking improved thermal mixing devices.

The degree of interaction between the opposing individual jets is governed by geometrical design parameters such as the spacing between the plates and the hydraulic conditions. The influence of these parameters is determined by extrapolating information from jet theory to the present problem, even though the problem involves multiple jets interacting within a confined space. For a single jet issuing from a circular orifice, the penetration distance of the jet into the surrounding fluid and the length of the core region of the jet increase with the jet orifice exit velocity and orifice hole size. Thus two jets, one hot and one cold, that originate in opposing perforated plates will interact within the tee chamber most intensely when they (1) impinge most nearly head-on and (2) have large core regions (i.e., regions with temperatures and velocities equal to their initial inlet orifice values and not altered before impact by turbulent action). Thus, the distance between perforated plate inserts for a given initial jet velocity and perforation hole diameter will influence mixing tee performance. The smaller the separation distance, the greater will be the intensity of the jet impact due to the larger jet core (and hence, better mixing).

Various perforated plate insert designs were performance-tested in a 4-in. (10-cm) mixing tee with 2-in. (5-cm) inlet reducer pipes. Figure 3.5-32 shows the effect of five void area ratios in the perforated-plate insert on the maximum temperature fluctuation amplitude at various locations along the mixer-exit flow pipe. A plate design with a void area fraction of 26.8% and seven 19-mm-dia beveled inlet holes in each perforated plate exhibited the best overall performance. The peak-to-peak temperature fluctuation amplitude in the tee exit leg was reduced 20 to 30%, below the case when mixing was achieved with no perforated plates present. Best mixing was achieved when the perforated plates in the two inlets were oriented such that the individual perforations were directly opposed, or “in-line.” This plate design also eliminated all traces of fluidic "flip-flop" and thus prevented tee shaking forces. More important, the testing also showed that when the percentage of plate hole void area exceeds a critical value, somewhere in the range between 26.8 and 35.5%, fluidic pulsations are not eliminated by the installation of perforated plates.

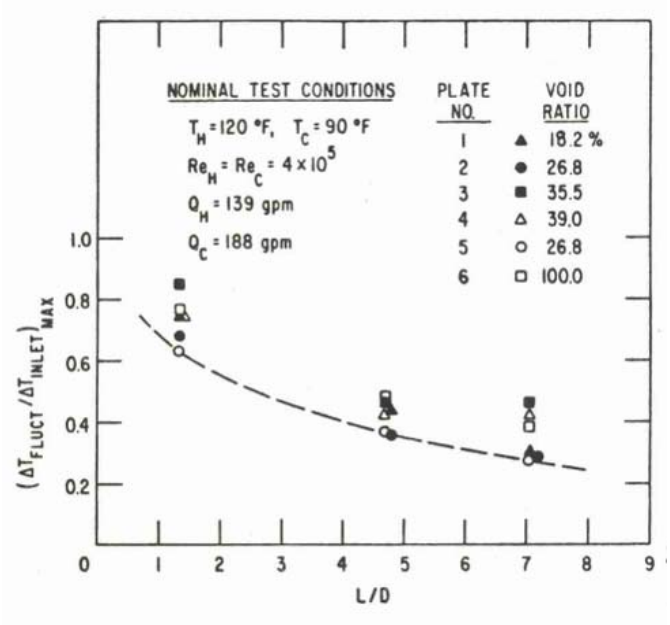

Figure 3.5-32 Effect of CRBR mixer perforated plate insert void area ratio on maximum temperature fluctuation amplitude along the mixer exit pipe L/D

Tee pressure-drop data also showed that tee pressure losses can be held to a reasonable level in the tee by careful smoothing and contouring the flow-inlet side of the plate holes. No attempt was made to experimentally explore the effect of perforated-plate separation distance on performance or to establish an optimum performance design in terms of all the delineated design parameters. Thus, additional experimental effort is needed to establish an optimum designed mixing tee of this configuration. The proposed CRBR mixer design was not optimum.

3.5.6.2 Improved 90^o Inlet-Leg Thermal Mixer

The CRBR mixer used perforated plate inserts in the inlet legs of a standard 180^o inlet tee to reduce mixer-produced, large-scale fluid transients and improve the thermal mixing performance. The perforated inserts reduced the exit-leg temperature fluctuation amplitude 20 to 30% over standard pipe tee performance with reasonably low pressure losses. However, in the tee chamber proper, fluctuations as large as 85% of the inlet-leg temperature difference occurred. A good mixer design must promote rapid thermal mixing of the fluids to minimize temperature-fluctuation effects both in the tee chamber and on components downstream of the mixer (e.g., piping, valves, elbows, and pump inlets). The design must also attempt to minimize pumping losses so as to maximize system hydraulic pumping efficiency, with the realization that the promotion of more rapid mixing usually is accompanied by increased pumping requirements.

A schematic of the Argonne-improved 90^o inlet-leg mixer is shown in Fig. 3.5-31. The two streams Q_c and Q_H enter the mixer and proceed part way through along two separate flow paths: Q_C through the outer annular region between the mixer pressure boundary and the central

perforated pipe, and Q_H through the central pipe. Eventually, Q_C is blocked by a baffle and thus is forced through the holes in the central pipe, forming a large number of jets, which promote rapid thermal mixing with Q_H. Because the mixing occurs primarily away from the walls of the central pipe, thermal-fatigue-producing temperature fluctuations can be minimized. Furthermore, because the central pipe is not a primary pressure boundary, the pipe wall can be made thinner than that of the primary boundary. This condition enhances resistance to thermal fatigue if complete elimination of wall temperature fluctuations at the inner pipe wall is not achieved. Also, by using a sufficiently large total perforated hole area relative to the Q_C flow which must be passed, the jet velocity can be maintained low enough to keep mixer pressure losses to a tolerable level consistent with rapid thermal mixing and low thermal-fatigue-producing propensity. The combined flows expand into the piping downstream of the mixer, and with proper mixer design the temperature fluctuations still persisting at the fluid-wall interface of this downstream primary pressure boundary piping can be maintained at a very low level.

Detailed information on mixer performance (both experimental and analytical) was generated on peak-to-peak temperature fluctuation amplitude, associated temperature fluctuation frequency, and flow pressure losses from the test article shown in Fig. 3.5-33. Figure 3.5-34 shows temperature fluctuation data from the test article for the inner perforated pipe region, where jet mixing occurs, and in the downstream pipe after the two flows are combined. In both regions the temperature fluctuations seen by the pipe walls are quite small; much smaller than for standard pipe tee mixers.

Argonne has developed a general correlation in terms of three basic mixing mechanisms which relates ΔT_{FLUCT} to all pertinent parameters. The mixer concept was shown to be capable of achieving rapid thermal mixing for which ΔT_{FLUCT} in all regions is less than 30% of the two-inlet stream temperature difference. In contrast, conventional pipe tee mixers as described earlier readily experience ΔT_{FLUCT} on the order of 90% of the inlet-leg temperature difference. The low level of ΔT_{FLUCT} achieved in the improved 90° inlet-leg mixer design qualifies it as a thermal-fatigue-free mixer for LMR service.

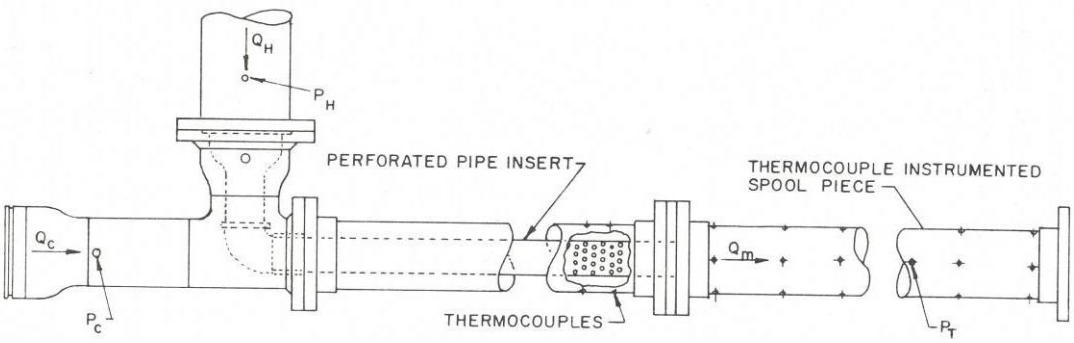

Figure 3.5-33 Argonne's developed improved 90° inlet-leg mixer test article

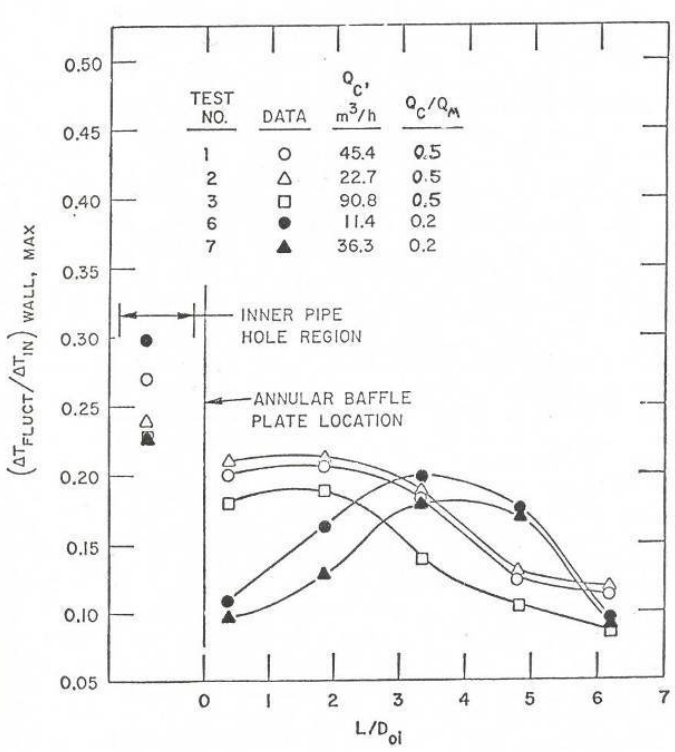

Figure 3.5-34 Normalized temperature fluctuation amplitude data for the Argonne improved 90° inlet-leg mixer

There are three flow mechanisms that influence the thermal mixing efficiency of the mixer and the flow losses through the mixer: the number of fluid jets created by the holes in the inner pipe, turbulent cross-flow interaction between the jets and the flow from the other leg, and the sudden expansion of the combined flows into the mixer exit pipe. A model incorporating all of these mechanisms was developed for predicting mixer pressure losses and correlating the maximum temperature fluctuations occurring in the exit pipe. In general, the larger the mixer flow losses, the greater the mixing and attenuation of temperature fluctuation amplitude at the walls of the exit pipe.

Modeling the above three mechanisms and their dependence on mixer design parameters yielded the parameter ζ below, which was used to correlate the data from the water experiments for the maximum amplitude of the normalized temperature fluctuations $\Delta T_{FLUCT}/\Delta T_{in}$ occurring in the mixer exit pipe:

$$\zeta = (V_j/V_H)\ (\ell/D_{ii})^{(2-Q_C/Q_M)} \left[1-\left(\frac{D_{ii}}{D_{oi}}\right)^2\right]^2$$

$$= \left(\frac{D_{ii}}{D_j}\right)^2 \frac{1}{N}\left[\frac{(Q_C/Q_M)}{1-(Q_C/Q_M)}\right]\left[\frac{s}{D_{ii}} + \phi\,\frac{D_j}{D_{ii}}\,(N_R-1)\right]^{(2-Q_C/Q_M)} \left[1-\left(\frac{D_{ii}}{D_{oi}}\right)^2\right]^2$$

This parameter incorporates all pertinent mixer hydraulic and geometric parameters into its formulation. Figure 3.5-35 shows $[\Delta T_{FLUCT}/(T_H-T_B)]_{MIXER,\ MAX}$ versus ζ for all 65 of the thermal mixing tests performed for the improved mixer. As shown, the temperature fluctuation amplitude correlates well with ζ. To make the data more useful to a mixer designer, they were fit with a second-order-polynomial least squares curve, which yielded the correlation function:

$$[\Delta T_{FLUCT}/(T_H - T_B)]_{MIXER,\ MAX} = 0.482 - 0.315\ \ell n\ (\zeta) + 0.056\ \ell n^2\ (\zeta),$$

where $\ell n(\zeta)$ denotes the natural logarithm.

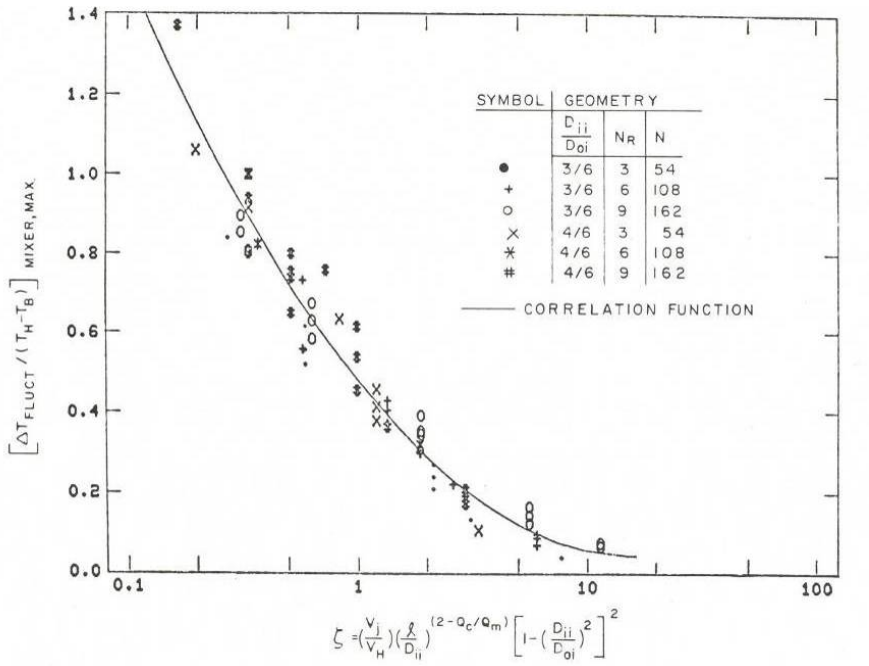

Figure 3.5-35 Maximum temperature fluctuation amplitude for Argonne improved 90° inlet-leg mixer as a function of correlation parameter ζ

The mixer is capable of being designed to achieve rapid thermal mixing for which ΔT_{FLUCT} at the pipe pressure boundary is less than 20% of the two-stream inlet temperature difference. In contrast, conventional pipe tee mixers previously tested readily experienced ΔT_{FLUCT} of order 90% of the inlet-leg temperature difference. The low level of ΔT_{FLUCT} achievable in this mixer design qualifies it to be considered a thermal-fatigue free mixer for LMR service. The frequency f associated with the temperature fluctuations ΔT_{FLUCT} in the exit pipe was shown to be correlated by the non-dimensional Strouhal frequency parameter $S_t = f D/V$, where D and V are, respectively, the pipe diameter and mean flow velocity in the combined flow exit pipe. A constant value of $S_t = 0.13$ was found to exist over a wide range of experimental conditions. The information furnished on ΔT_{FLUCT} and f allow a thermal stress analyst to evaluate thermal fatigue propensity of this mixer for a specific application. The mixer was also shown to be capable of achieving good thermal mixing with a pumping loss penalty being no larger than for a conventional pipe tee mixer. The information generated was formulated into a thermal-hydraulic Design Guide for the mixer [19]. The Guide does not cover the evaluation of actual thermal stresses produced by thermal mixing, and hence, no guidelines are given for making life predictions for a thermal-fatigue-free mixer. The Guide does contain an example on how to

size an improved mixer for use in combining the liquid sodium outflows from two paired evaporators in the CRBR intermediate heat transport system, where the temperature unbalance between the two streams occurs as the result of an off-normal condition, such as the loss of one evaporator.

References

1. Bump, T.R., "LMFBR Problems Due to Large Temperature Differences," Trans. Am. Nucl. Soc., *17*, 421 (1973).
2. Uherka, K.L., "An Evaluation of Available Experimental Results and Service Performance Data for Mixing Components," ANL-CT-73-26 (November 1973).
3. Creer, J.M., Watt, J.A., and Yatabe, J.M., "Thermal Mixing in FFTF Secondary Piping Tees," HEDL-TME 73-21 (January 1973).
4. Landoni, J.A., "Mixing Tee Cold Transients," Liquid Metal Engineering Center, 73-LMEC-DRF-3416 (April 1973).
5. Oras, J., "A Survey and Evaluation of LMFBR Thermal Stratification Problems, Applicable Analytical Models, and Devices for Counteracting Thermal Stratification," Argonne National Laboratory, ANL-CT-76-3 (July 1976).
6. Kasza, K.E., "Temperature Fluctuations and Shaking Forces in Certain Mixing Tee Configurations," Trans. Am. Nucl. Soc., *22*, 579 (1975).
7. Kasza, K., and Uherka, K., "Development and Testing of an Improved Mixing Tee," Trans. Am. Nucl. Soc., *23*, 389 (1976).
8. Kasza, K., and Uherka, K., "Thermal Phenomena in Mixing Tees: MCTF Flow-Visualization Studies," Trans. Am. Nucl. Soc., *24*, 373 (1976).
9. Kasza, K., "Test Plan For ANL/FFM Mixing Tees No. 2a and 2b," ANL-T0028-0010-SE-00 (October 1976).
10. Kasza, K., and Oras, J., "Water/Sodium Temperature-Fluctuation Correlation Mixing-Tee Experiments," Trans. Am. Nucl. Soc., *26*, 432, (1977).
11. Kasza, K.E., and Uherka, K.L., "Thermal Phenomena in Mixing Tees: MCTF Flow-Visualization Studies," Trans. Am. Nucl. Soc. *24*, 373 (1976).
12. Oras, J.J., and Kasza, K.E., "The Use of Laser Flow Visualization Techniques in Reactor Component Thermal-Hydraulics Studies," Trans. Am. Nucl. Soc., Vol. 47 (1984).
13. Kasza, K.E., and Colwell, W.S., "Characterization of the Temperature Fluctuations Generated in a Thermal Mixing Tee (Sodium Versus Water Behavior)," ANL-CT-78-2 (November 1977).
14. Kasza, K.E., and Oras, J.J., "Water/Sodium Temperature-Fluctuation Correlation Mixing-Tee Experiments," Trans. Am. Nucl. Soc., *26*, 432 (1977).
15. Debler, W., "The Intrusion of Fluid into the Inflow Branch of a 180°-Approach Mixing Tee," ANL-CT-76-47 (September 1976).

16. Fraser, J.P., and Oakley, D.J., "Turbulent Free Convection Heat Transfer Rates in a Horizontal Pipe," KAPL 1494 (1956).

17. Kasza, K.E., Oras, J.J. and Colwell, W.S., "CRBR/IHTS Mixer Thermal-Hydraulic Model Tests (In Support of GE/CRBRP:DRS 51.32)," ANL-CT-77-26 (May 1977).

18. Kasza, K.E., and Uherka, K.L., "Development and Testing of an Improved Mixing Tee," ANL-CT-76-42 (July 1976).

19. Kasza, K.E., and Bobis, J.P., "Thermal-Hydraulic Design Guide for an Advanced Design Thermal Mixer (Including Development/Testing Details)," ANL-CT-79-4 (October 1978).

20. Kasza, K.E. and Oras, J.J., "Mixing-tee Temperature-fluctuation Size-scaling Experiments: MCTF Test Section No. 4," ANL-RDP-59 (March 1977).

21. Kasza, K.E., and Uherka, K.L., "Mixing Components: Flow-visualization Studies," ANL-RDP-49 (March 1976).

22. Huebotter, P.R., "Report of the National Task Force on Thermal Stripping in LMFBRs," ANL-CT-78-46 (September 1978).

4.0 Past Argonne Studies on In-vessel Thermal-Hydraulics

Argonne in the 1970s and 1980s conducted ground-breaking studies based on water experiments addressing the flow and thermal behavior in LMR core outlets and plenums. The early studies, covered in Section 4.1, were in support of CRBR and used simplified models of the core outlet and upper plenums to explore thermal plume behavior above the core and stratification in the plenum. These studies also addressed the potential for thermal stripping at the core outlets and on the upper internals structures due to outlet temperature non-uniformities in the core sub-region. Starting in the early 1980s, covered in Section 4.2, Argonne conducted complete in-vessel thermal–hydraulic studies of the proposed GE/PRISM and RI/CE/SAFR reactor concepts.

Section 4 describes the Argonne studies, which focused on the complex thermal-hydraulic interactions that occur between the in-vessel components during the low-flow thermal transients associated with transition to natural circulation and decay heat removal. These interactions are produced by very strong thermal-buoyancy fluid forces, which not only effect individual-component thermal and structural behavior but also strongly influence global-reactor decay heat removal and general-reactor cooling under low-flow operation. The thermal-buoyancy forces cause the momentum and energy equations to become strongly coupled and the flow and thermal fields to be highly non 1-D. This causes gross errors in component and system design results that are based on 1-D flow-distribution modeling, in which the thermal effects are transported solely as a passive scalar with the only dependence on temperature being through the fluid properties. Gross design errors can also be introduced if the design is based on experimental data correlations or performance verification using isothermal flow testing..

4.1 Early Argonne Studies of CRBR Core-Plenum

The early core-plenum studies by Argonne were conducted in the Outlet Plenum Mixing Test Facility [1-6]. Figure 4.1-1 shows a schematic of the water facility. Figure 4.1-2 shows photos of the plenum containment tank and the simplified (1/10 scale) CRBR core internal test article used for studying core-outlet thermal plume and plenum interactions. Figure 4.1-3 shows the thermocouple-instrumented, seven-tube model of a core outlet used for studying thermal stripping.

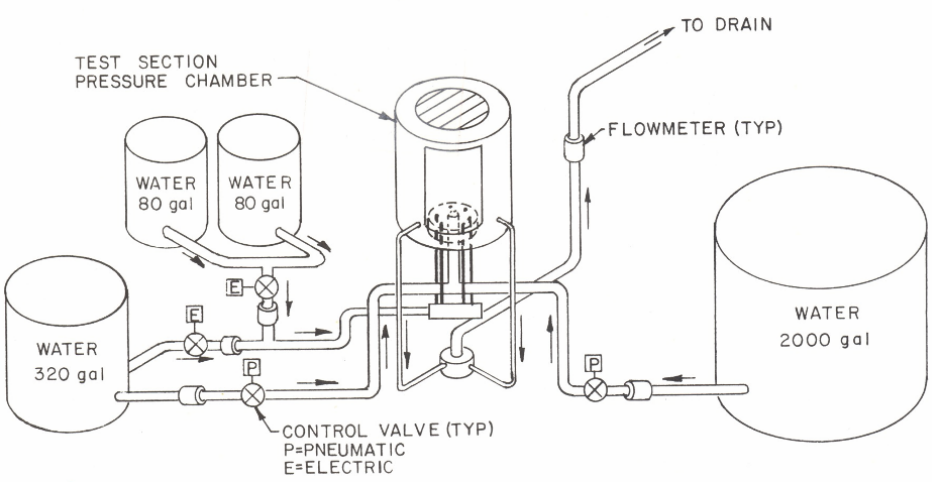

Figure 4.1-1 Schematic of Argonne Outlet Plenum Mixing Test Facility

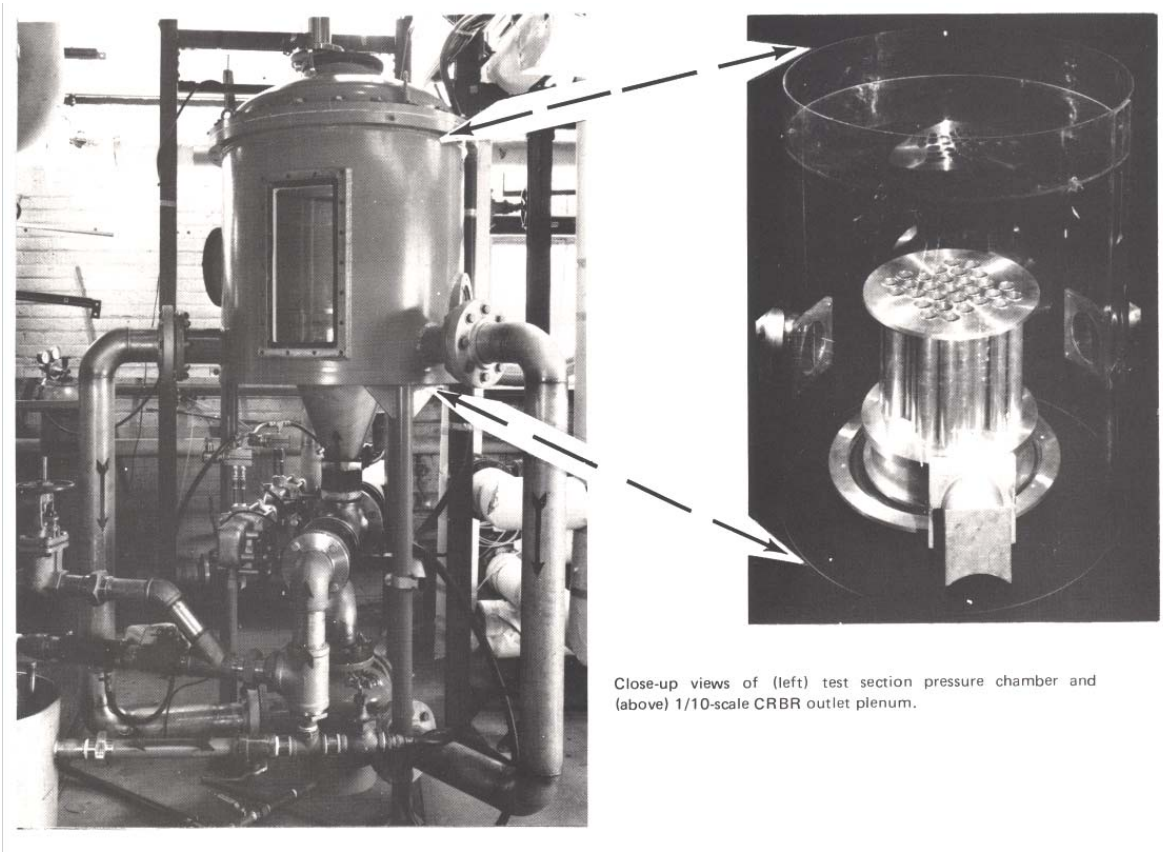

Close-up views of (left) test section pressure chamber and (above) 1/10-scale CRBR outlet plenum.

Figure 4.1-2 Argonne Outlet Plenum Mixing Test Facility; pressure vessel containment (left) and 1/10-scale model of CRBR outlet plenum (right)

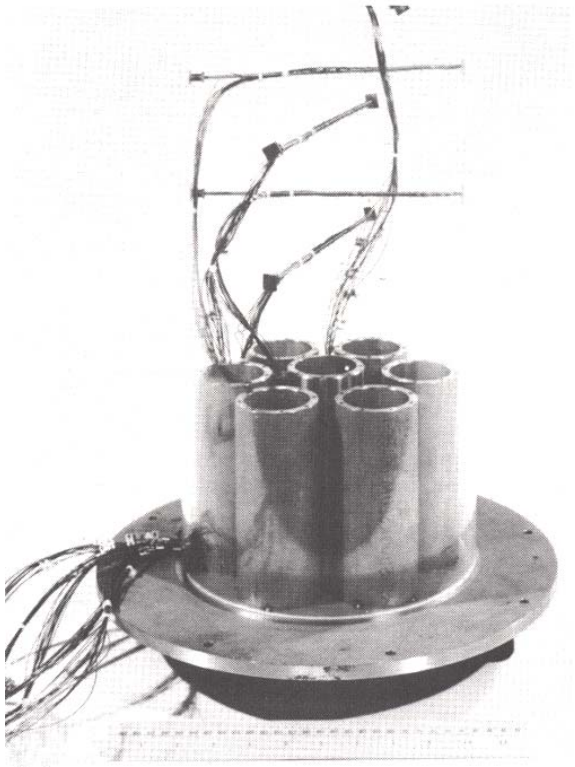

Figure 4.1-3 Argonne thermocouple-instrumented, seven-tube core outlet model for studying above core thermal stripping

The Argonne testing facility operated in the steady-state or transient modes. Studies in the steady-state mode focused on phenomena such as flow distribution between flow and blanket regions using dye injection, thermal stripping, and average temperature fields. Studies in the transient mode focused on phenomena associated with normal or constant-flow reactor scrams such as thermal plume formation, plenum stratification, and stratified-interface thermal oscillations. Exploratory use of 3-D CFD modeling was also used to simulate plenum mixing [3].

During steady-state operation, hot water from the 2000-gal tank would enter the bottom of the containment pressure vessel and flow upward through the reduced-scale simulated reactor core into the outlet plenum. Shown in Fig. 4.1-2 is the 1/10-scale CRBR simulated core. Cold water with brine added to simulate the thermal density differences between the two fluid streams for correctly modeling thermal buoyancy was introduced from the 320-gal tank and flowed up through a simulated blanket region.

Transients was also simulated by first achieving steady state with hot water flow and then reducing the flow while simultaneously introducing colder water to simulate reactor shutdown. The changes in flow and temperature were performed under computer control to model a prototype transient. Various core and plenum geometries were tested. Highlights of the results from these early studies can be found in Refs. [1-6].

References

1. Lorenz, J.J., and Carlson, R.D., "Transient Thermal-Hydraulic Behavior of a 1/15 Scale LMFBR Outlet Plenum," Trans. Am. Nucl. Soc. *19*, 307 (1974).

2. Lorenz, J.J., et al., "Influence of Scale Size and Fluid Thermal Properties in Simulating LMFBR Outlet Plenum Behavior," AIChE Symp. Series, No. 164, Vol. 73 (1977).

3. Sha, W.T., et al., "Three Dimensional Numerical Simulation of LMFBR Outlet Plenum Mixing," Trans. Am. Nucl. Soc. *26*, 434 (1977).

4. Lorenz, J.J., et al., "The Influence of Scale Size and Fluid Thermal Properties in Simulating LMFBR Outlet Plenum Behavior," AIChE Symposium Series, *73*, 120 (1977).

5. Lorenz, J.J., and Howard, P.A., "Entrainment by a Jet at a Density Interface in a Thermally Stratified Vessel," ASME J. Heat Transfer, Vol. 101, No. 3 (August 1979).

6. Oras, J.J., et al., "Conceptual Design Studies; Phase II: Plenum Mixing Studies,"ANL-CT-81-24 (April 1981).

4.2 Argonne Studies of Complete In-vessel GE/PRISM and RI-CE/SAFR Systems

The broadly stated objective of this DOE-funded program in collaboration with industry performed at Argonne was to conduct, in the Argonne MCTF, transient and steady-state thermal-hydraulic water tests in scaled complete in-vessel models of both the GE/PRISM and RI-CE/SAFR reactor concepts. These tests studied important high flow and low flow natural-convection operation scenarios to assess factors that inf1uence:

- Thermal-hydraulic performance
- Reactor emergency cooling
- Structural thermal distributions

For each reactor design concept, a complete in-vessel model was built for testing. Complete in-vessel models were used because the flow and thermal behavior in a given sub-region is the result of complex interactions with, and feedbacks from, the rest of the reactor vessel components (which is especially true under low-flow conditions during the transition to natural convection). With separate sub-region models, it would be very difficult to properly simulate inlet and outlet conditions for these models. Experimental simulations of in-vessel thermal hydraulics for PRISM and SAFR, under key postulated reactor operation scenarios, were conducted to provide the designers with performance information that is vital to the assessment

of the workability of the various design features that were being incorporated into their innovative and inherently safe reactor systems. As the GE and RI/CE designs evolved during the program, the Argonne models were altered to incorporate the new features.

Both reactor concepts were of the pool type with the intermediate heat exchangers (IHXs) and primary pumps immersed in sodium within the reactor vessel (RV). Hence, to establish the reliability and inherent safety of these reactor concepts, it is very important to understand the thermal hydraulics that are associated with the interplay and feedback between the various invessel components and the heat rejection out of the RV LMRs must be able to ride out, with minimal operator intervention, such events as a loss of normal heat sink with reactor scram or a loss of coolant pumping power and normal heat sink with failure to scram by relying on passive means for heat rejection from the RV. As a consequence, knowledge of the temperature and flow distributions during these low-flow, transient, and steady state conditions with mixed- and natural-circulation flow is essential for two reasons: (1) the validation of core coolability and component and structural performance under conditions of possibly detrimental thermal distributions and (2) the provision of information to aid in the development and validation of the thermal-hydraulic computer codes. Additionally, the influence of individual IHX, pump, and internals design and placement must be assessed with regard to general thermal-hydraulic performance and reliability of the system, as well as the individual components.

The research and testing for the DOE LMR program were performed in Argonne's MCTF located in Bldg. 212 (see Section 4.2.2). This facility was dismantled in the mid-1990s to make way for new facilities supporting the NRC program on Nuclear Steam Generator Tube Integrity. Expertise and space exists currently in Bldg. 212 for building a new DOE National Thermal-Hydraulic Test Facility supporting future GNEP programs and private-sector reactor development.

4.2.1 Non-dimensional Modeling/Scaling

The pertinent "similarity parameters" that were used in modeling the PRISM and SAFR prototypes are highlighted in Refs. [1-3]. Complete in-vessel models were built because the thermal-hydraulic behavior of one sub-region of the prototype under a variety of important engineering and safety conditions depends upon the conditions that prevail elsewhere in the reactor. Therefore, a similarity analysis of the model design to ensure the model incorporates the important attributes of the prototype should consider the whole RV. A 1-D similarity analysis applicable to such a complete system was followed in developing scaling for the two models. The parameters used are as listed below. Their values for each of the Argonne-built experimental models are given in Refs. [1,2]. In addition to these parameters, geometric similarity was also imposed between the models and prototypes. Additional information on modeling LMRs is contained in Ref. [4] and Appendix 1 , which discuss modeling and implications regarding the use of lead and sodium as coolants.

Modeling parameters used for PRISM and SAFR water experiments:

Richardson No.; $$R_i \equiv \frac{g\beta\Delta T_o \ell_o}{u_o^2} = \frac{\text{Buoyancy}}{\text{Inertia Force}}$$

Friction No.; $$F_i \equiv \left(\frac{f\ell}{d} + K\right)_i = \frac{\text{Friction}}{\text{Inertia Force}}$$

Modified Stanton No.; $$St_i \equiv \left(\frac{4h\ell_o}{\rho C_p u_o d}\right)_i = \frac{\text{Wall Convection}}{\text{Axial Convection}}$$

Time Ratio; $$T_i^* \equiv \left(\frac{\alpha_s}{\delta^2}\frac{\ell_o}{u_o}\right)_i = \frac{\text{Transport Time}}{\text{Conduction Time}}$$

Biot No.; $$B_i \equiv \left(\frac{h\delta}{k_s}\right)_i = \frac{\text{Wall Convection}}{\text{Conduction}}$$

Heat Source No.; $$Q_{si} \equiv \left(\frac{\dot{q}_s \ell_o}{\rho_s C_{ps} u_o \Delta T_o}\right)_i = \frac{\text{Heat Source}}{\text{Axial Energy Change}}$$

The Reynolds number, Re, does not appear in the above list of similarity parameters because the modeling analysis is one-dimensional. Re, which normally appears because of the boundary-layer-type shear zones, enters only implicitly through the boundary conditions. By the same token, the Prandtl number, Pr, enters through the surface heat transfer coefficient, h. The steady-state solutions of the conservation equations provide for ΔT_o, the scaling temperature differential, and, u_o, the scaling velocity given by:

$$\Delta T_o = \frac{\dot{q}_o \ell_o}{\rho C_p u_o}\left(\frac{a_{so}}{a_o}\right)$$

$$u_o = \frac{\beta\left(\frac{\dot{q}_o \ell_o}{\rho C_p}\right)\ell_h\left(\frac{a_{so}}{a_o}\right)^{1/3}}{\frac{1}{2g}\sum_i\left(F_i/A_i^2\right)}$$

Complete similarity between the model and prototype would be achieved by matching all the above parametric groups of the model, M, to those of the prototype, P. The resultant ratios are denoted below with the subscript "R". It is generally accepted that, for complex thermal-hydraulic models, complete similarity cannot be achieved. Furthermore, it is often the case that different materials are utilized in fabrication of a model (e.g., glass or plastic in the model versus steel in the prototype). From the governing equations, the following geometrical parameters should be satisfied for complete similarity:

$$A_{iR} = \frac{(a_i/a_o)_M}{(a_i/a_o)_P} = 1 \qquad \text{(kinematic similarity from continuity)}$$

$$t_R = \ell_R^3/(\text{volumetric flow})_R$$

$$\left(\sum_i L_i/A_i\right)_R = 1$$

$$L_{i_R} = L_{hR} = 1 \qquad \text{(for dynamic similarity from the momentum equation)}$$

$$\left(\sum_i F_i/A_i^2\right)_R = 1$$

The last condition was satisfied by flow resistance orificing of the PRISM and SAFR models to ensure proper pressure drops around their flow circuits. Because the friction and form contributions to F_i are very complex, model and prototype similarity could not be achieved exactly over the entire flow range but was achieved at a point corresponding to 10% of prototype flow. Resistance orificing was used in the model core and the IHXs. Once $R_{iR} = 1$ is satisfied (Richardson number equality exists between model and prototype), the correct similarity in U_{oR}, the reference velocity, is established. Hence, maintaining $R_{iR} = 1$ was a key constraint in designing the two reactor models and in conducting the tests. The ΔT_{oR}, the reference temperature ratio between model and prototype to satisfy $R_{iR} = 1$, is thus given by

$$\Delta T_{oR} = \frac{\Delta T_{om}}{\Delta T_{op}} = \dot{q}_{oR} \left(\frac{1}{\rho C_p}\right)_R \frac{\ell_{oR}}{u_{oR}} \frac{\delta_{oR}}{d_{oR}}$$

This condition was used to establish power requirements for the electrical heaters in the models. Similarity in the following parameters was not maintained:

$$St_{iR} \neq 1$$

$$T^*_{iR} \neq 1$$

$$B_{iR} \neq 1$$

$$Q_{soR} \neq 1$$

However, once the model is fully specified (i.e., scale, materials, temperature, power, and flow) the model/prototype parameter ratios can be evaluated to check on distortions between model and prototype. It is generally agreed that full similarity in St_{iR} and B_{iR} is difficult to attain in testing of complex thermal-hydraulic models because these two parameters signify the temperature drops at and in the walls. With major emphasis on simulating buoyancy effects around the flow circuits of the reactors, their full satisfaction was not of first order importance in these studies. The simulation of buoyancy effects was achieved by maintaining $R_{iR} = 1$ and the pressure ratio = 1 in the model tests. The collective consideration of the preceding modeling and the MCTF-imposed operating conditions led to fixing the model designs as described in Refs. [1,2] and highlighted in the following table for PRISM:

PRISM Model Operating Conditions and Similarity Parameters for Full Power and Flow

Scale	= 5.24
P	= 275 kW
Q	= 128 gpm
ΔT	= 14.7°F
U_R	= 0.086
$\Delta\rho_R$	= 0.0085
Q_R	= 0.00313
Re_R	= 0.046
Pe_R	= 7.41
t_R	= 2.22
ST_R	= 1.69

4.2.2 Argonne Water Test Facility (MCTF)

Argonne's MCTF conducted experimental studies and supporting analytical and computer modeling simulations of the fluid and heat-transfer phenomena that occur in various generic LMR reactor-plant components and for interactions among components. Piping, heat exchangers, steam generators, plenums, thermal mixers, and complete in-vessel systems were studied. The objective was to develop thermal-hydraulic data guidelines and tools for design of reactor plant components and systems with optimal flow distribution and heat transfer consistent with minimal detrimental thermal stripping/fatigue, structural problems induced by thermal stratification, and pressure drop under both steady-state normal operation and transient safety-related modes of operation, where maintaining core cooling is of vital importance.

General features and operating characteristics of the facility were:

- Closed-loop thermal-hydraulic water facility operating under computer control for simulating steady or transient conditions
- Capable of multiple stream testing with flow rates in the range 0 to 2200 gpm, and pressures in the range 0 to 100 psig over temperature excursions from 240 to 40^{o}F
- State-of-the-art flow and thermal characterization techniques: laser Doppler, hot film, and ultrasonic velocity measurement, laser-sheet flow visualization with dye/particle tracers, and fast-response temperature and pressure measurement
- Dedicated computer for data acquisition and facility control
- Ability to conduct multiple concurrent research programs

A simplified schematic of the MCTF is shown in Figure 4.2-1. The flow from a 2200-gpm pump was split into two streams: one stream went to a controllable steam-heated heat exchanger; the other went to a controllable water-cooled heat exchanger. The hot and cold

streams at their set temperatures went to separate 3000-gal reservoir tanks, from which flows at the two respective temperatures and desired flow rates were supplied to a test article. The supply-line flow rates were measured with turbine flow meters. The return leg to the pump contained an ASME orifice-plate flow meter that was used as a check on system flow.

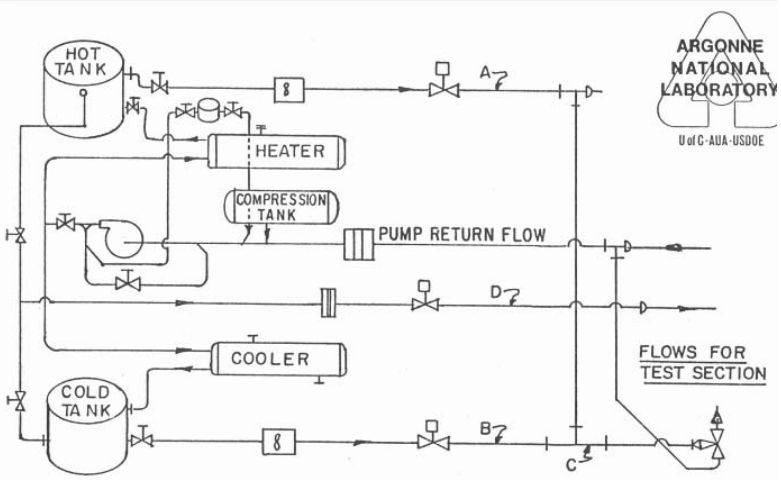

Figure 4.2-1 Schematic of Argonne's MCTF thermal-hydraulic water flow loop

Figure 4.2-2 shows an overview photo of the facility, and Fig. 4.2-3 shows a photo of the facility during tests on the GE / PRISM model. The same test stand was used to test the RI-CE/SAFR model on an interchangeable basis.

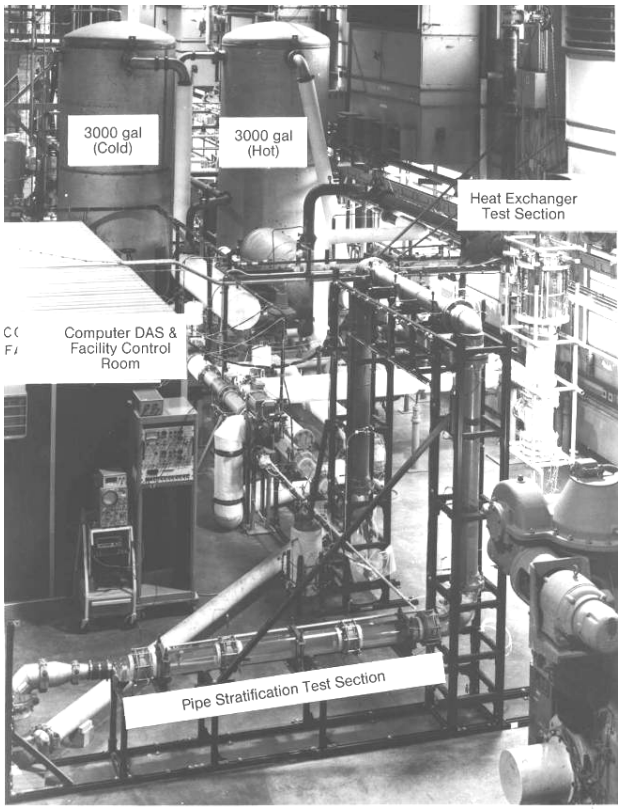

Figure 4.2-2 Photo of Argonne's MCTF

Figure 4.2-3 Complete in-vessel model of GE / PRISM interfaced with MCTF

The test facility functioned in two modes: steady-state and transient computer-controlled.

Steady State. In this mode, fluid streams at individually selected constant flow rates and constant temperature, were delivered to a test article. The streams could be set at the supply tank temperatures, or the flow from the two tanks could be combined by means of valves to achieve intermediate temperatures.

Transient Computer-Controlled. Transient streams were created by combining, at a given instant, the appropriate relative amounts of the hot and cold fluids to obtain the desired instantaneous flow rate and temperature. Control valves and turbine flow meters in lines A and B were interfaced with the MCTF computer system. A control loop between the valve and the flow meter, in conjunction with computer-stored functions which described the desired transient flow and temperature, allowed transient simulation. The two transient-controlled streams were combined at flow-mixer point C, and the resulting thermal-hydraulic transient was supplied to the test article.

4.2.3 Modes of Reactor Operation Explored and Phenomena Studied

This section describes the PRISM and SAFR reactor models built by Argonne for GE, RI, and the DOE; the modes of reactor operation explored experimentally; and the phenomena studied. The test program conducted by Argonne involved the most detailed and complex thermal-hydraulic water models and test facility ever built for a U.S. LMR program.

4.2.3.1 Modes of Testing

The complete in-vessel models for the PRISM and SAFR reactors were tested in three modes to explore their behavior under a variety of important prototype operational scenarios. Even more complex test scenarios were possible in the form of transient simulations composed of the following three modes of operation.

First, in an externally driven forced flow mode, high-to-intermediate flow rates were supplied to the cores of the reactor models from the MCTF flow loop under computer control. The flow passing through the models was returned to the MCTF via exit manifolds located in the cold plenums. In this mode, the flow rate and the temperature of the flow supplied to the core were controlled by the MCTF thermal-hydraulic system and computer as a function of time.

Secondly, in an internally driven forced flow mode, the models were isolated from the MCTF by closing valves between the models and the flow loop. In this mode, low-level forced flow and transition to natural circulation were studied. The flow for these tests was provided by internal model pumps driven by programmable dc motors with core simulation electrical immersion heaters as the heat source and operable IHXs as heat sinks. Both the flow rate provided by the dc-driven pumps and the power supplied by the immersion heater were controlled in this mode by the MCTF computer as a function of time to allow simulation of complex reactor low flow transients.

Finally, in the third mode of testing, an internally driven natural-convection flow mode, the situation is the same as in the second mode except that no internal pumps were operating. The natural convection flow was driven by the temperature differences caused by the core heater, the intermediate heat exchangers, and the reactor vessel auxiliary cooling system (RVACS) simulated by a cold RV wall.

4.2.3.2 Phenomena Studied

The following phenomena were studied for each test article:

1. Characterization of hot, intermediate, and cold plenum mixing; thermal distributions; and location of stratified interfaces with time for various reactor steady and transient events

2. Influence of formation of a stratified interface in a plenum on (a) flow and thermal ramps into and out of IHXs, pumps, and the core, and on critical 1iquid/solid structural interfaces (i.e., redan), (b) availability of in-vessel heat sinks associated with internals structure and sodium, and (c) RV heat-rejection capability to ambient air

3. Influence of flow path resistance (magnitude and possible disparity between multiple paths consisting of IHXs, pumps, and core) between hot and cold plenums on (a) general reactor coolability, (b) start-up time constant for natural-circulation flow, and (c) potential for instabilities created by multiple flow paths or reverse-flow siphoning or

blockage (produced, for example, by thermal distributions in the IHXs prior to transition to the natural-convection circulation mode, resulting in flow-opposing thermal density heads)

4. Influence of upper internals structure (UIS) on upper-plenum mixing and thermal distributions

5. Possible formation of a core/upper-hot-plenum recirculation loop, which may short circuit the preferred flow paths (through IHXs and pumps) between upper and lower plenums and thereby reduce heat sink availability and/or cause core hot spots

6. Influence of proximity and grouping of outlets and inlets of IHXs, pumps, and core on (a) potential for flow shunting (unequal flow split between the flow paths connecting the hot and cold plenums) and (b) mixing in the plenums

7. The potential for cover-gas/sodium interface flow disturbances and gas entrainment at high flow

In addition, by simulation of a "cold" RV wall, the influence of wall-driven, in-vessel, natural-convection currents was assessed for (a) plenum stratified-interface behavior, (b) heat rejection to ambient, and (c) temperature distribution in annular overflow gap. Furthermore, experimental data were generated to support initial development and validation of CFD codes to be used to guide design of the PRISM and SAFR prototypes.

The above studies highlighted the complexity of the phenomena associated with the complex in-vessel geometries and the presence of strongly interacting sub-regions which strongly supported the need for improved CFD simulation capabilities. The generated experimental data obtained in these studies were used to guide preliminary code improvements. However, further development of computational capabilities is still needed to establish validated tools for designing an efficient and safe LMR in the future.

4.2.4 GE/PRISM Results

A schematic and photo of the PRISM model are shown in Figs. 4.2-4 and -5. The GE/PRISM model built by Argonne for GE and the DOE had the following general features:

- It was a 1/5-scale model of the GE PRISM design.
- All major in-vessel components were modeled.
- It was constructed of transparent polycarbonate and cast acrylic plastics.
- The model was housed in a two-piece cylindrical containment vessel with large windows allowing for laser flow visualization using fluorescent dyes.

- The reactor core was simulated by a 60-kW electrical-resistance immersion heater with computer-interfaced power control.

- Programmable computer-controlled forced flow was provided in two ways:

    - for low-flow conditions, four in-vessel pumps (propellers driven by 1/4-hp dc motors with SCR controllers) were used, and
    - for high-flow conditions, the MCTF water loop pump was used.

- Computer control of the immersion heater, in-vessel pumps, and the MCTF allowed complex flow and thermal transient simulations.

- The two in-vessel IHXs contained water-cooled heat sinks, and the cold wall of the containment vessel simulated cooling by the RVACS.

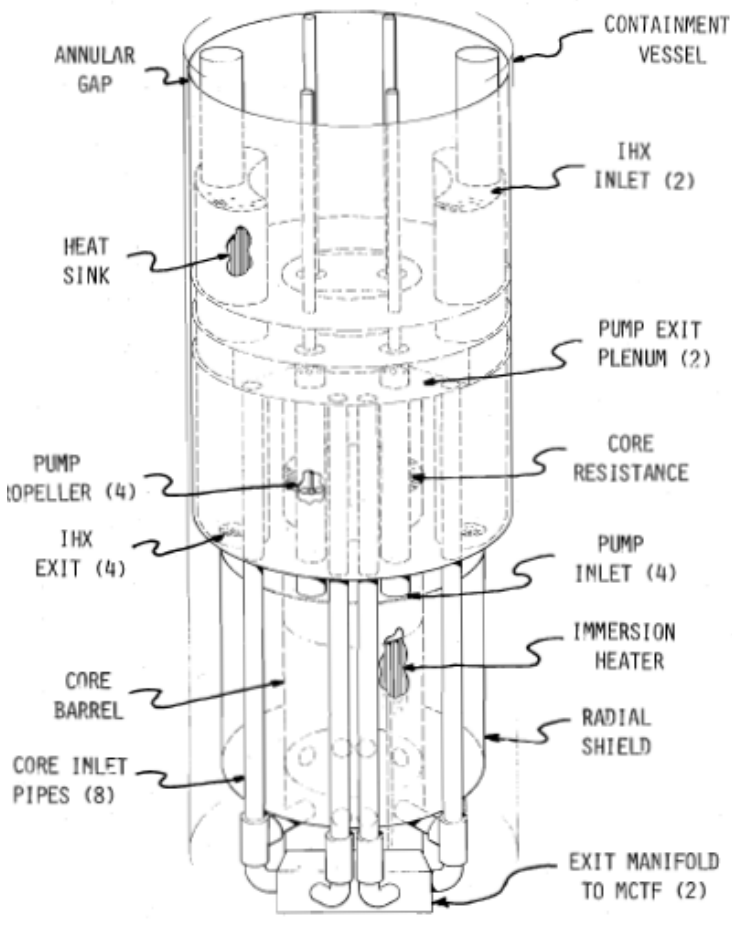

Figure 4.2-4 Argonne thermal-hydraulic model of GE/PRISM

Figure 4.2-5 Photo of Argonne 1/5-scale complete in-vessel thermal-hydraulic model for GE/PRISM (bottom enclosed in containment tank)

Various plant transients postulated by GE for PRISM [5,6] were simulated in testing at Argonne. The following summarizes some of the important thermal-hydraulic information obtained from testing of GE/PRISM [1] under the experimental modes described in Section 4.2.3 (see Fig. 4.2-4 for the location of components and geometrical features):

a) At flows yielding 20% of prototype Froude number, the free surface in the upper plenum was extremely quiescent; thus cover gas entrainment was not a problem. However, this observation was not conclusive since 100% of prototype Froude number simulation was not attainable in testing.

b) Under isothermal conditions at about 10% of simulated prototype flow, the annular flow downstream of the IHX exits turned radially inward just below the radial-shield bottom and then proceeded up through the radial shield, leaving a stagnant recirculation region in the lower plenum. For higher flow rates, there was no stagnant recirculation region in the lower plenum.

c) In all the thermal up-ramp tests at constant flow (5, 15, 30, and 60% of simulated full flow with a 16.7ºC step change in temperature) a cold, thermally stratified stagnant region initially formed below the radial shield in the lower plenum, as in the isothermal tests. However, unlike the isothermal tests, the cold stagnant region also formed at flow rates greater than 10% of simulated prototype flow because of the strong thermal-buoyancy forces, which oppose the downward-acting inertia forces of the fluid. This cold stagnant region is a potential thermal stress concern to designers because of the large temperature gradients in a region with many welds (e.g., core inlet pipes). There is also the potential for sodium freeze-up in this region, depending on the level of RVACS heat rejection.

d) All thermal up-ramp tests at constant flow exhibited stratification in the lower plenum; Richardson numbers (based on the radial-gap diameter outside the radial shield) ranged from 34.6 to 4914. Thus, a threshold value of Richardson number below which stratification does not exist in the lower plenum could not be determined from these tests. Additional testing is needed to determine the Richardson number below which stratification would not occur. The persistence time of the cold stagnant region varies inversely with flow rate, i.e., the higher the flow rate, the shorter the persistence time. At higher flow rates the stagnant region is washed away owing to turbulent mixing (Reynolds numbers of these tests varied between 634.9 and 7258.2).

e) Flow caused by natural-convection currents was found in the overflow gap during the thermal up-ramp tests at constant flow. This is important to the designer when estimating RVAC capacity and vessel heat losses, especially if it is assumed that heat transfer occurs by conduction alone.

f) In the pure natural-convection tests, the lower plenum stratified, whereas the upper plenum did not stratify. The Richardson numbers that were based on the radial-gap diameter ranged between 1276 and 5142 for these tests. These large Richardson numbers indicate that the buoyancy forces are very much larger than the inertia forces in the lower plenum. The Reynolds numbers (based on the radial-gap diameter) ranged between 203 and 314 for these tests. These small values indicate that the flows in the lower plenum are laminar.

g) In the mixed natural-convection tests, both the upper and lower plenums stratified. This behavior is a design concern because of the large temperature gradients, which could cause structural stress problems. In the upper plenum, the Richardson number (based on the core barrel diameter) for those tests varied between 56 and 99, an indication that the thermal-buoyancy forces are much larger than the inertia forces in the upper plenum. The Reynolds number (based on the core barrel diameter) for these tests varied between 4307 and 6374, an indication that the flows are turbulent. In the lower plenum, the Richardson number (based on the radial-gap diameter outside the radial shield) varied between 181 and 206 for these tests, an indication that the thermal-buoyancy forces are also much larger than the inertia forces in the lower plenum. The Reynolds number (based on the radial-gap diameter outside the radial shield) varied between 999 and 1307, an indication that the flows in the lower plenum were laminar for these tests.

h) Experimental simulation of a reactor trip from full power with maximum decay heat indicates the existence of some stratification in the upper plenum for a short period of time and a generally favorable cooling of the entire model after the scram.

i) Experimental simulation of loss of power to one primary pump indicates some stratification in the upper plenum for a short period of time. Also, reverse flow in the shutdown pump was observed during portions of the transient as the relative strengths of the buoyancy and inertia forces changed. The presence of reverse flow in the shutdown pump may cause design problems in that overall reactor cooling is affected, and reverse flow of cold fluid from the lower plenum may create large temperature gradients, causing structural stress concerns.

j) Under the conditions of i), the Richardson number (based on the core diameter) ranged between 87 and 549 for these tests, an indication that the buoyancy forces are much larger than the inertia forces in the upper plenum. This condition, together with the buoyancy forces opposing the inertia forces, gives rise to stratification in the upper plenum.

k) Also under the conditions of i), steady-state flow patterns in the UIS region indicate a slowly rotating body of fluid within the UIS, with some fluid near the slot being entrained by the flow in the annular gap around the UIS. There was not enough flow through the UIS to locate the source of fission product release. Additional flow holes in the top and bottom of the UIS would help this situation.

4.2.5 RI-CE/SAFR Results

Schematics and photos of the RI-CE/SAFR model are shown in Figs. 4.2-6, -7, -8, and -9. The RI-CE/SAFR model built by Argonne for Rockwell International and the DOE had the following features:

- It was a 1/11.2-scale model of the RI-CE/SAFR design.
- All major in-vessel components were modeled.
- It was constructed of transparent polycarbonate and cast acrylic plastics.
- The model was housed in a cylindrical containment vessel with large windows allowing for laser flow visualization using fluorescent dyes.
- The reactor core was simulated by a 60-kW electrical-resistance immersion heater with computer-interfaced SCR power control.
- Programmable computer-controlled forced flow was provided in two ways:

- for low-flow conditions, four in-vessel pumps (propellers driven by 1/4-hp dc motors with SCR controllers) were used, and
- for high-flow conditions, the MCTF water loop pump was used.

- Computer control of the immersion heater, in-vessel pumps, and the MCTF allowed complex flow and thermal transient simulations.

- The four in-vessel IHXs contained water-cooled heat sinks, and the cold wall of the containment vessel simulated cooling by the reactor air cooling system (RACS).

- Like the PRISM model, the SAFR model was the most complete thermal-hydraulic water model ever built for a DOE LMR program.

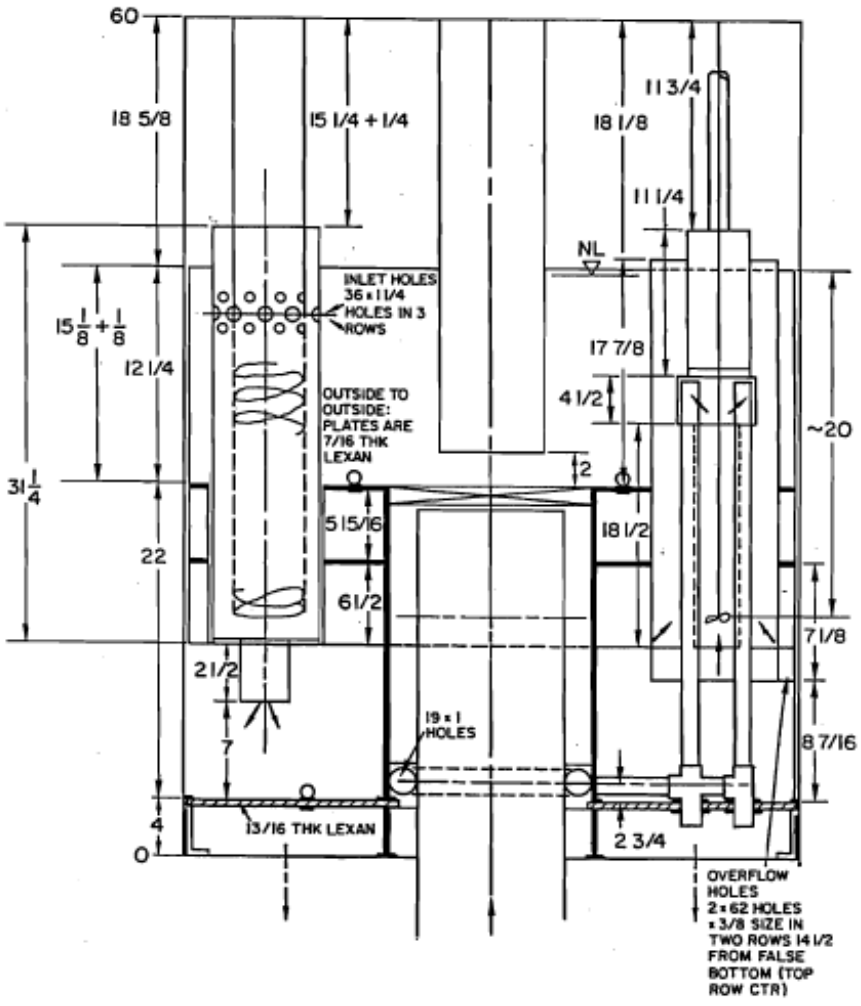

Figure 4.2-6 Elevation view of RI/CE SAFR model (dimensions in inches)

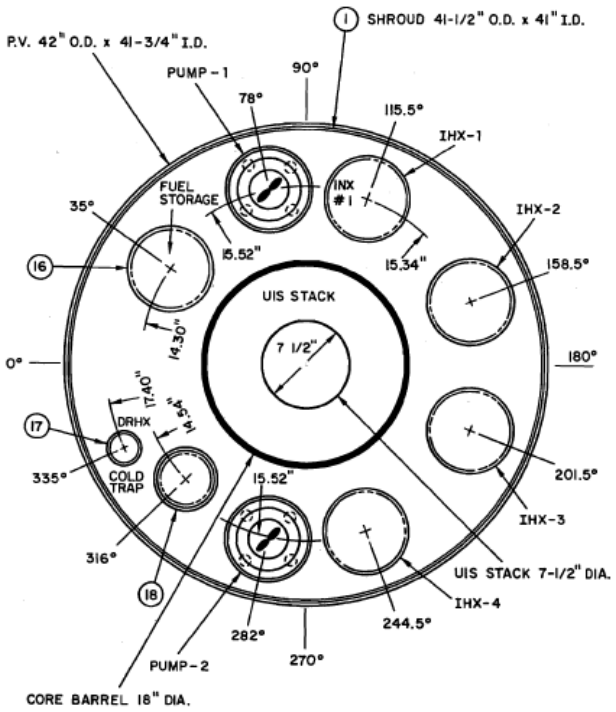

Figure 4.2-7 Top view of RI-CE SAFR model

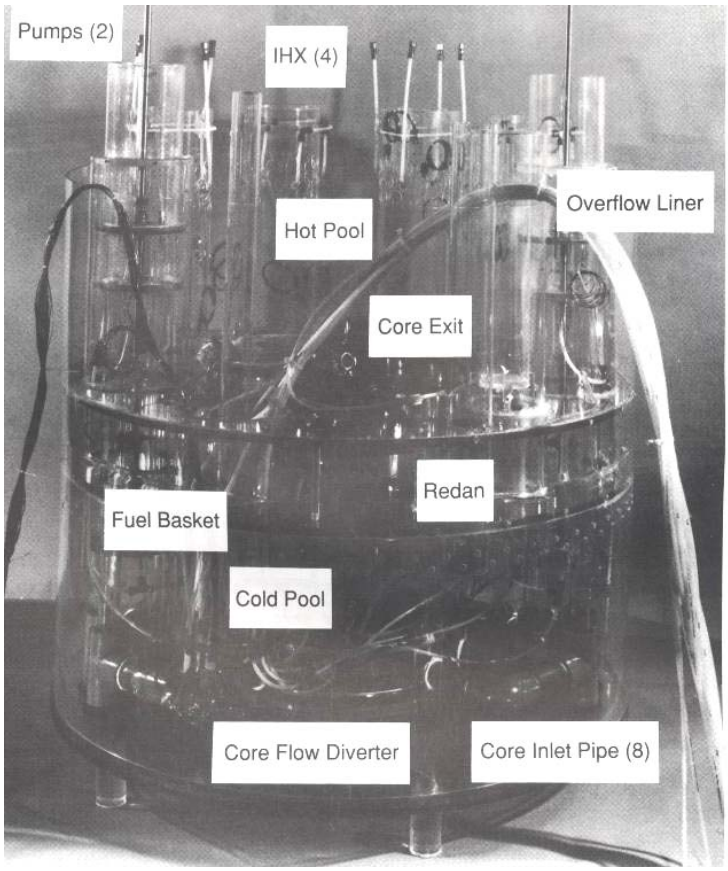

Figure 4.2-8 Photo of RI-CE/SAFR model

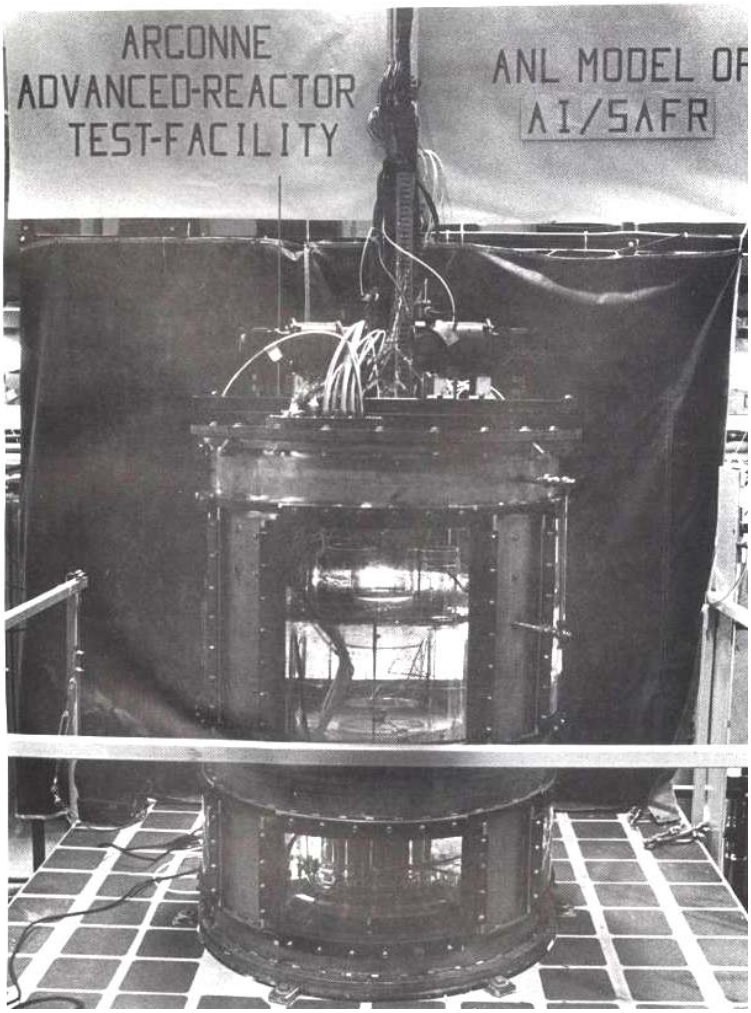

Figure 4.2-9 Photo of RI-CE/SAFR model in containment tank on MCTF test stand

The following describes some of the important types of thermal-hydraulic information obtained for the RI-CE/SAFR model [2] under the testing described in Section 4.2.3. Testing was conducted in two phases.

4.2.5.1 Phase I Testing/Results

Phase I testing facilitated the shakedown of the experimental protocols and the development of the many complex control features and subsystems that were incorporated into the SAFR model. After this shakedown, tests were conducted in the following general phenomena categories: isothermal flow distribution, hot plenum free-surface behavior, constant-flow thermal transients, natural-convection flows, and mixed forced-natural-convection flows. Also at the request of RI, several simulation tests of postulated plant transients were conducted as well as tests involving two asymmetric operation modes resulting from a down-flow loop. In Phase I testing the IHXs were not active heat sinks. Phase II had active IHXs. The following conclusions were reached from Phase I:

- At flows simulating 30% of the prototype Froude number, the free surface in the upper plenum was extremely quiescent; thus, cover gas entrainment was not a problem. However, this observation was not conclusive for the prototype since 100% of the prototype Froude number was unattainable in these tests due to the size scaling limitations.

- Under isothermal test conditions, at about 10% of simulated prototype flow and lower, the flow downstream of the four asymmetric IHXs exited and turned radially outward and then proceeded up toward the respective pump zones, leaving a stagnant recirculation region in the lower plenum. For higher flow rates, there was no stagnant recirculation region in the lower plenum.

- For the thermal up-ramp tests at constant flow (at 5, 10, 15, and 50% of simulated full flow with a 22.2°C step change in temperature), a cold, thermally stratified stagnant region initially formed below the radial shield in the lower plenum, as in the steady-state tests. However, unlike the steady-state tests, the cold stagnant region also formed at flow rates that were 15% of simulated prototype flow because of the strong thermal-buoyancy forces that oppose the downward-acting inertia forces of the fluid. This cold stagnant region is a potential thermal stress concern to the designers because of the large temperature gradients in the region. There is also the potential for sodium freeze-up in this region, depending on the level of RVACS heat rejection.

- In the thermal up-ramp test with 15% constant flow and a 22.2°C step change, the cold plenum remained stratified almost 1-1/2 hr into the test. The hot plenum was also stratified; however, the initial stratification dissipated approximately 1/2 hr into the test.

- In isothermal flow tests, dye injection from the IHX exits revealed very good hydraulic symmetry across the geometric symmetry plane in the lower plenum.

- In nonisothermal tests (constant flow at 15%, thermal up-ramp with a 22.2°C step change), some mixing occurred across the geometric symmetry plane in the lower plenum.

- In thermal up-ramp tests, the thermocouples at the core exit plane and the special thermocouples placed around the body of the IHX #4 in the cold plenum indicated no thermal gradients.

- In the pure natural-convection tests, the lower plenum stratified severely, whereas the upper plenum did not stratify. Even under the stratified conditions, the cold plenum exhibited azimuthal thermal uniformity at all elevations. The thermal stratification in the cold plenum occupied over half the height of the plenum.

- The redan functioned very well under all conditions by thermally separating the cold and the hot plenums. Mixing was always very poor in the redan, and it was thermally isolated from the external thermal-hydraulic phenomenon to a large extent.

- No thermal isolation existed for the pump wells. The wells were always convectively active in a given test, and whenever the non-isothermal test ceased, they readily stratified. The pump wells warranted further design attention.

- The natural circulation tests verified good circulation around the in-vessel flow circuits. The 2.5% core power test generated 3.3% flow 3-1/2 hr into the test. The 5.0, 7.5, and 10% core power tests yielded 6.6% flow around the loop established in shorter times.

- For the mixed convection tests, at 20% internally pumped flow, the cold plenum again stratified strongly. The thickness of the upper warm-water zone increased in proportion to the core power. At 20% flow, significant thermal stratification in the cold plenum starts in the 2.8-5.0% power range. It is very important for an LMR design that the stratification regimes of the cold plenum be carefully mapped out under mixed convection conditions by holding flow constant and varying the core power, then changing the flow rate and repeating the power sequence, and so on. Stratification in the cold plenum can be mitigated by changing the elevations of the IHX exits and/or pump inlets.

- The following results were obtained from the prototypic transient simulation tests:

    1. For a cold shock to the hot pool, both plenums were stratified.
    2. For a severe cold shock to the hot pool, strong thermal stratification was set up in the hot plenum; however, no circumferential thermal gradients were found at any level. Along with the cold shock to the hot pool, the cold plenum went through a hot shock in this transient. The resulting stratification is persistent, unlike the stratification in the hot pool. This result demonstrated that the mixing in the hot pool is very good, but needs improvement in the cold pool.
    3. A hot shock transient to the cold pool resulted in a minor stratification in the hot pool and moderate stratification with a mild thermal shock in the cold pool. The core exit was subject to large thermal fluctuations during this transient, creating the potential for thermal shock/thermal stripping of the UIS bottom surfaces.

- For the asymmetric simulation modes, in which only a single pump and only two of the four IHXs were allowed to operate, the hot plenum was found to be mildly affected by the imposed thermal-hydraulic asymmetry. In both variations of this test (the operating pump and the two plugged IHXs were in the same half or in different halves of the reactor cross section), the core exit exhibited strong thermal oscillations, potentially subjecting the UIS bottom to thermal stripping. The cold plenum was severely and persistently stratified. The circulating pump inlet was also found to be subject to large thermal oscillations. One notable difference between the two asymmetric operations manifests itself in the hot plenum stratification. When the operating pump and the two

non-plugged IHXs were in the same half of the reactor cross section, the 0-degree axis zone of the hot plenum became stratified initially, whereas the 180-degree axis zone was not stratified. When the operating pump and the non-plugged IHXs were in different halves of the reactor cross section, no stratification or thermal asymmetry was noted in the hot plenum. An important outcome from the asymmetric testing was the observed large thermal oscillations at the core exit, at the performing pump inlet, around the core barrel and the instrumented IHX #4 body, and at the non-performing IHX inlets and exits.

4.3.5.2 Phase II Testing/Results

Phase II tests consisted of simulations of five prototypic transients that were chosen by RI because their severity and frequency of occurrence could pose potential design concerns, such as stress problems caused by rapid temperature changes and inadequate heat rejection due to inadequate flow. The following conclusions were reached:

- Formation of a stratified hot/cold interface in the cold plenum, backflow in a shutdown pump, and unanticipated natural-convection currents in the overflow gap are some of the phenomena that were discovered during these tests. These phenomena are of very high importance to the designer.

- Several of the generic tests of Phase I were repeated in Phase II with the installation of heat removal capability in the IHXs.

- For the mixed forced natural-convection tests conducted at constant internal flow of about 17% and at core power levels of 3.8, 5.1, 7.5, and 10%, better than 70% of the input heat was removed by the IHX secondary side. The heat removal, in contrast to the Phase I tests of similar nature, affected the stratification patterns in the plenums as well as the thermal symmetry.

- In the cold plenum, the 180-degree zone of the symmetry plane (mid-plane of the IHX bank) exhibited fast decay of existing stratification, whereas in the opposite 0-degree zone, stratification lingered on. In the hot plenum, the opposite occurred. Therefore, the presence of heat removal by the skewed IHX bank in the SAFR geometry promoted thermal asymmetry and the potential for structural stressing.

- On the other hand, the presence of heat removal by the IHXs mitigates the conditions, causing stratification in the cold plenum (lesser hot shock), which was more severe than that encountered in similar Phase I tests.

- In the mixed forced natural-convection tests at 7.6% flow levels, the exit flow from the IHXs in the cold plenum would only reach downward halfway to the bottom [3-5/8 in. (9.2 cm) in the model, corresponding to 3-5/8 ft (1.1 m) in the prototype].

- Under pure natural-circulation conditions, the thermal stratification in the hot plenum was not significant. In the cold plenum, the tendency for thermal stratification was lessened. The 180-degree end zone of the symmetry plane experienced larger and longer-lasting stratification than the 0-degree end zone.

The following are important issues that were not studied in the SAFR program but should be evaluated for any future LMR initiative:

- The thermal-hydraulic asymmetry in the upper and lower plenums promoted by the skewed placement of the IHX bank suggests this design feature should be reevaluated.

- The asymmetric operations tests (N-1 loop operation) performed in Phase I should be repeated under IHX heat removal conditions.

- While the redan remains little affected by the thermal-hydraulic phenomena explored in the upper and lower plenums, the pump wells participate convectively with the phenomena. The role of the pump wells as convective heat transfer paths between the hot and cold plenums warrants investigation.

- Limits of the cold plenum stratification need to be more precisely defined in special feature tests.

- Convection paths through the overflow gap in an overflow regime have not been studied. This regime should be studied using flow visualization techniques.

- RVACS cooling tests should be conducted to investigate the performance/adequacy of the emergency cooling system.

References

1. Oras, J.J., Kasza, K.E., Argonne National Laboratory, unpublished information, 1988.

2. Kuzay, T.M., Kasza, K.E., Argonne National Laboratory, unpublished information, 1989.

3. Kuzay, T.M., Argonne National Laboratory, unpublished information, 1985.

4. Kasza, K.E., and Amorosi, A., Argonne National Laboratory, unpublished information, September 1992.

5. Halfen, F J., and Baig, K., "PRISM Plant Transient Analysis," General Electric Company Report, GEFR-00755 (August 1985).

6. Halfen, F.J., and Switick, D.M., “PRISM Plant Transient Analysis," General Electric Company Report, GEFR-00791 (September 1986).

5.0 Pathway Forward Supporting Development and Demonstration of GNEP/LM-ABR

5.1 Summary of Past Argonne Studies and Needed Research

In this Argonne white paper we provide an overview and status report on the LMR thermal-hydraulic R&D, both experimental and computational, mostly conducted at Argonne National Laboratory. Argonne during the period of time from 1970 through the mid-1990s was DOE's lead laboratory for LMR thermal-hydraulic development. During the 1970s and into the mid-1980s, Argonne conducted thermal-hydraulic studies and experiments on individual reactor components, supporting EBR-II, FFTF, and CRBR. In the 1980s and into the early 1990s, Argonne studied forced- and natural-convection phenomena in complete in-vessel models of GE/PRISM and RI/SAFR. These two reactor initiatives involved Argonne working closely with U.S. industry and the DOE. This paper describes the very important impact of thermal hydraulics on reactor global operation and on individual-component behavior/performance (thermal duty, structural impact, and safe operation) during normal operation and off-normal postulated scenarios for safety-related low-flow accidents. Argonne's LMR expertise and design knowledge are vital to the further development of safe, reliable, and high-performance LM-ABRs as part of the GNEP initiative.

Argonne believes there remains an important need for continued thermal-hydraulic research and development in support of the DOE's and the international community's renewed thrust for developing and demonstrating GNEP and the ABR. The support should come in the form of testing infrastructure for technology development, improved science-based engineering knowledge, and improved computational modeling design tools that have been validated.

As highlighted in this white paper, one technology area needing further understanding is associated with low-flow reactor coolant events. These safety-related events are associated with the transition to natural circulation and pure natural circulation. These events are the most difficult to design for because they involve thermal-hydraulic and component-interaction phenomena which are not adequately understood or appreciated by reactor designers as to their impact on reactor performance and safety. Argonne pioneered the study of thermal-buoyancy-force governed flows under transient conditions, including transition from forced to natural convection, instabilities generated by parallel flow paths, structural thermal stressing caused by thermal stratification, and influence on heat-sink effectiveness.

Argonne has highlighted the importance of and studied off-normal flow and thermal behavior in various individual LMR reactor components, as listed below:

- Sodium versus water thermal oscillations during multiple stream mixing
- Pipe flow stratification that produces pipe stress and influences energy transport between components

- Steam-generator and heat-exchanger flow channeling and instabilities that cause tube-bundle, tube-sheet, and shell thermal stressing
- Flow recirculation zones induced by thermal buoyancy at pipe nozzle/plenum interfaces and cause nozzle/tank stresses
- Periodic flow eddies generated by large-scale shear flow that strongly influences thermal-plume behavior and plenum mixing, and can cause thermal-cycling-induced structural fatigue (thermal stripping)
- Laminarization of stratified shear layers induced by thermal buoyancy forces, which can mitigate thermal stripping and reduce plenum mixing, enhancing stratification
- Suppression or enhancement of surface heat transfer under low-flow by thermal buoyancy forces, which can strongly influence heat exchanger performance
- Recirculation zones in baffled tube bundles and other components induced by thermal buoyancy forces, which can reduce heat transfer and produce radial temperature variation and "cold" spots, thereby causing detrimental structural stress in large components

Argonne also conducted the most complete thermal-hydraulic in-vessel tests ever performed in the U.S. on the advanced LMR designs GE/PRISM and RI/SAFR, addressing:

- Thermal-hydraulic performance
- Reactor emergency cooling
- Structurally detrimental thermal distributions
- Heat-sink effectiveness

Complete in-vessel model experiments were used because the flow and thermal behavior in a given sub-region is the result of complex interactions with the rest of the reactor in-vessel components (especially important for pool designs under low-flow conditions and the transition to natural convection). In-vessel behavior under key postulated reactor operation scenarios was studied. It was shown that an improved understanding of flows dominated or driven by thermal buoyancy forces is essential to developing improved inherently safe, robust, and reliable reactors.

Argonne was the first to use 3-D CFD analysis (starting in the early 1970s) to study transient reactor flows governed by thermal buoyancy forces. This work was in conjunction with Argonne's pioneering thermal-hydraulic buoyancy experiments on reactor components. The Argonne 3-D COMMIX code was used. Preliminary COMMIX simulation results for pipe thermal stratification strongly suggested that 3-D CFD codes are essential as tools in designing piping systems and other components and in correctly predicting the movement of transient fronts between components in an LMR. These early Argonne simulations with COMMIX, which were also extended to plenums and tube bundles, highlighted (1) the restrictiveness and short comings of several of the assumptions used in the constituent computer models and (2) the need for efficient and robust computational schemes for handling the very large complex

geometries during transients when the momentum and energy equations are strongly coupled by thermal buoyancy forces. At the time of the COMMIX simulations, the code took several hours to run a simulation of pipe flow behavior. Future CFD simulations of this type when addressing more complex systems for long-duration transients must be done on powerful computers.

Fluid flow and heat transfer in LMR components and systems are three-dimensional and complex. The system geometry is characterized by a large range of geometric scales (from a few millimeters to tens of meters). The fluid flow and heat transfer cover the whole range from highly turbulent (normal reactor operation) to laminar, and from forced flow to mixed flow (forced and thermal-buoyancy influenced) and to natural circulation (thermal-buoyancy dominated). As highlighted, low-flow events are where improvements in understanding of thermal-hydraulic phenomena and computational simulation tools are needed in the form of validated CFD and structural analysis codes for modeling of individual and several simultaneous-interacting components. Of particular importance is the ability to model stratified interfaces, turbulence behavior (enhanced or suppressed) involving large-scale transient thermal buoyancy forces and resulting in shear-formed eddies and flow instabilities. Since the early 1990s, when DOE cancelled the LMFBR program, little has been done regarding incorporation of the following into the CFD codes: thermal-buoyancy force terms, improved turbulence modeling, and improved flow instability modeling.

Furthermore, the CFD and structural analysis codes for aiding design of future reactors need to be coupled together and benchmarked/validated against an experimental data base for analyzing important phenomena, such as time-dependent structural stresses imposed by transient thermal-hydraulic phenomena associated with large-scale thermal stratification and structural fatigue induced by localized thermal stripping. Thermal stripping is related to localized surface regions being subjected to thermal oscillations, which induce cyclic structural stresses and lead to cracking. It is frequently produced by liquid metal transient flows that are inadequately thermally mixed and impinge on structures or by undulating stratified interfaces and eddies. Also, as shown by Argonne, strong thermal buoyancy forces occurring in plenums, heat exchangers, and piping under low-flow conditions can produce significant thermal stratification, flow instabilities, and poor flow distribution with large thermal gradients. These factors can induce large-scale structural thermal asymmetries and significant thermal distortion/stressing.

5.2 Proposed National GNEP-LMR Center at Argonne

Improved thermal-hydraulic data bases are needed for the phenomena described in this report. The information should be generated in new state-of-art test facilities utilizing state-of-art instrumentation. The improved data bases in conjunction with the improved benchmarked and validated codes proposed in this white paper, based on a science-based approach, will greatly facilitate the development of improved reactor components and operational scenarios resulting in even safer LMRs. Improved validated codes will also facilitate scale-up from small-scale test results to prototype size and will facilitate comparing performance of one reactor/component design with another. These codes would also benefit the safety assessment of current light

water reactors (LWRs) by virtue of the fact that many of the same important generic phenomena occur in LWRs.

To accomplish the preceding, a National GNEP-LMR Center should be established at Argonne having as its foundation state-of-art thermal-hydraulic experimental capabilities for conducting both water and sodium testing of individual reactor components and complete reactor in-vessel models. This Center should also contain a computational modeling capability of national stature that is strongly interfaced with the Argonne experimental facilities.

The proposed Center would greatly advance capabilities for reactor development by establishing the validity of high-fidelity (i.e., close to first principles) models and tools. Such tools could be used directly for reactor design or for qualification/tuning of lower-fidelity models, which now require costly experimental qualification for each different design application. Capabilities required to establish and operate this center are found primarily in Argonne's Nuclear Engineering and Mathematics and Computer Science Divisions. Funding for the center would be sought from DOE-NE (GNEP/Advanced Burner Reactor and Generation IV programs), DOE-SC/ASCR, and the commercial nuclear industry.

Having both capabilities at Argonne would constitute a highly focused and efficient national/international center of excellence for conducting the research and engineering design tool development needed to support the DOE GNEP/ LM-ABR initiative in developing safe high-performance reactors.

The experimental test facilities proposed for the Argonne National GNEP-LMR Center are as follows:

5.2.1 Water Facility

Argonne would conduct thermal-hydraulic studies and experiments similar to the past DOE-funded simulation testing of complete in-vessel behavior performed in support of the GE-PRISM and RI-SAFR reactor designs. Additionally, GE in its wrap-up document of 1994 for the PRISM program design specified that in-vessel water testing would be conducted at Argonne if PRISM went forward into final design/construction. Many important phenomena can be studied with water testing in reduced-scale component models (1/5 to 1/10 scale). The water testing is justified by non-dimensional modeling considerations described in this white paper. Testing at reduced scale allows use of smaller flow loops. Instead of a testing program costing $80 million or more, testing may be possible with a $15 to 20 million program. Argonne's past testing for the DOE LMR program was performed in the Mixing Components Test Facility, which was dismantled in the mid-1990s. Argonne expertise and space exists in the original building for constructing a new national thermal-hydraulic water test facility.

5.2.2 Sodium Facility

Argonne would also conduct highly focused sodium experiments on key phenomena (such as large-eddy and turbulence-induced structural thermal stripping and cracking, stratified interface thermal gradients, and turbulence behavior) and, where needed, studies exploring the behavior of critical sodium components like plenums, pumps, heat exchangers, and piping. The facility would have the capability of generating two flow streams of different temperature and be able to combine the flows under computer control to generate thermal-hydraulic transients and steady-state flows; in much the same manner as performed in the past Argonne water facility and the proposed new water facility. The sodium facility would also conduct a limited number of experiments on some of the basic phenomena for a direct comparison with water facility data as a check on, and confirmation of, the important modeling assumptions used to support water testing and for guiding / validating CFD code improvement.

5.2.3 Computer Modeling/Simulation

This white paper has also highlighted some previous pioneering Argonne research associated with assessing the usefulness of 1-D and 3-D computer modeling/simulations of thermal-buoyancy-dominated flows in reactor components and systems. One-dimensional models such as the W-DEMO code were shown to be inadequate, and early Argonne COMMIX code results showed that properly featured and implemented 3-D CFD codes are promising and essential as tools for designing reactor components and correctly predicting the movement of transient flow and thermal fronts within and between components in an LMR system. The restrictiveness and correctness of several of the assumptions used in past 3-D CFD simulations, especially in modeling turbulence and large-scale eddy behavior as modified by thermal buoyancy, must be investigated more thoroughly and benchmarked/validated with both water and sodium experimental data to better understand the stratification phenomena dependence on fluid properties and their occurrence during various modes of reactor operation.

The improved CFD codes developed for application to the next generation of LM-ABRs under GNEP would also benefit the safety assessment of current LWRs by virtue of the fact that many of the same important generic phenomena that are important to LMR development occur in both types of reactors under off-normal reactor operation and influence individual components as well as the entire plant. These phenomena, which affect much more than just core behavior, cause feedback with the core and are currently not adequately understood and have not been simulated with current CFD codes.

The 3-D CFD code(s) to be used in future LMR computational modeling could be a commercial code like FLUENT or STAR-CD or the Argonne NEK 5000 code of Argonne's Mathematics and Computer Science Division [1]. An approach using both a commercial code (for near term design guidance) and the Argonne in-house code for the long term pathway forward takes advantage of the fact that the in-house code, for which Argonne staff understand the internal algorithms and have complete access to the source code, would greatly facilitate

developing new models and improved computational algorithms, and implementing them in the codes for validation with experimental data and then making the new features available to the reactor and code community. This approach is believed to yield the most rapid progress and be the most flexible.

In CFD simulation of single-phase flows, which is predominately the case for LMRs, one of the most challenging problems is the simulation of turbulence and large-spatial-scale frequently ordered eddies or vortexes. This white paper has highlighted the potential for structural thermal stripping induced by large-scale eddies impinging on surfaces or by undulating thermally stratified interfaces. Although direct numerical simulation of turbulence and large eddy simulation (LES) of turbulence are feasible with some CFD codes, they are currently computationally practical only for problems of small geometrical scale and for flows of relatively small Reynolds number. For this reason, the simulation of turbulence by CFD codes would probably use RANS (Reynolds Averaged Navier-Stokes) turbulence models, which, although being better than the use of correlations for friction (pressure drop) and heat transfer, are not of universal applicability. Thus, the improved CFD codes will need validation, and at this time their validation for problems of interest to the nuclear industry (natural-circulation turbulence models) has been very limited. The experience to date shows that the simulations using RANS models for heat transfer coefficients in buoyant flows and in liquid metal flows can be quite inaccurate. The use of research-based codes like Argonne's NEK 5000 code, which uses LES, with additional improvements incorporated by modeling smaller scale turbulence effects, promises to significantly improve simulation capabilities and speed up computation considerably, especially when done in combination with parallel processing computers. Argonne will soon be installing a cutting-edge IBM Blue Gene Computer. This computer will play an important role in advancing the improved thermal-hydraulic simulation capabilities proposed in this white paper.

Further improvements in code thermal-hydraulic simulations for the complex geometries associated with LMRs will require further optimization and improvements in the generation of computational grids for CFD simulations. Additionally, the use of coupled CFD and structural codes in the future will require grid generation software that meets the needs of both codes with minimal computer user intervention. Specifically, in LMRs, thermal expansion of primary system components provides reactivity feedbacks that are very important in safety analyses. Thermal expansion of the liquid coolant can be very important also in the performance of some shutdown heat removal systems like the RVACS. Although CFD codes have models for the simulation of the motion of free surfaces like the interface between the surface of the sodium in the reactor tank and the cover gas, these models are not computationally efficient in large-scale problems involving long duration transients. There is a need for improved models and simulations of these important thermal-hydraulic phenomena.

In some reactor analyses, the use of the porous media approximation has been used to make these analyses more efficient. Some consideration should be given to incorporating a porous media model like the one used in the past Argonne COMMIX code into a new CFD code. The porous media model used in the commercial codes is awkward and in many analyses inappropriate because it forces the flow to be one-dimensional.

The Argonne efforts to couple a 3-D CFD and a structural code would initially start with uncoupled codes but would quickly focus on development of coupled codes to allow simulations of thermal stratification and other phenomena which have the potential for causing structural thermal stressing of the large components in an LMR. Two commercial 3-D coupled codes currently under development are the FLUENT CFD and ABAQUS structural codes and the ANSYS structural and BMX CFD codes. Both of these code pairings are in the early stages and Argonne's progress in this direction would be greatly enhanced by learning from the commercial experience and possibly collaborating with the commercial companies.

The proposed pathway forward focuses on the objectives/tasks that most directly provide the important foundational understanding and validation data for the most important phenomena to be modeled to support development of improved computer simulation methodologies which can then be applied to improving both 3-D CFD codes and lower order code simulations. This approach also facilitates creating an understanding with regard to what the limitations are of each code and which is best to use under a wide range of reactor operating conditions.

5.3 Closing Remarks

In conclusion, Argonne is in an excellent position based on historical accomplishments in the area of thermal-hydraulic research and simulation to be a key technical player supporting the new DOE GNEP-ABR initiative in the research and development area of thermal hydraulics and structures interactions and to make significant contributions to the design of safe and reliable nuclear reactors.

There is a significant need for a high-quality data bank utilizing state-of-art test facilities and measurement techniques focused on the thermal-hydraulic phenomena of high importance to the design of safe reactors. Many of these phenomena have been highlighted in this white paper. The phenomenological data bank will be used to guide development and validation of a variety of computational simulation tools that will contribute significantly to the vision for a nuclear reactor program at Argonne that serves both research and commercial needs related to validation of thermo-fluid models (and possibly models for coupled multi-physics problems) and deployment of the next generation of reactors. Under this initiative, reactor phenomenological research experimentalists, advanced reactor concept engineers, and computer computational simulation scientists/modelers would work together shoulder to shoulder in planning facilities, designing code features/computational algorithms, defining benchmark thermal-hydraulic phenomena to focus on, interpreting the experimental data, and evaluating the goodness of the simulations. This new Argonne thrust will constitute a science-based strategic initiative leading to improved understanding of the important thermal-hydraulic phenomena occurring under reactor off-normal behavior and development of the computational simulation tools to model individual components as well as the entire plant.

This science-based initiative and resulting reactor engineering design tools have the potential for revolutionizing reactor design, accelerating the design process, and reducing costs associated with developing new prototype designs much in the same way the use of computer

simulation has revolutionized the design of jet aircraft and the study of nuclear weapons. The preceding will benefit the GNEP initiative as well as the currently deployed generation of LWRs.

Reference

1. Fischer, P., Knoll. D., Pointer, D., Siegel, A., Argonne National Laboratory, unpublished information, March 2007.

Appendix 1

LMR Modeling:
Comparison of Sodium and Lead Cooled Reactors

This section provides a comparison based on thermal-hydraulic modeling of sodium versus lead liquid metal cooled reactors, using the French Superphenix Sodium Fast Reactor of 1200 MW(e) and the Russian Lead Fast Reactor (LFR 1000) of 1000 MW(e) as examples. Based on non-dimensional modeling parameters for various important phenomena influencing the behavior of LMRs, a qualitative introductory comparison illustrating the influence of the two metal coolants is provided. The appendix first focuses on large-scale thermal-hydraulic behavior under natural circulation operation and addresses how design and fluid coolant type influence core cooling. The appendix then focuses on comparing behavior between the two coolants for smaller scale behavior issues under both normal and low flow. This section is extracted from a previous Argonne internal study [1].

Tables A-1 and A-2 highlight important features of the Russian lead-cooled and the French sodium-cooled Superphenix fast reactors and some of the thermal-hydraulic properties of the two liquid metals. These parameters are used in the discussions to follows. While this discussion focuses on comparing behavior of the two reactors with different coolants, the same non-dimensional modeling parameters could be used to explore qualitatively the influence of geometrical and operational design trade-offs on the behavior of a reactor for a given coolant.

Table A-1 Comparison of lead and sodium LMRs

	Russian Lead Fast Reactor (LFR 1000)	French Superphenix Sodium Fast Reactor
Core inlet temperature (°F)	878	743
Core outlet temperature (°F)	1076	1013
Average (°F)	977	878
ΔT (°F)	198	270
Velocity design point (ft/s)	4.6	24
Power [MW(e)]	1000	1200
Primary tank height/diameter (ft)	70 / 45	61 / 69
Coolant mass flow rate (lb/s)	342,199	35,380

Table A-2 Fluid properties of lead and sodium at 1000ºF

	ρ (lbm/ft^3)	μ (lbm/ft-hr)	ν (ft^2/hr)	K (BTU/hr-ft-°F)	C_p (BTU/lbm-°R)	α (ft^2/hr)	β (1/°F) (700°F)	Pr = ν/α
Lead	646	4.07	0.0063	8.9	0.037	0.37	6.3×10^{-5}	0.017
Sodium	51.2	0.49	0.0096	37.8	0.30	2.4	1.6×10^{-4}	0.0040
Pb / Na	12.62	8.31	0.66	0.24	0.12	0.15	0.39	4.25

Global Natural Circulation Operation

Under quasi-steady-state conditions associated with the natural-circulation coolant flow around an LMR circuit, the flow is driven around the reactor solely by the core and heat-sink thermal induced density difference, causing a thermal-buoyancy head pressure differential (ΔP_H) across the core in balance with the core flow frictional pressure drop (ΔP_C) (assuming that the dominant flow resistance exists in the core). The frictional pressure drop through the core is a function of the core average velocity U_C, the geometry of the core, and fluid properties.

The simplified natural circulation flow circuit shown in Fig. A-1.1 is used along with the assumptions that the hot–leg flow coming out of the core heat source is of uniform temperature T_C, and the cold–leg flow returning from the heat sink to the core is of uniform temperature T_S. This simplified model can be used to evaluate the influence of design parameters on core cooling.

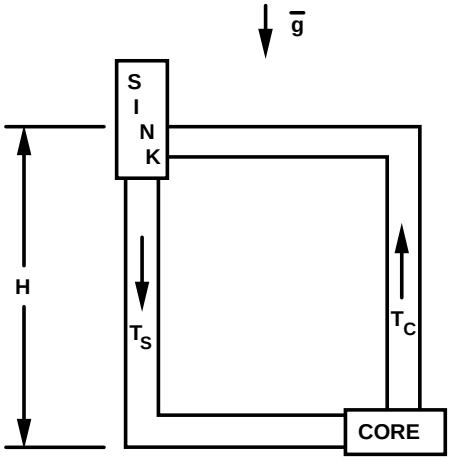

Figure A-1.1 Simplified schematic of LMR flow circuit

In the model H is the vertical distance between the heat source and sink thermal centers. Because this model neglects all heat transfer and coolant mixing around the circuit (except at the source and sink) as well as other flow resistances not in the core, it will yield an upper bound on the natural-circulation cooling velocity. Additionally, because very little information is available on core design, only very simplified modeling is used for the core resistance. The model developed is useful for showing general parametric influences and trends. Under the preceding conditions

$$\Delta P_H = \Delta P_C$$

which yields an equation for U_C and, in turn, allows calculation of decay heat removal from the core where

$$\Delta P_H = H\,\rho_{ave}\beta(T_C - T_S)$$

For sodium LMR designs, H can range from 2 to 15 ft, and

$$\Delta P_C = K_1\, f\, \rho_{ave}\, U_C^2$$

with K_1 a constant and a function of core geometry, and $f = K_2 Re^{-1/4}$ is a friction factor for the core. In the equation for f, Re is the core Reynolds number given by $Re = D_C U_C/\nu$, and K_2 is a constant and function of geometry. Thus

$$\Delta P_C = K_1 K_2\, \rho_{ave}\, U_C^{7/4}\left(\frac{\nu}{D_C}\right)^{1/4}$$

Some results are now presented for ΔP_H for both coolants:

Case I: $H_{Pb} = H_{Na} = 5$ ft and $\Delta T_{Pb} = 198°F$, $\Delta T_{Na} = 270°F$

$$\underline{\underline{\Delta P_{H_{Pb}}}} = \frac{5\,\text{ft}}{144\,\text{in.}^2/\text{ft}^2}\,646\,\text{lbm/ft}^3\;6.3\times10^{-5}\,\frac{1}{°F}\,198°F = \underline{\underline{0.28\,\text{psi}}}$$

$$\underline{\underline{\Delta P_{H_{Na}}}} = \frac{5}{144}\,51\,2\;16\times10^{-4}\,270 = \underline{\underline{0.077\,\text{psi}}}$$

Hence, in case I, the thermal head is larger in Pb than in Na.

Case II: $H_{Pb} = H_{Na} = 5$ ft, $\Delta T_{Pb} = \Delta T_{Na} = 270°F$

$$\underline{\underline{\Delta P_{H_{Pb}}}} = \underline{\underline{0.38\,\text{psi}}}$$

$$\underline{\underline{\Delta P_{H_{Na}}}} = \underline{\underline{0.077\,\text{psi}}}$$

Hence, for the same geometries and equal ΔTs, the thermal head is still larger in Pb.

The ratio of thermal heads for the two coolant circuits in general is given by

$$\frac{\Delta P_{H_{Pb}}}{\Delta P_{H_{Na}}} = \left(\frac{H_{Pb}}{H_{Na}}\right)\left(\frac{\rho_{Pb}}{\rho_{Na}}\right)\left(\frac{\beta_{Pb}}{\beta_{Na}}\right)\left(\frac{\Delta T_{Pb}}{\Delta T_{Na}}\right)$$

and for average fluid properties

$$= 4.97\left(\frac{H_{Pb}}{H_{Na}}\right)\left(\frac{\Delta T_{Pb}}{\Delta T_{Na}}\right)$$

Case I: for $H_{Pb}/H_{Na} = 1$ and $\frac{\Delta T_{Pb}}{\Delta T_{Na}} \equiv 1$

$$\underline{\underline{\Delta P_{H_{Pb}} / \Delta P_{H_{Na}}}} = \underline{\underline{4.97}}$$

Case II: for $H_{Pb} = 5\ H_{Na}$, $\Delta T_{Pb} = 198°F$ and $\Delta T_{Na} = 270°F$

$$\underline{\underline{\Delta P_{H_{Pb}} / \Delta P_{H_{Na}}}} = 4.97(5)\left(\frac{198}{270}\right) = \underline{\underline{18.22}}$$

By setting $\Delta P_H = \Delta P_C$, an equation is obtained for relating geometry, fluid properties, and thermal–hydraulics around the coolant circuit. This equation can be solved for the coolant velocity U_C through the core, yielding

$$U_C = \left[\frac{H\beta\Delta T_C}{K_1 K_2}\right]^{4/7} (D_C / \nu_C)^{1/7}$$

Interestingly this relation shows that U_C is not an explicit function of density ρ. Furthermore, H, D_C, K_1, and K_2 are difficult to quantify without knowing considerable reactor design detail, and even then it is still difficult because of the complex flow passages and heat transfer occurring around the circuit. Thus, an attempt was made to quantify the result.

The ratio of natural-circulation coolant core velocities for Pb and Na is given by

$$U_{C_{Pb}} / U_{C_{Na}} = \left[\frac{(K_1 K_2)_{Na}}{(K_1 K_2)_{Pb}}\right]^{4/7} \left[\left(\frac{H_{Pb}}{H_{Na}}\right)\left(\frac{\beta_{Pb}}{\beta_{Na}}\right)\frac{\Delta T_{Pb}}{\Delta T_{Na}}\right]^{4/7} \left[\left(\frac{D_{C_{Pb}}}{D_{C_{Na}}}\right)\left(\frac{\nu_{Na}}{\nu_{Pb}}\right)\right]^{1/7}$$

Note this expression is not sensitive to changing the core hydraulic diameter ratio due to the 1/7 power on the last term.

The above relation is next used to make parametric sample calculations for

$$U_{C_{Pb}}/U_{C_{Na}}$$

Case I: Same core designs, $D_{C_{Pb}} = D_{C_{Na}}$, with

$(K_1K_2)_{Na} + (K_1K_2)_{Pb}$, $H_{Pb} = H_{Na}$, and $\Delta T_{Pb} = \Delta T_{Na}$ which yields

$$\underline{\underline{U_{C_{Pb}}/U_{C_{Na}}}} = [1]^{4/7}[(1)(0.39)(1)]^{4/7}\left[(1)\left(\frac{1}{0.66}\right)\right]^{1/7}$$
$$= [1][0.585][1.06] = \underline{0.62}$$

Hence, core coolant velocity is less in Pb than in Na.

Case II: $\Delta T_{Pb}/\Delta T_{Na} = 198/270$, $H_{Pb} = 5\ H_{Na}$, and same core design because of not knowing how to quantify D_C and the influence on K_1, K_2. Even if $D_{C_{Pb}} > D_{C_{Na}}$, which is believed to be the case for the Russian LFR 1000, the impact on $U_{C_{Pb}}/U_{C_{Na}}$ is reduced by the 1/7 power.

$$\underline{\underline{U_{C_{Pb}}/U_{C_{Na}}}} = [1]^{4/7}\left[(5)(0.39)\left(\frac{198}{270}\right)\right]^{4/7}\left[\left(\frac{1}{0.66}\right)\right]^{1/7}$$
$$= [1][1.43][1.06] = \underline{1.52}$$

Hence, the increase in thermal center vertical separation distance has made the core coolant velocity greater in lead than in sodium.

With the knowledge of core coolant velocities, one can calculate the ratio of core decay heat removal for the two coolants occurring under natural circulation conditions, Q_{Pb}/Q_{Na},

$$\frac{Q_{Pb}}{Q_{Na}} = \left(\frac{\rho_{Pb}}{\rho_{Na}}\right)\left(\frac{U_{C_{Pb}}}{U_{C_{Na}}}\right)\left(\frac{A_{Pb}}{A_{Na}}\right)\left(\frac{C_{P_{Pb}}}{C_{P_{Na}}}\right)\left(\frac{\Delta T_{C_{Pb}}}{\Delta T_{C_{Na}}}\right)$$

where A is the coolant flow area in the core.

Sample calculation for Q_{Pb}/Q_{Na}:

Case I: Same reactor size, component locations and ΔTs ($A_{Pb} = A_{Na}$, $\Delta T_{C_{Pb}} = \Delta T_{C_{Na}}$)

$$\frac{Q_{Pb}}{Q_{Na}} = (12.62)(0.62)(1)(0.12)(1) = \underline{0.94}$$

Hence, the rate of decay heat removal is about the same under these assumptions for the two different coolants.

The claim that the LFR 1000 has a very large Q_{Pb} (= 15%) for the design-point reactor heat generation is in marked contrast to claims of Q_{Na} = 2% for sodium-cooled reactors, which would yield a $Q_{Pb}/Q_{Na} = 0.15(2400)/ 0.02(3000) = 6$.

The question to be answered is: how have the Russians designed the LFR 1000 to achieve such large values of decay heat removal? Looking at the general equations for $U_{C_{Pb}}/U_{C_{Na}}$ and Q_{Pb}/Q_{Na} yields some insight. By increasing the ratio of $U_{C_{Pb}}/U_{C_{Na}}$ and A_{Pb}/A_{Na}, Q_{Pb}/Q_{Na} can be increased. Also, $U_{C_{Pb}}/U_{C_{Na}}$ can be increased by increasing H_{Pb}/H_{Na} and the ratio of core hydraulic diameters $D_{C_{Pb}}/D_{C_{Na}}$. Hence, opening up the core coolant flow areas for the lead reactor would increase the D_C ratio as well as the flow area ratio in the core. (The Russians do state that the "low neutron moderation rate by lead allows increasing its volume fraction in the core compared to Na.") Also the height of the Russian reactor is larger than that of the Na reactor and thereby allows for the possibility of a larger H in the lead reactor.

The core flow area A_{Pb}/A_{Na} can be computed from the given design-point information for the two reactors using

$$\frac{A_{Pb}}{A_{Na}} = \frac{m_{Pb}}{m_{Na}} \frac{\rho_{Na}}{\rho_{Pb}} \frac{U_{C_{Na}}}{U_{C_{Pb}}}$$

$$\frac{A_{Pb}}{A_{Na}} = \left(\frac{342,199}{35,380}\right)\left(\frac{512}{646}\right)\left(\frac{24}{4.6}\right) = (9.67)(0.07926)(5.217)$$

$$= \underline{4.00}$$

Hence, the core flow area is much larger in the LFR 1000 than in the French SPX.

Sample calculations for Q_{Pb}/Q_{Na}:

Case I: $A_{Pb}/A_{Na} = 4.0$, $\Delta T_{Pb} = \Delta T_{Na}$, $H_{Pb} = H_{Na}$, and because of not knowing what to do with D_C, keep this ratio at unity (remember this appears to 1/7 power) with $U_{C_{Pb}}/U_{C_{Na}} = 0.62$ from earlier calculation. Thus, we get

$$\frac{Q_{Pb}}{Q_{Na}} = (12.62)(0.62)(4.00)(0.12)(1) = \underline{3.76}$$

Hence, Q_{Pb}/Q_{Na} is getting close to the Russian claim of 6.0 as a result of a larger Pb coolant flow area.

Case II: $H_{Pb} = 5\ H_{Na}$, $\Delta T_{Pb} = 198°F$, $\Delta T_{Na} = 270°F$, with the other parameters the same as in Case I and with $U_{C_{Pb}}/U_{C_{Na}} = 1.52$ from earlier calculation.

$$\frac{Q_{Pb}}{Q_{Na}} = (12.62)(152)(4.00)(0.12)\left(\frac{198}{270}\right) = \underline{6.75}$$

This ratio is close to the value claimed by the Russians and shows that there are design options which allow the Russian LFR 1000 to achieve high decay heat removal with the lead coolant.

Because of all the assumptions used in this simple model and lack of reactor design detailed information, however, this analysis can only reflect qualitative parametric trends between Pb and Na as coolants. As can be deduced, there appear to be no overwhelming benefits, from the thermal-hydraulics viewpoint, in using Pb versus Na coolants in the areas considered. In fact, the estimate for thermal density head is probably an upper bound. In reality, even though the LFR 1000 could be designed with a larger H, because of heat transfer and mixing in the plenums, the actual thermal head could be considerably less and a much weaker function of H (which is found to be the case in Na-cooled LMRs when more detailed analysis is used to study the coolant behavior). This part of the Na versus Pb coolant comparison could also be improved by more detailed modeling of the core pressure drop ΔP_C by using correlations reflecting specific details of the core geometry for each reactor.

Local Behavior

This section provides additional observations on local thermal-hydraulic behavior differences, based on modeling considerations, for the two coolant-based reactors for the conditions given in Tables A-1 and A-2.

- Lead is more dense (ρ) and viscous (μ) and has a lower thermal conductivity (k), coefficient of volumetric thermal expansion (β) and specific heat (C_p) than sodium.
- Energy capacity ratio $= (\rho C_p)_{Pb}/(\rho C_p)_{Na} = 1.56$. Hence, for the same volumes of coolant and equal thermal energy addition, the lead will undergo a smaller temperature rise

$$\left(\frac{\Delta T_{Pb}}{\Delta T_{Na}} = \frac{1}{1.56} = 0.64\right)$$

  This result indicates less thermal-buoyancy-driving temperature difference induced in the coolant for lead. (Note Pb also has a lower volumetric thermal expansion coefficient β than Na.)

- The turbulence level of the coolants is important to heat transfer at a surface. The ratio of Reynolds numbers for the two coolants is given by

$$Re_{Pb}/Re_{Na} = (\nu_{Na}/\nu_{Pb})[(VD)_{Pb}/(VD)_{Na}] = 1.52.$$

  Hence, for the same size reactors ($D_{Pb} = D_{Na}$) with the same coolant velocities ($V_{Pb} = V_{Na}$), the lead coolant will be more turbulent. Additionally, for the same Re in each reactor ($Re_{Pb} = Re_{Na}$) of the same size and hence the same turbulence, the coolants would have to be pumped with $V_{Pb} = 0.66\ V_{Na}$. For liquid metal flowing turbulently in a boundary layer fashion over flat surfaces, the ratio of hydrodynamic boundary-layer thickness (δ) to thermal layer thickness (δ_t) is given by $\delta/\delta_t = 164\sqrt{Pr}$. Hence, because $Pr_{Pb} = 4.25\ Pr_{Na}$ and $(\delta/\delta_t)_{Pb}/(\delta/\delta_t)_{Na} = \sqrt{4.25} = 2.06$ the thermal layer

in lead does not extend as far outside the hydrodynamic layer as does the thermal layer in sodium. This condition dictates the zone of influence of temperature normal to a heated surface.

- For forced convection in fully developed turbulent flow of liquid metal, the no-dimensional Nusselt heat transfer coefficient $Nu = hd/K$ is proportional to $(RePr)^m = (Pe)^m$, and m varies from 0.4 to 0.8, where $Pe = VD/\alpha$. Hence

$$Nu_{Pb} / Nu_{Na} \propto (Re_{Pb} / Re_{Na})^{1/2} (Pr_{Pb} / Pr_{Na})^{1/2}$$

or in terms of the surface heat transfer coefficient

$$h_{Pb} / h_{Na} \propto (Re_{Pb} / Re_{Na})^{1/2} (Pr_{Pb} / Pr_{Na})^{1/2} (D_{Na} / D_{Pb}) (K_{Pb} / K_{Na})$$

Thus, for same size reactors with same coolant velocity

$$h_{Pb} / h_{Na} \propto (152)^{1/2} (4.25)^{1/2} (0.24) = 0.60$$

and for same size reactors with the same Re

$$h_{Pb} / h_{Na} \propto (4.25)^{1/2} (0.24) = 0.49$$

In both limits the heat transfer coefficient is smaller for lead than for the sodium coolant under full turbulent conditions, and thus the low thermal conductivity of lead hurts overall heat transfer.

- For pure free convection flows where viscous forces dominate over inertia force and the fluid velocity is created solely by gravitation acting on fluid density variations, the non-dimensional Nusselt heat transfer coefficient is given by

$$Nu = C(Gr\ Pr)^n$$

where n can vary from 0.2 to 0.4, and the Grashof number $Gr = g\beta\Delta TD^3/\nu^2$ is the dimensionless ratio of buoyancy to viscous forces strength. When $Gr > 10^8 - 10^9$ flows tend to be turbulent. Thus, in terms of the heat transfer coefficient h ratio for the surface of the two coolants, we get

$$\frac{h_{Pb}}{h_{Na}} = \left(\frac{Pr_{Pb}}{Pr_{Na}}\right)^{1/4} \left(\frac{\beta_{Pb}}{\beta_{Na}} \frac{\Delta T_{Pb}}{\Delta T_{Na}} \frac{\nu_{Na}^2}{\nu_{Pb}^2} \frac{D_{Na}}{D_{Pb}}\right)^{1/4} \left(\frac{K_{Pb}}{K_{Na}}\right)$$

$$= 0.34 \left(\frac{\Delta T_{Pb}}{\Delta T_{Na}} \frac{D_{Na}}{D_{Pb}}\right)^{1/4}$$

If the two reactors have the same ΔT and size D, this ratio yields

$$\frac{h_{Pb}}{h_{Na}} = 0.34$$

Hence, in pure convection for the case where viscous forces dominate over inertia, the heat transfer coefficient is less in lead than sodium, and moderate changes in ΔT and D ratios do not significantly change the result.

- For many postulated accidents, the reactor is designed to undergo a flow coast-down from forced pumped flow to a state where coolant is driven solely by thermal-induced density differences via thermal buoyancy forces. Under this condition the local thermal–hydraulics can go from forced convection through mixed forced–free convection to possibly free convection. However, even under 100% natural circulating flow, because of the large reactor size, the coolant flow in many sub-regions can still be turbulent with rather large Re. Hence, the controlling force ratio will be between thermal buoyancy and inertia forces. Under this condition the non-dimensional modeling parameter is the Richardson number Ri given by

$$= \frac{g \beta D \Delta T}{u^2}$$

Ri is used to model the effects of buoyancy around a circuit as well as the nature of stratified interfaces within plenums. Thermal buoyancy starts to alter flow and temperature fields when $Ri > 0.2 – 0.4$.

- When computing the Ri ratio for the two coolants based on the parameters given in Tables A-1 and A-2 for a natural-circulation low-flow condition through the cores of each reactor, we get

$$\frac{Ri_{Pb}}{Ri_{Na}} = \left(\frac{\beta_{Pb}}{\beta_{Na}}\right)\left(\frac{D_{Pb}}{D_{Na}}\right)\left(\frac{\Delta T_{Pb}}{\Delta T_{Na}}\right)\left(\frac{u_{Na}}{u_{Pb}}\right)^2$$
$$= 0.16$$

This calculation indicates that the lead-cooled reactor Ri value is much lower than the sodium reactor, implying that thermal buoyancy will be much smaller under natural circulation conditions. Setting $Ri_{Pb} = Ri_{Na}$ imposes equal influence of buoyancy (good or bad) in both reactors. Thus

$$\frac{Ri_{Pb}}{Ri_{Na}} = \left(\frac{\beta_{Pb}}{\beta_{Na}}\right)\left(\frac{D_{Pb}}{D_{Na}}\right)\left(\frac{\Delta T_{Pb}}{\Delta T_{Na}}\right)\left(\frac{u_{Na}}{u_{Pb}}\right)^2 \equiv 1$$

Hence, for reactors having the same size D and ΔT, we get for the velocity ratio between the reactors

$$u_{Pb}/u_{Na} = (\beta_{Pb}/\beta_{Na})^{1/2}$$

Hence, flow velocity needs to be lower with a lead coolant = $(0.39)^{1/2} = 0.62$ to achieve the same thermal buoyancy effect. Note this ratio is 0.19 for LFR and Superphenix, which differ in size as shown in Table A-1.

Reference

1. Kasza, K.E., Amorosi, A., Argonne National Laboratory, unpublished information, September 1992.

Nuclear Engineering Division
Argonne National Laboratory
9700 South Cass Avenue, Bldg. 212
Argonne, IL 60439-4838

www.anl.gov

UChicago ▶ Argonne LLC

A U.S. Department of Energy laboratory
managed by UChicago Argonne, LLC